A CRYSTALLOGRAPHIC AND MECHANISTIC INVESTIGATION OF RHENIUM(I) TRICARBONYL COMPLEXES FOR MODEL DRUG DESIGN

by

MARAKE THABO DANIEL

A dissertation submitted to fulfil the requirements for the degree of

MAGISTER SCIENTIAE

in the

DEPARTMENT OF CHEMISTRY

FACULTY OF NATURAL AND AGRICULTURAL SCIENCES

at the

UNIVERSITY OF THE FREE STATE

SUPERVISOR: DR. ALICE BRINK

CO-SUPERVISOR: PROF. ANDREAS ROODT

FEBRUARY 2015

ACKNOWLEDGEMENTS

First and foremost, I would like to extend my sincere gratitude to my God and Heavenly Father for all the countless blessings You have showered me with. Thank You for giving me enough courage, wisdom and powerful knowledge to complete this dissertation.

Thank you to Prof. Andreas Roodt for giving me the opportunity to pursue my M.Sc. degree and for the patience and enthusiasm he showed in answering numerous questions. It is really an honour to be associated with a scientist of you calibre.

Thank you to Dr. Alice Brink for always being just a phone call away to answer questions. Your guidance and fresh ideas contributed a lot towards the successful completion of this M.Sc. study.

Thank you to the inorganic group for all the advice and knowledge you shared. Special thanks to the crystallographic team for all the effort they put in for collecting our crystal data. Your work does not go unnoticed.

Thank you to my friends, Majoang Seun, Mokheseng Khotso, Mokolokolo Pennie, Kama Tom and Alexander Orbett for all the jokes and laughter we shared which reminded me that there are more important things in life than being depressed for not obtaining crystals.

To my mother, Marake Mpoetsi Regina, thank you for all the sacrifices you made raising me up. Being a single parent must have not been easy. Thank you for the warm love and support you have given me over the years. But most importantly, I thank you for teaching me humility. To my siblings, Ntjabane Pulane Elizabeth, Marake Mathunya Meshack and Marake Kahlai Abednego thank you for all the support and encouragements. Special thanks to Kahlai for being a father figure in the family at a really tender age. You are my hero.

To my newly born son, Marake Neo Kelebohile and his mother, Lesesa Masekoala Joyce, you guys mean the world to me. I thank God every day for bringing the both of you into my life and making me complete.

Thank you to the University of the Free State and the South African National Research Foundation (NRF) for financial support.

TABLE OF CONTENTS

Chapter 3

Theoretical Aspects of Characterization Techniques (IR, UV-Vis, XRD, ^{1}H and ^{13}C NMR)

Chapter 4

Synthesis of Schiff-base Ligands and Re(I) Tricarbonyl Complexes

Chapter 5

Single Crystal X-ray Structures of fac-[Re(L,L'-Bid)(CO)$_3$(L)] complexes

Chapter 6

Preliminary Formation Kinetics of fac-[Re(L,L'-Bid)(CO)$_3$] complexes with L,L'-Bid = N,O- and N,N'-Bid Type Ligands

ABBREVIATIONS AND SYMBOLS

ABBREVIATION	MEANING
L,L'-Bid	Bidentate ligand
Sal	Salicylidene
Me	Methyl
α	Alpha
β	Beta
γ	Gamma
$\Delta S^{\neq}$	Entropy of activation
$\Delta H^{\neq}$	Enthalpy of activation
π	Pi
Z	Number of molecules in a unit cell
IR	Infrared spectroscopy
UV	Ultraviolet region in light spectrum
Vis	Visible region in light spectrum
NMR	Nuclear magnetic resonance spectroscopy
XRD	X-ray diffraction
ν	Stretching frequency on IR
ppm	(Units of chemical shift) parts per million
MeOH	Methanol
Py	Pyridine
Im	Imidazole
iProp	Isopropyl
CyPent	Cyclopentyl
KBr	Potassium bromide
k_{obs}	Observed pseudo first-order rate constant
en	Ethylenediamine
dien	Diethylenetriamine
κO	Coordination through oxygen donor atom

ABSTRACT

***Keywords*:** Rhenium, technetium, tricarbonyl complexes, radiopharmaceuticals, salicylidene, Schiff-base, formation kinetics

Four new complexes of the type *fac*-[Re(L,L'-Bid)$(CO)_3$(L)] (L,L'-Bid = monoanionic *N,O* bidentate Schiff-base ligands: 5Me-SalH-iProp = 2-(isopropylimino)methyl-5-methylphenol, 5Me-SalH-CyPent = 2-(cyclopentylimino)methyl-5-methylphenol and 5Me-SalH-Hist = 2-(2-imidazol-4-yl)ethyliminomethyl-5-methylphenol; *L* = pyridine or imidazole ligand) and a polymorphic form of a complex previously reported were synthesized during this study. The ligands were consciously selected due to their varying steric and electronic character afforded by the substituent bonded to the nitrogen imine donor atom. The complexes obtained were characterized by single crystal X-ray diffraction as well as other spectroscopic techniques (IR, NMR, UV-Vis) and included the following: *fac*-[Re(5Me-Sal-iProp)$(CO)_3$(Pyridine)], *fac*-[Re(5Me-Sal-CyPent)$(CO)_3$(Pyridine)], *fac*-[Re(5Me-Sal-CyPent)$(CO)_3$(Imidazole)], *fac*-[Re(*κO*-5Me-Sal-CyPent)$(CO)_3$(Pyridine)(Br)] and *fac*-[Re(5Me-Sal-Hist)$(CO)_3$].MeOH.

The new crystal structures reported all crystallize in the same crystal system (monoclinic), same space group ($P2_1/c$) and contain the same number of molecules in the unit cell ($Z = 4$). Two of the complexes, *fac*-[Re(5Me-Sal-CyPent)$(CO)_3$(Pyridine)] and *fac*-[Re(5Me-Sal-CyPent)$(CO)_3$(Imidazole)] were found to be iso-structural. The different substituents on the nitrogen imine donor atom do not affect the bond distances significantly. However, the bond distance of the imidazole ligand coordinated to the sixth position is significantly shorter than that of the coordinated pyridine ligand. Thus, imidazole coordinates more strongly to the metal center than pyridine.

Multiple reactions were observed for the reaction between the *fac*-$[Re(CO)_3]^+$ core and *N,O* bidentate ligands, therefore the preliminary formation kinetics was studied with more simple and symmetric ethylene amine type ligands. The preliminary formation reactions between the *fac*-$[Re(CO)_3]^+$ core and ethylene amine type ligands, ethylenediamine and diethylenetriamine were performed at 25 ^oC. Two separate reaction were identified, a rapid first reaction, followed by a slower second reaction. The second reaction was investigated during this study.

The second reaction followed *pseudo* first-order conditions with equilibrium rate constant, K_2 of 27(8) $M^{-1}s^{-1}$ for the reaction with ethylenediamine and 31(1) $M^{-1}s^{-1}$ for the reaction with diethylenetriamine at 25 ^{o}C. The second order rate constant, k_2 for the reaction between the *fac*-$[Re(CO)_3]^+$ core and ethylenediamine as well as diethylenetriamine was found to be 0.00826(4) $M^{-1}s^{-1}$ and 0.00715(3) $M^{-1}s^{-1}$ respectively. The reaction with ethylenediamine is faster than that with diethylenetriamine, which can be attributed to the simple, symmetrical nature of ethylenediamine ligand as opposed to the large steric demand of diethylenetriamine ligand.

OPSOMMING

***Sleutelwoorde*:** Renium, tegnesium, trikarboniel-komplekse, radiofarmasie, salisilideen, Schiff-basis, vormingskinetika

Vier nuwe komplekse van die tipe *fac*-[Re(L,L'-Bid)$(CO)_3$(L)] (L,L'-Bid = monoanioniese *N,O* bidentate Schiff-basis ligande: 5Me-SalH-iProp = 2-(isopropielimino)metiel-5-metielfenol, 5Me-SalH-CyPent = 2-(siklopentielimino)metiel-5-metielfenol en 5Me-SalH-Hist = 2-(2-imidasool-4-iel)etieliminometiel-5-metielfenol; *L* = piridien of imidasool ligand), en `n polimorfiese vorm van `n voorheen gerapporteerde kompleks is tydens hierdie studie vervaardig. Die ligande is bewustelik gekies as gevolg van hulle veranderlike steriese en elektroniese karakters wat veroorsaak word deur die substituent wat aan die imien se stikstof skenkeratoom gebind is. Die vervaardigde komplekse is deur X-straal diffraksie asook ander spektroskopiese metodes (IR, KMR, UV-Sig) gekarakteriseer en sluit die volgende in: *fac*-[Re(5Me-Sal-iProp)$(CO)_3$(piridien)], *fac*-[Re(5Me-Sal-CyPent)$(CO)_3$(piridien)], *fac*-[Re(5Me-Sal-CyPent)$(CO)_3$(imidasool)], *fac*-[Re(*κO*-5Me-Sal-CyPent)$(CO)_3$(piridien)(Br)] en *fac*-[Re(5Me-Sal-Hist)$(CO)_3$].MeOH.

Die nuwe gerapporteerde kristalstrukture kristalliseer almal in dieselfde kristalstelsel (monoklinies) en ruimtegroep ($P2_1/c$) en bevat dieselfde getal molekule in die eenheidsel (Z = 4). Daar is vasgestel dat twee van die komplekse, *fac*-[Re(5Me-Sal-CyPent)$(CO)_3$(piridien)] en *fac*-[Re(5Me-Sal-CyPent)$(CO)_3$(imidasool)], iso-struktureel is. Die verskillende substituente op die stikstof imien skenkeratoom het nie `n beduidende invloed op die bindingsafstande nie. Die bindingsafstand van die imidasool ligand wat aan die sesde posisie gekoördineer is is egter beduidend korter as dié van die gekoördineerde piridien ligand. Imidasool koördineer dus sterker aan die metaalsenter as piridien.

Veelvoudige reaksies is waargeneem vir die reaksie tussen die *fac*-$[Re(CO)_3]^+$ kern en *N,O* bidentate ligande, daarom is voorlopige vormingskinetika met meer eenvoudige en simmetriese etileenamien-tipe ligande bestudeer. Die voorlopige vormingsreaksies tussen die *fac*-$[Re(CO)_3]^+$ kern en etileenamine-tipe ligande, etileendiamien en dietileentriamien is uitgevoer teen 25 ^oC. Twee afsonderlike reaksies is geïdentifiseer; `n vinnige eerste reaksie gevolg deur `n stadiger tweede reaksie. Die tweede reaksie is tydens hierdie studie ondersoek.

Die tweede reaksie volg *pseudo* eerste-orde toestande met `n ewewigstempokonstante, K_2, van 27(8) $M^{-1}s^{-1}$ vir die reaksie met etileendiamien en 31(1) $M^{-1}s^{-1}$ vir die reaksie met dietileentriamien teen 25 ^{o}C. Die tweede orde tempokonstante, k_2, vir die reaksie tussen die *fac*-$[Re(CO)_3]^+$ kern en etileendiamien asook dietileentriamien is bepaal as onderskeidelik 0.00826(4) $M^{-1}s^{-1}$ en 0.00715(3) $M^{-1}s^{-1}$. Die reaksie met etileendiamien is vinniger as die reaksie met dietileentriamien, wat toegeskryf kan word aan die eenvoudige, simmetriese natuur van etileendiamien in kontras met die groot steriese aanvraag van die dietileentriamien ligand.

1 Introduction and Aim

1.1 Introduction

Cancer is a deadly disease with a high morbidity and mortality rate,[1] due to late detection and diagnosis. It is a disease in which abnormal cells divide without control and are able to invade other tissues. These cancer cells are carried to other parts of the body through the bloodstream and lymphatic system. The similarities that exists between normal and abnormal DNA, means that a given drug will react with a cancerous cell as much as it would with a normal cell. This poses great difficulties when designing cancer chemotherapeutic agents that will completely kill the cancer cell while causing minimal toxicity to normal cells in the body. In USA, an estimated 1.6 million new cases of cancer and approximately 900 000 deaths were reported in 2014.[1] The four most common types of cancer contributing to the total death rate include lung cancer, colon cancer, breast cancer and prostate cancer.[2]

1.2 Nuclear Medicine – History and Discovery

X-rays were discovered by C. W. Röntgen in 1895 after taking an X-ray image of his wife's hand.[3] A year later, A. H. Becquerel discovered radioactivity in the uranium salt, potassium uranyl sulphate. A large contribution has since been made by a number of scientists to the discovery of many other radionuclides and hence to the development of nuclear medicine. I. Curie and F. Joliot were the first scientists to report artificial radioactivity in 1934. The duo irradiated boron and aluminium targets with α particles from polonium and could observe positrons being emitted from the target even after the removal of the α particle source. The discovery of the cyclotron, deuteron and neutron facilitated the discovery of many more artificial radionuclides.

[1] National Cancer Institute, 2014. Available: http://www.cancer.gov/cancertopics/cancerlibrary/what-is-cancer. Last Accessed 06/01/2015.
[2] American Cancer Society, *Cancer Facts and Figures 2014*, 2014. Available: http://www.cancer.org/research/cancerfactsstatistics/cancerfactsfigures2014/. Last accessed 06/01/2015.
[3] R. R. Morris, *Society of Nuclear Medicine*, 20, 1954, 2005.

1.3 The Role of Metals in Medicine

Medicinal inorganic chemistry consists of introducing a metal ion into a biological system either by chance or by intention. The intentional introduction of a metal ion into a biological system will lead to either therapeutic or diagnostic agents. The resulting therapeutic or diagnostic agent is subject to the limitations in the Bertrand diagram (see Figure 1.1), which is used to indicate the benefit and/or detriment of an element and its concentration.[4] The area of optimum physiological response is dependent on the element's speciation and oxidation state, as well as the biochemistry of the specific compound in which it is found. Thus, the areas of deficiency, toxicity, and optimum physiological response can be changed significantly by considering a combination of these variables and utilizing a suitable ligand system that can easily be manipulated to tune the delivery of the metal ion into the biological system.

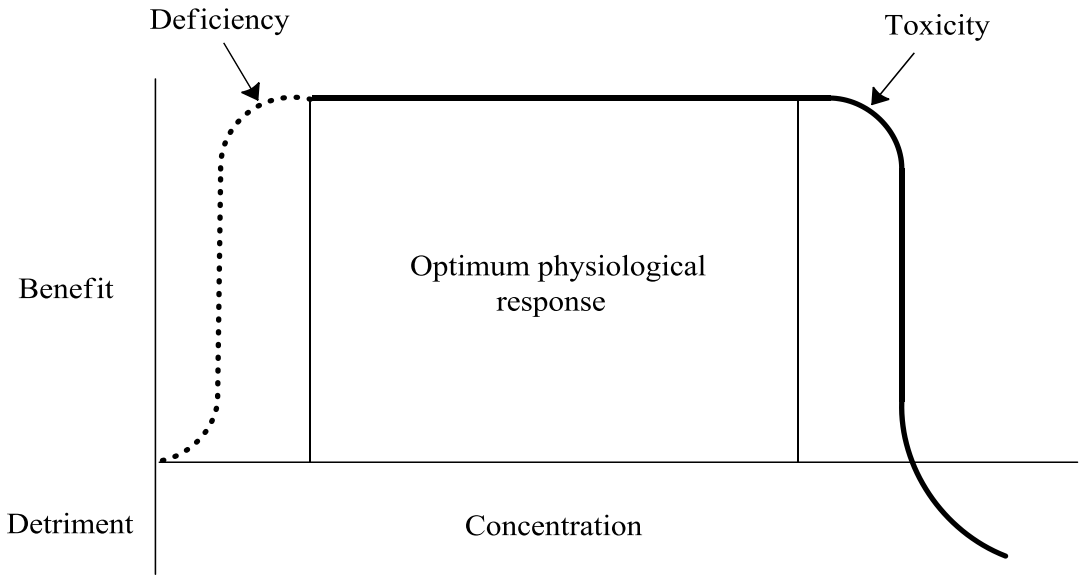

Figure 1.1: Bertrand diagram showing the relationship between benefit/detriment and concentration of an element.[4]

A large number of metallic elements play an important role in living systems. Metals are suited in medicinal applications because of their ability to loose electrons relatively easy from their familiar elemental or metallic state to form positively charged ions that are soluble in biological fluids. The cationic form of metals play a vital role in biology since it is electron poor, whereas most biological molecules such as proteins and DNA are electron rich. The

[4] G. Bertrand, *8th Int. Conf. Appl. Chem.*, 1912, 28, 30.

attraction of these opposing charges causes metal ions to bind and interact with biological molecules. This principle explains the affinity of metal ions for many small molecules and ions crucial to life, such as O_2.[5]

Metals perform a wide variety of tasks in the human body. Calcium forms a major part of the bone structure. Electrical transmission within the brain and heart, as well as muscle contraction in both skeletal and smooth muscles is made possible by the presence of Ca^{2+} ions. Haemoglobin, an iron-containing protein, transports oxygen throughout the body tissues. Zinc ions provide the structural framework for the zinc fingers that regulate the function of genes in the nuclei of cells. Furthermore, it is a component of insulin, a substance that is used to regulate sugar metabolism.

The role of metals in medicinal chemistry has been practiced since ancient times.[6,7] In the year, 3000 BC, the Egyptians used copper to sterilize water. In Egypt, various iron remedies were used about 1500 BC, around the same time that zinc was discovered to promote the healing of wounds. Mercurous chloride was used as a diuretic during the Renaissance era in Europe and the nutritional value of iron was discovered around the same era. During the early 20^{th} century, the freshness of milk was prolonged by placing silver coins in milk bottles. But, the rational development of inorganic compounds in medicinal use, started with the discovery of $K[Au(CN)_2]$, in the early 1900s, which was used for the treatment of tuberculosis.[5]

1.4 Radiopharmaceuticals

Radiopharmaceuticals are radionuclide containing drugs widely used in nuclear medicine and can be divided into two primary classes, namely diagnostic and therapeutic. Diagnostic radiopharmaceuticals are labeled with photon emitting (γ or β^+) radionuclides, whereas therapeutic radiopharmaceuticals are labeled with particle (α, β or Auger electron emission) radionuclides. ^{99m}Tc is the most successful radionuclide used in nearly 80 % of all diagnostic scans currently performed in clinical nuclear medicine applications, because of its attractive nuclear properties.[8] A number of other radionuclides with nuclear properties suitable for

[5] C. Orvig, M. J. Abrams, *Chem. Rev*., 1999, 99**,** 2202.
[6] H. E. Howard-Lock, C. J. L. Lock, *Comprehensive Coordination Chemistry*, Eds.: G. Wilkinson, R. D. Gillard, J. A. McCleverty, Pergamon, Oxford, 1987.
[7] P. J. Sadler, *Adv. Inorg. Chem*., 1991, 36, 1.
[8] S. Liu, D.S. Edwards, *Chem. Rev.*, 1999, 99, 2235.

nuclear medical applications will be discussed in chapter 2, with special attention given to ^{99m}Tc and $^{186/188}$Re.

1.5 Aim of this Study

Rhenium and technetium tricarbonyl complexes received little attention from nuclear medical applications because of their unfeasible synthetic procedures. The novel, mild reaction conditions described by Alberto *et al*.[9,10,11,12] for the synthesis of *fac*-$[M(CO)_3(H_2O)_3]^+$ (M = $^{186/188}$Re, ^{99m}Tc) precursor opened new possibilities for future development of metal based radiopharmaceutical agents bearing the *fac*-$[M(CO)_3]^+$ core. Tricarbonyl aqua complexes of rhenium and technetium are suited in nuclear medical application because of their stable *fac*-$[M(CO)_3]^+$ core in water and the relatively labile water molecules that can be substituted by a wide variety of mono-, bi-, tridentate ligands and a combination thereof. The *fac*-$[M(CO)_3]^+$ core possesses a d^6 electronic configuration in an octahedral field. Complexes which adopt this configuration are generally known to be kinetically inert.

Characterization of a newly synthesized radiopharmaceutical drug by chemical kinetics is vital since useful information relating to its stability *in vivo*, biodistribution and the rate of clearance from the body can be gathered.[13] Substitution kinetics investigates the reactivity of the synthesized complex, whereas formation kinetics deals with studying the factors that govern complex formation, specifically the time it takes for a complex to form at a given metal and ligand concentration. The latter was investigated in this study. The study of formation kinetics is important when designing radiopharmaceutical drugs for routine clinical applications because a few stringent limitations must be considered: The preparation must be a one-step mechanism yielding a product with a high purity (preferably > 98 % yield). The biomolecule concentration should be 1:1 with respect to the radionuclide and practical time restrictions should be designed to meet the half-life of the radionuclide. Thus, the time it takes for the preparation, i.e. for the ligand to coordinate to the *fac*-$[M(CO)_3]^+$ (M = $^{186/188}$Re,

[9] R. Waibel, R. Alberto, J. Willuda, R. Finnern, R. Schibli, A. Stichelberger, A. Egli, U. Abram, J. P. Mach, A. Plueckthun, P. A. Schubiger, *Nature Biotechnol*., 1999, 17, 897.
[10] R. Alberto, R. Schibli, U. Abram, B. Johannsen, H. J. Pietzsch, P. A. Schubiger, *J. Am. Chem. Soc*., 1999, 121, 6076.
[11] R. Schibli, K. V. Katti, C. Higginbotham, W. A. Volkert, R. Alberto, *Nucl. Med. Biol*., 1999, 26, 711.
[12] A. Egli, R. Alberto, L. Tannahill, R. Schibli, U. Abram, A. Schaffland, R. Waibel, D. Tourwe, L. Jeannin, K. Iterbeke, P. A. Schubiger, *J. Nucl. Med*., 1999, 40, 1913.
[13] C. Capellos, B. H. J. Bielski, *Kinetic Systems*, Wiley-Interscience, New York, 1972.

^{99m}Tc) core, is vital when designing metal based radiopharmaceutical drugs and it should be well below the half-life of the radionuclide of choice, which is about 60 minutes for ^{99m}Tc.

This study focused on investigating the coordinative ability of Schiff-base ligands to the *fac*-$[Re(CO)_3]^+$ core and exploring the formation kinetics with ethylene amine ligands. Schiff-bases are one of the most widely used ligand system because they form stable complexes with most transitional metals. In nuclear medical applications, the manipulative capabilities of Schiff-base ligands make them suitable to tune the delivery of the metal ion into the biological system. Furthermore, Schiff-bases also make it possible to design ligands with varying steric and electronic character, leading to novel radiopharmaceutical drugs. The advantage of using bidentate ligands with the *fac*-$[Re(CO)_3]^+$ core is that the sixth position on the metal center is left "opened" and can be occupied by a different monodentate ligand leading to the [2+1] mixed ligand approach suggested by Mundwiler *et al.*[14] The main objectives of this M.Sc. study are summarized as follows:

1. Synthesize Schiff-base ligands with varying steric and electronic properties afforded by the substituent bonded to the nitrogen imine donor atom.
2. Coordinate the ligands onto the *fac*-$[Re(CO)_3]^+$ core to form complexes of the type *fac* [Re(L,L'-Bid)$(CO)_3$(MeOH)] (L,L'-Bid = *N,O* Sal bidentate ligand)
3. To characterize and confirm the formation of complexes with X-ray diffraction and different spectroscopic techniques such as IR, UV-Vis and NMR.
4. Exploring preliminary formation kinetics for the reactions between *fac*-$[Re(CO)_3]^+$ core and *N,O* as well as *N,N'* bidentate ligand systems.

Chapter 2 discusses some of the rhenium and technetium compounds found in literature that have contributed to the development of radiopharmaceutical drugs over the years.

[14] S. Mundwiler, M. Kündig, K. Ortner, R. Alberto, *Dalton Trans*., 2004, 1320.

2 Literature Study

2.1 Discovery of Rhenium and Technetium

Rhenium was first discovered in 1925 by German chemists, W. Noddack, I. Tacke-Noddack and O. Berg.[1] It was detected by its X-ray spectrum in platinum ores and columbite minerals. In 1928, the discoverers managed to extract 1 g of rhenium from 660 kg of molybdenite ores, which was the highest that could be extracted at the time. Rhenium is usually left in solution as the perrhenate ion, $[ReO_4]^-$, which can be precipitated as the slightly soluble $KReO_4$ salt by addition of KCl. It is situated in the third row of transition metals in the periodic table and is the lowest element in the manganese triad which consist of Mn, Tc and Re. Rhenium is the highest known element with two stable isotopes, ^{185}Re (37.4 %) and ^{187}Re (62.6 %).[2] The radioactive isotopes involved in nuclear medicine are ^{186}Re and ^{188}Re.

Technetium, an artificially made element, was discovered in 1937 by C. Perrier and E. Segre by irradiating a molybdenum foil with deuterons and was obtained as ^{95}Tc and ^{97}Tc isotopes.[3] It only became available in large amounts after the discovery of uranium fission with thermal neutrons. The most stable isotopes are ^{98}Tc ($t_{1/2}$ = 4.2 x 10^6 yr), ^{97}Tc ($t_{1/2}$ = 2.6 x 10^6 yr) and ^{99}Tc ($t_{1/2}$ = 2.11 x 10^5 yr). ^{99m}Tc is the only radioactive isotope utilized in nuclear medicine and its use in this field was introduced in the early 1960's after the development of the ^{99}Mo/^{99m}Tc generator by Brookhaven National Laboratory in 1959.[4,5] Studies into coordination chemistry began with research in ^{99m}Tc radiopharmaceuticals as it relates to diagnostic imaging. There is practically no use for ^{98}Tc and the fact that it is the longest lived isotope, poses a major problem in nuclear waste deposition.

[1] I. Noddack, W. Z. Noddack, *Phys. Chem*., 1927, 125, 264.
[2] M. Gielen, E. Tiekink, *Metallotherapeutic Drugs and Metal-based Diagnostic Agents: The Use of Metals in Medicine*, John Wiley & Sons Ltd, Chichester, England, 2005.
[3] J. P. Icenhower, N. P. Qafoku, J. M. Zachara, W. J. Martin, *Am. J. Sci*., 2010, 310, 721.
[4] P. Richards, W. D. Tucker, S. C. Srivastava, *Int. J. Appl. Radiat. Isot*., 1982, 33, 793.
[5] W. D. Tucker, M. W. Greene, A. J. Weiss, A. P. Murenhoff, *Trans. Am. Nucl. Soc*., 1958, 1, 160.

2.2 Radiopharmaceuticals

Radiopharmaceuticals are radiolabeled compounds widely used in nuclear medicine for diagnosis of various diseases or to deliver therapeutic doses of ionizing radiation to specific disease sites.[6] They are usually small inorganic or organic compounds with a well-known composition. Radiopharmaceuticals can be divided into two primary classes: diagnostic and therapeutic.

2.2.1 Diagnostic Radionuclides

Diagnostic radiopharmaceuticals are labeled with a γ-emitting radionuclide for single-photon emission computed tomography (SPECT) or a β^+-emitting radionuclide for positron emission tomography (PET). Table 2.1 and 2.2 shows some of the radionuclides used in labeling diagnostic radiopharmaceuticals for SPECT and PET scintigraphy respectively. An ideal imaging agent utilizes a radionuclide which emits radiation that can be readily detected as it leaves the body but has little effect on the surrounding tissues. The most commonly used radionuclide is ^{99m}Tc and is used in over 85 % of all diagnostic scans currently performed in clinical nuclear medicine applications.

Table 2.1: Radionuclides utilized in labeling diagnostic radiopharmaceuticals for SPECT.[6,7]

Isotope	$t_{1/2}$ (h)	Production	Decay Mode	E_γ (keV)
SPECT IMAGING				
^{67}Ga	78.3	Cyclotron, ^{68}Zn(p, 2n)-^{67}Ga	EC (100%)	93(10%), 185(24%, 296(22%)
^{99m}Tc	6	^{99}Mo-^{99m}Tc Generator	IT (100%)	141(89%)
^{111}In	67.9	Cyclotron, ^{111}Cd(p, n)-^{111}In	EC (100%)	171(88%), 247(94%)

m = metastable isotope, EC = electron capture, IT = isomeric transition.

[6] S. Liu, D.S. Edwards, *Chem. Rev.*, 1999, 99, 2235.
[7] E. Brown, J. Dairiki, R. E. Doebler, A. A. Shibab-Elden, L. J. Jardine, J. K. Tuli, A. B. Byurn, *Table of Isotopes*, 7th Ed., Eds.: C. M. Lederer, V. S. Shirley, John Wiley & Sons, New York, 1978.

Table 2.2: Radionuclides utilized in labeling diagnostic radiopharmaceuticals for PET.[8,9,10,11,12]

Isotope	$t_{1/2}$ (h)	Production	Decay mode	$E_{\beta+}$ (keV)
PET IMAGING				
^{60}Cu	0.4	Cyclotron, ^{60}Ni(p, n)-^{60}Co	EC (7%)	3920, 3000, 2000
^{61}Cu	3.3	Cyclotron, ^{61}Ni(p, n)-^{61}Cu	EC (38%)	1220, 1150, 940, 560
^{62}Cu	0.16	^{62}Zn-^{62}Cu Generator	EC (2%)	2910
^{64}Cu	12.7	Cyclotron, ^{64}Ni(p, n)-^{64}Cu	EC (41%)	656
^{66}Ga	9.5	Cyclotron, ^{63}Cu(α, nγ)-^{66}Ga	EC (44%)	4150, 935
^{68}Ga	1.1	^{68}Ge- ^{68}Ga Generator	EC (10%)	1880, 770
^{86}Y	14.7	Cyclotron, ^{111}Cd(p, n)-^{111}In	EC (66%)	2335, 2019, 1603, 1248, 1043

EC = electron capture.

2.2.2 Therapeutic Radionuclides

Therapeutic radiopharmaceuticals are designed to deliver therapeutic doses of ionizing or sterilizing radiation to specific diseased sites with high specificity. An ideal therapeutic radiopharmaceutical should localize at the disease site whilst clearing rapidly from the blood stream and normal tissues to prevent excessive damage to healthy organs. Table 2.3 shows some of the radionuclides utilized in labeling therapeutic radiopharmaceuticals. Therapeutic drugs are

[8] D. W. McCarthy, R. E. Shefer, R. E. Klinkowstein, L. A. Bass, W. H. Margeneau, C. S. Cutler, C. J. Anderson, M. J. Welch, *Nucl. Med. Biol*., 1997, 24, 35.
[9] P. J. Blower, J. S. Lewis, J. Zweit, *Nucl. Med. Biol*., 1996, 23, 957.
[10] M. R. Zaman, S. M. Qaim, *Radiochim. Acta*, 1996, 75, 59.
[11] L. A. Bass, D. W. McCarthy, L. A. Jones, P. D. Cutler, R. E. Shefer, R. E. Klinkowstein, S. W. Schwarz, C. S. Cutler, J. S. Lewis, C. J. Anderson, M. J. Welch, *J. Labeled Compd. Radiopharm*., 1997, 40, 325.
[12] C. Loc'h, B. Mazièré, D. J. Comar, *Nucl. Med*., 1979, 21, 171.

normally labeled with particle emitting (α, β or Auger electron emission) radionuclides since they are suitable for delivering localized cytotoxic doses of ionizing radiation.[13,14,15,16] If the radionuclide also emits γ-photons, they can be used to simultaneously image the distribution of the therapeutic radiopharmaceutical at the diseased site. Such emissions should however be of low abundance to limit the radiation dose to non-target tissues.[17]

Table 2.3: Selected radionuclides utilized in labeling therapeutic radiopharmaceuticals.[16]

Isotope	$t_{1/2}$ (days)	Max range in tissue (mm)	Max E_β (MeV)	E_γ (MeV)
$^{67}Cu^a$	2.6	1.8	0.57	0.184 (48 %)
$^{89}Sr^b$	50.5	8	1.46	
$^{90}Y^c$	2.7	12	2.27	
$^{131}I^b$	8	4	0.81	0.364 (81%)
$^{153}Sm^b$	1.9	3.1	0.8	0.103 (29 %)
$^{166}Ho^b$	1.1	8	1.6	0.81 (6.33)
$^{177}Lu^b$	6.7	1.5	0.50	0.113 (6.4 %)
$^{186}Re^b$	3.8	5	1.07	0.137 (9 %)
$^{188}Re^c$	0.7	11	2.12	0.155 (15 %)

[a] ^{67}Cu is produced in a charged particle accelerator. [b] Radionuclides produced in nuclear reactors. [c] Radionuclides produced in generator systems.

2.2.3 Ideal Radionuclide Properties

The selection of an appropriate radionuclide is vital in designing any radiopharmaceutical drug. Important factors that should be considered include the half-life of the radionuclide, decay mode, cost and availability. An ideal radiopharmaceutical drug should be labeled with a radionuclide whose half-life is long enough to provide sufficient time for the drug to be synthesized,

[13] P. A. Schubiger, R. Alberto, A. Smith, *Bioconjugate Chem*., 1996, 7, 165.
[14] T. E. Wheldon, J. A. O'Donoghue, *Int. J. Radiat. Biol.*, 1990, 58, 1.
[15] V. K. Langmuir, R. M. Sutherland, *Antibody Immunoconjugates Radiopharm.*, 1988, 1, 195.
[16] R. W. Howell, M. T. Azure, V. R. Narra, D. V. Rao, *Radiat. Res.*, 1994, 137, 352.
[17] W. A. Volkert, T. J. Hoffman, *Chem. Rev*., 1999, 99, 2269.

administered and to accumulate at the specific diseased site while having fast clearance from the blood stream and normal tissues to limit the radiation dose to the patient.

The cost and availability of the radionuclide are two other important factors that should be considered. For example, ^{99m}Tc is produced from the commercially available ^{99}Mo/ ^{99m}Tc generator at low cost. Radionuclide generators consist of a parent radionuclide with a longer half-life that decays into a daughter radionuclide with a shorter half-life. Separation of the daughter from the parent radionuclide is done by ion exchange chromatography or solvent extraction. Other radionuclides are produced in charged particle accelerators and cyclotrons.

2.3 Designing of Radiopharmaceutical

Coordination chemistry plays an important role in designing and developing new metal based radiopharmaceuticals. Three general techniques (integrated, bifunctional and peptide-hybrid approach) are used to design radiopharmaceutical agents and are illustrated in Figure 2.1. Inorganic chemistry forms the basis of the labeling of the radiopharmaceutical in all three approaches. In the drug, the radionuclide is the source of radiation for diagnosis or therapy.

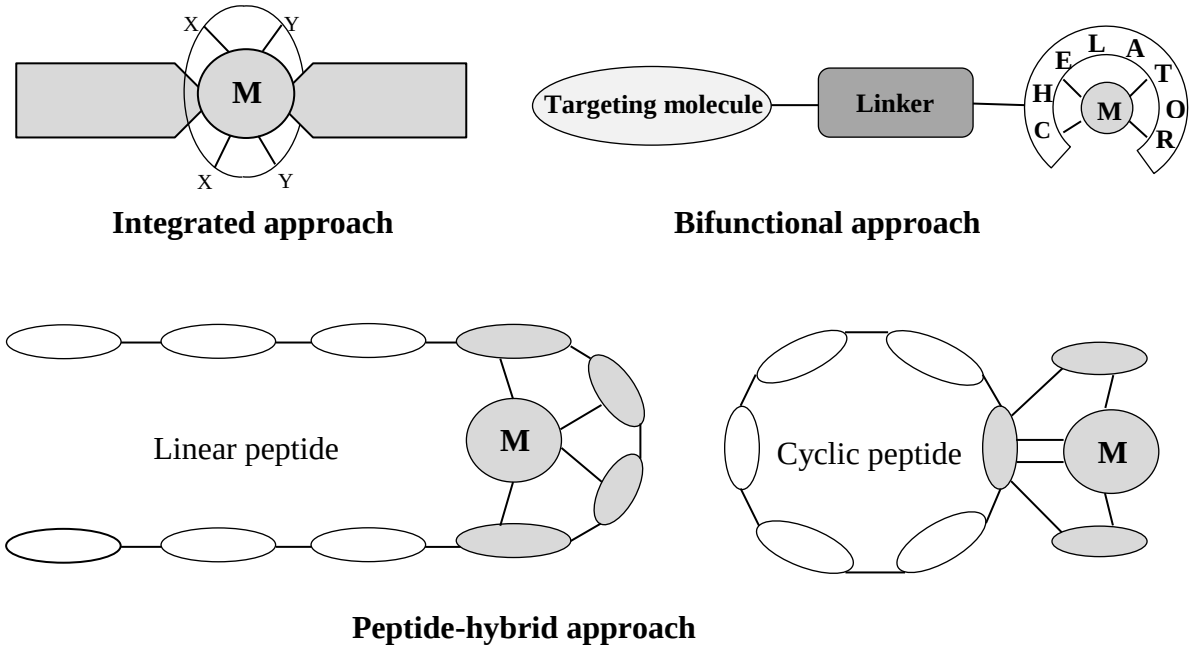

Figure 2.1: Three approaches used in designing radiopharmaceutical drugs.[18]

[18] S. Liu, *Chem. Soc. Rev*., 2004, 33, 445.

2.3.1 Integrated Approach

The integrated approach involves replacing a part of a known high affinity receptor ligand with a metal chelate in such a way that causes minimal changes in size, conformation and receptor binding affinity. The radionuclide plays an important part of the receptor binding molecule. In metal chelation, all the parts are arranged in such a way that makes the entire complex to become a high affinity receptor ligand. This approach however consists of challenging synthetic methods that produce target molecules with relatively low receptor binding affinity.[19]

2.3.2 Bifunctional Approach

This approach utilizes a high affinity receptor ligand as the targeting biomolecule, a bifunctional chelator (BFC) for conjugation of the receptor ligand and chelation of the radionuclide (^{99m}Tc, ^{186}Re, and ^{188}Re) as well as a linker for pharmacokinetic modification. The biomolecule used can be monoclonal antibodies, small peptides or non-peptide receptor ligands while the choice of the bifunctional chelator depend to a large extend on the nature and oxidation state of the radionuclide. The radionuclide chelate is usually kept away from the receptor binding molecule to minimize possible interference with receptor binding by the radionuclide chelate. A number of target-specific radiopharmaceuticals (*e.g.* OctreoScan® and NeoTect®) have been developed using this approach and its advantage is that the receptor binding affinity can be retained by a careful selection of the BFC for radiolabeling.

In the [2+1] mixed ligand approach suggested by Mundwiler *et al.*[20] for *fac*-$[M(CO)_3(H_2O)_3]^+$ (M = Re, $^{99/99m}$Tc), the three labile water molecules are substituted with a bidentate and a monodentate ligand. The biomolecule can be attached to either the bidentate, leading to the $[2_B+1]$ concept or the monodentate ligand ($[2+1_B]$ concept) as shown in Figure 2.2. The [2+1] mixed ligand approach makes it possible to synthesize *fac*-$[M(CO)_3]^+$ complexes in water which potentially have high kinetic stability.

[19] R. K. Hom, J. A. Katzenellenbogen, *Nucl. Med. Biol*., 1997, 24, 485.
[20] S. Mundwiler, M. Kündig, K. Ortner, R. Alberto, *Dalton Trans*., 2004, 1320.

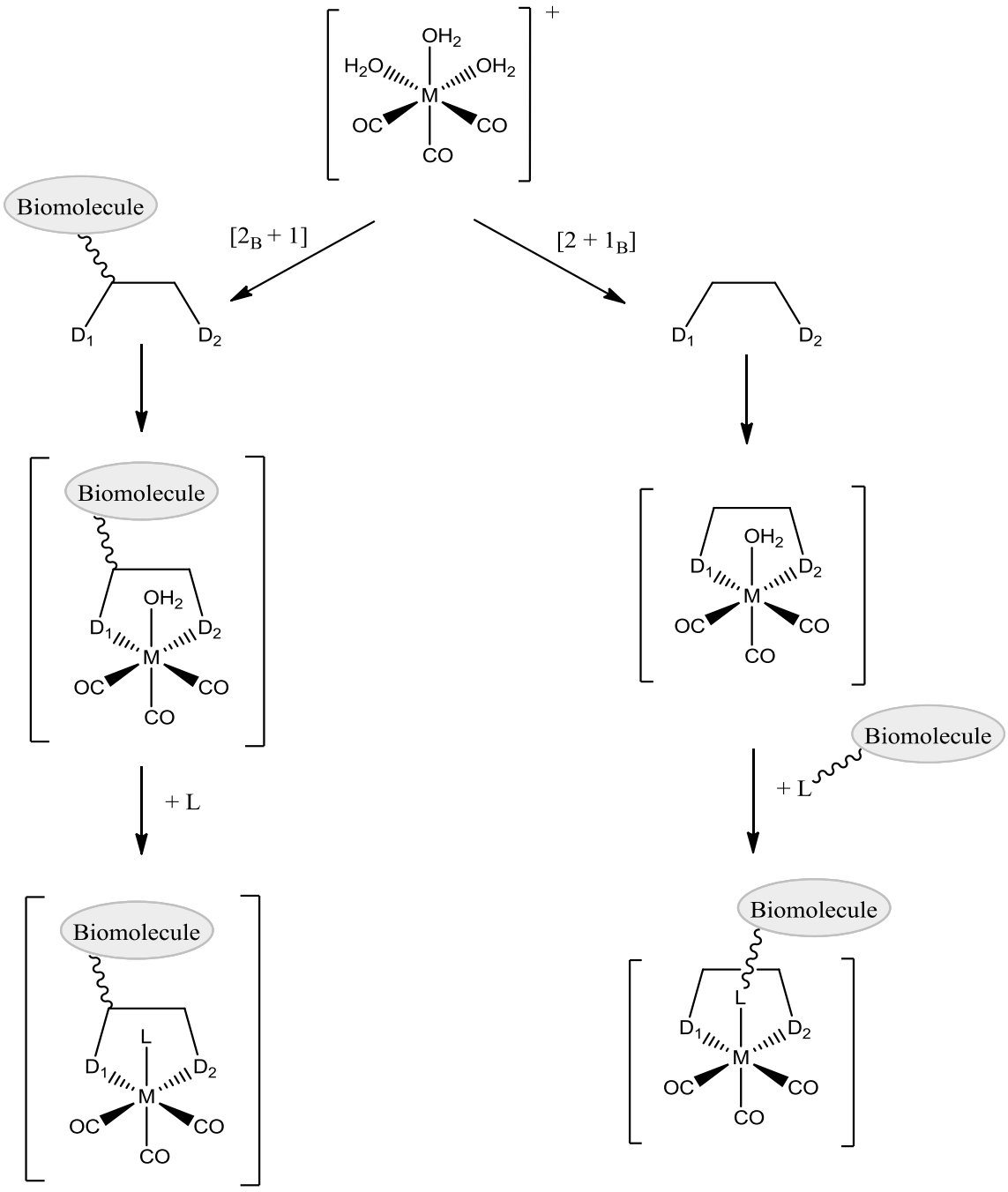

Figure 2.2: Illustration of the [2+1] mixed ligand approach for *fac*-$[M(CO)_3]^+$ complexes (D_1, D_2 = different donor atoms; L = entering monodentate ligand).[20]

2.3.3 Peptide-Hybrid Approach

The radionuclide in peptide-hybrid approach is chelated by a tripeptide sequence containing N_4, N_3S or N_2S_2 donor atoms set. The tripeptide sequence can be part of a linear polypeptide or a cyclic peptide backbone. It is also possible to incorporate the radionuclide as part of a macrocyclic peptide framework. The free linear peptide has a low binding affinity for the intended receptor. A major advantage of this approach is that bonding of the radionuclide induces macrocyclic metallopeptide which increases the receptor binding affinity of the polypeptide.

2.4 Technetium Isotopes Involved in Nuclear Medicine

^{99}Tc is produced from a parent radionuclide, ^{99}Mo, a fission product of ^{235}U with a 66 h half-life, *via* the metastable, ^{99m}Tc, as shown in Figure 2.3. Metastable radionuclides are formed, for example, when β^- -decay results in an excited state of the daughter radionuclide. Since the transition from the excited to the ground state occurs mainly by γ-emission (140 keV), the dose burden to the patient is low since it is free of particulate emission. ^{99m}Tc became widely used in nuclear medicine following the development of a ^{99}Mo/^{99m}Tc generator. In this generator, ^{99}Mo radionuclide is in the form of molybdate ion, $[^{99}MoO_4]^{2-}$. Molybdate is strongly absorbed on an Al_2O_3 column. The decay of $[^{99}MoO_4]^{2-}$ leads to $[^{99m}TcO_4]^-$ which is weakly bound to the alumina column due to the lower negative charge and is eluted by saline solution. The eluted ^{99m}Tc radiopharmaceuticals are usually utilized at dilute concentrations (10^{-8} - 10^{-6} M) and do not possess any pharmacological effect.[18] However, one of the difficulties encountered when synthesizing this kind of radiopharmaceuticals is that the low concentration of $[^{99m}TcO_4]^-$ complexes in solution can only be characterized by HPLC or other chromatographic methods with gamma detection in order to follow the chemistry, since it is almost impossible to characterize these complexes with analytical or spectroscopic methods. The majority of diagnostic radiopharmaceuticals available for treatment in clinical nuclear medicine today use ^{99m}Tc radionuclide because of its attractive nuclear properties. The 6 h half-life is sufficiently long for the drug to be synthesized, administered, collect useful images and yet short enough to limit the radiation dose to the patient. The monochromatic 140 keV photons emitted by the radionuclide are readily collimated to give images of high spatial resolution.

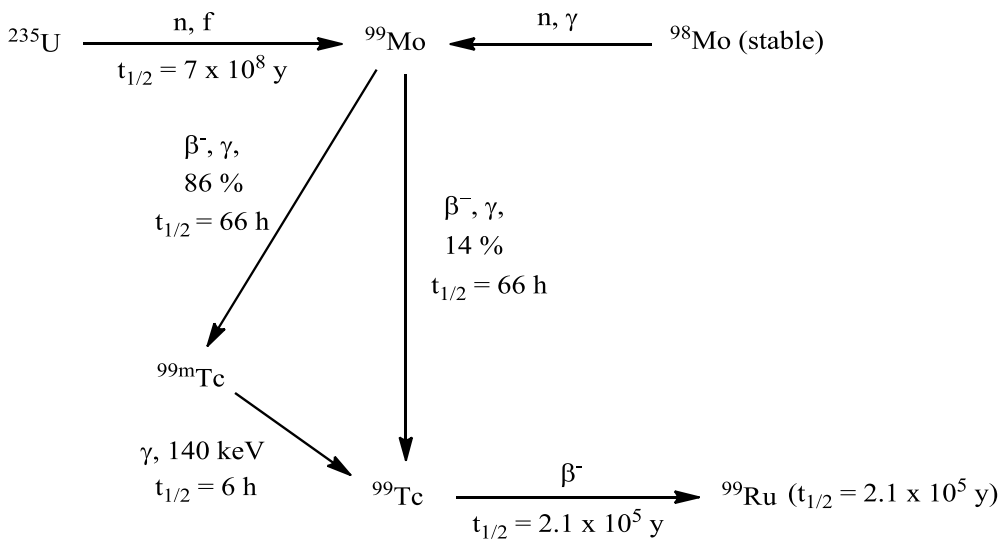

Figure 2.3: ^{99}Mo decay sequence to produce $^{99/99m}$Tc.[21]

2.4.1 First Generation Agents

^{99m}Tc imaging began in 1961 when [^{99m}TcO$_4$]$^-$ was used to image the thyroid gland. This was possible because [^{99m}TcO$_4$]$^-$ accumulates in the thyroid as it mimics the iodide contained in this gland. This was the first of the so called technetium essential agents where the biodistribution was dependent on the physical properties of the complex such as the charge, lipophilicity and size.[22] The pertechnetate ion is also considered to be the first generation of ^{99m}Tc radiopharmaceuticals complexes.[23,24] Many more ^{99m}Tc complexes were then subsequently designed to image various organs such as the liver (^{99m}Tc-EHIDA), kidneys (Technescan®), heart (Cardiolite®), brain (Ceretec®) or bone (^{99m}Tc-MDP) and are described in details hereafter. They represent perfusion (blood-flow) agents that follow a particular biological pathway or targets specific organs.

2.4.1.1 Kidney and Liver Imaging

This field of ^{99m}Tc imaging radiopharmaceuticals has been extensively investigated over the years and the complexone ligand system were the first ligands used. Complexone ligands are

[21] U. Abram, R. Alberto, *J. Braz. Chem. Soc.*, 2006, 17, 1486.
[22] J. R. Dilworth, S. J. Parrott, *Chem. Rev*., 1998, 27, 43.
[23] D. Jain, *Semin. Nucl. Med*., 1999, 29, 221.
[24] S. Banerjee, M. R. A. Pillai, N. Ramamoorthy, *Semin. Nucl. Med*., 2001, 21, 260.

aminoacetic acid derivatives (see Figure 2.4) and they form negatively charged complexes with technetium. Complexes of the type ^{99m}Tc-DTPA and ^{99m}Tc-DMSA (DTPA = diethylenetriamine pentaacetic acid; DMSA = dimercaptosuccinic acid) have been used for kidney imaging, but the well-known and most widely utilized complex in renal clearing studies is [^{99m}TcO(MAG3)]$^-$ (MAG3 = mercaptoacytyltriglycine) or Technescan®.[25,26] This anionic agent was designed by Fritzberg[27] and contains a free carboxylic acid which is vital for excretion by the kidney. Upon coordination with technetium, this tetradentate ligand loses four protons and forms a mono-anionic, square pyramidal ^{99m}Tc(V) complex with an apical oxo group.

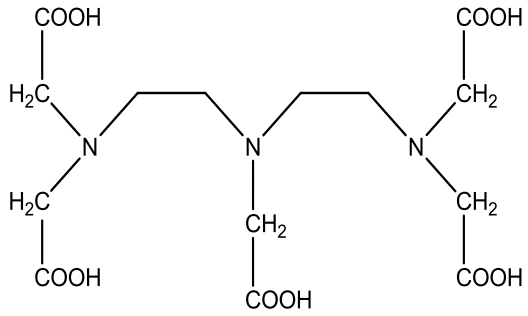

DTPA

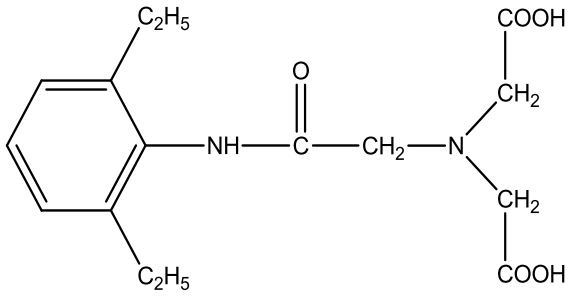

EHIDA

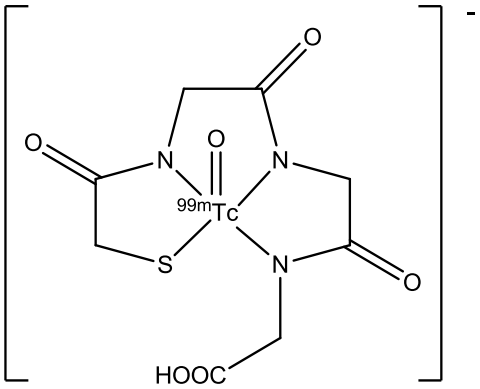

Technescan®

Figure 2.4: Selected complexone-type ligands and ^{99m}Tc complex used for kidney imaging.

[25] D. Eshima, T. J. Andrew, A. R. Fritzberg, S. Kasina, L. Hansen, J. F. Sorenson, *J. Nucl. Med*., 1987, 28, 1180.
[26] D. Eshima, A. R. Fritzberg, A. Taylor, *Semin. Nucl. Med*., 1990, 20, 28.
[27] A. R. Fritzberg, S. Kasina, D. Eshima, D. L. Johnson, *J. Nucl. Med.*, 1986, 27, 111.

^{99m}Tc-EHIDA (EHIDA = N-(2, 6-diethylacetanilido) iminodiacetic acid) have been shown to be suitable for liver imaging. Modification of the periphery of this type of ligand system helps with the excretion of the complex from the body after treatment. Similarly to [^{99m}TcO(MAG3)]$^{-}$, the highly hydrophilic nature of ^{99m}Tc-DTPA complex forces it to be excreted through the renal system while the more lipophilic ^{99m}Tc-EHIDA complex is excreted through the hepatobiliary tract.

2.4.1.2 Cardiac Imaging

Originally, heart imaging was dominated by the radioactive ^{201}Tl isotope since it is taken up into the myocytes by the Na^{+}/K^{+} ATPase pump and showed myocardial blood flow clearly. However, this radioactive isotope is expensive, has unfavourable physicochemical properties and is not readily available.[22,28,29] This led to more research whereby ^{201}Tl was replaced with ^{99m}Tc. Monocationic complexes of the type [$^{99m}TcCl_2(diars)_2]^{+}$ (diars = 1, 2-bis(dimethylarsino) benzene) and [$^{99m}TcCl_2(DMPE)_2]^{+}$ (DMPE = 1, 2-bis(dimethylphosphino)-ethane) were the first agents to show good myocardial uptake. But, these complexes showed good myocardial uptake in animals and not humans. Their retention in the human heart was also low, which can be explained by the quick reduction of redox-labile compounds in the myocardial cells.[30]

Further attempts whereby monodentate isonitrile ligands were coordinated to the ^{99m}Tc(I) centre led to the formation of stable complexes that were soluble in water.[31] This was facilitated by the kinetically inert nature of [$^{99m}Tc(L)_6]^{+}$ complexes. The low spin d^6 electronic state is stable towards dissociative ligand loss or associative substitution by other ligands in biological systems. Complexes of this type are prepared from $^{99m}TcO_4^{-}$ using $S_2O_4^{2-}$ ions as a reductant in the presence of the desired isocyanide ligand. Many complexes with different substituents on the isocyanide ligand have been prepared on a microscopic level and structurally elucidated.

[28] B. E. Backus, F. A. Verburg, R. L. Romijn, M. W. Konijnenberg, F. J. Beekman, J. F. Verzijlbergen, *J. Nucl. Cardiol*., 2009, 16, 97.
[29] T. Dey, H. Wieczorek, R. Bippus, B. E. Backus, R. L. Romijn, J. F. Verzijlbergen, T. Aach, *Eur. Heart J. Suppl*., 2011, 13, A106.
[30] E. Deutsch, K. A. Glavan, V. J. Sodd, H. Nishiyama, D. L. Ferguson, S. J. Lukes, *J. Nucl. Med.*, 1981, 22, 897.
[31] M. J. Abrams, A. Davison, A. G. Jones, C. E. Costello, H. Pang, *Inorg. Chem.*, 1983, 22, 2798.

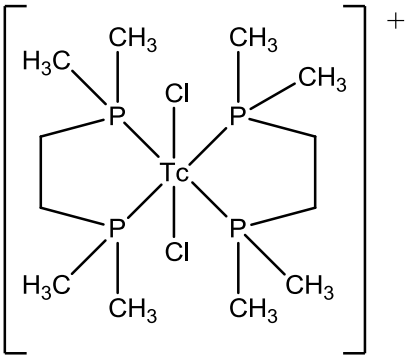

$[^{99m}TcCl_2(DMPE)_2]^+$

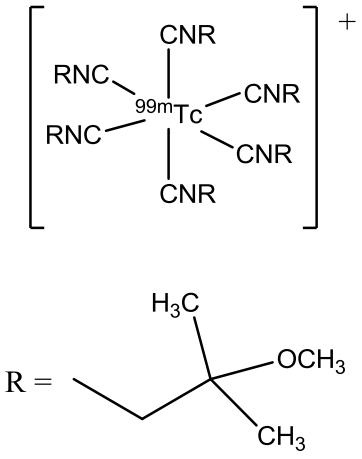

Cardiolite®

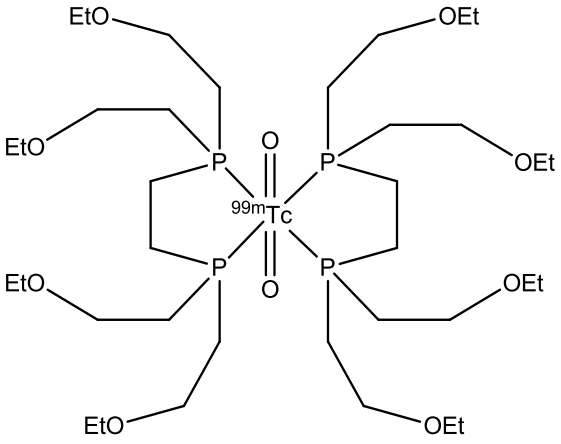

Myoview®

Figure 2.5: Selected ^{99m}Tc complexes used for cardiac imaging.

The real breakthrough in heart imaging came about with the discovery of an organometallic $^{99m}Tc(I)$ complex which uses MIBI (methoxyisobutylisocyanide) as a ligand and is commonly known as Cardiolite®.[32,33] $[^{99m}Tc(MIBI)_6]^+$ is prepared in a routine radiopharmaceutical way from $^{99m}TcO_4^-$ in saline using $SnCl_2$ as a reductant. The MIBI ligand is provided by the cationic $[Cu(MIBI)_4]^+$ complex. Although monocationic, this agent is not taken up into the heart by the Na^+/K^+ ATPase mechanism, but by the diffusion of cations across the membranes. Cardiolite® clears very quickly from the blood stream and accumulates in the heart, which allows for good

[32] E. Meggers, *Curr. Opin. Chem. Biol*., 2007, 11, 287.

[33] A. G. Jones, M. J. Abrams, A. Davison, J. W. Brodack, A. K. Toothaker, S. J. Adelstein, A. I. Kassis, *Int. J. Nucl. Med. Biol*., 1984, 11, 225.

imaging of the heart with excellent organ-to-background ratio.[34] This complex has also shown uptake in various tumors.[35,36]

Following the same routine which led to the development of $[^{99m}Tc(MIBI)_6]^+$, numerous other monocationic complexes with peripheral ether functionalities were designed for heart imaging. These complexes made use of ligands such as dioximes, phosphines and Schiff-bases with different technetium oxidation states, ^{99m}Tc(III) and ^{99m}Tc(V). Myoview®,[37] an octahedral dioxo ^{99m}Tc(V) complex with eight alkoxy groups on the two bidentate phosphine ligand is one complex of commercial interest that was developed from this routine. The structure of this complex is derived from that of $[^{99m}TcCl_2(DMPE)_2]^+$ complex, but it is more difficult to reduce since it is a ^{99m}Tc(V) species. Cardiolite® and Myoview® are two agents which are extensively used today in cardiac imaging, substituting ^{201}Tl.

2.4.1.3 Brain Imaging

A few stringent requirements must be met by a radiopharmaceutical if successful targeting of neuroreceptors is to be achieved. The overall charge of the complex should be neutral making it possible for the agent to cross the blood brain barrier by diffusion and accumulate in the brain. The complex should be small, lipophilic and must have high selectivity and specificity for the particular receptor.[38] A number of neutral amine-oxime complexes were developed in the 1980's by the University of Missouri. These complexes were later modified by Amersham International which led to the commercially available Ceretec®.[39]

The ligand used in Ceretec® is hexamethylpropyleneamineoxime[40,41] (HMPAO) which loses three protons upon coordination with technetium to form a neutral, square pyramidal ^{99m}Tc(V)

[34] K. A. Narahara, J. Villanuevameyer, C. J. Thompson, M. Brizendine, I. Mena, *Am. J. Cardiol*., 1990, 66, 1438.
[35] E. Barbarics, J. F. Kronauge, A. Davison, A. G. Jones, *Nucl.Med. Biol.*, 1998, 25, 667.
[36] D. Piwnica-Worms, B. L. Holman, *J. Nucl. Med.*, 1990, 31, 1166.
[37] E. Deutsch, K. Libson, *Prog. Inorg. Chem.*, 1983, 30, 75.
[38] D. D. Dishino, M. J. Welch, M. R. Kilbourne, M. E. Raichle, *J. Nucl. Med.*, 1983, 24, 1030.
[39] J. P. Leonard, D. P. Novotnik, R. D. Neirinckx, *J. Nucl. Med.*, 1986, 27, 1819.
[40] T. J. Hoffman, R. M. Seger, E. H. Mckenzie, W. A. Volkert, R. A. Holmes, R. P. Pettit, L. Canning, S. A. Cumming, G. Nechvatal, *J. Nucl. Med*., 1985, 26, 129.
[41] D. P. Nowotnik, L. R. Canning, A. Cumming, R. C. Harrison, B. Higley, G. Nechvatal, R. D. Pickett, I. M. Piper, V. J. Bayne, A. M. Forster, P. S. Weisner, R. D. Neirinckx, W. A. Volkert, D. E. Troutner, R. A. Holmes, *Nucl. Med. Commun.*, 1985, 6, 499.

mono-oxo complex. HMPAO ligand exists in two forms, *d, l* and *meso*-isomers. The *d, l* isomer becomes more hydrophilic once it has crossed the blood brain barrier and thus can no longer leave the brain making it more suitable for brain imaging than its *meso* counterpart. Neurolite® is another commercially available agent used for brain imaging.

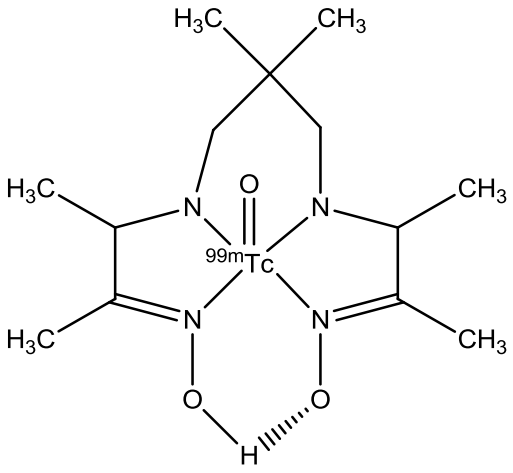

Ceretec®

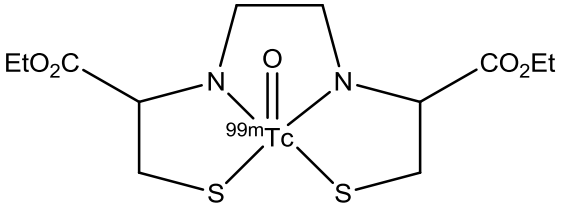

Neurolite®

Figure 2.6: Commercially available ^{99m}Tc radiopharmaceuticals used for brain imaging.

2.4.1.4 Bone imaging

Bone imaging agents[42] of ^{99m}Tc with diphosphonate ligands were among the first ^{99m}Tc-based radiopharmaceuticals developed for routine clinical use. Methylenediphosphonate (MDP) shown in Figure 2.7, is one example that is widely used for bone imaging, but its derivatives such as hydroxymethylenediphosphonate (HMDP) and 1-hydroxyethylenediphosphonate (HEDP) are also in routine use. The structure of ^{99m}Tc-MDP is however not known. It was introduced into the market when structure elucidation was not necessary for Federal Drug Administration (FDA) approval. But this is no longer the case as new emerging radiopharmaceutical agents for routine imaging should be fully characterized (composition and structure) to be approved. ^{99m}Tc-MDP is believed to accumulate in sites of actively growing bone such as bone metastases or fractures by coordination of the free phosphoryl oxygens to the calcium ions on the surface of the hydroxyapatite bone.

[42] W. Volkert, E. A. Deutsch, *Adv. Met. Med.*, 1993, 1, 115.

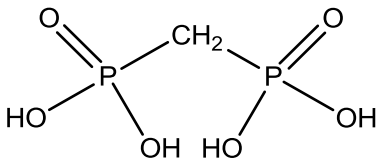

Figure 2.7: Structure of methylenediphosphonic acid ($MDPH_4$).

2.4.2 Second Generation Agents

Second generation complexes make use of biological functions such as peptide proteins which are covalently linked to bifunctional chelators (BFC). In these complexes, one part coordinates to the radioactive $^{186/188}$Re or ^{99m}Tc isotope and the other function is designed for conjugation. Labeling of this bioconjugates with a radioactive $^{186/188}$Re or ^{99m}Tc isotope must produce a product of high purity (preferably > 98 % yield) in a reasonably short time without affecting the targeting ability of the biologically active molecule. Factors such as the size of ^{99m}Tc isotope, charge, lipophilicity of the conjugate and the length of the covalent linker affect the targeting ability of the biological function.

2.4.2.1 Steroid Receptors

Three receptors namely, progesterone, estrogen and androgen have been explored for breast and prostate cancer.[43,44] Breast tumors are estrogen or progesterone receptor positive, while most prostate cancers are both estrogen and androgen receptor positive.

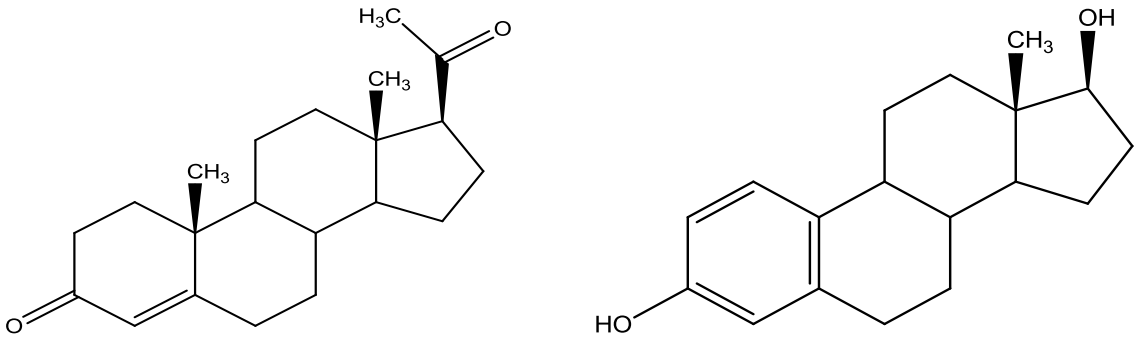

(A) **(B)**

Figure 2.8: Structures of progesterone **(A)** and estradiol **(B)** receptor hormones.

[43] S. S. Jurisson, J. D. Lydon, *Chem. Rev*., 1999, 99, 2205.
[44] R. M. Hoyte, N. J. MacLusky, R. B. Hochberg, *J. Steroid Biochem*., 1990, 36, 125.

Labeling of progesterone receptor with radioactive ^{99m}Tc isotope has been studied and is achieved by coordination *via* the N_2S_2 ligands, which contains progesterone receptor linked by a phenyl spacer, to technetium as shown in Figure 2.9. The key is to find an attachment site on the steroid which does not affect receptor binding.

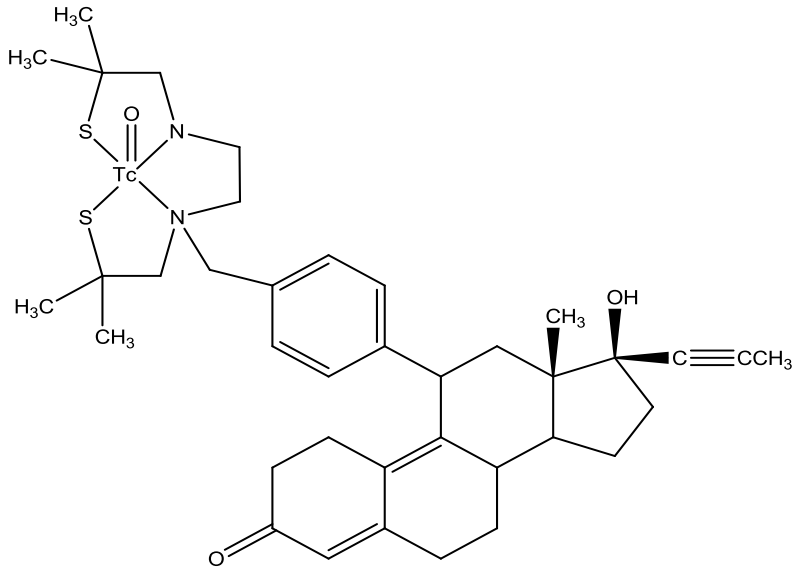

Figure 2.9: Labeling of progesterone receptor with ^{99m}Tc.

Figure 2.10 shows an alternative way that can be used to label these receptor hormones with ^{99m}Tc whereby the linker has been omitted. These structures resemble those of progesterone and estradiol respectively.[45]

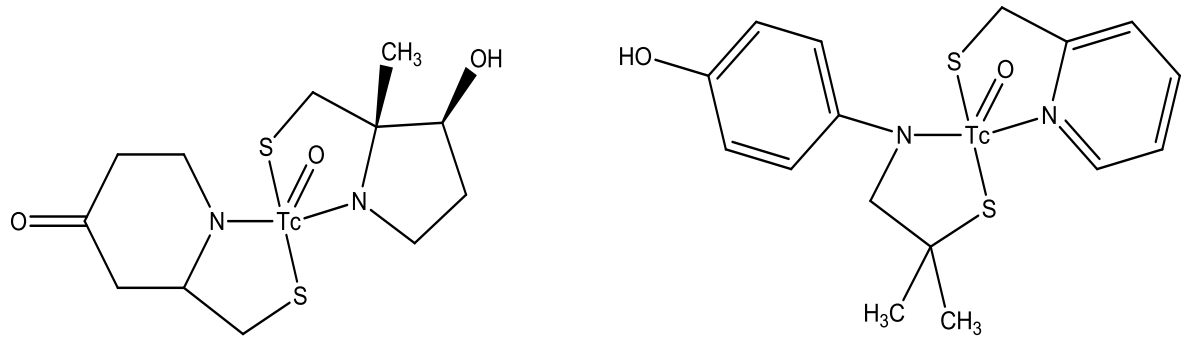

(A) **(B)**

Figure 2.10: ^{99m}Tc labeling of progesterone **(A)** and estradiol **(B)** derivatives.

[45] D. Y. Chi, J. P. O'Neil, C. J. Anderson, M. J. Welch, J. A. Katzenellenbogen, *J. Med. Chem*., 1994, 37, 928.

2.4.2.2 Multidrug Resistance (MDR) Targeting Molecules

A pathological state which shows the development of resistance by tumor cells towards chemotherapeutic agents is termed multidrug resistance (MDR). This is one of the reasons for the failure of treatment in cancer patients. This pathological state is characterized by the over expression of P-glycoprotein (Pgp), a trans-membrane pump that carries cytotoxic materials out of the cells.[46,47,48] MDR mostly affect complexes that are lipophilic and monocationic at physiologic pH. The development of MDR regulators which can block the action of Pgp is important because they can re-establish the cytotoxic effects of chemotherapeutic agents in tumor cells when administered simultaneously. Cardiolite® and Myoview® are two heart imaging agents that have been evaluated for diagnosing and monitoring MDR. Cardiolite® has been shown to be carried out of tumor cells expressing MDR by P-glycoprotein.[49] Both agents show similar multidrug resistance behaviour in MDR human carcinoma cells and non-MDR cells.

2.4.2.3 Central Nervous System (CNS) Receptors

Many radiopharmaceuticals labeled with ^{99m}Tc have targeted neuroreceptors because of their implications in various diseases such as Alzheimer's disease, Parkinson disease, schizophrenia and epilepsy. A neuroreceptor that has received most attention recently and shown promise for a ^{99m}Tc labeled neuroreceptor targeting is dopamine transporter (DAT). This neuroreceptor has been implicated in Parkinson's disease and schizophrenia. Kung *et al*.[50,51,52] synthesized ^{99m}Tc-TRODAT which uses an N_2S_2 ligand coordinated to technetium and a tropane analogue derivatized from one nitrogen as shown in Figure 2.11. Serotonin receptors have been implicated

[46] L. W. Herman, V. Sharma, J. F. Kronauge, E. Barbarics, L. A. Herman, D. Piwnica-Worms, *J. Med. Chem.*, 1995, 38, 2955.
[47] J. R. Ballinger, J. Bannerman, I. Boxen, P. Firby, N. G. Hartmen, M. J. Moore, *J. Nucl. Med.*, 1996, 37, 1578.
[48] C. L. Crankshaw, M. Marmion, G. D. Luker, V. Rao, J. Dahlheimer, B. D. Burleigh, E. Webb, K. F. Deutsch, D. Piwnica-Worms, *J. Nucl. Med.*, 1998, 39, 77.
[49] V. Rao, M. L. Chiu, J. F. Kronauge, D. Piwnica-Worms, *J. Nucl. Med.*, 1994, 35, 510.
[50] S. K. Meegalla, K. Plossl, M. P. Kung, S. Chumpradit, D. A. Stevenson, S. A. Kushner, W. T. McElgin, P. D. Mozley, H. F. Kung, *J. Med. Chem.*, 1997, 40, 9.
[51] M. P. Kung, D. A. Stevenson, K. Plossl, S. K. Meegalla, A. Beckwith, W. D. Essman, M. Mu, I. Lucki, H. F. Kung, *Eur. J. Nucl. Med.*, 1997, 24, 372.
[52] S. K. Meegalla, K. Plossl, M. P. Kung, D. A. Stevenson, M. Mu, S. Kushner, L. M. Liable-Sands, A. L. Rheingold, H. F. Kung, *J. Med. Chem.*, 1998, 41, 428.

in Alzheimer's disease, schizophrenia, anxiety, depression and suicide. Kentanserin is a prototypic serotonin receptor antagonist.

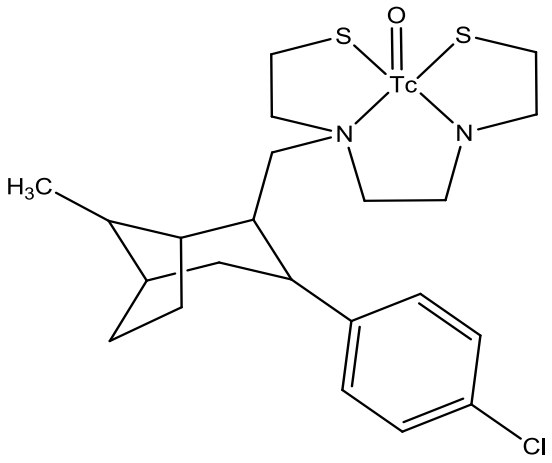

(A)

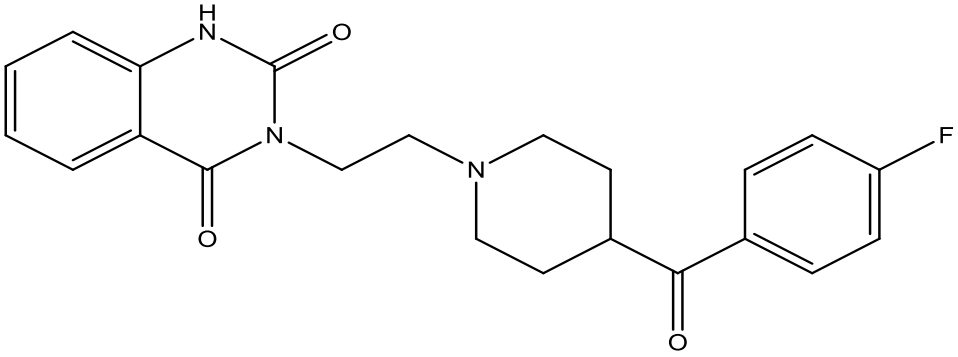

(B)

Figure 2.11: Structures of ^{99m}Tc-TRODAT **(A)** and Kentanserin **(B)**.

2.5 Current Studies in ^{99}Tc Chemistry

The radioactive isotope, ^{99}Tc, is a fission product that is produced in large amounts in nuclear reactors. The long half-life ($t_{1/2}$ = 2.11 x 10^5 yr) of this isotope poses a major problem in nuclear waste deposition. In industry, ^{99}Tc is handled in the form of pertechnetate, $[^{99}TcO_4]^-$ and is separated from used nuclear fuel in a method known as the plutonium-uranium extraction process (PUREX process). $[^{99}TcO_4]^-$ is kinetically inert and can be a potential hazard when accidentally released into the environment due to its high solubility in water. Environmental contamination by this isotope may last several years because of its long half-life. The selective

recognition of pertechnetate in water is difficult to achieve because of its big size and relatively low charge density.[53,54,55] Until recently, most of the studies on $[^{99}TcO_4]^-$ recognition have been based on neutral organic molecules and done in pure organic solvents.[56,57,58]

Amendola *et al*.[59,60] recently reported the first hexaprotonated *p*-xylyl azacryptand receptor which has a high affinity for $[^{99}TcO_4]^-$ in water and fluoresce when it is in contact with this anion. The azacryptand receptor consists of a macro-bicyclic polyamine, made of two bis-tren units linked by *p*-xylyl spacers as shown in Figure 2.12. The secondary amino groups of the azacryptand receptor are fully protonated at a pH of 2 in water. This expands the cavity of the receptor and is the most suitable form for anion binding.[61]

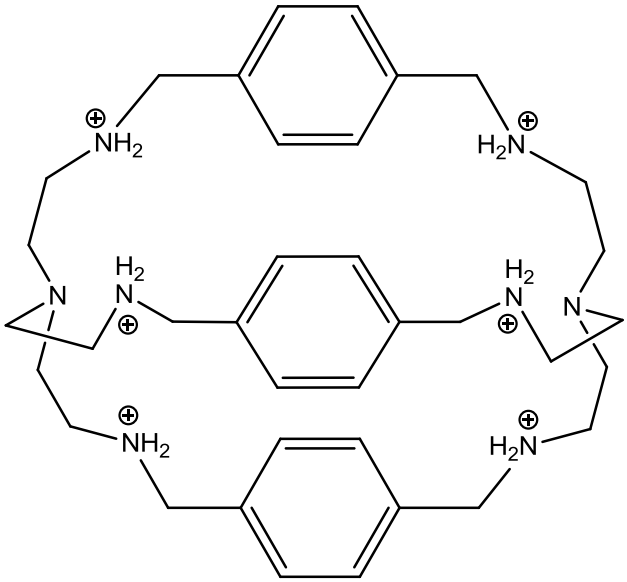

Figure 2.12: Structure of hexaprotonated azacryptand receptor, LH_6^{6+}.

[53] S. Kubik, *Chem. Soc. Rev*., 2010, 39, 3648.
[54] M. Wenzel, J. R. Hiscock, P. A. Gale, *Chem. Soc. Rev*., 2012, 41, 480.
[55] B. A. Moyer, R. Custelcean, B. P. Hay, J. L. Sessler, K. Bowman-James, V. W. Day, S. O. Kang, *Inorg. Chem*., 2013, 52, 3473.
[56] J. A. Gawenis, K. T. Holman, J. L. Atwood, S. S. Jurisson, *Inorg. Chem*., 2002, 41, 6028.
[57] E. A. Katayev, N. V. Boev, V. N. Khrustalev, Y. A. Ustynyuck, I. G. Tananaev, J. L. Sessler, *J. Org. Chem*., 2007, 72, 2886.
[58] M. Saeki, Y. Sasaki, A. Nakai, A. Ohashi, D. Banerjee, A. C. Scheinost, H. Foerstendorf, *Inorg. Chem*., 2012, 51, 5814.
[59] R. Alberto, G. Bergamaschi, H. Braband, T. Fox, V. Amendola, *Angew. Chem. Int. Ed*., 2012, 51, 9772.
[60] V. Amendola, G. Bergamaschi, M. Boiocchi, R. Alberto, H. Braband, *Chem. Sci*., 2014, 5, 1820.
[61] V. Amendola, G. Alberti, G. Bergamaschi, R. Biesuz, M. Boiocchi, S. Ferrito, F. P. Schmidtchen, *Eur. J. Inorg. Chem*., 2012, 21, 3410.

2.6 Rhenium Isotopes Involved in Nuclear Medicine

Rhenium consists of two radioactive isotopes which are used in therapeutic nuclear medicine by means of β-irradiation, ^{186}Re and ^{188}Re. ^{186}Re is produced from ^{185}Re by means of neutron radiation but is inevitably contaminated with the non-radioactive ^{185}Re. ^{188}Re is obtained as a solution of $[^{188}ReO_4]^-$ in high specific activity from ^{188}W-^{188}Re generator system similar to that of ^{99}Mo/^{99m}Tc (see Figure 2.13).[62] When ^{186}W is bombarded with neutrons, two neutrons are captured to give ^{188}W in the form of tungstate, $[^{188}WO_4]^{2-}$. Similarly to the ^{99}Mo/^{99m}Tc generator, $[^{188}WO_4]^{2-}$ is absorbed onto the alumina column and decays to give $[^{188}ReO_4]^-$ which is eluted with saline solution. A generator with 0.5 Ci of ^{188}W has a lifetime of 2-6 months and can provide enough radioactive ^{188}Re for the therapy of several hundred patients. ^{186}Re is a medium energy β-emitter (E_β = 1.07 MeV) with a range of 5 mm in tissue which makes it suitable for the therapy of small tumors. The long-half ($t_{1/2}$ = 3 days) makes it more suitable in labeling large biomolecules that tend to stay longer in the blood stream. ^{188}Re on the other hand is a high energy β-emitter (E_β = 2.12 MeV) with a range of 11 mm in tissue and a short half-life of 17 h which makes it suitable to design radiopharmaceuticals for the therapy of larger tumors.[63,64] Considering the fact that rhenium and technetium are both in the same group in the periodic table, it was thought that ^{99m}Tc could be used for therapy and ^{188}Re for diagnostic purposes. But, although the chemistry of these two transitional metals is similar, it is not sufficiently similar to allow for this comparative leap.

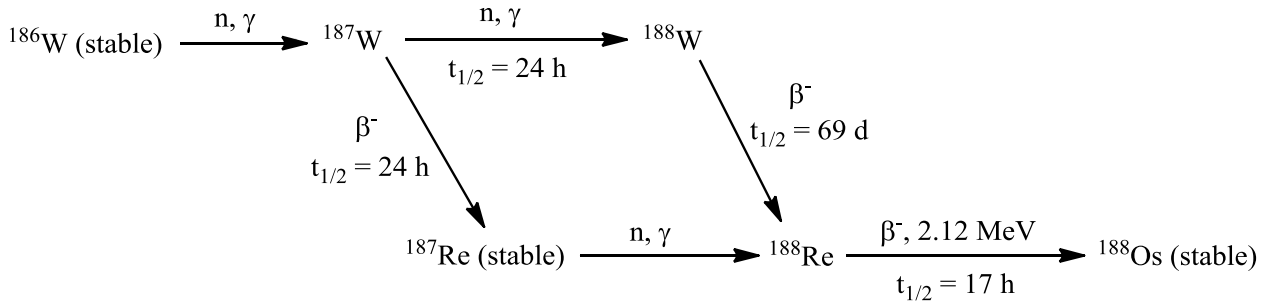

Figure 2.13: Production of ^{188}Re isotope from ^{188}W-^{188}Re generator system.

[62] F. F. Knapp Jr, S. Mirzadeh, A. L. Beets, *Appl. Radiat. Isot*., 1998, 49, 309.
[63] J. R. Dilworth, S. J. Parrott, *J. Chem. Soc. Rev*., 1999, 43.
[64] P. J. Blower, S. Prakash, *Perspect. Bioinorg. Chem*., 1999, 4, 91.

2.6.1 Rhenium Radiopharmaceuticals

As previously mentioned, rhenium consists of two radionuclides, ^{186}Re and ^{188}Re, which are widely used for therapy in nuclear medicine. Since both isotopes are β-emitting particles, any radiopharmaceutical agent labeled with them must meet a few strict requirements. Firstly, the agent should be stable towards oxidation or reduction which in turn could help with modifying the biodistribution. Secondly, it must be kinetically inert to ensure that the highly toxic radionuclide is not lost in the body. Finally, the agent should have high specificity for the target, which is normally a cancerous cell or a tumor. First generation complexes of rhenium for therapy are rare and their biodistribution is governed by their chemical and physical properties. A number of therapeutic radiopharmaceuticals labeled with rhenium radionuclides utilizes bifunctional, polydentate chelating ligands which offer kinetic stability and is conjugated to a biologically active molecule (BAM), normally by an amide bond. Two polydentate chelating ligands that are frequently used to link rhenium to the biologically active molecule include MAG3 and MAG2-GABA.[65]

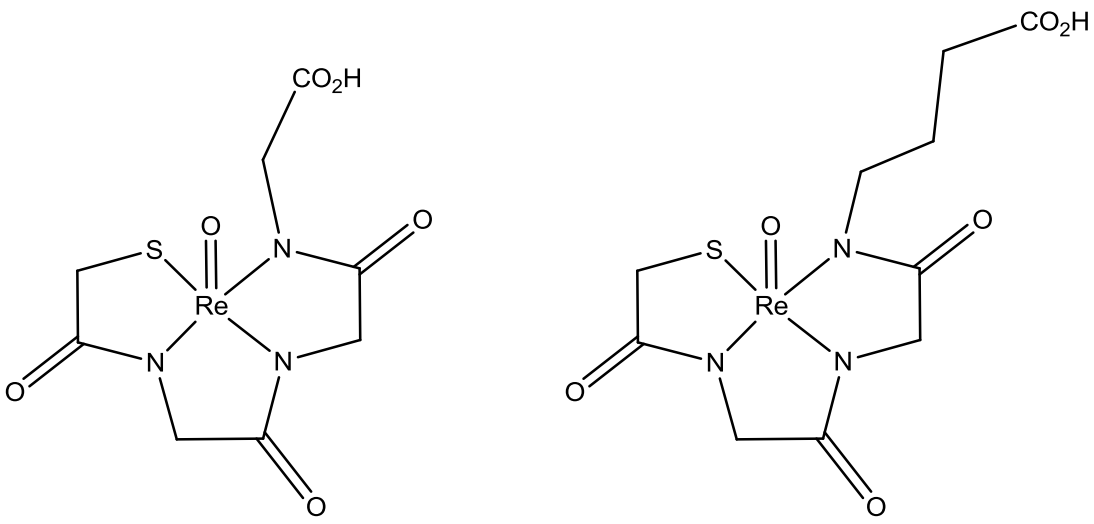

(A) **(B)**

Figure 2.14: Chelation of MAG3 **(A)** and MAG2-GABA **(B)** ligands to rhenium metal center.

[65] T. Kneiss, S. Noll, B. Noll, H. Spies, B. Johannsen, *J. Radioanal. Nucl. Chem*., 1999, 240, 357.

2.6.1.1 Bone Targeting Complexes

Rhenium complexes using diphosphonate ligands have been studied extensively as bone targeting radiopharmaceuticals since they have been shown to be suitable for relieving pain associated with bone metastases. The cause of pain in bone metastases and the mechanism of relief by these types of complexes are not entirely understood.[58] An example of a rhenium radiopharmaceutical that is well established and widely used for bone therapy is [^{186}Re-HEDP] (HEDP = hydroxyethylidenediphosphonate).[66,67] The synthesis of this complex involves reacting [$^{186}ReO_4]^-$ with HEDP in the presence of $SnCl_2$ which act as a reducing agent and ascorbic acid which act as an anti-oxidant. However, the structure of this complex is not completely known.

[^{186}Re-HEDP] is believed to accumulate in sites of actively growing bone such as bone metastases or fractures by coordination of the free phosphoryl oxygens to the calcium ions on the surface of the hydroxyapatite bone. The ^{188}Re analogue is a safer radiopharmaceutical for prostate cancer patients with osseous metastases.[68] Both agents have similar benefits and toxicity in patients with skeletal metastases. Their biodistribution and radiation dosimetry characteristics also appear similar. Another complex that has been studied as a potential therapeutic bone agent is [^{188}Re-EDTMP] (EDTMP = ethylenediamine-*N*,*N*,*N'*,*N'*-tetrakis(methylenephosphonate)) and its biodistribution studies done in rats showed high bone uptake and clearance from other organs.[69]

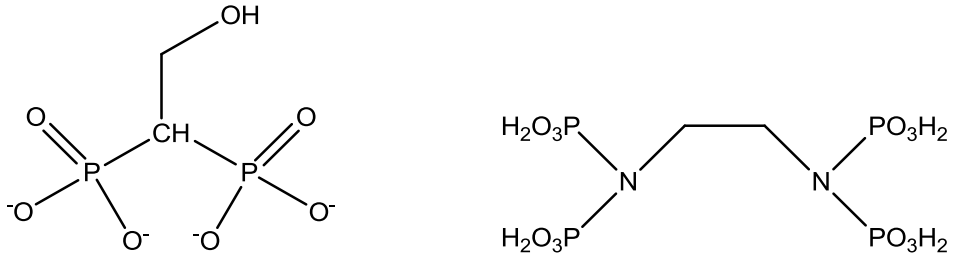

(A) **(B)**

Figure 2.15: Structures of hydroxyethylidenediphosphonate **(A)** and ethylenediamine-*N*,*N*,*N'*,*N'*-tetrakis(methylenephosphonic acid) **(B).**

[66] L. Mathieu, P. Chevalier, G. Galy, M. Berger, *Int. J. Appl. Radiat. Isot*., 1979, 30, 725.
[67] K. Liepe, R. Runge, J. Kotzerke, *J. Cancer Res. Clin. Oncol*., 2005, 131, 60.
[68] H. Palmedo, S. Guhlke, H. Bender, *Eur. J. Nucl. Med*., 2000, 27, 123.
[69] S. J. Oh, K. S. Won, D. H. Moon, *Nucl. Med. Commun*., 2002, 23, 75.

2.6.1.2 Medullary Thyroid Carcinoma

^{188}Re(V)-oxo complex of *meso*-2,3-dimercaptosuccinic acid (DMSA) has been investigated as a therapeutic analogue of [^{99m}Tc-DMSA], which is widely used as an imaging agent of a relatively rare medullary thyroid carcinoma. The ^{188}Re(V) complex exist as a mixture of three isomers in solution depending on the orientation of the carboxylate groups and all three isomers have a square pyramidal geometry.

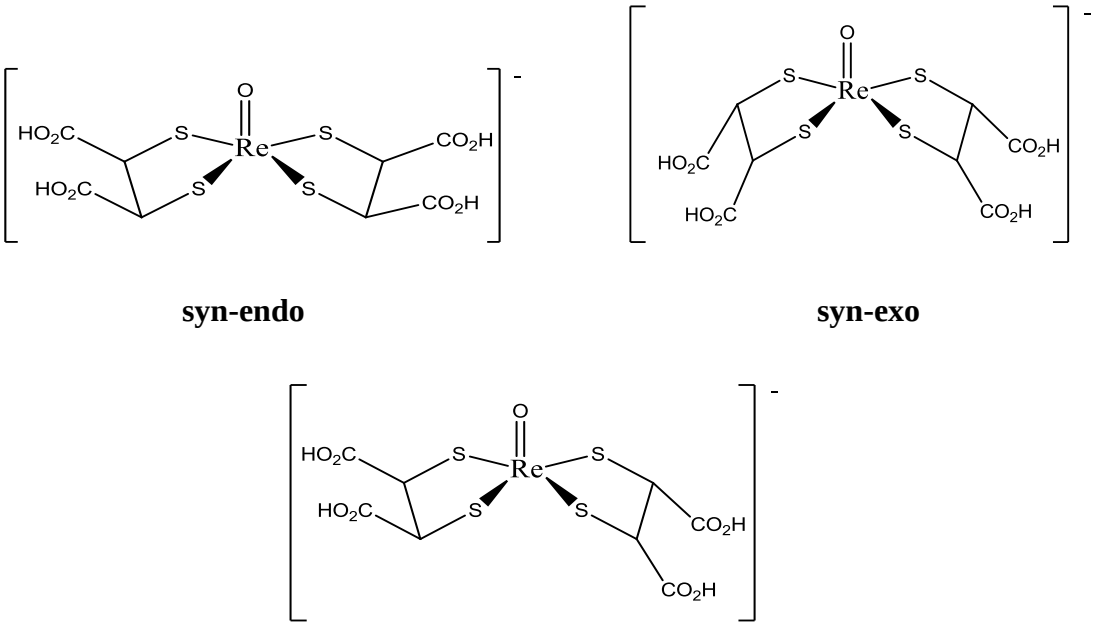

Figure 2.16: Structural isomers of [^{188}Re(O)DMSA]$^{-}$.

Studies of the biological properties of [^{188}Re(O)DMSA] done in humans with medullary thyroid carcinoma showed selective uptake of this complex in tumour tissue and selective uptake in bone metastases. An advantage of [^{188}Re(O)DMSA] over [^{188}Re-HEDP] in the palliation of painful bone metastases is that it is taken up in lower quantities in normal bone, thus limiting the radiation dose to healthy bone marrow.[70,71,72] Selective uptake of this agent in bone metastases is

[70] P. J. Blower, J. Singh, S. E. M. Clarke, M.M. Bisundan, M. J. Went, *J. Nucl. Med.*,1990, 31, 768.
[71] P. J. Blower, A. S. K. Lam, M. J. O'Doherty, *Eur. J. Nucl. Med*., 1998, 25, 613.
[72] P. J. Blower, A. G. Kettle, M. J. O'Doherty, *Eur. J. Nucl. Med*., 2000, 27, 1405.

believed to be achieved by the interaction of the carboxylate and oxo groups with the calcium ions on the surface of the hydroxyapatite bone.

2.7 Rhenium and Technetium Cyanido Complexes

Roodt *et al.*[73,74,75] investigated the reactivity of complexes of the type *trans*-$[MO_2(CN)_4]^{3-}$ (M = Re(V), ^{99}Tc(V)) with respect to protonation and ligand substitution. The kinetic behaviour of rhenium and technetium complexes play a vital role when designing model radiopharmaceutical for potential use in therapy or diagnosis, since useful information relating to the preparation of the drug, stability in *vivo*, biodistribution tendencies and the rate of decomposition or clearance can be gathered. Protonation of $[ReO_2(CN)_4]^{3-}$ to form $[ReO(OH)(CN)_4]^{2-}$ and $[Re(OH_2)(CN)_4]^{-}$ respectively,[76,77] resulted in a significant decrease in the metal-oxo (Re=O) bond length along the apical O=Re–OH and O=Re–OH_2 axis, thus weakening the protonated Re–O bond. The implication of this effect was an increase in the distortion of the octahedral geometry around the metal center. The weakening of the Re–OH and Re–OH_2 bond strength induces pronounced effects on the reactivity of these types of complexes towards oxygen exchange.

The $[M=O]^{3+}$ (M = $^{186/188}$Re, ^{99m}Tc) core has without a shadow of doubt played an important role in the development and designing of new metal based radiopharmaceutical agents over the years. The majority of complexes described in this literature study so far all bear the $[M=O]^{3+}$ core, with a few bearing the $[O=M=O]^{+}$ core and the so-called naked metal "M" core. The *fac*-$[M(CO)_3]^{+}$ core holds great promise for future development of rhenium and technetium radiopharmaceuticals and is described in details hereafter.

2.8 Rhenium and Technetium Tricarbonyl Complexes

Rhenium and technetium tricarbonyl complexes only started receiving more attention from nuclear medical application after the synthesis of *fac*-$[M(CO)_3(H_2O)_3]^{+}$ (M = $^{186/188}$Re, ^{99m}Tc)

[73] A. Roodt, H. P. Engelbrecht, J. M. Botha, S. Otto, S. *Technetium, Rhenium and Other Metals in Chemistry and Nuclear Medicine*: Eds.: M. Nicolini, U. Mazzi, Cortina International: Verona, 1999, 5, 161.
[74] A. Roodt, A. Abou-Hamdan, H. P. Engelbrecht, A. E. Merbach, *Adv. Inorg. Chem*., 1999, 40, 59.
[75] A. Roodt, H. G. Visser, A. Brink, *Cryst. Rev*., 2011, 17, 241.
[76] W. Purcell, A. Roodt, S. S. Basson, J. G. Leipoldt, *Transit. Met. Chem*., 1989, 14, 224.
[77] W. Purcell, A. Roodt, S. S. Basson, J. G. Leipoldt, *Transit. Met. Chem*., 1990, 15, 239.

under mild reaction conditions described by Alberto *et al.*[78,79,80,81] This important precursor can be prepared in a single-step procedure from aqueous permetallates, $[MO_4]^-$ in the presence of CO gas, using BH_4^- as a reducing agent.[82] However, the preparation of *fac*-$[M(CO)_3(H_2O)_3]^+$ relying on gaseous carbon monoxide is not suitable for use in commercial radiopharmaceutical "kits". The key is to use a solid, air-stable source of carbon monoxide that can possibly act as a reducing agent at the same time. The first commercially feasible preparation of an organometallic transition metal complex in physiological media was described by Alberto *et al.*[83] The preparation uses a boron based carbonylating agent which acts as a carbon monoxide source and a reducing agent simultaneously.

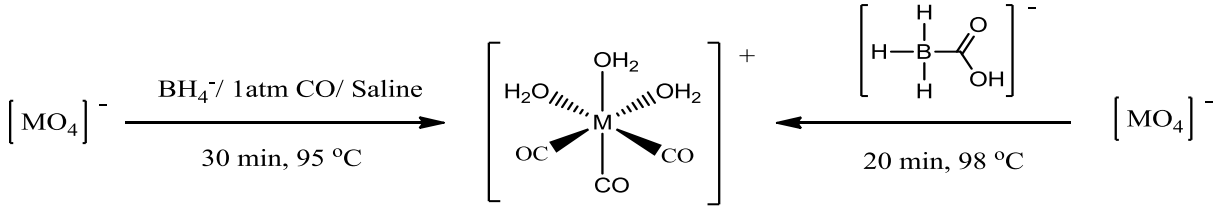

Figure 2.17: Two ways to synthesis *fac*-$[M(CO)_3(H_2O)_3]^+$ from permetallates (M = Re, $^{99/99m}$Tc).

Alternatively to permetallates, *fac*-$[Et_4N]_2[M(CO)_3X_3]$ (M = Re, $^{99/99m}$Tc; X = Cl, Br), can also be used as a starting material to prepare *fac*-$[M(CO)_3(H_2O)_3]^+$. This complex is soluble in water and the halides are readily substituted by the H_2O molecules. Tricarbonyl aqua complexes consist of two very important and perhaps conflicting features. Firstly, they bear carbon monoxide, which is an important and versatile ligand in the organometallic chemistry of transition metals. Secondly, they bear water, which is considered to be a green solvent.

Complexes of the type *fac*-$[M(CO)_3(H_2O)_3]^+$ (M = $^{186/188}$Re, ^{99m}Tc) are suitable for radiopharmaceutical design because of their stable, near spherical *fac*-$[M(CO)_3]^+$ core[84] in water and the potential of exchanging the labile solvent molecules. The low valency of a majority of

[78] R. Waibel, R. Alberto, J. Willuda, R. Finnern, R. Schibli, A. Stichelberger, A. Egli, U. Abram, J. P. Mach, A. Plueckthun, P. A. Schubiger, *Nature Biotechnol*., 1999, 17, 897.
[79] R. Alberto, R. Schibli, U. Abram, B. Johannsen, H. J. Pietzsch, P. A. Schubiger, *J. Am. Chem. Soc*., 1999, 25, 6076.
[80] R. Schibli, K. V. Katti, C. Higginbotham, W. A. Volkert, R. Alberto, *Nucl. Med. Biol.*, 1999, 26, 711.
[81] A. Egli, R. Alberto, L. Tannahill, R. Schibli, U. Abram, A. Schaffland, R. Waibel, D. Tourwe, L. Jeannin, K. Iterbeke, P. A. Schubiger, *J. Nucl. Med*., 1999, 40, 1913.
[82] R. Alberto, R. Schibli, A. Egli, U. Abram, T. A. Kaden, P. A. Schubiger, *J. Am. Chem. Soc*., 1998, 120, 7987.
[83] R. Alberto, K. Ortner, N. Wheatley, R Schibli, P. A. Schubiger, *J. Am. Chem. Soc.*, 2001, 123, 3135.
[84] R. Alberto, R. Schibli, R. Waibel, U. Abram, P. A. Schubiger, *Coord. Chem. Rev*., 1999, 190-192, 901.

Re(I) and $^{99/99m}$Tc(I) complexes is stabilized by pH independent ligands such as phosphanes which are hardly substituted by other incoming chelators. The *fac*-$[M(CO)_3]^+$ core possesses a d^6 electronic configuration in an octahedral field. Complexes which adopt this configuration are generally known to be kinetically inert. Combining these two features, it may be possible for monodentate ligands, which provides low thermodynamic stability, to form inert complexes.[84] A number of biomolecules such as peptides,[85,86] central nervous system (CNS) receptor ligands,[87] glucose[88,89] and many small molecules[90,91,92] have already been labeled with rhenium and technetium utilizing *fac*-$[M(CO)_3(H_2O)_3]^+$ demonstrating its potential for radiopharmaceutical development.

2.9 Current Studies in Rhenium Chemistry

Since the preparation of *fac*-$[Re(CO)_3(H_2O)_3]^+$ was described, much of the research have focused on reactions between this precursor and biomolecules. Although a lot of research has been done in investigating the interactions between rhenium tricarbonyl based compounds and nucleic acids,[93,94,95] amino acids and oligopeptides,[96,97] the interactions between rhenium prodrug or drug model complexes and proteins have received little attention. These interactions can be very useful for the biological processing of rhenium and technetium radiopharmaceutical agents since proteins are encountered in the plasma and not necleotides or single amino acids. Furthermore, the rhenium and technetium protein adducts could be used as novel therapeutic and diagnostic

[85] R. La Bella, E. Garcia-Garayoa, M. Bahler, P. Blauenstein, R. Schibli, P. Conrath, D. Tourwe, P. A. Schubiger, *Bioconjugate Chem*., 2002, 13, 599.
[86] C. J. Smith, G. L. Sieckman, N. K. Owen, D. L. Hayes, D. G. Mazuru, R. Kannan, W. A. Volkert, T. J. Hoffman, *Cancer Res*., 2003, 63, 4082.
[87] J. Bernard, K. Ortner, B. Spingler, H. J. Pietzsch, R. Alberto, *Inorg. Chem*., 2003, 42, 1014.
[88] C. L. Ferreira, C. B. Ewart, C. A. Barta, S. Little, V. Yardley, C. Martins, E. Polishchuk, P. J. Smith, J. R. Moss, M. Merkel, M. J. Adam, C. Orvig, *Inorg. Chem*., 2006, 45, 8414.
[89] C. L. Ferreira, C. B. Ewart, S. R. Bayly, B. O. Patrick, J. Steele, M. J. Adam, C. Orvig, *Inorg. Chem*., 2006, 45, 6979.
[90] L. Maria, C. Fernandes, R. Garcia, L. Gano, A. Paulo, I. C. Santos, I. Santos, *Dalton Trans*., 2009, 603.
[91] Y. Liu, J. K. Pak, P. Schmutz, M. Bauwens, J. Mertens, H. Knight, R. Alberto, *J. Am. Chem. Soc*., 2006, 128, 15996.
[92] H. W. P. N'Dongo, P. D. Raposinho, C. Fernandes, I. Santos, D. Can, P. Schmutz, B. Spingler, R. Alberto, *Nucl. Med. Biol*., 2010, 37, 255.
[93] F. Zobi, O. Blacque, H. W. Schmalle, B. Spingler, R. Alberto, *Inorg. Chem*., 2004, 43, 2087.
[94] F. Zobi, O. Blacque, R. K. O. Sigel, R. Alberto, *Inorg. Chem*., 2007, 46, 10458.
[95] K. M. Adams, P. A. Marzilli, L. G. Marzilli, *Inorg. Chem*., 2007, 46, 9172.
[96] H. He, M. Lipowska, X. Xu, A. T. Taylor, M. Carlone, L. G. Marzilli, *Inorg. Chem*., 2005, 44, 5437.
[97] H. He, M. Lipowska, X. Xu, A. T. Taylor, L. G. Marzilli, *Inorg. Chem*., 2007, 46, 3385.

agents. Binkley and co-workers[98,99] reported the first crystal structure of a protein-bound *fac*-$[Re(CO)_3(H_2O)_2]^+$ complex by reacting *fac*-$[Re(CO)_3(H_2O)_3]^+$ with the protein hen egg white lysozyme in aqueous medium. In the crystal structure, the cation binds to a single amino acid side chain at the periphery of the protein hen egg white lysozyme *via* the nitrogen imine donor atom of the His15 imidazole ring. The His15 imidazole ligand replaces one water molecule on the cation forming a mono-substituted complex.

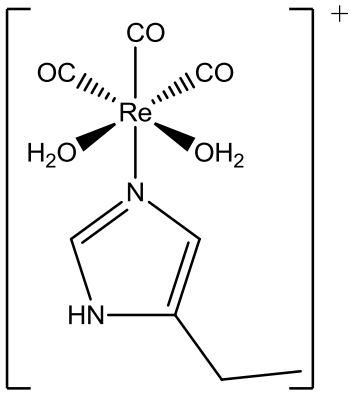

Figure 2.18: A structure of the mono-substituted *fac*-$[Re(CO)_3(His15)(H_2O)_2]^+$ complex.

Zobi *et al*.[100] later showed that the chemistry of the lysozyme-bound *fac*-$[Re(CO)_3(H_2O)_2]^+$ complex is affected by the nature of the chiral protein environment when compared to the cationic *fac*-$[Re(CO)_3(H_2O)_3]^+$ precursor. This complex retains its reactivity towards selected mono- and bidentate ligands, while ligands bearing primary amines induced demetalation.

2.10 Kinetic Behavior of *fac*-$[M(CO)_3]^+$ (M = Re, ^{99}Tc, Mn) Core

2.10.1 Aqueous Chemistry of *fac*-$[M(CO)_3(H_2O)_3]^+$

The first thermodynamic and kinetic data for water exchange on *fac*-$[Re(CO)_3(H_2O)_3]^+$ was obtained by Salignac *et al*.[101] using a variety of NMR techniques. The water exchange rate constants on *fac*-$[Re(CO)_3(H_2O)_3]^+$and the monohydroxo species *fac*-$[Re(CO)_3(H_2O)_2(OH)]$, were found to be $k_{ex} = 6.3 \pm 0.1 \times 10^{-3}$ s^{-1} and $k_{OH} = 27 \pm 1$ s^{-1} respectively at 298 K. The kinetic

[98] S. L. Binkley, T. C. Leeper, R. S. Rowlett, R. S. Herrick, C. J. Ziegler, *Metallomics*, 2011, 3, 909.
[99] S. L. Binkley, C. J. Ziegler, R. S. Herrick, R. S. Rowlett, *Chem. Commun.*, 2010, 46, 1203.
[100] F. Zobi, B. Spingler, *Inorg. Chem*., 2012, 51, 1210.
[101] B. Salignac, P. V. Grundler, S. Cayemittes, U. Frey, R. Scopelliti, A. E. Merbach, *Inorg. Chem*., 2003, 42, 3516.

contribution of the basic form was significant only at $[H^+] < 3 \times 10^{-3}$ M. Above this $[H^+]$ concentration, kinetic studies can be carried out solely on the triaqua cation. The activation parameters for the water exchange were found to be $\Delta H^{\neq}_{ex} = 90 \pm 3$ kJ mol^{-1}, $\Delta S^{\neq}_{ex} = +14 \pm 10$ J K^{-1} mol^{-1}, with the latter indicating a dissociative interchange mechanism, I_d. To supplement these findings, water substitution studies on the *fac*-$[Re(CO)_3(H_2O)_3]^+$ with a variety of ligands (trifluoroacetate = TFA; acetonitrile = CH_3CN; 2,2'-bipyridine = bipy; 1,10-phenanthroline = phen; dimethylsulfide = DMS and thiourea = TU) were conducted and followed with different NMR (^{17}O, ^{1}H, ^{13}C, ^{19}F) nuclei. The calculated interchange rate constants k_i' for each ligand used were found to be similar to the water exchange rate constant k_{ex}, which further support an I_d mechanism.

Water substitution on the *fac*-$[Re(CO)_3(H_2O)_3]^+$ with a variety of unidentate ligands (TFA, CH_3CN, TU, DMS and I^-), except Br^-, led to the formation of mono-, di-, and trisubstituted complexes.[101,102,103] In the cases of CH_3CN and DMS, the substitution of each H_2O molecule by the unidentate ligand could be identified stepwise. The kinetic data for the reaction of *fac*-$[M(CO)_3(H_2O)_3]^+$ (M = Mn, ^{99}Tc, Re) complexes with CH_3CN and DMS shows that these complexes are less stable with CH_3CN than with DMS, and have a higher affinity for the *S*-donor DMS than the *N*-donor CH_3CN. The activation volumes, $\Delta V^{\neq}$, of these *S* and *N* bonded ligands[103,104] range from slightly negative for *S* bonded ligands, to slightly positive for *N* bonded ligands, indicating a shift from I_a for the *S* ligands to I_d for the *N* ligands.

The water exchange rates for complexes of the type *fac*-$[M(CO)_3(H_2O)_3]^+$ (M = Mn, ^{99}Tc, Re) vary over several orders of magnitude, with Mn reactions being the fastest followed by ^{99}Tc and then Re. The slower water exchange rates observed for Re(I) as compared to the similar reactions for ^{99}Tc(I) does not exclude it totally as a potential radionuclide. The advantage of starting with rhenium is that its stable isotope found in nature is non-radioactive as opposed to the radioactive Tc isotopes. Thus, the reactions of Re complexes are less laborious and can be studied as models for the Tc analogues.

[102] L. Helm, *Coord. Chem*., 2008, 252, 2346.
[103] P. V. Grundler, L. Helm, R. Alberto, A. E. Merbach, *Inorg. Chem*., 2006, 45, 10378.
[104] P. V. Grundler, B. Salignac, S. Cayemittes, R. Alberto, A. E. Merbach, *Inorg. Chem*., 2004, 43, 865.

2.10.2 Substitution Reactions of *fac*-[Re(L,L'-Bid)(CO)$_3$(MeOH)]

Schutte *et al*.[105] synthesized a range of *fac*-[Re(L,L'-Bid)(CO)$_3$(H$_2$O)]$^{n+}$ (L,L'-Bid = neutral or monoanionic *N*,*N*', *O*,*O*', *N*,*O* bidentate ligands, *n* = 0, 1) complexes and evaluated the lability and mechanism of substitution of the coordinated H$_2$O/MeOH with a variety of monodentate nucleophiles. The investigation was primarily prompted by the fact that the influence that other ligands (*e.g.* different bidentates), except the coordinated carbonyl ligands, have on the rate of aqueous substitution had not yet been investigated. The bidentate ligands; 1,10-phenanthroline (Phen), 2,2'-bipyridine (Bipy), 2,4-pyridinedicarboxylic acid (2,4-dPicoH), 2,4-quinolinedicarboxylic acid (2,4-dQuinH), 2-picolinic acid (PicoH), 2-quinolinecarboxylic acid (QuinH), 3,5,7-tribromotropolone (TropBr$_3$) and 3-hydroxyflavone (Flav), were consciously chosen to obtain complexes that were positively or neutrally charged, with varied Bronsted basicities afforded by the pKa values of the bidentate ligands. The major advantage of using bidentate ligands is that they "block" two of the reactive aqua ligands on the *fac*-[M(CO)$_3$(H$_2$O)$_3$]$^+$ complex leaving the third site available for substitution.

The majority of the isolated mono-aqua complexes were converted to the corresponding MeOH species, upon dissolution in methanol for the kinetic studies. Thus, the reported kinetic investigations were of the substitution of the coordinated MeOH in *fac*-[Re(L,L'-Bid)(CO)$_3$(MeOH)]^n with various monodentate entering nucleophiles, ranging from halides to pyridines as well as S and P donor groups. The kinetic studies were the first of its kind and the rates as well as concentration dependencies obtained, assumed that the mono-aqua complexes immediately formed the corresponding MeOH coordinated complexes, upon dissolution in methanol. This effect was confirmed by X-ray diffraction, clearly showing a coordinated MeOH in the aqua site.[106,107] The substitution of MeOH in the *fac*-[Re(L,L'-Bid)(CO)$_3$(H$_2$O)]^n complexes by a range of entering ligands was studied under *pseudo* first-order conditions ([*L*] >> [*M*]).

The rates of formation, k_1, obtained for the reactions of *N*,*N'* positively charged complexes with various halides (Cl^-, Br^-, and I^-) as entering ligands are comparable, and 300−400 times faster

[105] M. Schutte, G. Kemp, H. G. Visser, A. Roodt, *Inorg. Chem*., 2011, 50, 12486.
[106] M. Schutte, H. G. Visser, G. Steyl, *Acta Cryst.*, 2007, E63, m3195.
[107] M. Schutte, H. G. Visser, A. Brink, *Acta Cryst.*, 2009, E65, m1575.

than the values obtained for the neutral pyridine type ligands. The higher affinity of these *N,N'* positively charged metal complex for the negatively charged halido ligands as well as the obtained negative value of $\Delta S^{\neq}$ pointed towards an associative mechanism, I_a. The substitution reaction with pyridine and *m*-methylpyridine as entering ligands shows that the sterically hindered *m*-methylpyridine reacts slower (4-6 times) than the unsubstituted pyridine. The value obtained by Salignac *et al.*[101] for the formation of *fac*-[Re(CO)$_3$(H$_2$O)$_2$Br] is about 20-30 times slower than the formation of *fac*-[Re(Phen)(CO)$_3$(Br)] and *fac*-[Re(Bipy)(CO)$_3$(Br)], which shows that Phen and Bipy activates the Re(I) metal center more than the aqua ligands in *fac*-[Re(CO)$_3$(H$_2$O)$_3$]$^+$.

The rate of formation for the reactions of *N,O* neutrally charged metal complexes with Br$^-$ as entering ligand is approximately 5-7 times faster than that observed with neutral ligands. When considering neutral ligands only, DMAP entering ligand is slightly faster than the other rate constants. The obtained activation parameters also pointed towards an associative mechanism.

In *O,O'* neutrally charged metal complexes, the rate of substitution of methanol in *fac*-[Re(Flav)(CO)$_3$(MeOH)] with 4-dimethylaminopyridine (DMAP) occurs almost 150 times faster than that in *fac*-[Re(CO)$_3$(TropBr$_3$)(MeOH)]. When pyridine was used as the entering ligand, the rate of substitution of methanol in *fac*-[Re(Flav)(CO)$_3$(MeOH)] occurs almost 70 times faster than that observed in *fac*-[Re(CO)$_3$(TropBr$_3$)(MeOH)].

The conclusion drawn was that the *O,O'* bidentate ligands activate the metal center more than the *N,O* bidentate ligands and that the *N,N'* positively charged metal complexes have slower methanol substitution rates. The reason behind this is that the *O,O'* bidentate ligands increase the electron density on the metal center substantially and thus increase the rate of the entering ligand.

Brink *et al.*[108,109,110] investigated the activation of Re(I) metal center by *N,O* bidentate Schiff-base ligands towards the methanol substitution in neutral *fac*-[Re(L,L'-Bid)(CO)$_3$(MeOH)] (L,L'-Bid = monoanionic *N,O* bidentate ligands) complexes with various neutral monodentate entering ligands. The bidentate ligands were chosen to investigate the possible effect that a range of aromatic and aliphatic substituents could have on the rate of substitution of the coordinated

[108] A. Brink, *Ph.D. Thesis*, University of the Free State, Bloemfontein, South Africa, 2011.
[109] A. Brink, H. G. Visser, A. Roodt, *Inorg. Chem.*, 2013, 52, 8950.
[110] A. Brink, H. G. Visser, A. Roodt, *Inorg. Chem.*, 2014, 53, 12480.

methanol. Substituted pyridine ligands, 3-chloropyridine, 4-picoline, 4-dimethylaminopyridine and pyridine, were selected as neutral monodentate entering ligands due to their varying pKa values. The substitution of the methanol in *fac*-[Re(L,L′-Bid)$(CO)_3$(MeOH)] complexes with substituted pyridine type ligands could also be studied under *pseudo* first-order conditions. However, from the obtained k_{obs} *vs* [*L*] profiles, an interchange mechanism was formed.

The k_{obs} *vs* [Ligand] plots, obtained from the substitution of methanol in a range of rhenium complexes with various entering ligands, produced linear plots in some cases and nonlinear (limiting plots) ones in others. This made assigning an intimate mechanism for the substitution of methanol complicated, therefore fits of the rate data *vs* [*L*] were interpreted with equations corresponding to a pure associative or an interchange mechanism, respectively.

The substitution of the axial methanol in *fac*-[Re(Sal-*m*Tol)$(CO)_3$(MeOH)] (Sal-*m*Tol = 2-(*m*-tolyliminomethyl)phenolatido) with different pyridine type ligands yielded linear plots of k_{obs} *vs* [*L*] with no obvious deviation from linearity when 3-chloropyridine (pKa = 2.81) and pyridine (pKa = 5.23) were used as entering ligands. The data obtained when 4-picoline (pKa = 5.99) was used as the entering ligand indicates slight deviation from linearity, while the reaction with DMAP (pKa = 9.8) indicates distinct curvature with near saturation limits. The calculated second order rate constants determined for either an associative or interchange type mechanism, decrease in the order 3-ClPy > Py > 4-Pic > DMAP, which is inversely proportional to the pKa values of the ligands. This is the opposite of what is expected for an associative type mechanism. The positive value of the entropy of activation $\Delta S^{\neq}$, as well as the stepwise increase in the pre-equilibrium constant (K_2), which is in direct agreement with the electron density on the *N*-atom of the pyridine type entering ligand pointed towards an interchange dissociative mechanism, I_d. The substitution of methanol in *fac*-[Re(Sal-*m*Tol)$(CO)_3$(MeOH)] with pyridine occurs faster than the reactions studied by Schutte[105] for analogous *N,O* bidentate ligands. Thus, salicylidene type Schiff-base ligands activate the Re(I) metal center more than the other *N,O* donor atoms.

In conclusion, the *N,O* salicylidene type ligands were found to activate the Re(I) metal center significantly leading to rapid methanol substitution reactions as indicated by the 3 orders of magnitude increase in reaction rates, which have only been reported for the *O,O′* bidentate flavonoid type ligand.[100] The obtained data shows that the primary influence towards metal activation comes from the basic Schiff-base backbone, whereas the contribution from the

substituents is relatively small. These rhenium salicylidene tricarbonyl complexes also made it possible to study the substitution reactions under limiting conditions for the first time.

2.11 Formation Kinetics of *fac*-$[M(CO)_3]^+$ (M = Re, ^{99m}Tc) core

Although our group has contributed significantly towards the substitution reactions of the coordinated methanol and aqua solvento molecules (*S*) in *fac*-[Re(L,L'-Bid)$(CO)_3$(S)] complexes with various monodentate entering ligands, the same can't be said for the formation reactions, i.e. the time it takes for the actual bidentate or tridentate ligand to coordinate to the *fac*-$[Re(CO)_3]^+$ core. Radiopharmaceutical drug design for routine clinical applications comes with a few stringent limitations that must be met: The preparation must be a one-step mechanism yielding a product with a high purity (preferably > 98 % yield). The biomolecule concentration should be 1:1 with respect to the radionuclide and practical time restrictions should be designed to meet the half-life of the radionuclide. Thus, the time it takes for the preparation, i.e. for the ligand to coordinate to the *fac*-$[M(CO)_3]^+$ (M = $^{186/188}$Re, $^{99/99m}$Tc) core, is vital when designing radiopharmaceutical drugs and it should be well below the half-life of the radionuclide of choice, which is about 60 minutes for ^{99m}Tc.

Alberto *et al.*[84] investigated formation reactions of the *fac*-$[M(CO)_3]^+$ (M = Re, ^{99m}Tc) moiety with the ligands imidazole, histamine and histidine utilizing ^{1}H NMR. The mono-, di- and trisubstituted complexes $[Re(im)(CO)_3\ Br_2]^-$, $[Re(im)_2(CO)_3Br]$ and $[Re(im)_3(CO)_3]^+$ were systematically synthesized as shown in Figure 2.19.

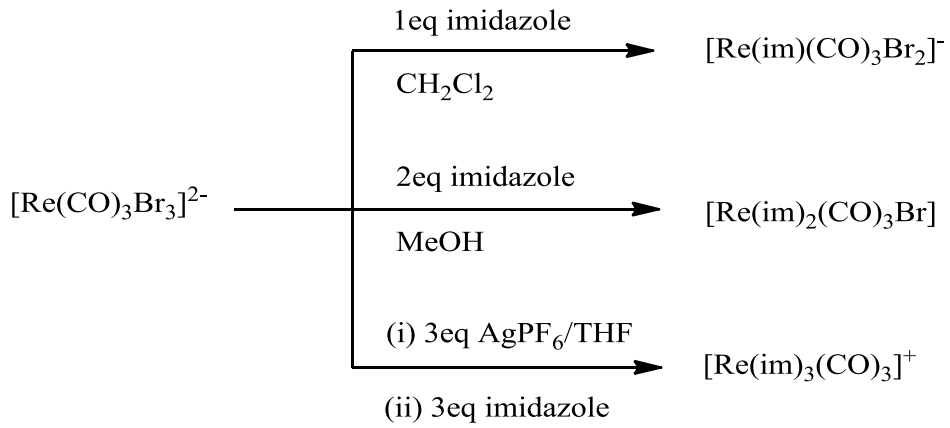

Figure 2.19: Stepwise synthesis of rhenium imidazole tricarbonyl complexes.

^{1}H NMR kinetics done in coordinating organic solvents such as methanol or DMSO at room temperature, showed a stepwise formation of the mono- and disubstituted intermediates $[M(im)(CO)_3(sol)_2]^+$ and $[M(im)_2(CO)_3(sol)]^+$ which were converted to their respective $[M(im)(CO)_3Br_2]^-$ and $[M(im)(CO)_3Br]$ final complexes. Existence of these solvent coordinated intermediates was proven by comparing the ^{1}H NMR spectra of the reaction mixtures with those of the final complexes. The final step however involves the re-coordination of Br^- and not the coordination of a third imidazole ligand even when present in excess amount. The kinetic investigations showed fast coordination for the first and second imidazole ligand, followed by a slow re-coordination of the bromido ligand. Reactions with $[^{99m}Tc(CO)_3(H_2O)_3]^+$ and imidazole in aqueous solutions (pH 6-8, phosphate buffer, 70°C) on the no carrier added level ($[^{99m}TcO_4]^-$ generator), showed similar substitution behavior as rhenium imidazole complexes in terms of the formed products, $[^{99m}Tc(im)(CO)_3(H_2O)_2]^+$ and $[^{99m}Tc(im)_2(CO)_3(H_2O)]^+$. However, the re-coordination of Br^- could not be detected with certainty. Complete complex formation could only be observed after increasing the reaction time at elevated temperature (2 h, 75 ^{o}C) and using relatively high ligand concentration, 10^{-4} M as opposed to 10^{-6} M of $[^{99m}Tc(CO)_3(H_2O)_3]$.

The neutral complex, $[Re(hist)(CO)_3Br]$ was synthesized from the reaction between $[Re(CO)_3Br_3]^{2-}$ and the bidentate ligand, histamine. A kinetic investigation of the formation of this complex was similar to that observed with imidazole. Thus, the coordination of the histamine ligand to the rhenium center was relatively fast ($t_{1/2}$ = 30 min), followed by the slow re-coordination of the bromido ligand. Complete complex formation for the reaction between $[^{99m}Tc(CO)_3(H_2O)_3]^+$ and histamine in aqueous solutions (pH = 7.4, phosphate buffer) on the *n.c.a.* level was observed only after 30 minutes at 75 ^{o}C, using ligand concentration as low as 10^{-5} M. Thus, the incorporation of the imidazole moiety with the primary amine function in histamine, resulted in fast complex formation rates with $[^{99m}Tc(CO)_3(H_2O)_3]^+$ using ten times lower ligand concentration than with imidazole only.

The neutral complex, $[Re(his)(CO)_3]$ was synthesized from $[Re(CO)_3Br_3]^{2-}$ and histidine in aqueous medium. In the complex, the histidine ligand coordinate to the metal center facially and in a tridentate manner. Complete complex formation with $[^{99m}Tc(CO)_3(H_2O)_3]^+$ and histidine on the *n.c.a.* level was observed after 60 minutes at 75 ^{o}C, using ligand concentrations lower than 10^{-6} M. The ratio of the ligand to the metal at this concentration level is 1:1, which is ideal when

designing radiopharmaceutical drugs. Thus, labeling of biomolecules with the *fac*-$[M(CO)_3]^+$ core using a histidine like chelator would lead to the preparation of radiopharmaceutical drugs with high specific activity, which can be applied without separation or purification from unlabeled material.

A major advantage of using *fac*-$[M(CO)_3(H_2O)_3]^+$ precursor in labeling is the wide variety of ligands which binds efficiently to the *fac*-$[M(CO)_3]^+$ core. The resulting complexes are generally stable and do not decompose *in vivo*. Different ligands have been used with hydrides,[111] carboranes[112,113,114] and cyclopentadienyl[115,116] being the more uncommon ones reported in literature. Many combinations of mono-, bi- and tridentate ligands are possible but the most versatile are tridentate ligands.[117] The synthesis can be done at low biomolecule concentration but heating is required to achieve quantitative yields. Our approach is to utilize Schiff-base ligand system in the mixed [2+1] concept, to substitute the three labile water molecules on the metal centre and coordinate to the *fac*-$[M(CO)_3]^+$ core.

2.12 Schiff-Base Ligands

Schiff-bases are condensation products of the reaction between primary amines and carbonyl compounds (aldehydes and ketones). The reaction can be acid-catalyzed but is not always necessary as the product forms in quantitative amounts within a reasonable time scale. Furthermore, the water that forms as a by-product can be removed from this reversible reaction to ensure maximum possible yields. Schiff-bases are one of the most extensively used ligand system because of their relative ease of formation and react with most transitional metals to form stable complexes.[118] These compounds possesses a common structural feature, the azomethine group with a general formula RHC=N-R1, where R and R1 are alkyl, aryl, cyclo alkyl or heterocyclic groups which may be varied. The choice of the appropriate amine and various

[111] R. Garcia, A. Paulo, A. Domingos, I. Santos, K. Ortner, R. Alberto, *J. Am. Chem. Soc*., 2000, 122, 11240.
[112] J. F. Valliant, O. O. Sogbein, P. Morel, P. Schaffer, K. J. Guenther, A. D. Bain, *Inorg. Chem*., 2002, 41, 2731.
[113] A. E. C. Green, L. E. Harrington, J. F. Valliant, *Can. J. Chem*., 2008, 86, 1063.
[114] A. E. C. Green, S. K. Parker, J. F. Valliant, *J. Organomet. Chem*., 2009, 694, 1736.
[115] J. Wald, R. Alberto, K. Ortner, L. Candreia, *Angew. Chem. Int. Ed*., 2001, 40, 3062.
[116] Y. Liu, B. Spingler, P. Schmultz, R. Alberto, *J. Am. Chem. Soc*., 2008, 130, 1554.
[117] R. Alberto, J. K. Pak, D. van Staveren, S. Mundwiler, P. Benny, *Biopolymers*, 2004, 76, 324.
[118] G. J. J. Steyn, A. Roodt, I. A. Poletaeva, Y. S. Varshavsky, *J. Organomet. Chem*., 1997, 536-537, 197.

substituents on the aromatic ring of the carbonyl precursor allows for great versatility and fine tuning of the steric and electronic properties.The C=N functionality makes Schiff bases excellent chelating agents, especially when a functional group like –OH or –SH is present close to the azomethine group to form a five or six membered ring with transition metal ions.[119]

Schiff-bases usually exhibit tautomerism between the phenol-imine and the keto-amine forms O—H···N and O···H—N. Salicylaldimines often gives the O—H···N tautomer.[120] Schiff-base ligands have interesting photo-physical properties as thermochromism and photochromism,[121] such as N-Salicylideneaniline which displays reversible photoreactivity and crystallizes as both non-planar and planar polymorphs,[119,122] In studies concerning quantitative structure-antitumor activity relationship of a number of Schiff-bases made from different substituted aromatic amines and aldehyde, it was shown that azomethines from salicylaldehydes gave the best correlation.[123,124]

A large number of rhenium and technetium Schiff-base complexes have been reported over the years.[125] Most of these ligands are however coordinated to Re(V) and ^{99}Tc(V)[126,127,128] because of the integral part played by the $[M=O]^{3+}$ core in radiopharmaceutical design. Schiff-bases with a salicylidene backbone have also been used with rhenium and technetium, but are mostly coordinated to Re(III), (V) and ^{99}Tc(III), (V).[129,130,131,132] To the best of our knowledge, only four similar[133,134] and three related[135] Re(I) salicylidene tricarbonyl complexes could be found in

[119] C. M. Metzler, A. Cahill, D. E. Metzler, *J. Am. Chem. Soc*., 1980, 102, 6075.
[120] F. Arod, M. Gardon, P. Pattison, G. Chapuis, *Acta Cryst*., 2005, C61, o317.
[121] S. Gakias, C. Rix, A. Fowless, G. Wills–Johnson, K. Latham, J. White, *J. Mol. Struct*., 2005, 737, 69.
[122] F. Arod, P. Pattison, K. J. Schenk, G. Chapuis, *Cryst. Growth Des*., 2007, 7, 1679.
[123] E. M. Hodnett, W. J. Dunn, *J. Med. Chem*., 1970, 13, 768.
[124] E. M. Hodnett, P. D. Mooney, *J. Med. Chem*., 1970, 13, 786.
[125] Cambridge Structural Database (CSD), Version 5.35, November 2013 update.
[126] S, Jurisson, L. F. Lindoy, K. P. Dancey, M. McPartlin, P. A. Tasker, D. K. Uppal, E. Deutsch, *Inorg. Chem*., 1984, 23, 227.
[127] P. D. Benny, C. L. Barnes, P. M. Piekarski, J. D. Lydon, S. S. Jurisson, *Inorg. Chem*., 2003, 42, 6519.
[128] P. D. Benny, J. L. Green, H. P. Engelbrecht, C. L. Barnes, S. S. Jurisson, *Inorg. Chem*., 2005, 44, 2381.
[129] V. Bertolasi, M. Sacerdoti, G. Gilli, U. Mazzi, *Acta Cryst*., 1982, B38, 424.
[130] A. Duatti, A. Marchi, S. A. Luna, G. Bandoli, U. Mazzi, F. Tisato, *J. Chem. Soc., Dalton Trans*., 1987, 867.
[131] G. Bandoli, U. Mazzi, H. J. Pietzsch, H. Spies, *Acta Cryst*., 1992, C48, 1422.
[132] I. N. Booysen, T. I. A. Gerber, P. Mayer, *Inorg. Chim. Acta*, 2010, 363, 1292.
[133] J. W. Faller, G. Mason, J. Parr, *J. Organomet. Chem*., 2001, 626, 181.
[134] Z. K. Li, Y. Li, L. Lei, C. M. Che, X. G. Zhou, *Inorg. Chem. Commun.*, 2005, 8, 307.
[135] R. Czerwieniec, A. Kapturkiewicz, R. Anulewicz-Ostrowska, J. Nowacki, *J. Chem. Soc., Dalton Trans*., 2002, 3434.

literature before the structures reported by Ju *et al.*[136] and Brink *et al.*[137,138,139,140] Our group is interested in the coordination chemistry of Schiff-base ligands to the *fac*-$[M(CO)_3]^+$ core towards radiopharmaceutical design because of the little research that has been done on this type of complexes and due to the manipulative capabilities of the ligand system.

2.13 Conclusion

When a compound is labeled with a radioactive isotope such as ^{99m}Tc or $^{186/188}$Re, the metal complex should be kept small in size and its physico-chemical properties should adopt those of the biomolecule. Apart from the chemical requirements, a number of other stringent limitations have to be taken into consideration when designing a radiopharmaceutical for routine clinical application. The preparation must be a one-step synthesis yielding a product with a very high purity (preferably 98 % yield), the biomolecule concentration should be 1:1 with respect to the radionuclide and the preparation should not exceed a certain time, depending on the half-life of the radionuclide. Therefore, any preparation has to be done in saline solution (0.9 % NaCl in water or buffer) and no purification should be needed.[84]

The above mentioned limitations, especially the preparation that has to be done in aqueous medium, made the introduction of the *fac*-$[M(CO)_3]^+$ (M = $^{186/188}$Re, ^{99m}Tc) core into nuclear medical application rather unattractive. The cores that have being prominent in metal based radiopharmaceutical agents over the years include $[M{=}O]^{3+}$, $[O{=}M{=}O]^+$ and $[M{\equiv}N]^{2+}$ (M = $^{186/188}$Re, ^{99m}Tc). The novel mild reaction conditions described by Alberto for preparing the all-important, *fac*-$[M(CO)_3(H_2O)_3]^+$ precursor, opened new possibilities for future development of metal based radiopharmaceutical agents bearing the *fac*-$[M(CO)_3]^+$ core. This complex is suited in nuclear medical application because of its stable *fac*-$[M(CO)_3]^+$ core in water and the relatively labile water molecules that can be substituted by other free ligands. The *fac*-$[M(CO)_3(H_2O)_3]^+$ complex accepts and forms stable complexes with a wide variety of mono-, bi- and tridentate ligands.

[136] C. C. Ju, A. G. Zhang, H. L. Sun, K. Z. Wang, W. L. Jiang, Z. G. Bian, C. H. Huang, *Organomet.*, 2011, 30, 712.
[137] A. Brink, H. G. Visser, A. Roodt, *J. Coord. Chem.*, 2011, 64, 122.
[138] A. Brink, H. G. Visser, A. Roodt, *Polyhedron*, 2013, 52, 416.
[139] A. Brink, H. G. Visser, A. Roodt, *Inorg. Chem*., 2013, 52, 8950.
[140] A. Brink, H. G. Visser, A. Roodt, *Inorg. Chem*., 2014, 53, 12480.

CHAPTER 2

This study focused on utilizing Schiff-base ligands in the mixed [2+1] concept for labeling of *fac*-$[M(CO)_3]^+$ complexes. Schiff-bases are one of the most widely used ligand system due to their relative ease of formation and because they form stable complexes with most transition metals. Our particular interest in Schiff-base ligand system was prompted by the fact that they can easily be manipulated. A wide variety of mono-, bi- and tridentate Schiff-base ligands with varying steric and electronic properties afforded by the substituent bonded to the nitrogen imine donor atom can be synthesized depending on the choice of the starting material (carbonyl compound and the amine). Chapter 4 describes in details the synthetic approach towards the Schiff-base ligands used in this study and how they were coordinated to the metal center to form the final complexes. Chapter 3 describes the spectroscopic techniques that were used to fully characterize and confirm the formation of the ligands and complexes synthesized in chapter 4.

3 Theoretical Aspects of Characterization Techniques (IR, UV-Vis, XRD, ^{1}H and ^{13}C NMR)

3.1 Introduction

In chemistry, newly synthesized compounds must be fully characterized to know the exact composition of the compound. Several characterization methods can be used in this regard and are divided into two groups, namely destructive and non-destructive techniques. Destructive methods include inductively coupled plasma (ICP), elemental mass (MS), atomic absorption (AA) and gas chromatography (GC). These methods are utilized in cases where a large amount of the sample is available for characterization. Non-destructive methods consist of infrared (IR) spectroscopy, nuclear magnetic resonance (NMR) spectroscopy, ultraviolet-visible (UV-Vis) spectroscopy as well as X-ray diffraction (XRD) crystallography, and are generally used in cases where small amounts of the sample is available for characterization.

Characterization of all the rhenium(I) salicylidene tricarbonyl complexes synthesized in this study was performed using the non-destructive methods. Five of the obtained complexes were characterized by X-ray diffraction (XRD). X-ray diffraction crystallography is a very powerful technique used in the characterization of complexes in their solid state and clearly shows the coordination of ligands around the metal center. The basic theory of the techniques used to characterize the ligands and complexes synthesized in this study will be discussed hereafter.

3.2 Spectroscopic Techniques

3.2.1 Infrared Spectroscopy

Infrared (IR) Spectroscopy is a valuable analytical tool used by scientists in the qualitative and quantitative identification of compounds and functional groups. This technique is however not effective when used alone since almost all organic and inorganic compounds containing covalent bonds, except homonuclear compounds such as H_2, N_2 and Cl_2, absorb infrared radiation. All

molecular compounds, except chiral compounds in the crystalline state, have a unique infrared spectrum.

The infrared region is situated between the visible and microwave regions on the electromagnetic spectrum and consists of a wavelength range that extends from 14 000-10 cm^{-1}. The infrared wavelength range is divided into three regions, namely near infrared region (14 000-4 000 cm^{-1}), mid infrared region (4 000-400 cm^{-1}) and far infrared region (400-10 cm^{-1}). The most important region for chemical analysis is mid infrared region while the far infrared region is mainly used for the analysis of inorganic compounds containing heavy metals.

The energy of infrared radiation is capable of exciting vibrational and rotational transitions but is not sufficient to induce electronic transitions. For every vibrational state, splitting of the peaks occur with change in rotational energy. This rotation is often hindered or prevented in solution and solid state, which causes the effects of these small energy differences to be undetected. Thus, a typical infrared spectrum originates in transitions between two vibrational levels of the molecule in the electronic ground state and is normally observed as an absorption spectrum.[1] Two types of molecular vibrations can occur, namely stretching and bending.

When a compound absorbs infrared radiation, the molecules are excited to a higher energy state. The energy of infrared radiation can only be absorbed by molecules if it corresponds to the natural stretching and bending vibrational frequencies of the molecule. The absorbed energy increases the amplitude of the vibrational motions of the bonds in the molecule.[2] Bonds that have a dipole moment that changes as a function of time can absorb infrared radiation while symmetrical bonds of H_2 or Cl_2 do not absorb infrared radiation. The energy of infrared radiation can only be transferred when a bond possesses an electrical dipole that changes at the same frequency as the incoming radiation.

Each type of bond has a unique natural frequency of vibration. When the same type of bond (*e.g.* C≡O) is present in two different compounds, the infrared frequency will be chemically different, because the bonds experience two slightly different environments. Thus, the infrared spectrum of each different molecule is unique and can be used to identify different compounds.

[1] D. A. Skoog, D. M. West, F. J. Holler, S. R. Crouch, *Fundamentals of Analytical Chemistry*, 8th Ed., 2004.
[2] K. Nakamoto, *Infrared Spectra of Inorganic and Coordination Compounds*, 2nd Ed., New York, John Wiley & Sons, Inc., 1970.

The carbonyl group is permanently polarized because of the difference in electro-negativity between the carbon and oxygen atoms. Any vibrational stretching of this C≡O bond will affect the dipole moment. The carbonyl stretching has a distinct absorption peak on the infrared spectrum and is often used for complex characterization.[3]

General carbonyl stretching and bending frequencies are observed in the range 2360-1080 cm^{-1}, while the stretching frequencies of metal carbonyl complexes (M-CO) are observed in the range 2200-1700 cm^{-1} on the infrared spectrum.[2] The carbonyl stretching frequency, $\nu_{(CO)}$, is highly sensitive to the groups bonded to the central metal ion. Generally, electron rich ligands will result in a lower carbonyl stretching frequency value in the infrared spectrum while electron poor ligands will result in a higher carbonyl stretching frequency value. Strong σ-donor ligands (see Figure 3.1) donate electron density to the metal which increases the electron back-donation from the metal into the M-CO bond. This strengthens the M-CO bond, weakens the C≡O bond and consequently decreases the carbonyl stretching frequency value.

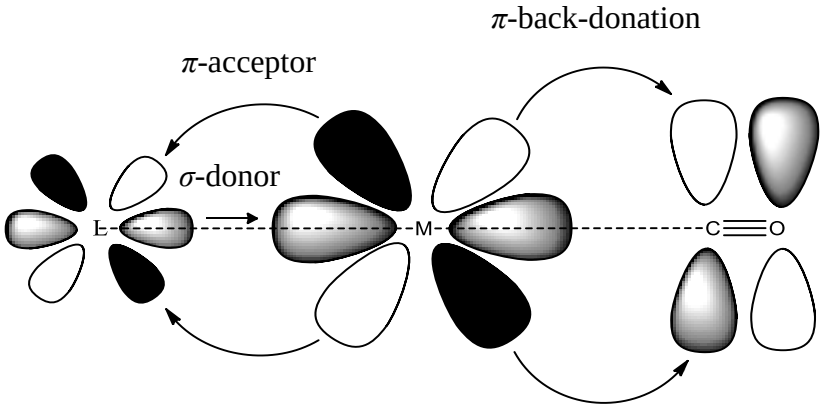

Figure 3.1: Strong σ-donor ligands increase the electron density around the metal and strengthen the M-CO bond through π-back-donation.

3.2.2 Ultraviolet-Visible Spectroscopy

Ultraviolet-visible (UV-Vis) spectroscopy is a helpful technique used primarily for quantitative analysis and following the formation or disappearance of different colored reactions.[4] The

[3] B. Stuart, *Modern Infrared Spectroscopy*, Ed.: D. J. Ando, John Wiley & Sons, Ltd., England,1996.
[4] C. N. R. Rao, *Ultra-violet and Visible Spectroscopy*: *Chemical Applications*, 2nd Ed., Butterworth and Co. Ltd., England, 1967.

ultraviolet (UV) region wavelength varies between 190–380 nm on the electromagnetic spectrum while the visible (Vis) region ranges between 380–750 nm. The wavelength of the majority of commercially available spectrophotometers ranges between 185–900 nm.[5] When a compound absorbs the energy of ultraviolet-visible radiation, its atoms or molecules pass from a lower energy (ground state) to a higher energy (excited state). The energy (ΔE) of the absorbed electromagnetic radiation is equal to the energy difference between the excited and ground state as shown in Figure 3.2. h is Planck's constant (6.626×10^{-34} J.s.) and v is the frequency of vibration.

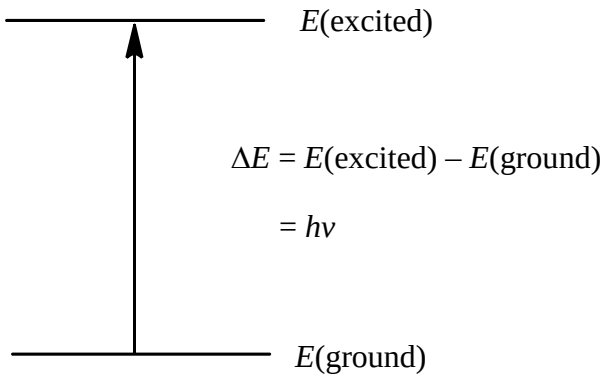

Figure 3.2: An illustration of the excitation of electrons from a lower energy (ground state) to a higher energy (excited state) as a result of energy absorption.

In ultraviolet-visible spectroscopy, the absorption of electromagnetic radiation energy by a compound causes transitions between electronic energy levels. The main types of electronic transitions that can occur include, transitions involving single (σ) bonding, double or triple (π) bonding and non-bonding (n, lone pair electrons) orbitals. When a molecule absorbs energy, its valence electrons are excited from the highest occupied molecular orbital (HOMO) to the lowest unoccupied molecular orbital (LUMO) as illustrated in Figure 3.3.

[5] F. Rouessac, A. Rouessac, *Chemical Analysis: Modern Instrumentation Methods and Techniques*, 2nd Ed., John Wiley & Sons, New York, 2007.

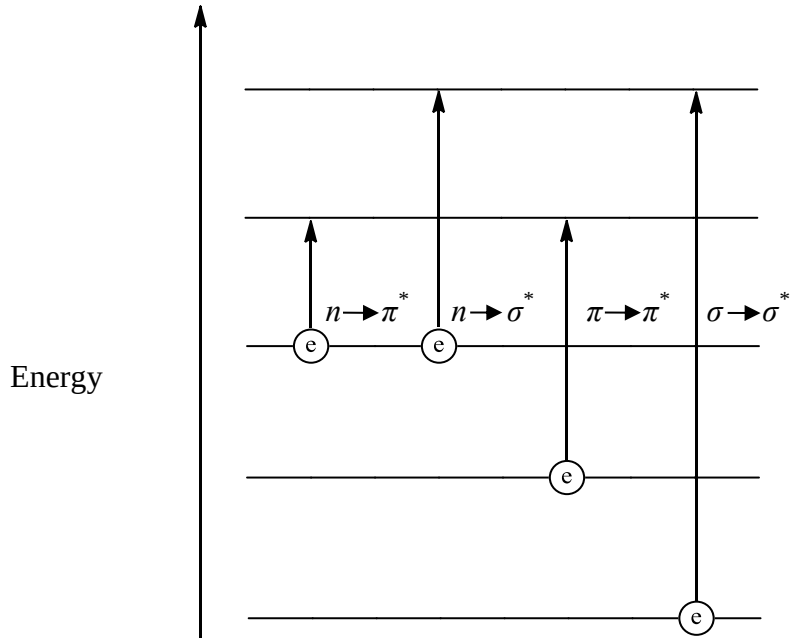

Figure 3.3: An illustration of electronic transitions from HOMO (σ-bonding, π-bonding and n-non-bonding) to LUMO (σ^*-anti-bonding and π^*-anti-bonding).

In the ultraviolet-visible region, interactions of photons with valence or lone pair electrons results in the absorption of energy by molecules. The wavelength at which the molecules will absorb the energy depends on how tight its electrons are bound to the atom. Electrons involved in double or triple bonds are loosely bound to the atom, and can easily be excited by electromagnetic radiation to give characteristic absorption peaks.

3.2.3 Nuclear Magnetic Resonance Spectroscopy

Nuclear magnetic resonance (NMR) spectroscopy is a powerful analytical tool available to modern science. NMR gives detailed information of chemical structures based on the quantum mechanical magnetic properties of the atom's nucleus. NMR is widely used in various fields such as chemistry, physics and biology as well as in living biological material for medical diagnosis (magnetic resonance imaging, MRI). The basic principles of NMR was first described and measured in molecular beams by Isidor Rabi in 1938.[6] The technique was later modified and improved by Felix Bloch and Edward Mills Purcell in 1946 and used it on liquids and solids. The duo shared a Nobel Prize in physics in 1952.

[6] I. I. Rabi, S. Millman, P. Kusch, J. R. Zacharias, *Phys. Rev.*, 1939, 55,526.

Magnetic nuclei, like ^{1}H, ^{13}C, ^{15}N, ^{19}F, ^{29}S and ^{31}P, absorbs radio frequency energy when placed in a magnetic field of a strength that is specific to the identity of the nuclei. When this absorption occurs, the nucleus is described as being in resonance. Different atoms within a molecule resonate at a particular frequency in the radio frequency range. From the small variations in the resonant frequency, detailed information about the molecular structure in which the atoms are located can be obtained.[7]

Electrons, neutrons and protons are considered to possess spinning properties and when these spins are paired against each other, the overall spin of the atom can be determined. The rules for determining the net spin of a nucleus are as follows:

- If the number of neutrons and the number of protons are both even, the nucleus has no spin.
- If the number of protons plus the number of neutrons is odd, the nucleus has a half-integer spin (1/2, 3/2, 5/2).
- If the number of neutrons and the number of protons are both odd, the nucleus has an integer spin (i.e. 1, 2, 3).
- Nucleus with spin quantum numbers greater than 1/2 generally give broad NMR lines[8]

The ^{1}H NMR spectra is produced from protons in a molecule that exist in slightly different chemical and hence electronic environments from one another. As a result, the protons absorb different frequencies. The effective magnetic field experienced by the nucleus is less than the applied magnetic field because of the shielding caused by the electrons around the nucleus. If the electron density around the nucleus is high, the magnetic field felt by the nucleus is stronger due to the electrons. The reverse is true if the electron density decreases. Deshielding occurs due to electron withdrawing groups and shielding results from electron donating groups. These varying resonance frequencies result in different signals known as chemical shifts, δ, observed on the NMR spectrum.

A proton can be affected by the presence of the magnetic field of a nearby proton or equivalent protons. This results in magnetic interactions between the nuclei of the protons, an effect known

[7] N. E. Jacobsen, *NMR Spectroscopy Explained*, John Wiley & Sons, New Jersey, 2007.
[8] P. J. Hore, *Nuclear Magnetic Resonance*, Oxford University Press, Inc., New York, 1995.

as spin-spin coupling, whereby the multiplicity in the resonance frequency of the first proton is given by the number of equivalent protons in neighboring atoms plus one (n + 1). The distance between the peaks of the split frequency is indicated by the coupling constant, J, and is measured in Hertz (Hz).[9]

^{13}C NMR is analogous to ^{1}H NMR and is used in many industrial applications such as quantification of drug purity and the determination of the composition of polymers. This technique allows for the identification of carbon atoms in a molecule by detecting the ^{13}C isotope, which has a natural abundance of 1.1 %. The ^{12}C isotope is not detected because it has a zero spin state. A few differences exist between ^{1}H and ^{13}C NMR:

- The intensity of a signal is not proportional to the number of equivalent ^{13}C atoms, but is dependent on the number of surrounding spins.
- The chemical shifts in ^{13}C NMR range between 0-220 ppm, while the range in ^{1}H NMR extends from 0-13 ppm.
- Coupling between protons occur in ^{1}H NMR, whereas coupling between carbons can be ignored in ^{13}C NMR, because of the relatively low natural abundance of ^{13}C isotope.
- In the spectrum ^{1}H NMR, multiplets are shown for each proton, but a typical ^{13}C NMR shows single peaks for each chemically non-equivalent carbon atom.

3.3 Theory of X-ray Diffraction

3.3.1 Introduction

Mineralogy, the study of naturally occurring chemical compounds, gave birth to the field of crystallography. The term crystal was derived from a Greek word *krystallos*, which means ice. X-ray diffraction is an extremely precise technique used to identify the exact molecular structures within a crystalline lattice. This method is used to determine the arrangement of atoms within a crystal when a beam of X-rays is irradiated onto a crystal sample and scatters into many different directions. From the angles and intensities of these scattered beams, it is possible to produce a three-dimensional picture of the electron density around the atoms in the crystal. From

[9]E. Breitmaier, G. Bauer, *^{13}C NMR Spectroscopy*, Vol. 3, Harwood Academic Publishers, London, 1984.

the electron density, the mean positions of the atoms in the crystal can be determined, as well as their chemical bonds and disorders.[10]

3.3.2 X-ray Diffraction

X-rays were discovered by C. W. Röntgen in 1895, but their scattering character by the atoms within a crystal was discovered by a German physicist, Max von Laue in 1912. This discovery made it possible to observe a crystal on the inside and obtain complete information on the structure and the size of the unit cell. Scientists believed that X-rays were a form of electromagnetic radiation by the observation made from the diffraction pattern of X-ray beams.[11] In 1922, the photon model was confirmed by the study of scattering of X-rays from electrons, which resolved all remaining doubt about the nature of X-rays.[12]

Spectroscopic techniques such as NMR and IR give information on the structure of a molecule according to a manner in which it absorbs or emits radiation. X-ray crystallography measures the variation in intensity with direction, in terms of the scattering of monochromatic radiation. X-rays are electromagnetic radiation with a short wavelengths (2×10^{-2}-100 Å) that is comparable to the size of atoms. Thus, an incoming beam of X-rays can be scattered by each atom in a crystal. The scattered electromagnetic radiation can add constructively or destructively depending on the direction of the diffracted beam and the atomic positions.[13] Diffraction or interference effects cause these intensity variations which create complex scattering patterns that can be analyzed quantitatively. From the scattered X-rays, it is possible to derive the position of each atom in the crystal.[14]

To simplify a crystal structure, each atom is represented by a single point, resulting in a regular array of points. The lattice of the structure is known as the array of identical points which are equivalent to each other by translation symmetry. A unit cell is the characteristic portion of the crystal, from which the entire part of the crystal can be reproduced, if it is repeated indefinitely

[10] S. A. Nelson, *X-Ray Crystallography*, 2008. Available: http://www.tulane.edu/~sanelson/eens211/x-ray.htm. Last accessed 25/11/2008.
[11] W. Friedrich, P. Knipping, M. von Laue, *Interferenz-Erscheinungenbie Rontgenstrahlen*, 1912.
[12] A. Compton, *Physical Review*, 21, 483, 1923.
[13] M. F. C. Ladd, R. A. Palmer, *Structure Determination by X-ray Crystallography*, Plenum Press, New York, 1977.
[14] W. Clegg, *Crystal Structure Determination*, Oxford University Press, Inc., New York, 1998.

in the direction of the crystal axes.[15] The lattice is made up of many unit cells, consisting of three sides (*a, b, c*) and three angles (α, β, γ). Crystal symmetry can be divided into the seven crystal systems. There are 230 possible three dimensional patterns or space groups which describes the symmetry of a unit cell. These space groups are listed in the *International Tables for Crystallography*.[16] Miller indices (*h, k, l*) are used to describe the directions and planes in a crystal lattice.

An overall diffraction pattern results from the X-rays that are being scattered by each atom in a crystal. To obtain a complete pattern, the crystal is rotated in the X-ray beam, with a detector producing two dimensional electron density maps for each angle of rotation. In a crystal, the atoms are arranged in highly ordered and repeating manner in three dimensions. This increases the signal to a more measurable level. The diffraction pattern consists of spots of different intensity that have three properties corresponding to three properties of the crystal structure:

- The pattern has a specific geometry and is related to the lattice and unit cell geometry of the crystal structure.
- The pattern has symmetry which is related to the symmetry of the unit cell of the crystal structure.
- The pattern has different intensities that reveal information about the position of the atoms in the unit cell.[14]

Max von Laue regarded crystals in terms of a three-dimensional network of rows of atoms that behaves like a three-dimensional diffraction grating. This led to the development of three Laue equations.[17] Although his equations are accurate, they are complicated to calculate. In order for constructive interference to occur simultaneously from all three atom rows, all three Laue equations must be satisfied simultaneously. An alternative equation to the complex von Laue's equations was derived by W. L. Bragg in 1912 and is known as Bragg's Law.[13]

[15] D. W. A. Sharpe, *The Penguin Dictionary of Chemistry*, 3rd Ed., Penguin Books Ltd., London, 2003.
[16] *International Tables for Crystallography*, Vol. A, 5th Ed., Kluwer Academic Publishers, Netherlands, 2002
[17] C. Hammond,*The Basics of Crystallography and Diffraction*, 2nd Ed., Oxford University Press, Inc., New York, 2001.

3.3.3 Bragg's Law

Bragg's law defines the conditions under which diffraction can occur and gives the position of a diffracted beam without any reference to its intensity.[18] When X-rays are diffracted by crystals, they act as though they were reflected by "atomic mirror planes" within the crystal. Not all parts of the X-ray beam may be reflected at a given crystal plane, some penetrate deeper into the crystal and undergo a similar process at another plane deep in the crystal as illustrated by Figure 3.7. All X-rays reflected from the same plane remain in phase after reflection, while the X-rays reflected from neighboring planes are out of phase after reflection because they have travelled different path lengths. Bragg's law is used to correct these differences in phase:

$$n\lambda = d_{hkl} sin\theta \tag{3.1}$$

where n is an integer, λ is the wavelength of the X-rays, d_{hkl} is the interplanar distance between the (hkl) planes and θ is the diffraction angle (Bragg angle).

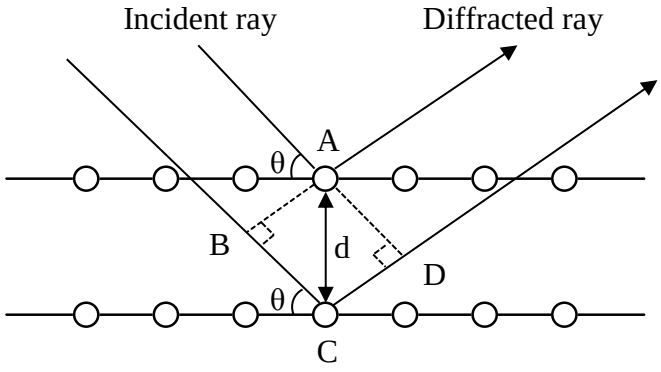

Figure 3.7: Scattering of X-rays by atoms as proposed by Bragg.

3.3.4 Structure Factor

The structure factor, $F(hkl)$, of any diffracted X-ray is the quantity that expresses both the amplitude, $|F(hkl)|$ and the phase angle, $\Phi(hkl)$ of that reflection. The amplitude of the structure factor is directly related to the intensity of a diffracted beam, but the phase must be calculated by indirect means. In structure determination, phases are estimated and an initial description of the positions and anisotropic displacements of the scattering atoms is deduced. From this initial

[18] D. Sherwood, J. Cooper, *Crystals, X-ray's and Proteins: Comprehensive Protein Crystallography*, Oxford University Press, New York, 2011.

model, structure factors are calculated and compared with those experimentally observed. The total scattering of all the atoms in the unit cell is given by the following equation:[13]

$$F(hkl) = = \sum_{j=1}^{N} f_j exp[i2\pi(hx_j + ky_j + lz_j)] \quad (3.2)$$

where f_j is the scattering factor of each of the N atoms.

The X-ray diffraction pattern created when X-rays are scattered by the electrons surrounding an atom in a crystal can be used to determine the crystal structure. Atoms with high atomic numbers provide a greater concentration of electrons than do atoms of low atomic numbers. This concentration of electrons and its distribution around the atom is called the electron density, ρ. Since the density of the electrons is a function of position, it can be specified at a point X, Y, Z as $\rho(X, Y, Z)$. The electron density can be expressed in terms of the structure factor as follows:[19]

$$\rho(x, y, z) = \frac{1}{V}\sum_h \sum_k \sum_l F(hkl) e^{-i2\pi(hx+ky+lz)} \quad (3.3)$$

where V is the volume of the unit cell.

3.3.5 The "Phase Problem"

To determine a crystal structure from the combined diffracted X-ray beams, both the amplitude and phase of each beam must be known. As previously mentioned, the amplitude, $|F(hkl)|$, can be determined from the intensity of the diffracted beam, while the corresponding phase angle, $\Phi(hkl)$ is not directly measurable. This inability to determine the phase is known as the 'Phase Problem'. The two most common methods used to overcome this problem include the direct method and Patterson function.

3.3.5.1 Direct Method

The direct method resolves the approximate reflection phases from measured X-ray intensities utilizing mathematical formulae.[20] This method is favored when solving crystal structures

[19] G. H. Stout, L. H. Jensen, *X-ray Structure Determination: A Practical Guide*, Macmillan Company, London,1968.
[20] J. Als-Nielsen, D. McMorrow, *Elements of Modern X-ray Physics*, 2nd Ed., John Wiley & Sons, West Sussex, 2011.

consisting only of light atoms, while the Patterson function is favored when solving crystal structures that contain a heavy atom.

3.3.5.2 Patterson Function

The Patterson Function, $P(u, v, w)$, looks like an electron density map with peaks of positive electron density in various positions.[21] These are not the positions of atoms in the structure. The Patterson Function is a map of vectors between pairs of atoms in the structure. In a Patterson cell, the coordinates are *u*, *v* and *w* with dimensions identical to the real cell. The Patterson peaks show where atoms lie relative to each other, but not relative to the unit cell origin.

$$P(u, v, w) = \frac{1}{V}\sum_h \sum_k \sum_l |F(hkl)|^2 \, exp[-i2\pi(hu + kv + lw)] \tag{3.4}$$

3.3.6 Least Squares Refinement

The least-squares refinement compares the calculated structure factor $|Fc|$ to the experimental data and the observed structure factor $|Fo|$. If the atoms of the model structure are in the approximate correct positions, then there should be a degree of resemblance between the calculated diffraction pattern and the observed one. This comparison is described in terms of the residual index or *R*-factor as follows:

$$R = \frac{\sum \big||F_0| - |F_c|\big|}{\sum |F_0|} \tag{3.5}$$

The value of the *R*-factor for a correct and complete crystal structure as determined from well measured experimental data is around 0.02-0.07.[22] A residual factor which is widely used for crystal structure determination uses F^2 values instead of $|F|$ values and incorporates the weight, *w*, of each reflection as indicated by equation 3.6. This is a more meaningful factor from a statistical point of view than the basic *R*-factor.[15]

$$wR2 = \sqrt{\frac{\sum w(F_0^2 - F_c^2)^2}{\sum \left(F_0^2\right)^2}} \tag{3.6}$$

[21] J. Drenth, *Principles of Protein X-ray Crystallography*, 2nd Ed., Springer, New York, 1999.
[22] J. P. Gluster, M. Lewis, M. Rossi, *Crystal Structure Analysis for Chemist and Biologists*, John Wiley & Sons, New York, 1994.

4 Synthesis of Schiff-base Ligands and Re(I) Tricarbonyl Complexes

4.1 Introduction

Tricarbonyl aqua complexes of the type *fac*-$[M(CO)_3(H_2O)_3]^+$ (M = $^{186/188}$Re, ^{99m}Tc) have displayed numerous attractive attributes over the past 20 odd years as precursors for the development of new metal based radiopharmaceutical agents.[1,2] These complexes consist of two important features. The *fac*-$[M(CO)_3]^+$ core[3] is generally known to be kinetically inert and stable towards dissociative ligand loss or associative substitution by other ligands. The coordinated water molecules on the other hand are relatively labile and can be readily substituted by a range of mono-, bi- and tridentate ligands. A number of biomolecules such as peptides and central nervous system (CNS) receptor ligands have already been labelled with technetium utilising the *fac*-$[^{99m}Tc(CO)_3(H_2O)_3]^+$ precursor.[3,4,5] Similarly, the methanol solvent coordinated to the *fac*-$[Re(CO)_3(MeOH)_3]^+$ precursor, can easily be substituted by other free ligands leading to the design of new model radiopharmaceuticals.[6] The similarity in the coordination chemistry of rhenium and technetium provides the opportunity to label biomolecules developed for technetium with rhenium and *vice versa*.

Three *N,O* ligands were synthesized by reacting 2-hydroxy-4-methylbenzaldehyde with three different amines *via* a Schiff-base reaction and are shown in Figure 4.1. 5Me-SalH-iProp (**1)** and 5Me-SalH-CyPent **(2)** are bidentate ligands while 5Me-SalH-Hist **(3)** is a tridentate ligand. The amines were chosen due to their varying electronic and steric character. The ligands were coordinated to the *fac*-$[Re(CO)_3(MeOH)_3]^+$ intermediate *in-situ* to form the final complex. In the case of the bidentate ligands, 5Me-SalH-iProp **(1)** and 5Me-SalH-CyPent **(2)**, the coordinated methanol solvent on the sixth position was substituted with either a pyridine

[1]R. Alberto, R. Schibli, U. Abram, B. Johannsen, H. J. Pietzsch, P. A. Schubiger, *J. Am. Chem. Soc*., 1999, 25, 6076.
[2] R. Waibel, R. Alberto, J. Willuda, R. Finnern, R. Schibli, A. Stichelberger, A. Egli, U. Abram, J. P. Mach, A. Plueckthun, P. A. Schubiger, *Nature Biotechnol.*, 1999, 17, 897.
[3] R. Alberto, R. Schibli, R. Waibel, U. Abram, P. A. Schubiger, *Coord. Chem. Rev*., 1999, 190-192, 901.
[4] R. Schibli, K. V. Katti, C. Higginbotham, W. A. Volkert, R. Alberto, *Nucl. Med. Biol.*, 1999, 26, 711.
[5] A. Egli, R. Alberto, L. Tannahill, R. Schibli, U. Abram, A. Schaffland, R. Waibel, D. Tourwe, L. Jeannin, K. Iterbeke, P. A. Schubiger, *J. Nucl. Med.*, 1999, 40, 1913.
[6] A. Brink, H. G. Visser, A. Roodt, *J. Coord. Chem.*, 2011, 64, 122.

or an imidazole ligand as it proved to be rather challenging to obtain single crystals of the methanol substituted product that were suitable for X-ray diffraction.

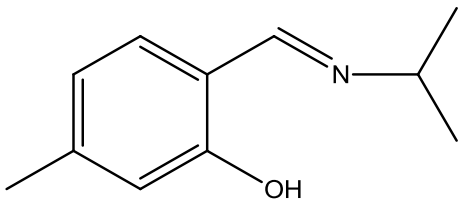

(1)

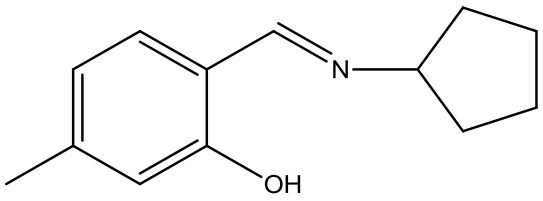

(2)

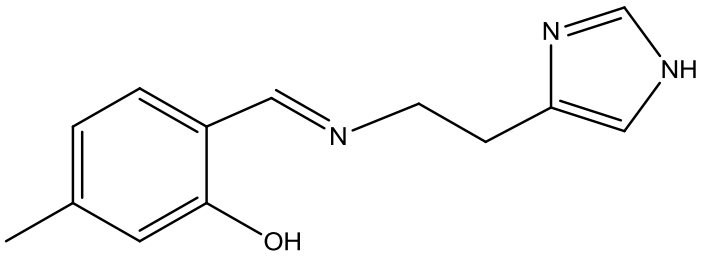

(3)

Figure 4.1: Schiff-base ligands synthesized during this study. **(1)** 2-(isopropylimino)methyl-5-methylphenol, **(2)** 2-(cyclopentylimino)methyl-5-methylphenol, **(3)** 2-(2-imidazol-4-yl)ethyliminomethyl-5-methylphenol.

4.2 Reagents and Apparatus

All reagents and solvents used in this study were of analytical grade purchased from Sigma Aldrich unless stated otherwise. Reagents and solvents were used as received without any further purification. Rhenium pentacarbonyl bromide was purchased from Strem chemicals, Newburyport in USA. ^{1}H and ^{13}C FT-NMR spectra of the ligands and rhenium complexes were recorded on a Bruker AXS 300 or 600 MHz at 25 ^{o}C using the following deuterated solvents: Acetone-d_6 (2.05 and 29.92 ppm), Methanol-d_4 (3.31 and 49.15ppm) and $CDCl_3$ (7.26 and 77.16 ppm). The infrared spectra of *fac*-[Re(5Me-Sal-Hist)$(CO)_3$].MeOH complex was analysed on a Bruker Tensor 27 ATR spectrophotometer, while those of the other complexes were analysed as KBr pellets on a Bruker Tensor 27 spectrophotometer. UV-Vis spectra of the complexes were recorded using 1 cm quartz cuvette cells on a Varian Cary 50 Conc. UV-Visible Spectrophotometer equipped with a Julabo F12-mV temperature cell regulator, accurate within 0.1 ^{o}C.

4.3 Synthesis of Schiff-base Ligands

4.3.1 2-(Isopropylimino)methyl-5-methylphenol – 5Me-SalH-iProp (1)

Isopropylamine (0.228 g, 3.857 x 10^{-3} mol) dissolved in methanol (5 ml) was added drop wise to a methanol (10 ml) solution of 2-hydroxy-4-methylbenzaldehyde (0.501 g, 3.680 x 10^{-3} mol). The reaction mixture was refluxed on an oil bath pre-heated to 80 ^{o}C for 4.5 h. The solution was cooled to room temperature and the solvent evaporated to dryness under vacuum to give the product as a yellow powder. (Yield: 0.582 g, 89.2 %).

^{1}H NMR (300 MHz, Methanol-d_4) δ 8.37 (s, 1H, HC=N), 7.17 (d, J = 8.1 Hz, 1H, Ar), 6.60 (m, 2H, Ar), 3.65 (m, 1H, CH), 2.28 (s, 3H, CH_3), 1.31 (d, 6H, J = 6.3 Hz, 2xCH_3). ^{13}C NMR (600 MHz, $CDCl_3$) δ 161.87, 161.69, 143.06, 131.08, 119.67, 117.63, 116.62 (Ar), 59.99 (CH), 24.42 (2xCH_3), 21.97 (CH_3).

4.3.2 2-(Cyclopentylimino)methyl-5-methylphenol – 5Me-SalH-CyPent (2)

5Me-SalH-CyPent, was synthesized in a similar manner as 5Me-SalH-iProp in 4.3.1, using cyclopentylamine (0.313 g, 3.676 x 10^{-3} mol) and 2-hydroxy-4-methylbenzaldehyde (0.500 g, 3.672 x 10^{-3} mol) in methanol. The reaction mixture was refluxed for 3 h. Removal of the solvent under vacuum afforded the product as a yellow powder. (Yield: 0.697 g, 93.4 %).

^{1}H NMR (300 MHz, Methanol-d_4) δ 8.36 (s, 1H, HC=N), 7.16 (d, J = 7.8 Hz, 1H, Ar), 6.61 (m, 2H, Ar), 3.88 (m, 1H, CH), 2.28 (s, 3H, CH_3), 2.10-1.61 (m, 8H, C_4H_8). ^{13}C NMR (300 MHz, Methanol-d_4) δ 166.64, 164.46, 145.80, 133.08, 120.03, 119.47, 117.11 (Ar), 69.14 (CH), 35.66, 25.23 (CH_2), 22.05 (CH_3).

4.3.3 2-[(2-Imidazol-4-yl)ethyliminomethyl]-5-methylphenol – 5Me-SalH-Hist (3)

5Me-SalH-Hist, was synthesized in a similar manner as 5Me-SalH-iProp in 4.3.1, using histamine (0.408 g, 3.671 x 10^{-3} mol) and 2-hydroxy-4-methylbenzaldehyde (0.504 g, 3.702 x 10^{-3} mol) in methanol. The reaction mixture was refluxed for 3 h. The product was obtained as a yellow powder after the solvent was removed. (Yield: 0.732 g, 86.9 %).

^{1}H NMR (300 MHz, Methanol-d_4) δ 8.23 (s, 1H, HC=N), 7.60 (s, 1H, Ar), 7.11 (d, 1H, J = 7.8 Hz, Ar), 6.85 (s, 1H, Ar), 6.59 (m, 2H, Ar), 3.85 (t, 2H, J = 6.9 Hz, CH_2), 2.96 (t, 2H, J = 6.9 Hz, CH_2), 2.27 (s, 3H, CH_3). ^{13}C NMR (600 MHz, Methanol-d_4) δ 165.36, 165.08, 144.42, 134.78, 131.66, 119.38, 118.48, 117.87, 115.95, 115.55 (Ar), 56.34, 28.07 (CH_2), 20.49 (CH_3).

4.4 Synthesis of Re(I) Tricarbonyl Complexes

4.4.1 *fac*-$[Et_4N]_2[Re(CO)_3Br_3]$ (ReAA)

The title complex was synthesized as described by Alberto *et al*. (1996).[7] $[Et_4N]Br$ was ground to a fine powder in a mortar and pestle and dried overnight in an oven at 100 ^{0}C. A round bottom flask containing the dry $[Et_4N]Br$ (4.79 g, 22.8 mmol) was placed in an oil bath, pre-heated to 80 ^{o}C and 2,5,8-trioxanone diglyme (150 ml) was added under an argon atmosphere. The flask was flushed and evacuated three times with argon. The solution was stirred vigorously for 30 minutes. $[Re(CO)_5Br]$ (5.0 g, 12.3 mmol) was added and the flask was purged and evacuated three times. The reaction mixture was heated to 115 ^{o}C and stirred for 19 h. The reaction mixture was cooled to room temperature. The precipitate was filtered, washed twice with cold ethanol and twice with cold dichloromethane. The product was obtained as a white powder and was dried overnight in a desiccator over phosphorus pentoxide. (Yield: 8.39 g, 88.5 %).

IR (KBr, cm^{-1}): $\nu_{(CO)}$ 1999.4, 1867.1.

4.4.2 *fac*-[Re(5Me-Sal-iProp)$(CO)_3$(Pyridine)] (4)

5Me-SalH-iProp (0.0363 g, 2.048 x 10^{-4} mol, 1.05eq) dissolved in methanol (5 ml) was added drop-wise to a methanol (5 ml) solution of ReAA (0.150 g, 1.947 x 10^{-4} mol). The reaction mixture was stirred at 60 ^{o}C for 5 h. Pyridine (0.0154 g, 1.947 x 10^{-4} mol, 1eq) dissolved in methanol (5 ml) was added and the reaction stirred for a further 16 h. The solution was cooled to room temperature and allowed to evaporate slowly to give white* and yellow crystals suitable for X-ray diffraction. The title complex was identified as the yellow crystals. (Crystalline yield: 0.0195 g, 19.1 %).

[7] R. Alberto, R. Schibli, P. A. Schubiger, *Polyhedron*, 1996, 15, 1079.

IR (KBr, cm^{-1}): $\nu_{(CO)}$ 2014.3, 1906.8, 1879.5. UV-Vis (nm, L mol^{-1} cm^{-1}): λ_{max} = 381.0, ε = 3.598 x 10^3. ^{1}H NMR (600 MHz, Acetone-d_6) δ 8.71 (m, 2H, Ar), 8.39 (s, 1H, HC=N), 8.06 (tt, 1H, *J* = 1.8, 7.8 Hz, Ar), 7.58 (m, 2H, Ar), 7.12 (d, 1H, *J* = 8.4 Hz, Ar), 6.61 (s, 1H, Ar), 6.38 (d, 1H, *J* = 8.4 Hz, Ar), 4.32 (m, 1H, CH), 2.20 (s, 3H, CH_3), 1.30 (dd, 6H, *J* = 6.6 Hz, 2xCH_3), 3.51 (q, *J* = 7.2 Hz, Et_4N^+), 1.40 (tt, *J* = 1.8, 7.2 Hz, Et_4N^+). ^{13}C NMR (600 MHz, Acetone-d_6) δ 166.94, 164.56, 153.08, 146.40, 140.34, 136.46, 126.88, 122.78, 119.88, 117.41 (Ar), 67.76 (CH), 24.09, 23.50, 21.90 (CH_3).

* The white crystals were manually separated from the yellow crystals under a microscope to give the title complex as a pure product.

4.4.3 *fac*-[Re(5Me-Sal-CyPent)(CO)$_3$(MeOH)]

5Me-SalH-CyPent (0.0317 g, 1.559 x 10^{-4} mol, 1.2eq) dissolved in methanol (4 ml) was added drop-wise to a methanol (4 ml) solution of ReAA (0.100 g, 1.298 x 10^{-4} mol). The reaction was refluxed at 70 ^{o}C for 7.5 h. The solution was cooled and allowed to evaporate slowly at room temperature. Slow evaporation of the solvent afforded crystals not suitable for X-ray diffraction. (Crystalline yield: 0.0312 g, 47.7 %).

The complex could also be obtained as follows:

$AgNO_3$ (0.0662 g, 3.897 x 10^{-4} mol, 3eq) was added to a methanol (10 ml) solution of ReAA (0.101 g, 1.311 x 10^{-4} mol) and stirred for 25 h at 25 ^{o}C. AgBr precipitated and was removed by filtration. 5Me-SalH-CyPent (0.0318 g, 1.564 x 10^{-4} mol, 1.2eq) dissolved in methanol (2 ml) was added and the reaction refluxed at 70 ^{o}C for 16.5 h. Excess solvent was removed under vacuum before allowing the solution to evaporate slowly at room temperature. Slow evaporation of the solvent also afforded crystals not suitable for X-ray diffraction. (Yield: 0.0249 g, 37.7 %).

IR (KBr, cm^{-1}): $\nu_{(CO)}$ 1999.7, 1868.0. UV-Vis (nm, L mol^{-1} cm^{-1}): λ_{max} = 270.2, ε = 1.229 x 10^3. ^{1}H NMR (300 MHz, Acetone-d_6) δ 8.36 (s, 1H, Ar), 7.15 (d, 1H, *J* = 8.1 Hz, Ar), 6.70 (s, 1H, Ar), 6.51 (d, 1H, *J* = 8.1 Hz, Ar), 4.53 (m, 1H, CH), 3.35 (s, 3H, CH_3), 2.27 (s, 3H, CH_3), 2.17-1.67 (m, 8H, C_4H_8), 1.29 (tt, *J* = 1.8, 7.2 Hz, Et_4N^+).

4.4.4 *fac*-[Re(5Me-Sal-CyPent)(CO)$_3$(Pyridine)] (5)

$AgNO_3$ (0.0663 g, 3.903 x 10^{-4} mol, 3eq) was added to a methanol (10 ml) solution of ReAA (0.100 g, 1.298 x 10^{-4} mol) and stirred at 25 ^oC for 29 h. AgBr precipitated and was removed by filtration. 5Me-SalH-CyPent (0.0279 g, 1.372 x 10^{-4} mol, 1.05 eq) dissolved in methanol (5 ml) was added drop-wise and the reaction mixture refluxed at 70 ^oC for 14 h. Pyridine (0.0105 g, 1.327 x 10^{-4} mol, 1eq) dissolved in methanol (1 ml) was added and stirred for 5 minutes. Excess solvent was removed under vacuum before allowing the solution to evaporate slowly at room temperature. Slow evaporation of the solvent afforded yellow crystals suitable for X-ray diffraction. (Yield: 0.0147 g, 20.3 %).

The title complex could also be obtained in a similar manner as *fac*-[Re(5Me-Sal-iProp)(CO)$_3$(Pyridine)] in 4.4.2 using 5Me-SalH-CyPent (0.0395 g, 1.943 x 10^{-4} mol, 1eq), ReAA (0.150 g, 1.947 x 10^{-4} mol) and pyridine (0.0153 g, 1.934 x 10^{-4} mol, 1 eq) in methanol. The majority of the solvent was removed under vacuum before allowing the solution to evaporate slowly at room temperature. Slow evaporation of the solvent afforded white and yellow crystals suitable for X-ray diffraction. The title complex was identified as the yellow crystals. (Crystalline yield: 0.0198 g, 18.5 %).

IR (KBr, cm^{-1}): $\nu_{(CO)}$ 2008.9, 1899.1, 1859.1. UV-Vis (nm, L mol^{-1} cm^{-1}): λ_{max} = 384.0, ε = 1.852 x 10^3. ^{1}H NMR (300 MHz, Acetone-d_6) δ 8.69 (m, 2H, Ar), 8.37 (s, 1H, HC=N), 8.05 (tt, 1H, *J* = 1.5, 7.8 Hz, Ar), 7.56 (m, 2H, Ar), 7.10 (d, 1H, *J* = 7.8 Hz, Ar), 6.60 (s, 1H, Ar), 6.36 (d, 1H, *J* = 7.8 Hz, Ar), 4.50 (m, 1H, CH), 2.19 (s, 3H, CH_3), 1.92-1.59 (m, 8H, C_4H_8), 3.50 (q, *J* = 7.2 Hz, Et_4N^+), 1.40 (tt, *J* = 1.8, 7.2 Hz, Et_4N^+). ^{13}C NMR (300 MHz, Acetone-d_6) δ 166.99, 164.47, 153.08, 146.39, 140.28, 136.55, 126.85, 122.77, 119.79, 117.36 (Ar), 78.29 (CH), 35.70, 33.73, 24.54, 24.29 (CH_2), 21.89 (CH_3).

4.4.5 *fac*-[Re(5Me-Sal-CyPent)(CO)$_3$(Imidazole)] (6)

5Me-SalH-CyPent (0.0263 g, 1.294 x 10^{-4} mol, 1.eq) dissolved in methanol (5 ml) was added drop-wise to a methanol (5 ml) ReAA (0.101 g, 1.311 x 10^{-4} mol). The reaction mixture was stirred at 60 ^oC for 6 h. Imidazole (0.0087 g, 1.278 x 10^{-4} mol, 1eq) dissolved in methanol (5 ml) was added and the reaction mixture stirred for a further 20 h. Excess solvent was removed under vacuum before allowing the concentrated methanol solution to evaporate slowly at room temperature. Slow evaporation of the solvent afforded yellow crystals suitable for X-ray diffraction. (Crystalline yield: 0.0144 g, 21.2 %).

IR (KBr, cm^{-1}): $\nu_{(CO)}$ 2007.5, 1879.3. UV-Vis (nm, L mol^{-1} cm^{-1}): λ_{max} = 383.9, ε = 2.405 x 10^3. ^{1}H NMR (300 MHz, Acetone-d_6) δ 8.28 (s, 1H, HC=N), 7.87 (s, 1H, Ar), 7.24 (m, 1H, Ar), 7.12 (m, 1H, Ar), 7.08 (d, 1H, J = 8.1 Hz, Ar), 6.54 (s, 1H, Ar), 6.33 (d, 1H, J = 7.8 Hz, Ar), 4.45 (m, 1H, CH), 2.18 (s, 3H, CH_3), 1.92-1.63 (m, 8H, C_4H_8), 3.51 (q, J = 7.2 Hz, Et_4N^+), 1.40 (tt, J = 1.8, 7.2 Hz, Et_4N^+). ^{13}C NMR (300 MHz, Acetone-d_6) δ 167.17, 163.76, 145.93, 138.65, 136.57, 129.72, 122.63, 119.69, 118.29, 116.71 (Ar), 78.42 (CH), 35.20, 33.93, 24.53, 24.29 (CH_2), 21.86 (CH_3), 53.11, 7.86 (Et_4N^+).

4.4.6 *fac*-[Re(*κO*-5Me-Sal-CyPent)(CO)$_3$(Pyridine)(Br)] (7)

5Me-SalH-CyPent (0.0264 g, 1.299 x 10^{-4} mol, 1eq) dissolved in methanol (5 ml) was added drop-wise to a methanol (5 ml) solution of ReAA (0.100 g, 1.315 x 10^{-4} mol). The reaction mixture was stirred at 25 ^{o}C for 6 h. Pyridine (0.0106 g, 1.340 x 10^{-4} mol, 1eq) dissolved in methanol (2 ml) was added and the reaction mixture stirred for a further 16 h. The precipitate was filtered and weighed. Recrystallization from acetone afforded yellow crystals suitable for X-ray diffraction. (Crystalline yield: 0.0325 g, 44.4 %).

IR (KBr, cm^{-1}): $\nu_{(CO)}$ 2016.8, 1891.0. UV-Vis (nm, L.mol^{-1}.cm^{-1}): λ_{max} = 404.8, 287.4, 253.0, ε = 5.412 x 10^3, 17.246 x 10^3, 19.196 x 10^3. ^{1}H NMR (300 MHz, Acetone-d_6) δ 8.90 (m, 1H, Ar), 8.45 (m, 1H, HC=N), 8.07 (m, 1H, Ar), 7.58 (m, 1H, Ar), 7.30 (d, 1H, J = 8.1 Hz, Ar), 6.97 (s, 1H, Ar), 6.58 (d, 1H, J = 7.8 Hz, Ar), 4.11 (m, 1H, CH), 2.34 (s, 3H, CH_3), 1.88-1.39 (m, 8H, C_4H_8), 1.31 (m, Et_4N^+). ^{13}C NMR (300 MHz, Acetone-d_6) δ 175.43, 165.92, 154.51, 151.46, 139.73, 136.46, 126.45, 122.37, 118.77, 114.84 (Ar), 64.46 (CH), 33.50, 33.19, 29.92, 24.84 (CH_2), 22.76 (CH_3).

4.4.7 *fac*-[Re(5Me-Sal-Hist)(CO)$_3$].MeOH (8)

$AgNO_3$ (0.0331 g, 1.949 x 10^{-4} mol, 3eq) was added to a methanol (10 ml) solution of ReAA (0.0504 g, 6.542 x 10^{-5} mol) and stirred at 25 ^{o}C for 27 hr. AgBr precipitated and was removed by filtration. 5Me-SalH-Hist (0.0302 g, 1.317 x 10^{-4} mol, 2eq) was added and the reaction mixture refluxed at 70 ^{o}C for 14 hr. Excess solvent was removed under vacuum before allowing the solution to evaporate slowly at 5 ^{o}C to give the title complex as yellow crystals. (Yield: 0.0211g, 64.7 %).

IR (ATR, cm^{-1}): $\nu_{(CO)}$ 1999.7, 1860.2. UV-Vis (nm, L mol^{-1} cm^{-1}): λ_{max} = 389.9, ε = 1.652 x 10^3. ^{1}H NMR (300 MHz, Methanol-d_4) δ 8.02 (s, 1H, HC=N), 8.00 (s, 1H, Ar), 7.07 (d, 1H, J

= 7.8 Hz, Ar), 6.99 (s, 1H, Ar), 6.59 (s, 1H, Ar), 6.46 (d, 1H, *J* = 7.5 Hz, Ar), 4.37 (m, 1H, CH_2), 4.11 (m,1H, CH_2), 3.33 (m, 1H, CH_2), 3.02 (m, 1H, CH_2), 2.23 (s, 3H, CH_3), 1.29 (tt, *J* = 1.8, 7.2 Hz, Et_4N^+).^{13}C NMR (600 MHz, Methanol-d_4) δ 166.48, 165.28, 146.75, 140.24, 137.19, 135.28, 122.43, 121.38, 118.98, 115.68 (Ar), 62.14, 29.46 (CH_2), 22.11 (CH_3), 53.35, 7.67 (Et_4N^+).

4.4.8 *fac*-[Re(en)(CO)$_3$(Br)]

Ethylenediamine (0.0041 g, 6.822 x 10^{-5} mol, 1eq) dissolved in methanol (5 ml) was added drop-wise to a methanol (5 ml) solution of ReAA (0.0503 g, 6.529 x 10^{-5} mol). The reaction was refluxed at 70 °C for 8 h. An excess of bromine was added in the form of solid KBr (0.0078 g, 6.555 x 10^{-5} mol, 1eq) to the warm solution and the reaction stirred for a further 2 h. The solvent was allowed to evaporate slowly at room temperature to give white crystals not suitable for X-ray diffraction. (Crystalline yield: 0.0210 g, 78.7 %).

IR (KBr, cm^{-1}): $\nu_{(CO)}$ 2018.22, 1906.1, 1876.3. UV-Vis (nm, $L.mol^{-1}.cm^{-1}$): λ_{max} = 265.6, ε = 2.107 x 10^3. ^{1}H NMR (300 MHz, Methanol-d_4) δ 5.12 (s, 1H, NH_2), 4.88 (s, 4H, 2xCH_2), 3.58 (s, 1H, NH_2), 3.00 (m, 1H, NH_2), 2.72 (m, 1H, NH_2), 3.33 (q, *J* = 7.2 Hz, Et_4N^+), 1.31 (tt, *J* = 1.8, 7.2 Hz, Et_4N^+). ^{13}C NMR (300 MHz, Acetone-d_6) δ 45.53 (2xCH_2), 53.45, 7.83 (Et_4N^+).

4.4.9 *fac*-[Re(dien)(CO)$_3$][NO$_3$]

$AgNO_3$ (0.0662 g, 3.897 x 10^{-4} mol, 3eq) was added to a methanol (5 ml) solution of ReAA (0.100 g, 1.315 x 10^{-4} mol) and stirred at 25 ^{o}C for 26 h. AgBr precipitated and was removed from by filtration. Diethylenetriamine (0.0133 g, 1.289 x 10^{-4} mol, 1eq) dissolved in methanol (5 ml) was added drop-wise and the reaction refluxed at 70 °C for 14 h. Excess solvent was removed under vacuum to give a yellow oil. The oil was left in open air to give white crystals suitable for X-ray diffraction. (Crystalline yield: 0.0307 g, 63.8 %).

IR (KBr, cm^{-1}): $\nu_{(CO)}$ 2020.8, 1887.5. UV-Vis (nm, L mol^{-1} cm^{-1}): λ_{max} = 257.9, ε = 4.34 x 10^3. ^{1}H NMR (300 MHz, Methanol-d_4) δ 6.85 (s, 1H, NH), 5.37 (s, 2H, NH_2), 4.03 (s, 2H, NH_2), 3.09-2.59 (m, 8H, 4xCH_2). ^{13}C NMR (300 MHz, Methanol-d_4) δ 53.68, 44.32 (4xCH_2).

4.5 Discussion

The initial aim of synthesizing complexes of the type *fac*-[Re(L,L'-Bid)$(CO)_3$(MeOH)] (L,L'-Bid = *N,O* Sal bidentate ligand) was achieved during this study. However, all attempts to obtain single crystals of the methanol substituted products that were suitable for X-ray diffraction were unsuccessful. The synthetic procedure was modified by substituting the more labile methanol solvento molecule with more rigid ligands such as pyridine and imidazole to give single crystals of complexes of the type *fac*-[Re(L,L'-Bid)$(CO)_3$(L)] (L,L'-Bid = *N,O* Sal bidentate ligand; *L* = coordinated pyridine or imidazole) that were suitable for X-ray diffraction. These complexes can be obtained by using one of the two synthetic procedures shown in Figure 4.2 below.

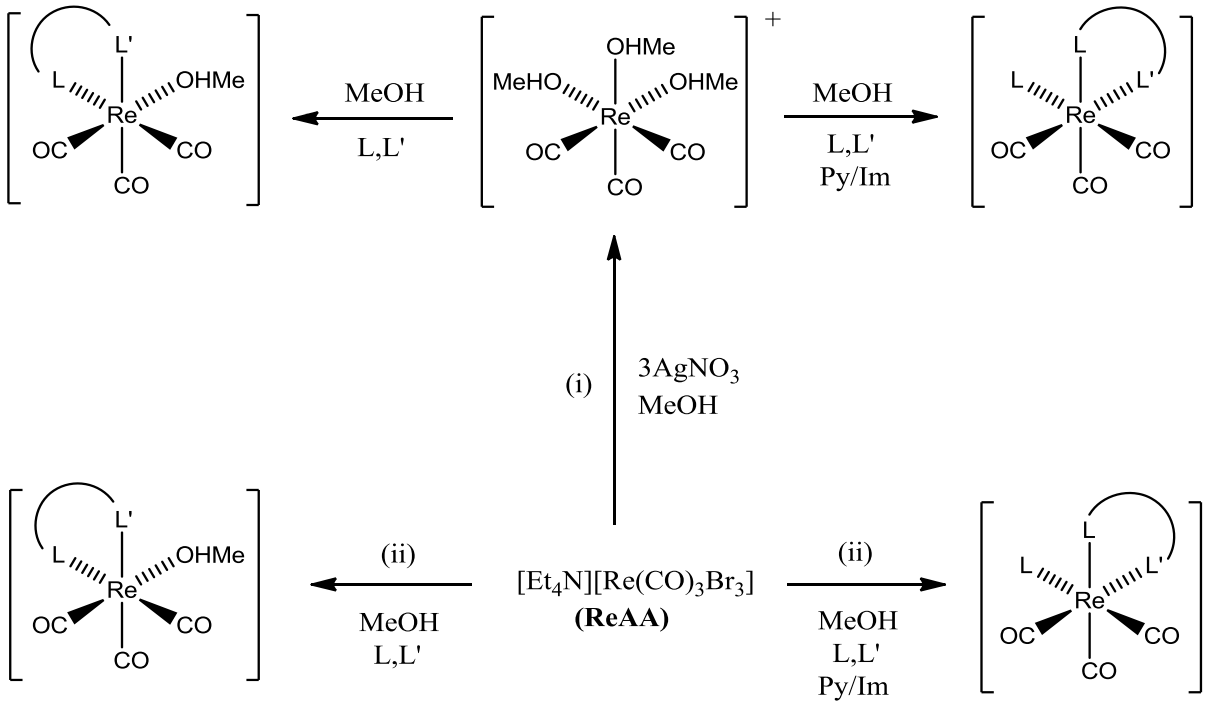

Figure 4.2: Synthetic procedures towards *fac*-[Re(L,L'-Bid)$(CO)_3$(L)] (L,L'-Bid = *N,O* Sal bidentate ligand; *L* = pyridine or imidazole) complexes.

The first method (i), consist of the removal of three bromido ligands coordinated to **ReAA** with three equivalence of silver nitrate to form *fac*-$[Re(CO)_3(MeOH)_3]^+$ intermediate. The bromide ions precipitate as silver bromide which is removed by filtration, dried and weighed

to ensure complete removal of the bromido ligands. The bidentate ligand is added to the *fac*-$[Re(CO)_3(MeOH)_3]^+$ intermediate *in-situ* together with pyridine or imidazole to give the final complex. In the second method (ii), the bidentate ligand together with pyridine or imidazole is added directly to **ReAA** without removing the bromido ligands. The latter gives a mixture of white and yellow crystals which can be separated manually under a microscope to give pure products of both. The disadvantage of this method is that it gives the desired product in fairly low yields since it forms a mixture of products. The first method however also gives the product in low yields. This can be attributed to the fact that the yields were calculated from the crystallized products. The formed complexes were characterized by IR, ^{1}H NMR, ^{13}C NMR, UV-vis and X-ray diffraction. The complexes are stable at room temperature for several months and dissolve in solvents such as methanol, acetone and dimethyl sulfoxide (DMSO).

The temperature at which the reaction is carried out plays an important role on how the bidentate ligand coordinates to rhenium in *fac*-[Re(L,L'-Bid)$(CO)_3$(L)] (L,L'-Bid = *N,O* Sal bidentate ligand; *L* = pyridine or imidazole) complexes. For example, when the reaction is carried out at high temperatures (70 ^{o}C), the Schiff-base ligand coordinates to rhenium center in a standard bidentate manner through the *N* and *O* donor atoms as seen in the synthetic procedure of *fac*-[Re(5Me-Sal-CyPent)$(CO)_3$(Pyridine)] **(5)** in 4.4.4. But, when the reaction is carried out at low temperatures (25 ^{o}C), the same ligand coordinates as a monodentate through the *O* donor atom as seen in the synthetic procedure of *fac*-[Re(*κO*-5Me-Sal-CyPent)$(CO)_3$(Pyridine)(Br)] **(7)** in 4.4.6. Chapter 5 clearly indicate the coordination of 5Me-Sal-CyPent **(2)** in complexes **(5)** and **(7)**.

The carbonyl stretching frequency, *ν*(CO) of the complexes synthesized during this study together with those of related complexes are given in Table 4.1 for comparison. The carbonyl stretching frequency of the CO ligands indicates the amount of *π*-back-donation from the metal centre into the M-CO bond. Different ligands change the stretching frequency because they change the electron density around the metal centre and consequently the amount of back-donation. In general, electron rich ligand result in a lower CO stretching frequency value in the infrared spectrum while electron poor ligand result in a higher CO stretching frequency value. Strong *σ*-donor ligands donate electron density to the metal centre which increases the electron back-donation from the metal centre into the M-CO bond. This strengthens the M-CO bond, weakens the C≡O bond and consequently decreases the CO stretching frequency value.

Table 4.1: Carbonyl stretching frequencies, *ν*(CO) of the complexes synthesized during this study as well as related complexes.

Complex	Carbonyl stretching, *ν*(CO), cm^{-1}			Ref
fac-$[Et_4N]_2[Re(CO)_3Br_3]$ **ReAA**	1999.4		1867.1	
***N,O* ligands**				
fac-[Re(5Me-Sal-iProp)$(CO)_3$(Py)]	2014.3	1906.8	1879.5	[a]
fac-[Re(5Me-Sal-CyPent)$(CO)_3$(MeOH)]	1999.7		1868.0	[a]
fac-[Re(5Me-Sal-CyPent)$(CO)_3$(Py)]	2008.9	1899.1	1859.1	[a]
fac-[Re(5Me-Sal-CyPent)$(CO)_3$(Im)]	2007.5		1879.3	[a]
fac-[Re(*κO*-5Me-Sal-CyPent)$(CO)_3$(Py)(Br)]	2016.8		1891.0	[a]
fac-[Re(5Me-Sal-Hist)$(CO)_3$].MeOH	1999.7		1860.2	[a]
fac-[Re(Sal-*m*Tol)$(CO)_3$(MeOH)]	2002.0		1868.8	[b]
fac-[Re(Sal-*m*Tol)$(CO)_3$(Py)]	2014.7		1890.5	[b]
fac-[Re(Sal-3MeBu)$(CO)_3$(MeOH)]	2001.4		1876.5	[b]
fac-[Re(Sal-3MeBu)$(CO)_3$(Py)]	2013.6	1904.8	1878.4	[b]
fac-[Re(5Me-Sal-Hist)$(CO)_3$]	2012.8	1902.6	1871.0	[b]
fac-[Re(2,4-dipic)$(CO)_3$(Im)]	2030	1926	1906	[c]
***O,O′* ligands**				
fac-$[Et_4N]_2[Re(acac)(CO)_3Br]$	2005.1	1901.7	1857.8	[b]
fac-[Re(Flav)$(CO)_3$(Py)]	2012	1897	1860	[c]
fac-[Re(Hfaa)$(CO)_3$(Py)]	2036	1939	1873	[d]
fac-[Re(Hfaa)$(CO)_3$(MeOH)]	2023		1879	[d]
***N,N′* ligands**				
fac-[Re(en)$(CO)_3$Br]	2018.2	1906.1	1876.3	[a]
fac-[Re(dien)$(CO)_3$]$[NO_3]$	2020.8		1887.5	[a]
fac-[Re(Bipy)$(CO)_3(H_2O)$]	2008	1904	1882	[c]

[a] Synthesized during this study; [b] Synthesized by A. Brink *et al.*[8,9,10]; [c] Synthesized by M. Schutte *et al.*[11]; [d] Synthesized by A. Manicum *et al.*[12]; Py = pyridine; Im = imidazole; Sal-*m*Tol = 2-(*m*-tolyliminomethyl)phenol; Sal-3MeBu = 2-(3-methylbutylimino)phenol; 2,4-dipic = pyridine-2,4-dicarboxylic acid; Flav = 3-hydroxyflavone; acac = acetylacetone; Hfaa = hexafluoroacetylacetone; Bipy = 2,2'-bipyridine.

[8] A. Brink, *P.hD. Thesis*, University of the Free State, Bloemfontein, South Africa, 2011.
[9] A. Brink, H. G. Visser, A. Roodt, *Inorg. Chem*., 2013, 52, 8950.
[10] A. Brink, H. G. Visser, A. Roodt, *Inorg. Chem*., 2014, 53, 12480.
[11] M. Schutte, G. Kemp, H. G. Visser, A. Roodt, *Inorg. Chem*., 2011, 50, 12486.
[12] A. Manicum, M. Schutte-Smith, G. Kemp, H.G. Visser, *Polyhedron*, 2015, 85, 190.

4.6 Conclusion

Complexes of the type *fac*-[Re(L,L'-Bid)$(CO)_3$(MeOH)] (L,L'-Bid = *N*,*O* Sal bidentate ligand) were synthesized during this study but could not be crystallized to obtain single crystals that were suitable for X-ray diffraction. Therefore, the methanol solvento molecule coordinated to the sixth position was substituted with more stable ligands like pyridine and imidazole to give single crystals of complexes of the type *fac*-[Re(L,L'-Bid)$(CO)_3$(L)] (L,L'-Bid = *N*,*O* Sal bidentate ligand; *L* = coordinated pyridine or imidazole) that were suitable for X-ray diffraction.

These complexes can be obtained by removing the bromido ligands coordinated to **ReAA** with silver nitrate followed by an *in-situ* addition of the bidentate and monodentate ligands to the rhenium(I) trimethanol intermediate, or by direct addition of the bidentate and monodentate ligands to **ReAA** without removing the bromido ligands. The second method forms a mixture of products and thus gives the desired complex in fairly low yields. Depending on the temperature at which the reaction is carried out when the second method is used, the bidentate ligand can coordinate to rhenium in a standard bidentate manner or as a monodentate ligand through the *O* donor atom. Chapter 5 describes the single crystal X-ray structures of the complexes obtained in this chapter and shows exactly how the ligands coordinate to the rhenium centre.

5 Single Crystal X-ray Structures of *fac*-[Re(L,L'-Bid)(CO)$_3$(L)] complexes

5.1 Introduction

Over the years, a large number of rhenium tricarbonyl crystal structures with various *N,N'*, *N,O*, and *O,O'* ligands have been reported.[1] The majority of Schiff-base ligands found in literature are coordinated to Re(III) and Re(V) because of the important role played by the $[M=O]^{3+}$ moiety in the radiopharmaceutical design as discussed in chapter 2. To the best of our knowledge, only four similar[2,3] and three related[4] crystal structures, whereby the salicylidene backbone is utilised and coordinated to the *fac*-$[Re(CO)_3]^+$ core could be found in literature before the structures reported by Brink *et al*.[5,6,7,8] and Ju *et al*.[9] Thus, our interest in rhenium salicylidene tricarbonyl complexes was prompted by the little interest they have received up to date. Our interests in Schiff-bases is further influenced by the fact that they can easily be manipulated into designing a range of mono-, bi- and tridentate ligands with varying steric and electronic character. Therefore, it is also possible to incorporate a biologically active molecule (BAM) into the ligand,[6] leading to the design of novel radiopharmaceutical drugs.

In this chapter, four new crystal structures of complexes of the type *fac*-[Re(L,L'-Bid)(CO)$_3$(L)] (L,L'-Bid = *N,O* Sal bidentate ligand, *L* = coordinated pyridine or imidazole) depicted in Figure 5.1 are reported. Complex **(8)** is a polymorph of a crystal structure reported by Brink *et al*. (2013).[6] The structural coordination chemistry of the Sal ligands to the *fac*-$[Re(CO)_3]^+$ core, packing modes of the complexes and the means by which the packing is stabilized within the unit cell are described in this chapter.

[1] Cambridge Structural Database (CSD), Version 5.35, November 2013 update.
[2] J. W. Faller, G. Mason, J. Parr, *J. Organomet. Chem*., 2001, 626, 181.
[3] Z. K. Li, Y. Li, L. Lei, C. M. Che, X. G. Zhou, *Inorg. Chem. Commun*., 2005, 8, 307.
[4] R. Czerwieniec, A. Kapturkiewicz, R. Anulewicz-Ostrowska, J. Nowacki, *J. Chem. Soc., Dalton Trans*., 2002, 3434.
[5] A. Brink, H. G. Visser, A. Roodt, *J. Coord. Chem.,* 2011, 64, 122.
[6] A. Brink, H. G. Visser, A. Roodt, *Polyhedron*, 2013, 52, 416.
[7] A. Brink, H. G. Visser, A. Roodt, *Inorg. Chem*., 2013, 52, 8950.
[8] A. Brink, H. G. Visser, A. Roodt, *Inorg. Chem*., 2014, 53, 12480.
[9] C. C. Ju, A. G. Zhang, H. L. Sun, K. Z. Wang, W. L. Jiang, Z. G. Bian, C. H. Huang, *Organomet.,* 2011, 30, 712.

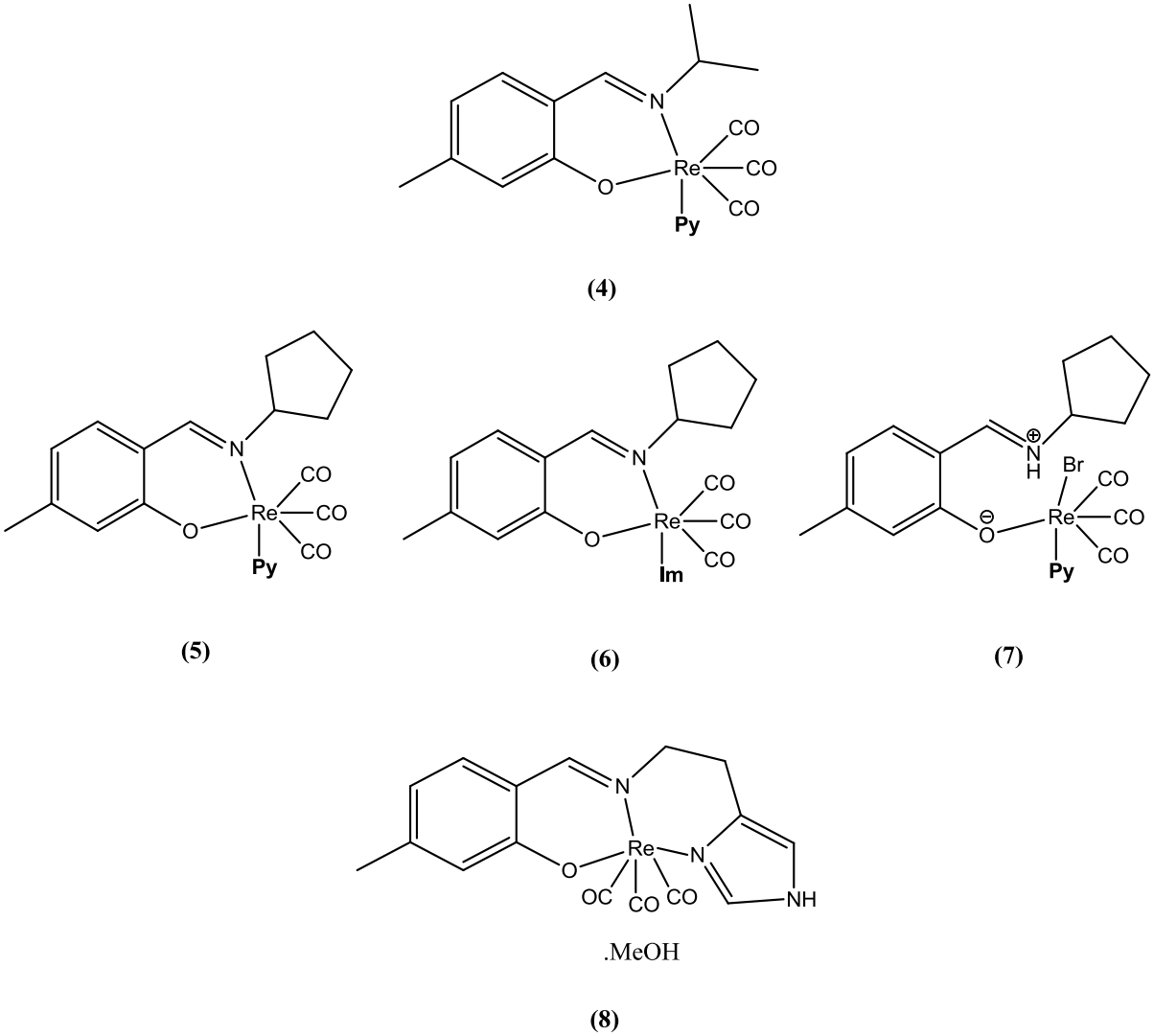

Figure 5.1: Crystal structures of rhenium(I) tricarbonyl complexes described in this chapter. (Py = pyridine, Im = imidazole).

(4) *fac*-[(tricarbonyl)(2-(isopropylimino)methyl-5-methylphenolatido)(pyridine)rhenium(I)].

(5) *fac*-[(tricarbonyl)(2-(cyclopentylimino)methyl-5-methylphenolatido)(pyridine) rhenium(I)].

(6) *fac*-[(tricarbonyl)(2-(cyclopentylimino)methyl-5-methylphenolatido)(imidazole) rhenium(I)].

(7) *fac*-[(bromido)(tricarbonyl)(2-(cyclopentylimino)methyl-5-methylphenolatido)(pyridine) rhenium(I)].

(8) *fac*-[(tricarbonyl)(2-(2-imidazol-4-yl)ethyliminomethyl-5-methylphenolatido)rhenium(I)] methanol solvate.

5.2 Experimental

The reflection data of the single crystals was collected on a Bruker X8 ApexII 4K diffractometer[10] using a molybdenum *Kα* radiation source with phi and omega scans at 100 K. The crystal structure of *fac*-[Re(5Me-Sal-iProp)$(CO)_3$(Pyridine)] **(4)** was collected at 293 K. COSMO[11] was used for optimum collection of more than a hemisphere of reciprocal space. Integration and reduction of the data were performed using the Bruker SAINT-Plus and XPREP software packages.[12] Absorption correction of the data was performed utilizing the multi-scan technique SADABS.[13] The structures were solved using SIR97[14] and refined with WINGX,[15] incorporating SHELXL.[16] The solved structures were doubled checked using OLEX2.[17] All non-hydrogen atoms were refined with anisotropic parameters. All H atoms were placed in geometrically idealized positions and constrained to ride on their parent atoms, with C-H = 0.95 Å and U_{iso}(H) = 1.2U_{eq}(C) for sp^2 CH, and with C-H = 0.98 Å and U_{iso}(H) = 1.5U_{eq}(C) for methyl groups. The methyl protons were located from a difference Fourier map and the group refined as a rigid motor. The thermal ellipsoids of the crystal structures are drawn at a 50 % probability. Graphical representation of the crystal structures were constructed using DIAMOND.[18] The crystal data and structure refinement details of the rhenium(I) tricarbonyl complexes are summarized in Table 5.1a and 5.1b. In the crystal structure of complexes **(5)**, (**6)** and **(7)**, high electron density peaks of 2.64, 4.17 and 2.36 e. $Å^{-3}$ are found 0.78, 0.89 and 0.82 Å from Re1 metal center respectively. The R_{int} of **(6)** is also quite high (R_{int} = 0.1241).

[10] Bruker APEX2 (Version 1.0-27), Bruker AXS Inc., Madison, Wisconsin, USA, 2005.
[11] Bruker, COSMO (Version 1.48), Bruker AXS Inc., Madison, Wisconsin, USA, 2003.
[12] Bruker, SAINT-Plus (Version 7.12) (including XPREP), Bruker AXS Inc., Madison, Wisconsin, USA, 2004.
[13] Bruker, SADABS (Version 2004/1), Bruker AXS Inc., Madison, Wisconsin, USA, 1998.
[14] A. Altomare, M. C. Burla, M. Camalli, G. L. Cascarano, C. Giacovazzo, A. Guagliardi, A. G. G. Moliterni, G. Polidori, R. Spagna, *J. Appl. Cryst.*, 1999, 32, 115.
[15] L. J. Farrugia, *J. Appl. Cryst.*, 1999, 32, 837.
[16] G. M. Sheldrick, SHELXL97, *Program for Solving Crystal Structures*, University of Göttingen, Germany, 1997.
[17] O. V. Dolomanov, L. J. Bourhis, R. J. Gildea, J. A. K. Howard, H. Puschmann, *J. Appl. Cryst.*, 2009, 42, 339.
[18] K. Brandenbug, H. Putz, DIAMOND, Release 3.0c, Crystal Impact GbR, Bonn, Germany, 2005.

Table 5.1a: Crystal data and structure refinement details of rhenium(I) tricarbonyl complexes

Complex	**(4)**	**(5)**	**(6)**
Empirical formula	$C_{19}H_{19}N_2O_4Re$	$C_{21}H_{21}N_2O_4Re$	$C_{19}H_{20}N_3O_4Re$
Formula weight	525.56	551.6	525.46
Temperature (K)	293(2)	100(2)	100(2)
λ (Å)	0.71073	0.71073 Å	0.71073
Crystal system	Monoclinic	Monoclinic	Monoclinic
Space group	$P2_1/c$	$P2_1/c$	$P2_1/c$
Unit cell dimensions			
a (Å)	8.2805(3)	8.2371(4)	15.746(5)
b (Å)	13.7325(5)	15.0284(7)	7.983(5)
c (Å)	16.3560(6)	16.2958(7)	19.170(4)
α (^{o})	90	90	90
β (^{o})	92.431(2)	91.040(1)	126.407(17)
γ (^{o})	90	90	90
Volume (Å^3)	1858.2(2)	2016.9(2)	1939.4(3)
Z	4	4	4
ρ_{calc} (g.cm^{-1})	1.878	1.817	1.800
M (mm^{-1})	6.565	6.054	6.293
F(000)	1016	1072	988
Crystal color	Yellow	Yellow	Yellow
Crystal shape	Cuboid	Cuboid	Cuboid
Crystal size (mm)	0.631x0.479x0.348	0.404x0.326x0.190	0.857x0.635x0.145
Theta range (^{o})	2.87 to 28.00	1.84 to 27.99	1.61 to 28.00
Index ranges	h = -10 to 10	h = -10 to 10	h = -20 to 20
	k = -18 to 18	k = -18 to 19	k = -10 to 10
	l = -21 to 21	l = -21 to 21	l = -25 to 25
Reflections collected	37928	46262	64555
Independent reflections	4472	4757	4687
R_{int}	0.0941	0.0857	0.1241
Completeness (%)	99.8	99.9	100.0
Refinement method	Full-matrix least-square on F^2	Full-matrix least-squares on F^2	Full-matrix least-squares on F^2
Data / restraints / parameters	4472/0/239	4757/0/254	4687 / 0 / 245
Goodness-of-fit on F^2	1.028	1.088	1.078
Final R indices [I>2sigma(I)]	R1 = 0.0346, wR2 = 0.0877	R1 = 0.0383, wR2 = 0.0818	R1 = 0.0596, wR2 = 0.164
R indices (all data)	R1 = 0.0422, wR2 = 0.0921	R1 = 0.0500, wR2 = 0.0874	R1 = 0.0676, wR2 = 0.1764
ρ_{max} and ρ_{min} (e. Å^{-3})	1.438 and -0.964	2.638 and -2.416	4.197 and -3.478

Table 5.1b: Crystal data and structure refinement details of rhenium(I) tricarbonyl complexes

Complex	**(7)**	**(8)**
Empirical formula	$C_{21}H_{21}N_2O_4BrRe$	$C_{16}H_{14}N_3O_4Re$
Formula weight	631.51	498.5
Temperature (K)	100(2)	100(2)
λ (Å)	0.71073	0.71073
Crystal system	Monoclinic	Orthorhombic
Space group	$P2_1/c$	*Pbcn*
Unit cell dimensions		
a (Å)	11.2105(5)	28.3997(39)
b (Å)	9.0638(5)	9.0380(11)
c (Å)	22.9499(12)	14.3900(17)
α (^{o})	90	90
β (^{o})	102.860(2)	90
γ (^{o})	90	90
Volume (Å^3)	2273.4(3)	3693.6(13)
Z	4	8
ρ_{calc} (g.cm^{-1})	1.845	1.793
μ (mm^{-1})	7.13	6.602
F(000)	1212	1904
Crystal color	Yellow	Yellow
Crystal shape	Cuboid	Cuboid
Crystal size (mm)	0.365x0.340x0.194	0.315x0.313x0.159
Theta range (^{o})	1.82 to 28.00	1.43 to 28.00
Index ranges	*h* = -14 to 14	*h* = -37 to 37
	k = -11 to 11	*k* = -11 to 11
	l = -30 to 30	*l* = -18 to 19
Reflections collected	80289	69990
Independent reflections	5471	4459
R_{int}	0.0940	0.0949
Completeness (%)	100.0	99.9
Refinement method	Full-matrix least-squares on F^2	Full-matrix least-squares on F^2
Data / restraints / parameters	5471/0/263	4459/0/238
Goodness-of-fit on F^2	1.121	1.218
Final *R* indices [*I*>2sigma(*I*)]	*R*1 = 0.0331, *wR*2 = 0.0868	*R*1 = 0.0303, *wR*2 = 0.0924
R indices (all data)	*R*1 = 0.0390, *wR*2 = 0.0978	*R*1 = 0.0462, *wR*2 = 0.1184
ρ_{max} and ρ_{min} (e. Å^{-3})	2.364 and -1.039	1.172 and -1.615

Three general planes are defined in this chapter and drawn through each rhenium complex as illustrated in Figure 5.2 below using one of the obtained crystal structures as an example.

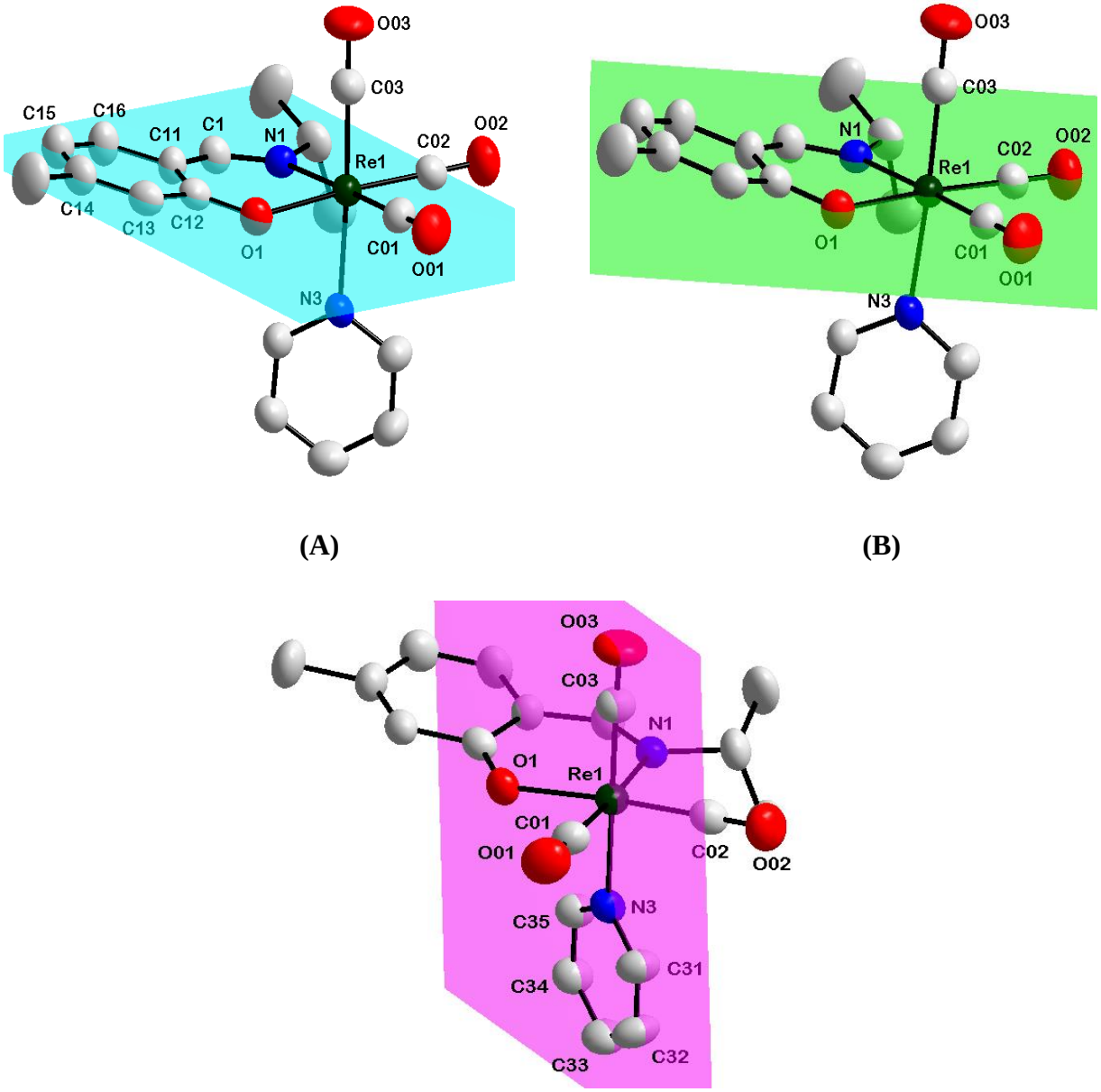

Figure 5.2: A schematic representation of the planes defined in this chapter and drawn through each rhenium complex. Plane 1 **(A)** is a salicylidene aromatic backbone plane and is drawn through atoms C11, C12, C13, C14, C15, C16 in blue. Plane 2 **(B)** is a rhenium equatorial plane and is drawn through atoms Re1, N1, O1, C01, C02 in green. Plane 3 **(C)** is drawn through the atoms of the ligand that is coordinated to the sixth position (pyridine or imidazole) in pink.

5.3 Crystal Structures of *fac*-[Re(L,L'-Bid)(CO)$_3$(L)] Complexes

5.3.1 *fac*-[Re(5Me-Sal-iProp)(CO)$_3$(Pyridine)] (4)

Complex **(4)** crystallizes in a monoclinic crystal system in the $P2_1/c$ space group and contains four molecules in the unit cell (Z = 4). The asymmetric unit contains one complete molecule of the metal complex. The molecular structure of **(4)** together with the numbering of the atoms is shown in Figure 5.3. Important bond lengths and angles are given in Table 5.2.

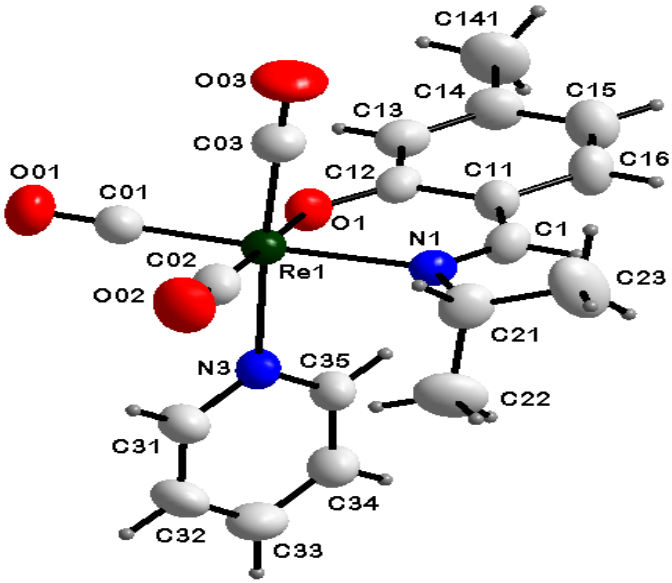

Figure 5.3: Molecular structure of **(4)** showing the numbering of the atoms. Displacement ellipsoids are drawn at a 50 % probability.

Table 5.2: Selected bond lengths and angles of complex **(4)**.

Atoms	Length (Å)	Atoms	Angle (°)
Re1-O1	2.107(3)	N1-Re1-O1	85.73(12)
Re1-N1	2.173(3)	N1-Re1-N3	87.23(13)
Re1-N3	2.231(4)	C03-Re1-N3	176.37(19)
Re1-C01	1.898(5)	C01-Re1-C02	86.95(19)
Re1-C02	1.905(5)	C02-Re1-N3	93.99(16)
Re1-C03	1.907(5)	O1-Re1-C02	176.21(16)
C01-O01	1.165(6)	N3-Re1-O1	83.44(12)
C02-O02	1.147(5)	C1-N1-C21	117.9(4)
N1-C1	1.300(6)		
N1-C21	1.510(5)		

In the title complex, the Schiff-base ligand coordinate to the rhenium center in a bidentate manner through the phenolatido oxygen and nitrogen imine donor atoms which result in the formation of a six-membered ring. Three carbonyl ligands are facially coordinated to the rhenium center with the last position occupied by the nitrogen donor atom from the pyridine ligand. The octahedron around the Re(I) center is slightly distorted with N1-Re1-O1 bite angle of 85.73(12)^{o} and C03-Re1-N3 angle of 176.37(19)^{o}.

The Re1-O1 and Re1-N1 bond lengths of 2.107(3) Å and 2.173(3) Å compares well to related salicylidene structures with bond lengths varying from 2.093-2.155 Å for Re-O and 2.148-2.198 Å for Re-N.[2,3,4,5,9] The Re1-N3 bond length of 2.231(4) Å compares well to related salicylidene structures with Re-N(pyridine) bond lengths ranging from 2.203-2.230 Å,[2,5,9] as well as to other *N,O* and *O,O'* ligand-to-metal structures with Re-N(pyridine) bond lengths varying from 2.203-2.334 Å.[19,20,21,22,23] The pyridine ligand is slightly bent towards the bidentate ligand with N3-Re1-O1 angle of 83.44(12)^{o}. The same bending of the pyridine ligand towards the bidentate ligand is also observed in structures reported by Brink *et al*. (2011),[5] Ju *et al*. (2011),[9] Czerwieniec *et al*. (2001, 2002),[4,19] Schutte-Smith *et al*. (2011, 2013)[20,22] and Manicum *et al*. (2015)[23] with N-Re-O angles ranging from 80.85-85.55^{o}.

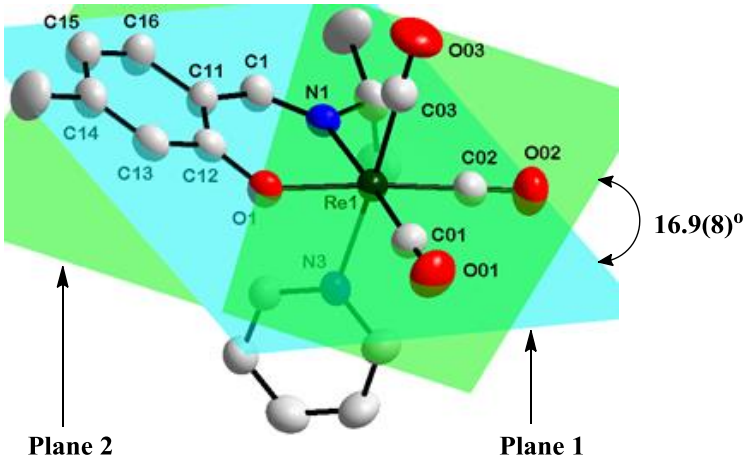

Figure 5.4: A graphical representation of the salicylidene aromatic ring plane (Plane 1) and rhenium equatorial plane (Plane 2). H atoms are omitted for clarity.

[19] R. Czerwieniec, A. Kapturkiewicz, R. Anulewicz-Ostrowska, J. Nowacki, *J. Chem. Soc., Dalton Trans*., 2001, 2756.
[20] M. Schutte, G. Kemp, H. G. Visser, *Inorg. Chem*., 2011, 50, 12486.
[21] M. Schutte, H. G. Visser, A. Roodt, *Inorg. Chem*., 2012, 51, 11996.
[22] M. Schutte-Smith, T. J. Muller, H. G. Visser, A. Roodt, *Acta Cryst*., 2013, C69, 1467.
[23] A. Manicum, M. Schutte-Smith, G. Kemp, H. G. Visser, *Polyhedron*, 2015, 85, 190.

The plane formed by the salicylidene aromatic ring (Plane 1: C11, C12, C13, C14, C15, C16) is bent away from the rhenium equatorial plane (Plane 2: Re1, N1, O1, C01, C02) with a dihedral angle of 16.9(8)^{o} (see Figure 5.4). The plane formed by the pyridine ligand (Plane 3: N3, C31, C32, C33, C34, C35) is orientated nearly perpendicular to the salicylidene aromatic backbone plane (Plane 1) and perpendicular to the rhenium equatorial plane (Plane 2) with dihedral angles of 87.3(6)^{o} and 89.9(6)^{o} respectively.

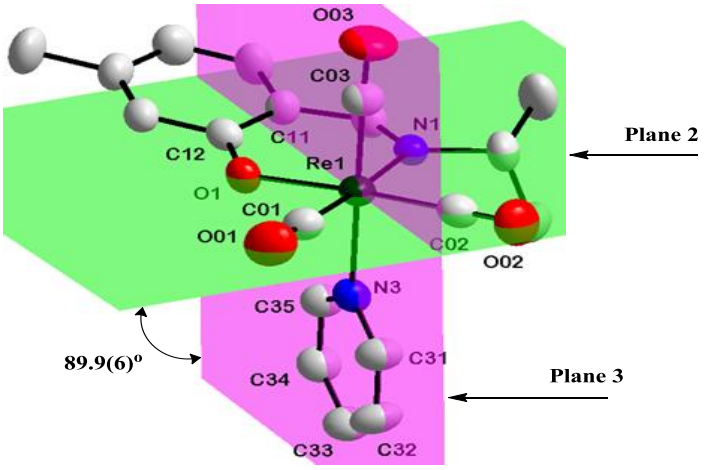

Figure 5.5: An illustration of the rhenium equatorial plane (Plane 2) and the pyridine ligand plane (Plane 3). H atoms are omitted for clarity.

One intramolecular hydrogen bond interaction is found between the pyridine atoms C35-H35 and the phenolatido oxygen atom O1 coordinated to the metal center as illustrated in Figure 5.6 and Table 5.3. The interaction forms a pseudo-tridentate ligand with a five-membered ring system.

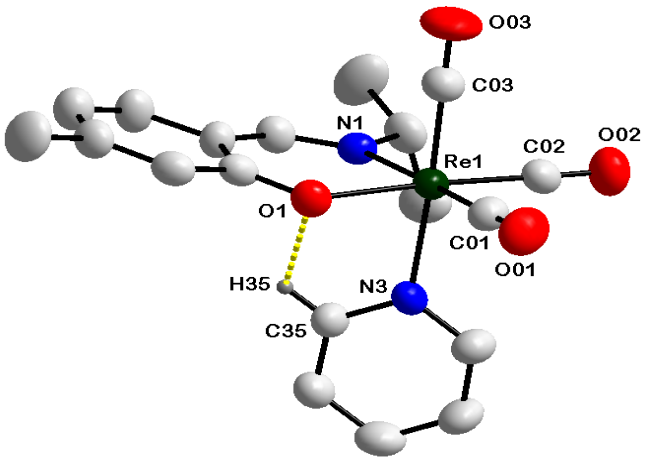

Figure 5.6: Intramolecular hydrogen bond interaction of the title complex. H atoms, not part of hydrogen interaction, are omitted for clarity.

Table 5.3: Intramolecular hydrogen bonding found in the title complex [Å and °].

D-H…A	*d*(*D-H*)	*d*(*H…A*)	*d*(*D…A*)	<(*DHA*)
C35-H35…O1 #1	0.93	2.58	3.015(6)	109

Symmetry codes:
#1 x, y, z

The molecular packing is stabilized by a C-O…π interaction observed between the carbonyl atoms C03-O03 and the six-membered ring atoms of the pyridine ligand as shown in Figure 5.7 and Table 5.4.

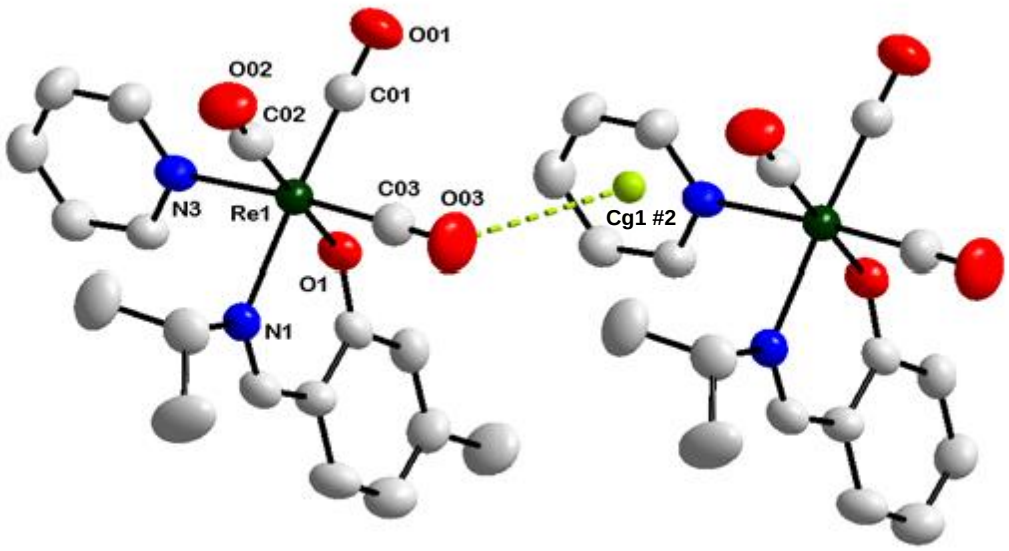

Figure 5.7: Graphical representation of the C-O...π interaction in the unit cell. H atoms are omitted for clarity.

Table 5.4: C-O…π interactions found in the title complex [Å and °].

C-O…Cg	*d*(O…Cg)	*d*(C…Cg)	<(C-O…Cg)
C03-O03…Cg1 #2	3.661(5)	4.025(6)	100.2(3)

Symmetry codes:
#2 1+x, y, z
Cg1 = centroid atom of N3, C31, C32, C33, C34, C35

The molecules in the unit cell pack in an alternating "head-to-tail' fashion when viewed along the *a*-axis as shown in Figure 5.8.

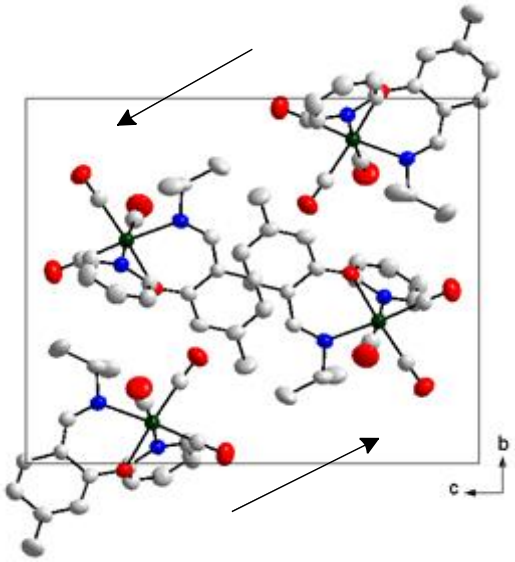

Figure 5.8: Molecular packing of the complex in the unit cell when viewed along the *a*-axis. H atoms are omitted for clarity.

5.3.2 *fac*-[Re(5Me-Sal-CyPent)(CO)$_3$(Pyridine)] (5)

Complex **(5)** crystallizes in a monoclinic crystal system in the $P2_1/c$ space group and contains four molecules in the unit cell (Z = 4). The asymmetric unit contains one complete molecule of the metal complex. The molecular structure of **(5)** is depicted in Figure 5.9 together with the numbering of the atoms. Important bond lengths and angles are given in Table 5.5.

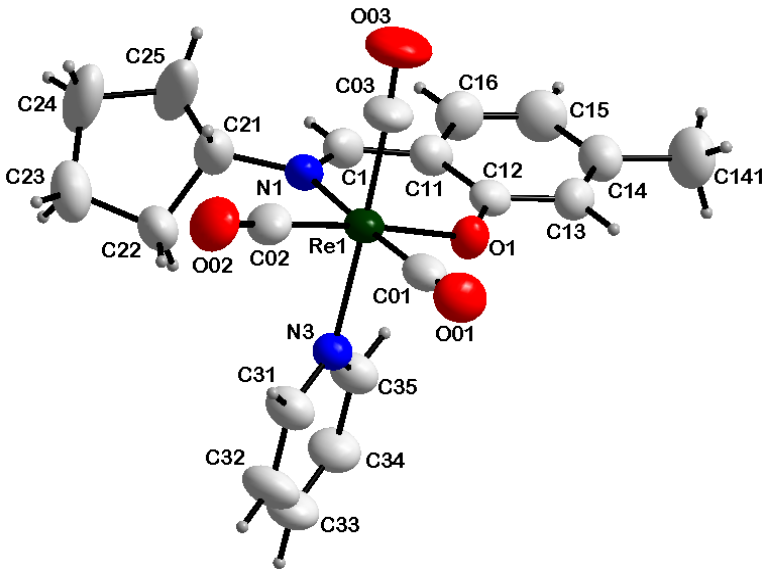

Figure 5.9: Molecular structure of **(5)** showing the numbering of the atoms. Displacement ellipsoids are drawn at a 50 % probability.

Table 5.5: Selected bond lengths and angles of complex **(5)**.

Atoms	Length (Å)	Atoms	Angle (°)
Re1-O1	2.093(4)	N1-Re1-O1	85.70(17)
Re1-N1	2.170(5)	N1-Re1-N3	86.22(18)
Re1-C01	1.933(7)	C03-Re1-N3	176.2(3)
Re1-C02	1.907(7)	C01-Re1-C02	86.2(3)
Re1-C03	1.921(6)	C02-Re1-N3	93.8(2)
C01-O01	1.141(7)	O1-Re1-C02	175.3(2)
C02-O02	1.148(7)	N3-Re1-O1	83.09(16)
C03-O03	1.124(8)	C1-N1-C21	118.3(6)
Re1-N3	2.229(5)		
N1-C1	1.291(8)		
N1-C21	1.489(8)		

In the crystal structure of the title complex, the *N* and *O* donor atoms of the bidentate ligand coordinate to the rhenium center forming a six-membered ring. Three carbonyl ligands are facially coordinated to rhenium and the last position is occupied by the *N* donor atom of the pyridine ligand. The octahedron around the Re(I) center is slightly distorted with N1-Re1-O1 bite angle of 85.70(17)^{o} and O1-Re1-C02 angle of 175.3(2)^{o}.

The Re1-O1 and Re1-N1 bond lengths of 2.093(4) Å and 2.170(5) Å are comparable to related salicylidene structures with bond lengths that vary between 2.093-2.155 Å for Re-O and 2.148-2.198 Å for Re-N. The bond lengths are also comparable to other *N,O* ligand-to-metal bond lengths varying between 2.099-2.146 Å and 2.162-2.247 Å for Re-O and Re-N respectively.[19,20,22] The Re1-N3 bond length of 2.229(4) Å is comparable to related salicylidene structures with Re-N(pyridine) bond lengths ranging from 2.203-2.230 Å. The bond length is also comparable to other *N,O* and *O,O'* ligand-to-metal structures with Re-N(pyridine) bond lengths varying from 2.203-2.334 Å. Similarly to *fac*-[Re(5Me-Sal-iProp)$(CO)_3$(Pyridine)] **(4)** and other reported structures as previously discussed, the pyridine ligand in *fac*-[Re(5Me-Sal-CyPent)$(CO)_3$(Pyridine)] **(5)** is slightly bent towards the bidentate ligand with N3-Re1-O1 angle of 83.09(16)^{o}. The bond length of Re1-N1 (2.170 Å) is shorter than that of Re1-N3 (2.229 Å), but longer than that of Re1-O1 (2.093 Å). Thus, the nitrogen imine atom of the bidentate ligand coordinates strongly to the rhenium center than the

nitrogen atom of the pyridine ligand and the phenolatido oxygen coordinates even more strongly to the metal center .[24,25,26]

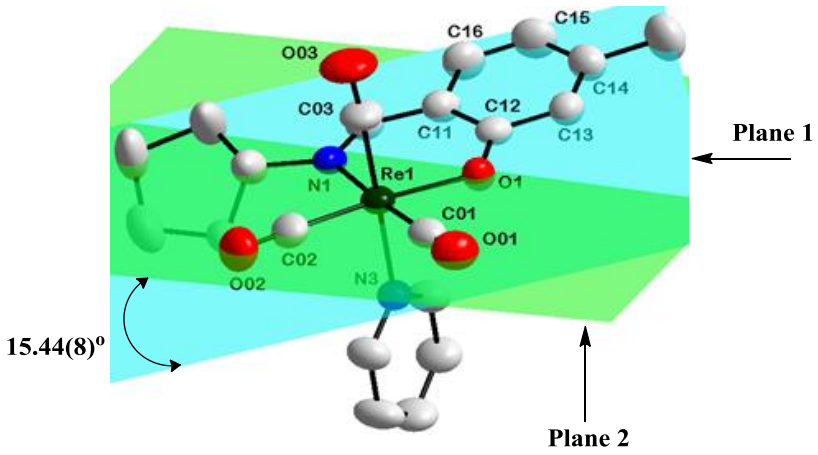

Figure 5.10: An illustration of the salicylidene aromatic ring plane (Plane 1) and rhenium equatorial plane (Plane 2). H atoms are omitted for clarity.

The plane formed by the salicylidene aromatic backbone (Plane 1: C11, C12, C13, C14, C15, C16) is bent away from the rhenium equatorial plane (Plane 2: Re1, N1, O1, C01, C02) with a dihedral angle of 15.44(8)°. The plane formed by the pyridine ligand (Plane 3: N3, C31, C32, C33, C34, C35) is perpendicularly oriented to both the salicylidene aromatic backbone plane (Plane 1) and the rhenium equatorial plane (Plane 2) with dihedral angles of 89.60(7)° and 89.87(6)° respectively.

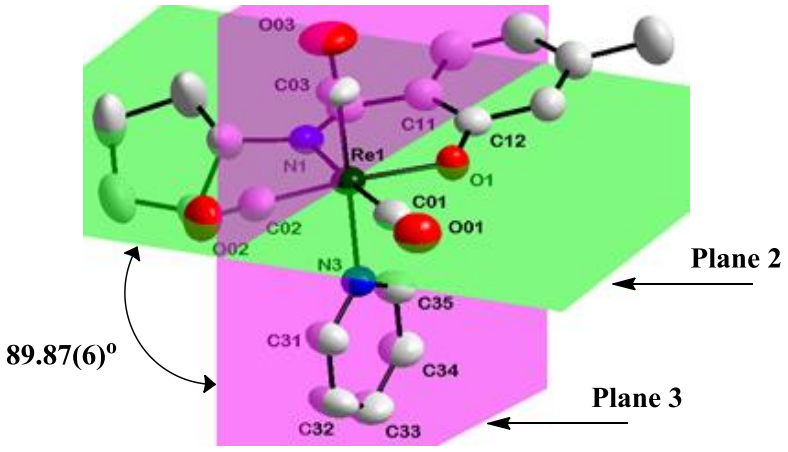

Figure 5.11: Demonstration of the rhenium equatorial plane (Plane 2) and the pyridine ligand plane (Plane 3). H atoms are omitted for clarity.

[24] R. Ballardini, G. Varani, M. T. Indelli, F. Scandola, *Inorg. Chem.*, 1986, 25, 3858.
[25] D. J. Donges, K. Nagle, H. Yersin, *J. Lumin.*, 1997, 72-74, 658.
[26] D. J. Donges, K. Nagle, H. Yersin, H. *Inorg. Chem.*, 1997, 36, 3040.

Similarly to *fac*-[Re(5Me-Sal-iProp)$(CO)_3$(Pyridine)] **(4)**, one intramolecular hydrogen bond interaction is found in *fac*-[Re(5Me-Sal-CyPent)$(CO)_3$(Pyridine)] **(5)** between the pyridine atoms C35-H35 and the phenolatido oxygen atom O1 coordinated to the metal center as shown in Figure 5.12 and Table 5.6. The interaction also forms a pseudo-tridentate ligand with a five-membered ring system.

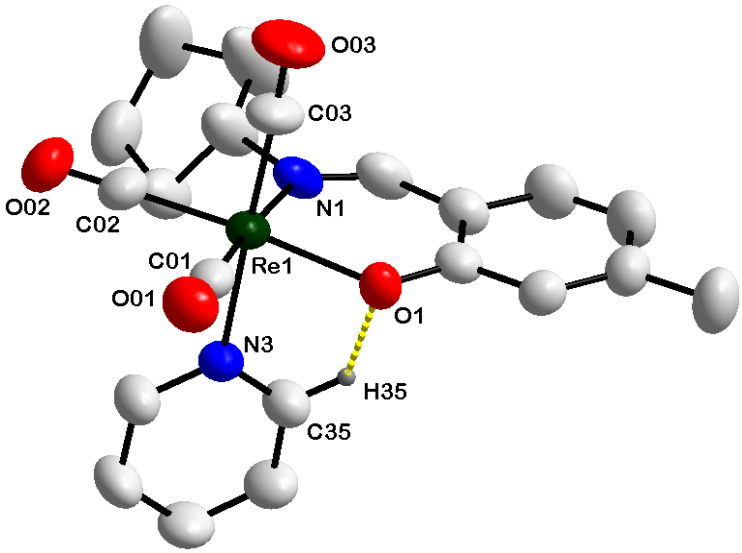

Figure 5.12: Intramolecular hydrogen bond interaction between the pyridine atoms C35-H35 and phenolatido oxygen O1 forming a pseudo-tridentate ligand. H atoms not part of hydrogen interaction are omitted for clarity.

Table 5.6: Intramolecular hydrogen bonding found in the title complex [Å and °].

D-H…A	*d*(*D-H*)	*d*(*H…A*)	*d*(*D…A*)	<(*DHA*)
C35-H35…O1 #1	0.95	2.48	2.972(7)	112

Symmetry codes:
#1 x, y, z

The molecular packing in the unit cell is stabilized by the formation of an intermolecular hydrogen bond interaction between the cyclopentyl substituent atoms C23-H23B and the phenolatido oxygen atom O1 of the neighbouring molecule as illustrated in Figure 5.13 and Table 5.7.

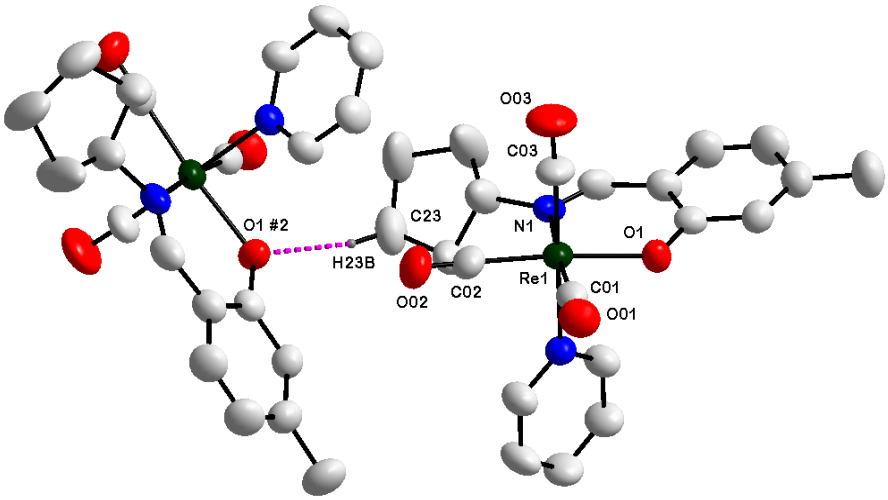

Figure 5.13: Intermolecular hydrogen bond interaction observed in the title complex. H atoms, not part of hydrogen interaction, are omitted for clarity.

Table 5.7: Intermolecular hydrogen bonding found in the title complex [Å and °].

D-H…A	*d*(*D-H*)	*d*(*H…A*)	*d*(*D…A*)	<(*DHA*)
C23-H23B…O1 #2	0.99	2.44	3.415(6)	169

Symmetry codes:
#2 1-x, 1/2+y, 1/2-z

The molecular packing in the unit cell is further stabilized by the formation of a C-O…π interaction found between the carbonyl atoms C03-O03 and the six-membered ring atoms of the pyridine ligand as illustrated in Figure 5.14 and Table 5.8.

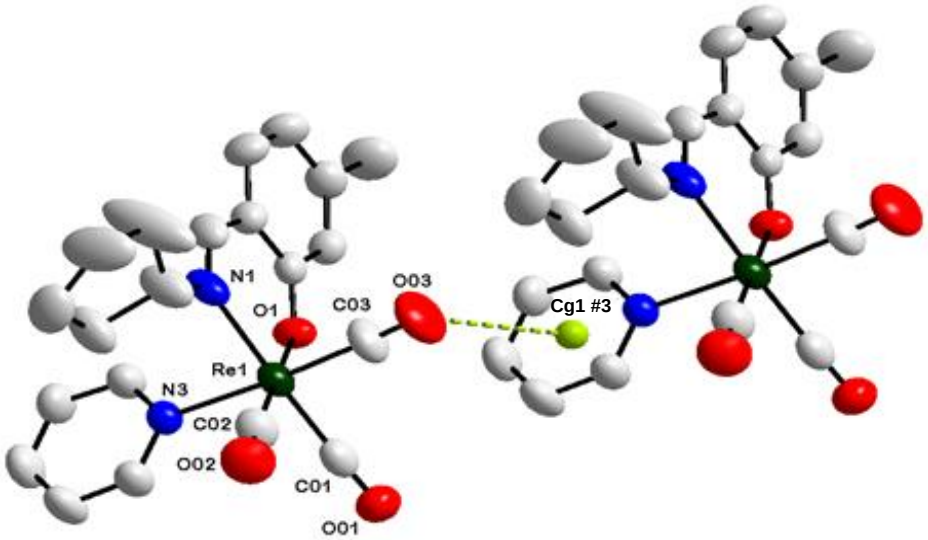

Figure 5.14: Graphical representation of the C-O...π interaction in the unit cell. H atoms are omitted for clarity.

Table 5.8: C-O…π interactions observed in the title complex [Å and °].

C-O…Cg	*d*(O…Cg)	*d*(C…Cg)	<(C-O…Cg)
C03-O03…Cg1 #3	3.786(7)	4.074(8)	96.8(5)

Symmetry codes:
#3 -1+x, y, z
Cg1 = centroid atom of N3, C31, C32, C33, C34, C35

Similarly to *fac*-[Re(5Me-Sal-iProp)$(CO)_3$(Pyridine)], The molecules in the unit cell pack in an alternating "head-to-tail" direction when viewed along the *a*-axis as illustrated in Figure 5.15.

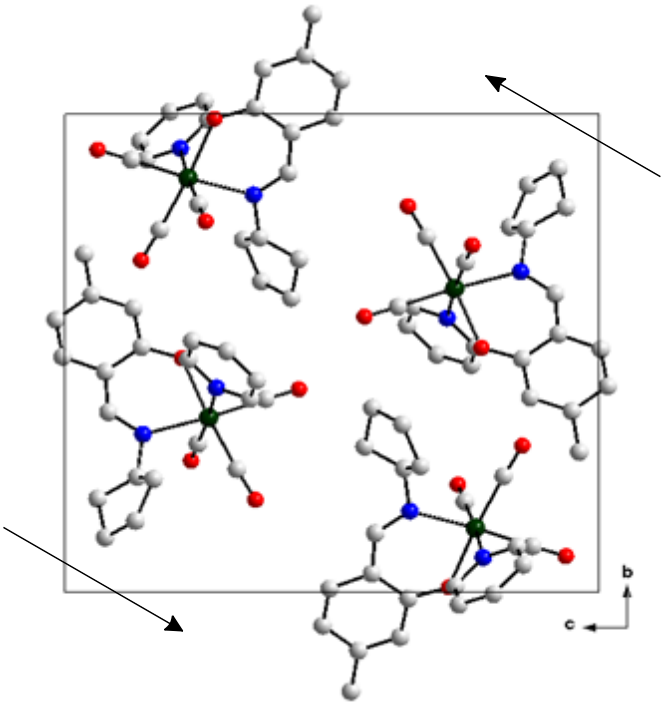

Figure 5.15: Packing of the molecules in the unit cell when viewed along the *a*-axis. H atoms are omitted for clarity.

5.3.3 *fac*-[Re(5Me-Sal-CyPent)$(CO)_3$(Imidazole)] (6)

Complex **(6)** crystallizes in a monoclinic crystal system in the $P2_1/c$ space group and contains four molecules in the unit cell (Z = 4). The asymmetric unit contains one complete molecule of the metal complex. The molecular structure of **(6)** is represented in Figure 5.16 together with the numbering of the atoms. Important bond lengths and angles are given in Table 5.9.

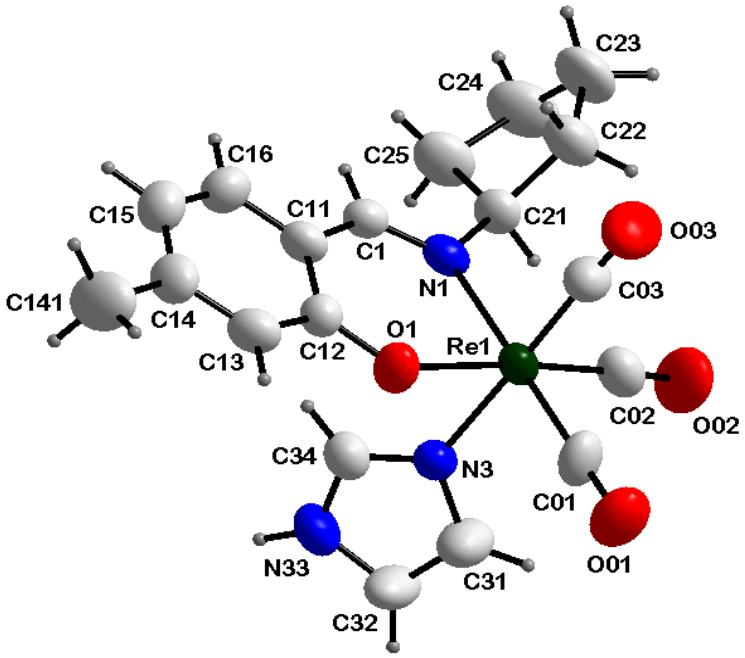

Figure 5.16: Molecular structure of **(6)** showing the numbering of the atoms. Displacement ellipsoids are drawn at a 50 % probability.

Table 5.9: Selected bond lengths and angles of complex **(6)**.

Atoms	Length (Å)	Atoms	Angle (°)
Re1-O1	2.114(5)	N1-Re1-O1	85.1(2)
Re1-N1	2.183(6)	N1-Re1-N3	87.1(2)
Re1-C01	1.896(8)	C03-Re1-N3	178.2(3)
Re1-C02	1.871(9	C01-Re1-C02	84.9(4)
Re1-C03	1.905(8)	C02-Re1-N3	92.3(3)
C01-O01	1.160(10)	O1-Re1-C02	173.8(3)
C02-O02	1.162(12)	C1-N1-C21	115.9(6)
C03-O03	1.151(10)		
Re1-N3	2.189(6)		
N1-C1	1.303(9)		
N1-C21	1.485(9)		

In the title complex, the *N* imine and *O* phenolatido donor atoms of the bidentate ligand coordinate to the rhenium center forming a six-membered ring. Three carbonyl ligands are facially coordinated to rhenium and the final position is occupied by the *N* donor atom of the imidazole ligand completing the octahedron around the metal center. The octahedron around the Re(I) center is slightly distorted as indicated by the N1-Re1-O1 bite angle of 85.1(2)^{o} and O1-Re1-C02 angle of 173.8(3)^{o}.

The Re1-O1 and Re1-N1 bond lengths of 2.114(5) Å and 2.183(6) Å are comparable to related salicylidene structures with bond lengths varying between 2.093-2.155 Å for Re-O and 2.148-2.198 Å for Re-N, as well as to other *N,O* ligand-to-metal bond lengths varying between 2.099-2.146 Å for Re-O and 2.162-2.247 Å for Re-N. The Re1-N3 bond length of 2.189(6) Å is similar to a related salicylidene structure reported by Brink *et al*. (2013)[6] with Re-N(histamine) bond length of 2.188(2) Å. The bond length is also within range of other related structures reported by Benny *et al*. (2011)[27] with Re-N(imidazole) bond lengths varying from 2.169-2.196 Å. The shorter N1-C1 bond length of 1.303(9) Å is an indication of a double bond and is well within range of similar salicylidene structure with bond lengths ranging between 1.275-1.347 Å whereas the longer N1-C21 bond length of 1.485(9) Å falls within range of single bonds (1.439-1.482 Å).[5,6]

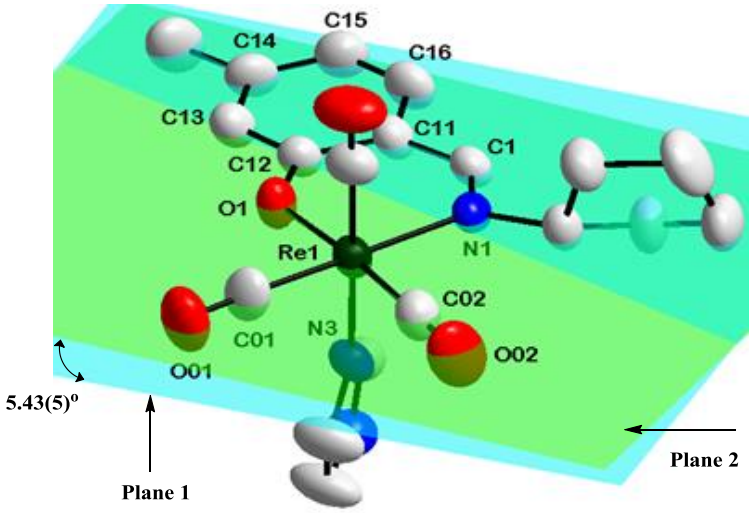

Figure 5.17: A graphical representation of the salicylidene aromatic ring plane (Plane 1) and rhenium equatorial plane (Plane 2). H atoms are omitted for clarity.

The plane formed by the salicylidene aromatic backbone (Plane 1: C11, C12, C13, C14, C15, C16) is lying almost in the same plane as the rhenium equatorial plane (Plane 2: Re1, N1, O1, C01, C02) with a dihedral angle of 5.43(5)°. The plane formed by the five-membered imidazole ring (Plane 3: N3, C31, C32, N33, C34) is slightly bent away from the cyclopentyl substituent on the *N* imine atom of the bidentate towards the C01 and O1 atoms with dihedral angles of 80.29(3)° and 82.81(4)° relative to the salicylidene aromatic backbone plane (Plane 1) and rhenium equatorial plane (Plane 2) respectively.

[27] P. D. Benny, G. A. Fugate, T. Ganguly, B. Twamley, D. K. Bučar, L. R. MacGillivray, *Inorg. Chim. Acta*, 2011, 365, 356.

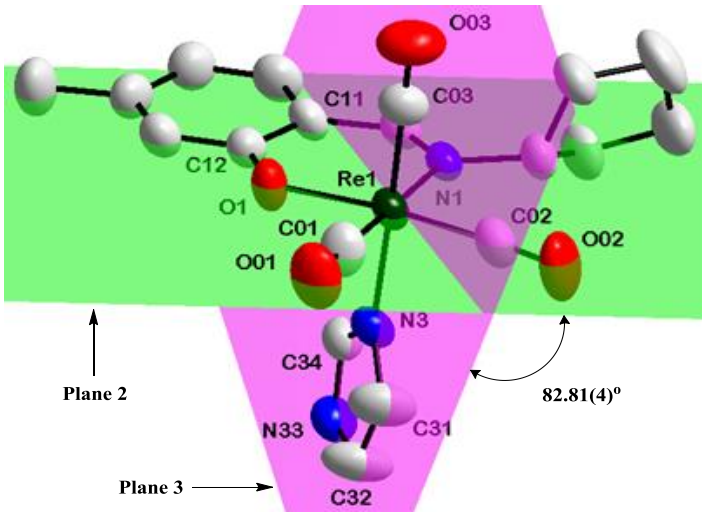

Figure 5.18: A graphical representation of the rhenium equatorial plane (Plane 2) and the imidazole ligand plane (Plane 3). H atoms are omitted for clarity.

The molecular packing is stabilized by an intermolecular hydrogen bond interaction found between the N33-H33 atoms of the imidazole ligand and the phenolatido oxygen atom O1 of the neighbouring molecule as shown in Figure 5.19 and Table 5.10.

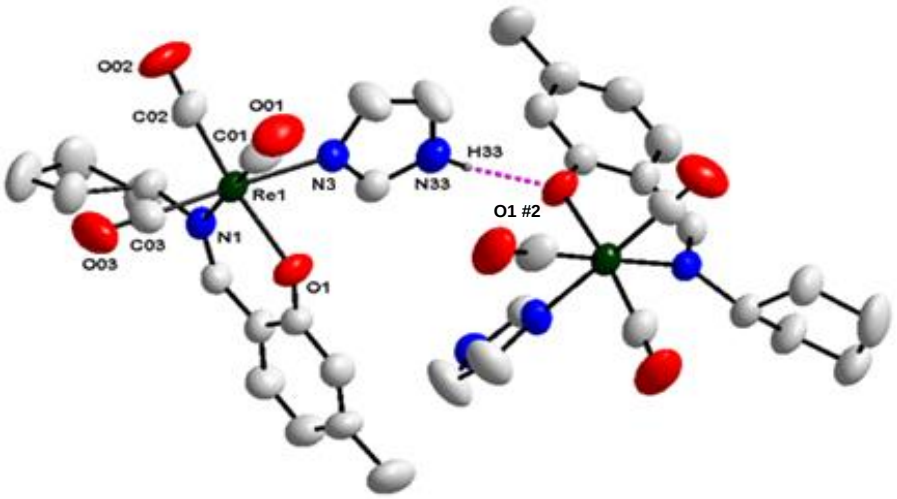

Figure 5.19: Intermolecular hydrogen bond interaction found in the molecular packing of the title complex. H atoms, not part of the hydrogen interaction, are omitted for clarity.

Table 5.10: Intermolecular hydrogen bonding of the title complex [Å and °]

D-H…A	*d*(*D-H*)	*d*(*H…A*)	*d*(*D…A*)	<(*DHA*)
N33-H33…O1 #2	0.88	1.89	2.722(9)	158

Symmetry codes:
#2 5/2-x, -1/2+y, 1/2-z

An intramolecular C-H…π interaction is observed between the C34-H34 atoms and the six-membered ring formed by the bidentate ligand coordinated to the metal center. The molecular packing is stabilized by a C-H…π interaction which exists between the C141-H14B atoms and the five-membered ring atoms of the imidazole ligand of a neighbouring molecule as demonstrated in Figure 5.20 and Table 5.11.

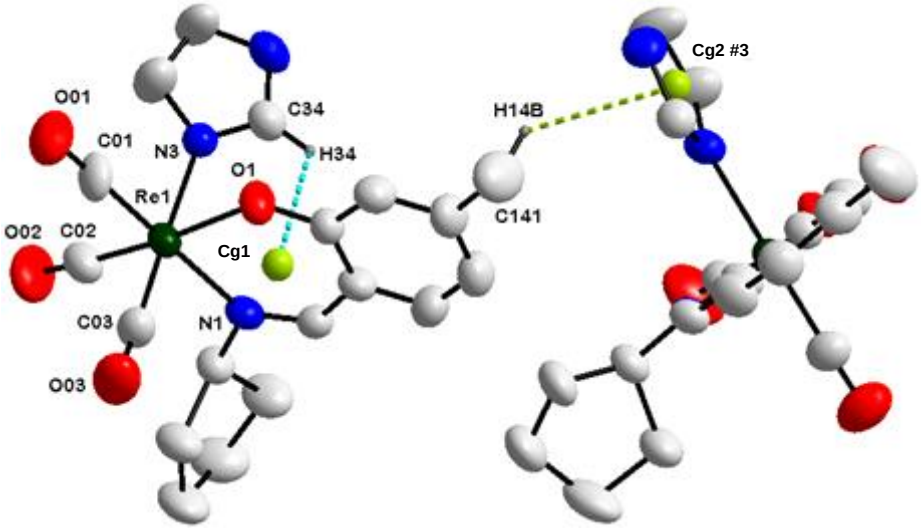

Figure 5.20: Schematic representation of the types of C-H…π interactions that exist in the molecular packing of the title complex. H atoms, not part of the hydrogen interactions, are omitted for clarity.

Table 5.11: C-H…π interaction found in the title complex [Å and °].

C-H…Cg	*d*(H…Cg)	*d*(C…Cg)	<(C-H…Cg)
C34-H34…Cg1 #1	2.46	2.947(9)	112
C141-H14B…Cg2 #3	2.98	3.567(15)	119

Symmetry codes:
#1 x, y, z; #3 1/2+x, 1/2-y, 1/2+z
Cg1 = centroid atom of Re1, N1, C1, C11, C12, O1; Cg2 = centroid atom of N3, C31, C32, N33, C34

A C-O…π interaction is observed between the carbonyl atoms C01-O01 and the imidazole ring of a neighbouring molecule as shown in Figure 5.21 and Table 5.12.

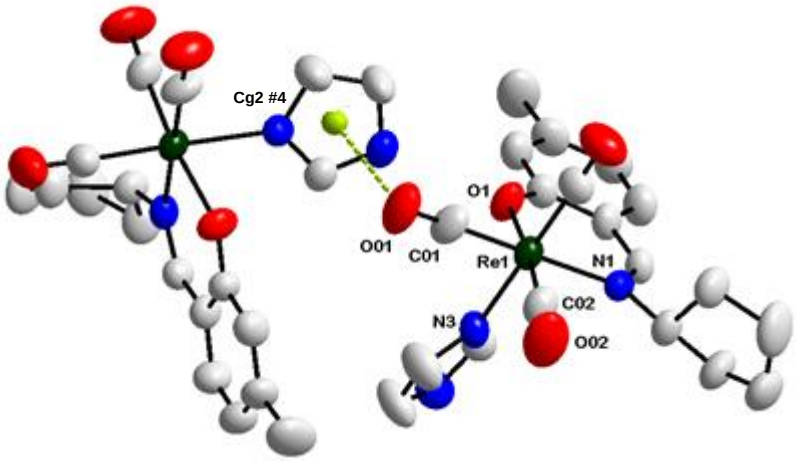

Figure 5.21: A schematic representation of the C-O…π interaction found in the molecular packing of the title complex. H atoms are omitted for clarity.

Table 5.12: C-O…π interactions found in the title complex [Å and °].

C-O…Cg	*d*(O…Cg)	*d*(C…Cg)	<(C-O…Cg)
C01-O01…Cg2 #4	3.432(9)	3.718(11)	95.0(7)

Symmetry codes:
#4 5/2-x, 1/2+y, 1/2-z
Cg2 = centroid atom of N3, C31, N32, C33, C34

The molecular layers in the unit cell pack in an alternating "head-to-tail" direction when viewed along the *b*-axis as illustrated in Figure 5.22 below.

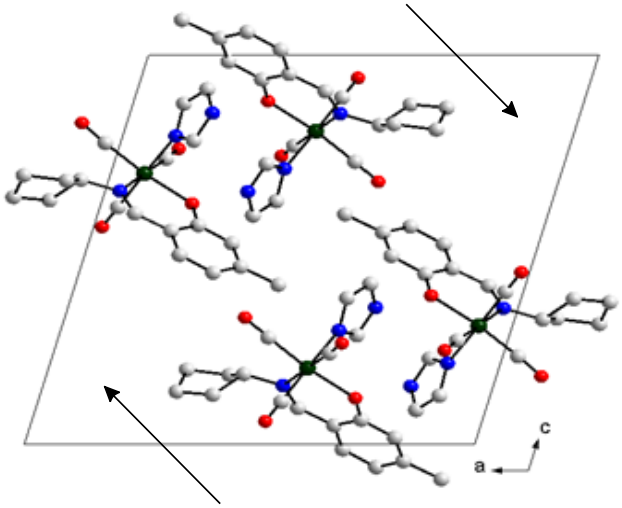

Figure 5.22: Molecular packing of the complex in the unit cell when viewed along the *b*-axis. H atoms are omitted for clarity.

5.3.4 *fac*-[Re(*κO*-5Me-Sal-CyPent)(CO)$_3$(Pyridine)(Br)] (7)

Complex **(7)** crystallizes in a monoclinic crystal system in the $P2_1/c$ space group and contains four molecules in the unit cell ($Z = 4$). The asymmetric unit consist of one complete molecule of the metal complex. The molecular structure of **(7)** is represented in Figure 5.23 together with the numbering of the atoms. Important bond lengths and angles are given in Table 5.13.

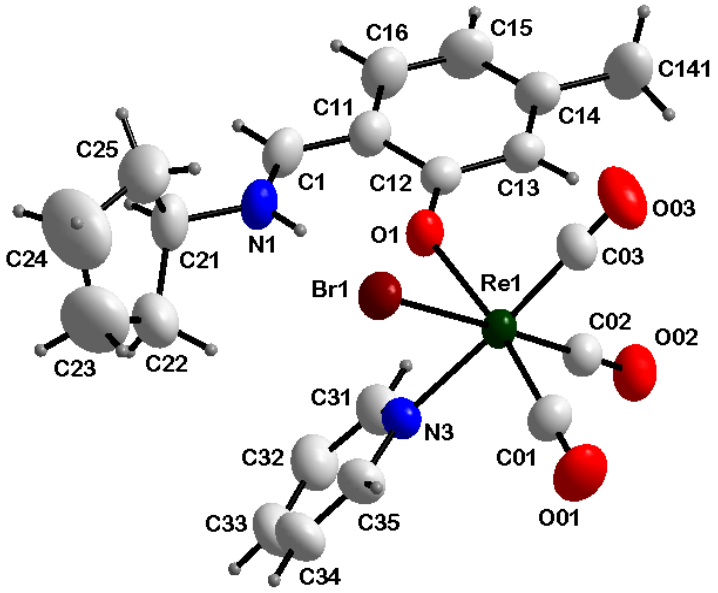

Figure 5.23: Molecular structure of **(7)** showing the numbering of the atoms. Displacement ellipsoids are drawn at a 50 % probability.

Table 5.13: Selected bond lengths and angles of complex **(7)**.

Atoms	Length (Å)	Atoms	Angle (°)
Re1-O1	2.132(3)	O1-Re1-Br1	80.47(9)
Re1-Br1	2.628(7)	N3-Re1-Br1	84.96(9)
Re1-N3	2.220(4)	C03-Re1-N3	175.93(15)
Re1-C01	1.896(4)	C01-Re1-C02	88.61(19)
Re1-C02	1.897(4)	C02-Re1-Br1	177.78(14)
Re1-C03	1.899(5)	O1-Re1-C02	98.96(15)
C01-O01	1.147(5)	N3-Re1-O1	80.73(13)
C02-O02	1.151(5)	C1-N1-C21	124.9(4)
C03-O03	1.149(6)		
N1-C1	1.304(6)		
N1-C21	1.459(6)		

In the title complex, the ligand coordinates to the rhenium center in a monodentate manner through the phenolatido *O* donor atom and not in a standard bidentate manner. The mono-coordinated Schiff-base ligand crystallizes as the *trans* keto-amine tautomer with a strong intramolecular hydrogen bond observed between the N1-H1B…O1 atoms (Table 5.14). Three carbonyl ligands are facially coordinated to rhenium as usual while the remaining two positions are occupied by the *N* donor atom of the pyridine ligand and a bromido ligand. The octahedron around the Re(I) center is slightly distorted as indicated by O1-Re1-Br1, C03-Re1-N3 and C01-Re1-C02 angles of 80.44(9)^{o}, 176.00(16)^{o} and 88.7(2)^{o} respectively.

The Re1-O1 bond length of 2.132(3) Å is significantly longer than the observed Re1-O1 bond lengths in *fac*-[Re(L,L'-Bid)$(CO)_3$(L)] complexes reported in this study which range between 2.093-2.114 Å. The C1-N1 bond length of 1.304(6) Å is longer than the C-N bond lengths in related non-coordinated salicylidene ligands which range between 1.278-1.287 Å and normally crystallizes as the *trans* phenol-imine tautomer.[28,29,30,31] The structure reported by Tahir *et al*. (2011)[31] crystallizes as a mixture of both the phenol-imine and keto-amine tautomers. The bond length is also longer than the observed C1-N1 bond length in a similar structure reported in this study, *fac*-[Re(5Me-Sal-CyPent)$(CO)_3$(Pyridine)] **(5)**, as shown in Figure 5.24. The increase in the C=N bond length is an indication of the transformation from the phenol-imine tautomer to the keto-amine form.[32]

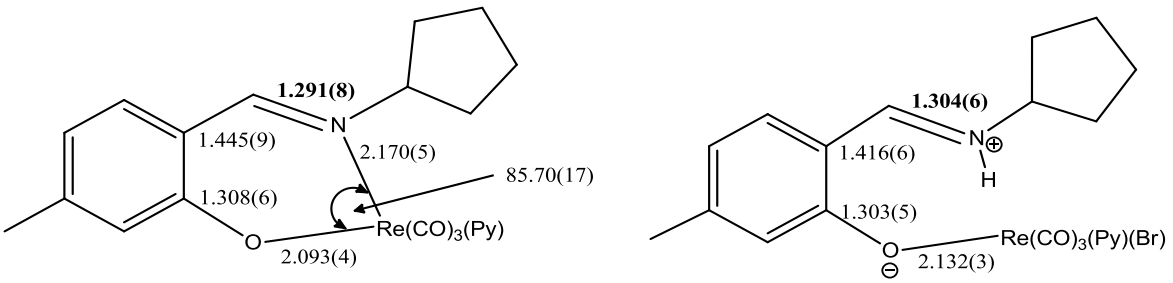

(5) **(7)**

Figure 5.24: Structural comparison, bond length (Å) and angle (^{o}), between bi- and mono-coordinated ligands of *fac*-[Re(5Me-Sal-CyPent)$(CO)_3$(Pyridine)] **(5)** and *fac*-[Re(*κO*-5Me-Sal-CyPent)$(CO)_3$(Pyridine)(Br)] **(7)** complexes.

[28] Y. Miura, Y, Aritake, T. Akitsu, *Acta Cryst*., 2009, E65, o2381.
[29] A. Brink, A. Roodt, H. G. Visser, *Acta Cryst*., 2009, E65, o3175.
[30] H. K. Fun, C. K. Quah, S. Viveka, D. J. Madhukumar, G. K. Nagaraja, *Acta Cryst*., 2011, E67, o1933.
[31] M. N. Tahir, H. A. Shad, R. H. Tariq, *Acta Cryst*., 2011, E67, o2319.
[32] R. Hernández-Molina, A. Merderos, *Comprehensive Coordination Chemistry II*, Eds.: J. A. McCleverty, T. J. Meyer, Pergamon Press, Oxford, UK, Vol. 1, 2004.

The Re1-Br1 bond length of 2.628(7) Å is well within range of other *N,O* ligand-to-metal structures with Re-Br bond lengths ranging between 2.611-2.641 Å.[33,34,35] The Re1-N3 bond length of 2.219(4) Å compares well to related salicylidene structures with Re-N(pyridine) bond lengths ranging from 2.203-2.230 Å, as well as to other *N,O* and *O,O'* ligand-to-metal structures with Re-N(pyridine) bond lengths varying from 2.203-2.334 Å. The pyridine ligand is slightly bent towards the cyclopentyl substituent on the *N* imine atom with N3-Re1-O1 angle of 80.68(13)°.

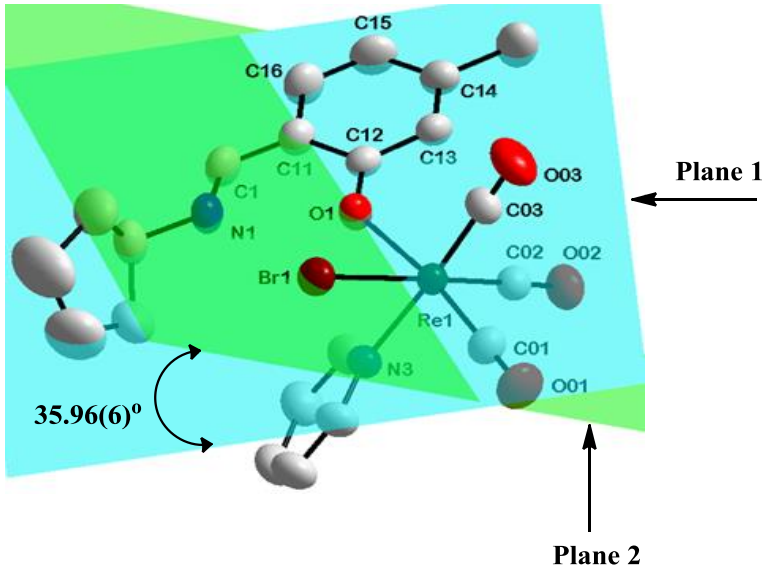

Figure 5.25: A graphical representation of the salicylidene aromatic ring plane (Plane 1) and rhenium equatorial plane (Plane 2). H atoms are omitted for clarity.

The salicylidene aromatic backbone plane (Plane 1: C11, C12, C13, C14, C15, C16) is rotated relative to the rhenium equatorial plane (Plane 2: Re1, Br1, O1, C01, C02) with a dihedral angle of 35.96(6)°. The plane formed by the pyridine ligand (Plane 3: N3, C31, C32, C33, C34) has a dihedral angle of 50.43(5)° relative to the salicylidene aromatic backbone plane (Plane 1) and a dihedral angle of 81.64(2)° relative to the rhenium equatorial plane (Plane 2).

[33] W. Wang, B. Spingler, R. Alberto, *Inorg. Chim. Acta*, 2003, 355, 386.
[34] L. Wei, J. Zubieta, *Acta Cryst*., 2005, C61, m95.
[35] J. Ho, W. Y. Lee, K. J. T. Koh, P. P. F. Lee, Y. K. Yan, *J. Inorg. Biochem*., 2013, 119, 10.

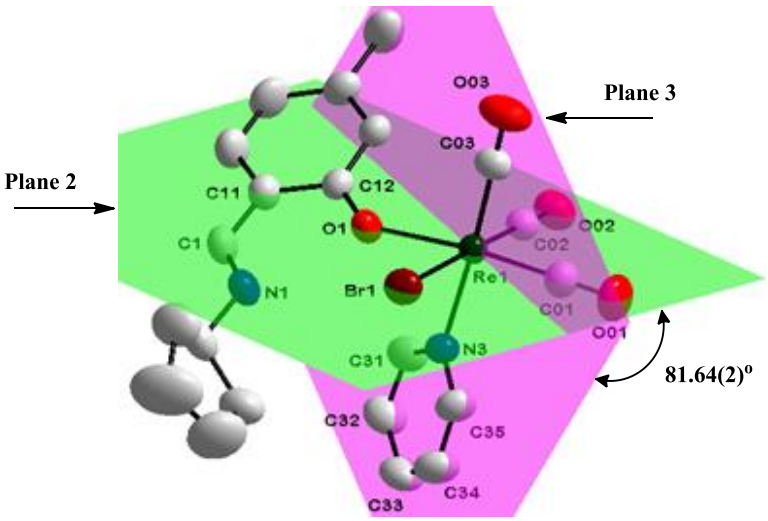

Figure 5.26: Illustration of the rhenium equatorial plane (Plane 2) and the pyridine ring plane (Plane 3). H atoms are omitted for clarity.

Two intramolecular hydrogen bond interactions occur between the N1-H1B…O1 and C31-H31…O1 atoms as shown in Figure 5.27 and Table 5.14. The former is a strong interaction with H1B…O1 bond length of 2.606 Å.

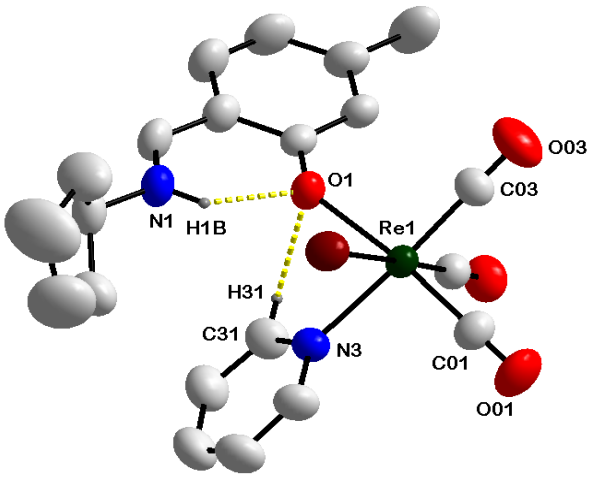

Figure 5.27: Intramolecular hydrogen bond interactions observed in the title complex. H atoms, not part of the hydrogen interactions, are omitted for clarity.

Table 5.14: Intramolecular hydrogen bonding observed in the title complex [Å and °].

D-H…A	*d*(*D-H*)	*d*(*H…A*)	*d*(*D…A*)	<(*DHA*)
N1-H1B…O1 #1	0.88	1.94	2.606(5)	131
C31-H31…O1 #1	0.95	2.60	2.972(6)	104

Symmetry codes:
#1 x, y, z

The packing of the molecules in the unit cell is further stabilized by three intermolecular hydrogen bond interactions as shown in Figure 5.28 and Table 5.15.

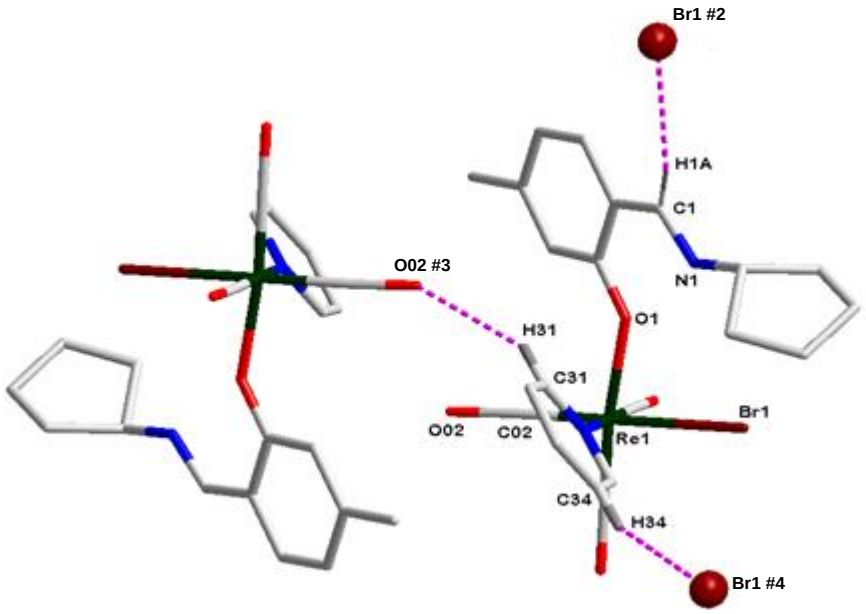

Figure 5.28: Intermolecular hydrogen bond interactions occurring in the title complex. Molecules are shown in "stick" format and H atoms not part of the hydrogen interactions omitted for clarity.

Table 5.15: Intermolecular hydrogen bonding observed in the title complex [Å and °].

D-H…A	*d*(*D-H*)	*d*(*H…A*)	*d*(*D…A*)	<(*DHA*)
C1-H1A…Br1 #2	0.95	2.79	3.722(5)	166
C31-H31…O02 #3	0.95	2.56	3.416(6)	150
C34-H34…Br1 #4	0.95	2.82	3.701(7)	156

Symmetry codes:
#2 1-x, -1/2+y, 1/2-z; #3 1-x, -y, 1-z; #4 –x, -1/2+y, 1/2-z

An intramolecular C-H…π interaction is observed between the C22-H22B atoms of the cyclopentyl substituent and the pyridine ligand while an intermolecular C-H…π interaction occurs between the C22-H22A atoms and the salicylidene aromatic ring of a neighbouring molecule as illustrated in Figure 5.29 and Table 5.16.

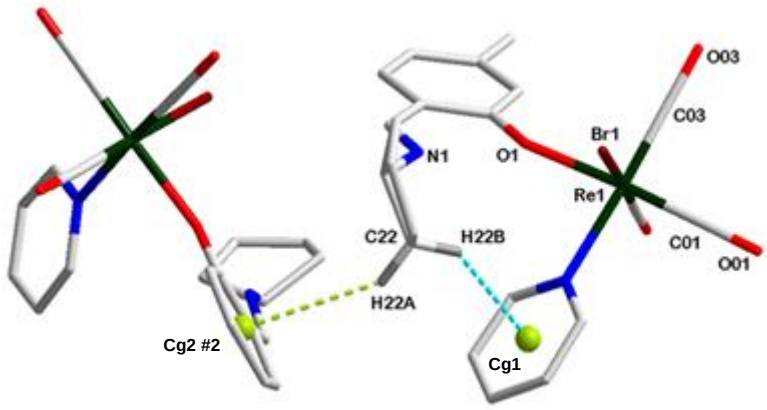

Figure 5.29: Intra- and intermolecular C-H…π interactions observed in the packing of the title complex. Molecules are illustrated in "stick" format and H atoms not part of the C-H…π interactions omitted for clarity.

Table 5.16: C-H…π interactions observed in the title complex [Å and °].

C-H…Cg	*d*(H…Cg)	*d*(C…Cg)	<(C-H…Cg)
C22-H22A…Cg1 #1	2.97	3.774(8)	139
C22-H22B…Cg2 #2	2.91	3.741(7)	142

Symmetry codes:
#1 x, y, z; #2 1-x, -1/2+y, 1/2-z
Cg1 = centroid atom of N3, C31, C32, N33, C34; Cg2 = centroid atom of C11, C12, C13, C14, C15, C16

The molecular packing is further stabilized by the formation of a C-O…π interaction between the carbonyl atoms C02-O02 and the salicylidene aromatic ring as demonstrated in Figure 5.30 and Table 5.17.

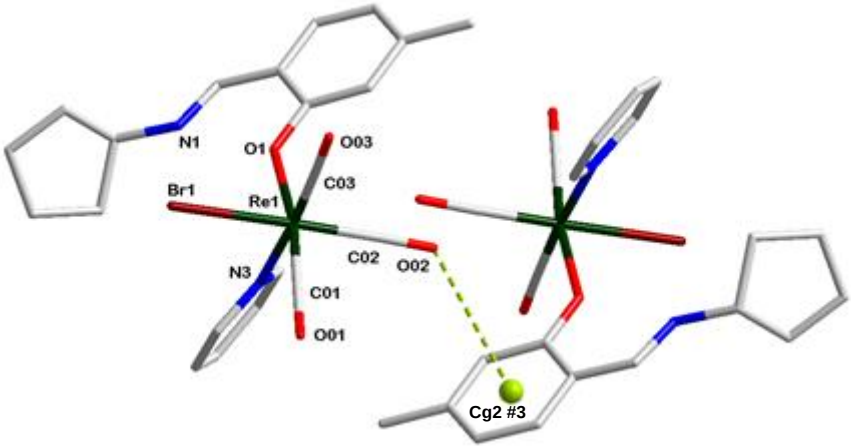

Figure 5.30: Schematic representation of the C-O…π interaction that exists in the packing of the title complex. Molecules are illustrated in "stick" format and H atoms omitted for clarity.

Table 5.17: C-O…π interactions observed in the title complex [Å and °].

C-O…Cg	*d*(O…Cg)	*d*(C…Cg)	<(C-O…Cg)
C02-O02…Cg2 #3	3.615(4)	4.450(5)	130.6(3)

Symmetry codes:
#3 1-x, -y, 1-z
Cg2 = centroid atom of C11, C12, C13, C14, C15, C16

The molecules in the unit cell pack in a "head-to-head" manner when viewed along the *b*-axis as depicted in Figure 5.31.

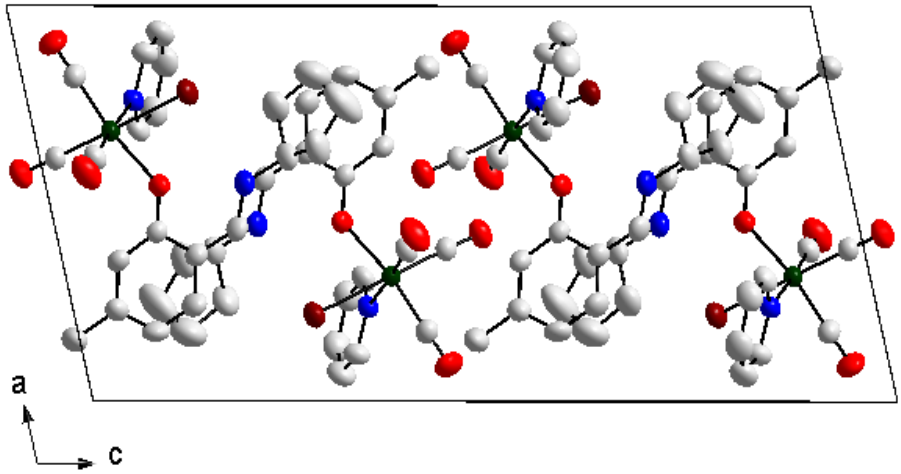

Figure 5.31: Molecular packing of the complex in the unit cell when viewed along the *b*-axis. H atoms are omitted for clarity.

5.3.5 *fac*-[Re(5Me-Sal-Hist)(CO)$_3$]. MeOH (8)

Complex **(8)** is a polymorphic form of a complex previously reported by Brink *et al*. (2013),[6] which crystallized in a triclinic crystal system in the $P\bar{1}$ space group and consists of 2 molecules in the unit cell (Z = 2). The title complex reported in this study crystallizes in an orthorhombic crystal system in the *Pbcn* space group and consists of eight molecules in the unit cell (Z = 8). The asymmetric unit consists of one complete molecule of the metal complex with a methanol solvent molecule. The molecular structure of **(8)** is depicted in Figure 5.32 together with the numbering of the atoms. Important bond lengths and angles are given in Table 5.18.

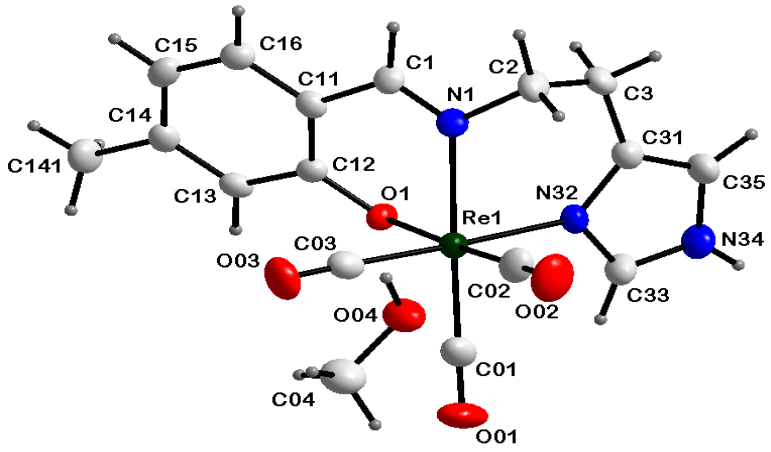

Figure 5.32: Molecular structure of **(8)** showing the numbering of the atoms. Displacement ellipsoids are drawn at a 50 % probability.

Table 5.18: Selected bond lengths and angles of complex **(8)**.

Atoms	Length (Å)	Atoms	Angle (°)
Re1-O1	2.138(4)	N1-Re1-O1	81.12(14)
Re1-N1	2.167(5)	N1-Re1-N32	81.23(18)
Re1-N32	2.184(4)	N1-Re1-C03	96.9(2)
Re1-C01	1.917(7)	N32-Re1-C02	93.4(2)
Re1-C02	1.894(6)	O1-Re1-C02	176.9(2)
Re1-C03	1.925(6)	N32-Re1-C03	178.0(2)
N1-C1	1.277(7)	N1-Re1-C03	178.0(2)
N1-C2	1.467(7)	C1-N1-C2	117.4(5)
C01-O01	1.150(8)		
C02-O02	1.162(8)		
C03-O03	1.150(7)		

In the title complex, the Schiff-base ligand coordinate to the rhenium center in a tridentate manner through the *N* imine donor atom, phenolatido *O* donor atom and *N* donor atom of the histamine moiety forming two six-membered rings. The complex crystallizes with a methanol solvent in the unit cell. The octahedron around the Re(I) center is distorted with N1-Re-O1, N1-Re-N32 bite angles of 81.12(14)° and 81.23(18)° respectively and the N1-Re-C01 angle of 173.6(2)°.

The Re1-O1, Re1-N1 and Re1-N32 bond lengths of 2.138(4), 2.167(5) and 2.184(4) Å are comparable to the polymorphic structure reported by Brink *et al*. (2013)[6] with Re1-O1, Re1-N1 and Re1-N32 bond lengths of 2.1454(16), 2.1599(19) and 2.1875(19) respectively.

The bond lengths also compare well to related salicylidene structures with bond lengths ranging from 2.093-2.155 Å for Re-O, 2.148-2.198 Å for Re-N and 2.169-2.196 for Re-N(imidazole).

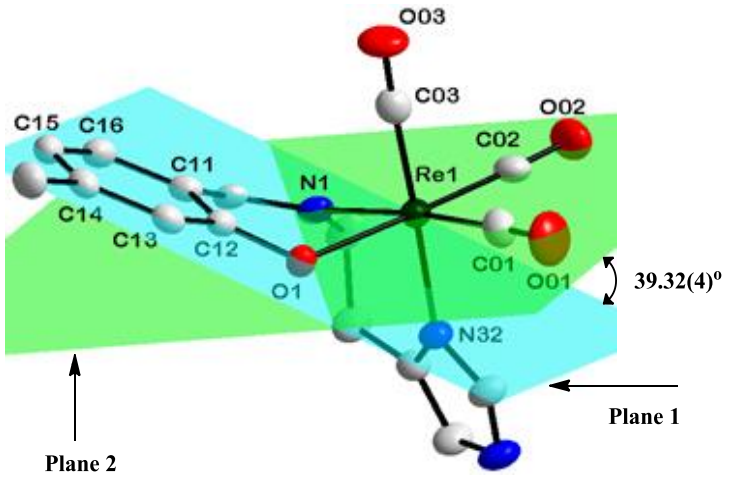

Figure 5.33: Illustration of the salicylidene aromatic backbone plane (Plane 1) and rhenium equatorial plane (Plane 2). H atoms and methanol solvent are omitted for clarity.

The salicylidene aromatic backbone plane (Plane 1: C11, C12, C13, C14, C15, C16) is bent away from the rhenium equatorial plane (Plane 2: Re1, N1, O1, C01, C02) with a dihedral angle of 39.32(4)°. The histamine moiety is slightly bent away from the bidentate ligand and the plane formed by this five-membered ring (Plane 3: C31 N32, C33, N34, C35) has a dihedral angle of 84.47(5)° relative to the rhenium equatorial plane (Plane 2) and 51.05(3)° relative to the salicylidene aromatic backbone (Plane 1).

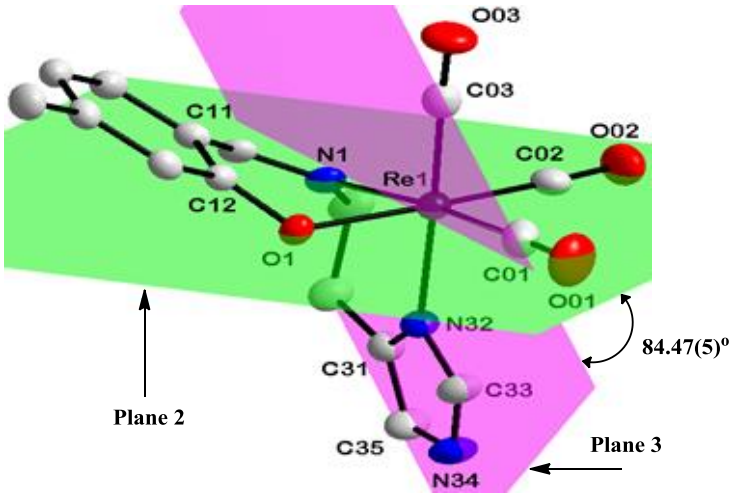

Figure 5.34: Graphical representation of the rhenium equatorial plane (Plane 2) and the histamine substituent plane (Plane 3). H atoms and methanol solvent are omitted for clarity.

An intramolecular hydrogen bond interaction of the type O-H…O occurs between the O04-H141 atoms of the methanol solvent molecule and the phenolatido oxygen atom O1 coordinated to the metal center. The packing is stabilized by two classic intermolecular hydrogen bond interactions. The first interaction occurs between the N34-H34 atoms of the histamine substituent and the methanol oxygen atom O04 while the second interaction is observed between the C35-H35 atoms and the carbonyl oxygen atom O01 of a neighbouring molecule as shown in Figure 5.35 and Table 5.19.

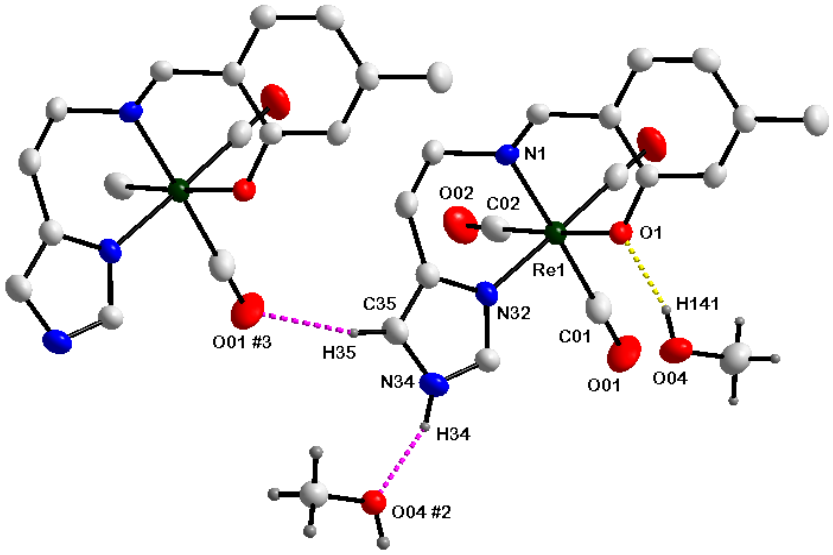

Figure 5.35: Types of hydrogen bond interactions that occur in the molecular packing of the title complex. Certain H atoms are omitted for clarity.

Table 5.19: Hydrogen bonding found in the title complex [Å and °].

D-H…A	*d*(*D-H*)	*d*(*H…A*)	*d*(*D…A*)	<(*DHA*)
O04-H141…O1 #1	0.84	1.88	2.659(6)	153
N34-H34…O04 #2	0.88	1.94	2.767(7)	157
C35-H35…O01 #3	0.95	2.38	3.317(7)	167

Symmetry codes:
#1 x, y, z; #2 1-x, 1-y, 1-z; #3 x, 1+y, z

The molecular packing is further stabilized by the formation of a C-H…π interaction that occurs between the C141-H14C atoms of the methyl moiety on the salicylidene aromatic backbone and the six-membered ring atoms of the salicylidene backbone of a neighbouring molecule as illustrated in Figure 5.36 and Table 5.20.

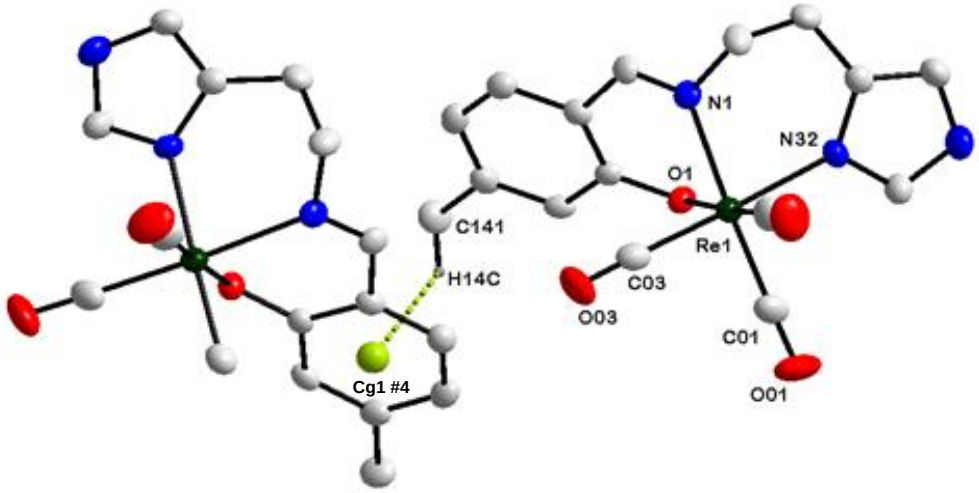

Figure 5.36: Graphical representation of the C-H…π interaction that stabilizes the molecular packing in the unit cell. H atoms, not part of the hydrogen interaction, are omitted for clarity.

Table 5.20: C-H…π interactions found in the title complex [Å and °].

C-H…Cg	*d*(H…Cg)	*d*(C…Cg)	<(C-H…Cg)
C141-H14C…Cg1 #4	2.82	3.480(7)	125

Symmetry codes:
#4 1/2-x, 1/2+y, z
Cg1 = centroid atom of C11, C12, C13, C14, C15, C16

A π-π interaction occurs between the five-membered histamine rings of the neighbouring molecules as shown in Figure 5.37 and Table 5.21.

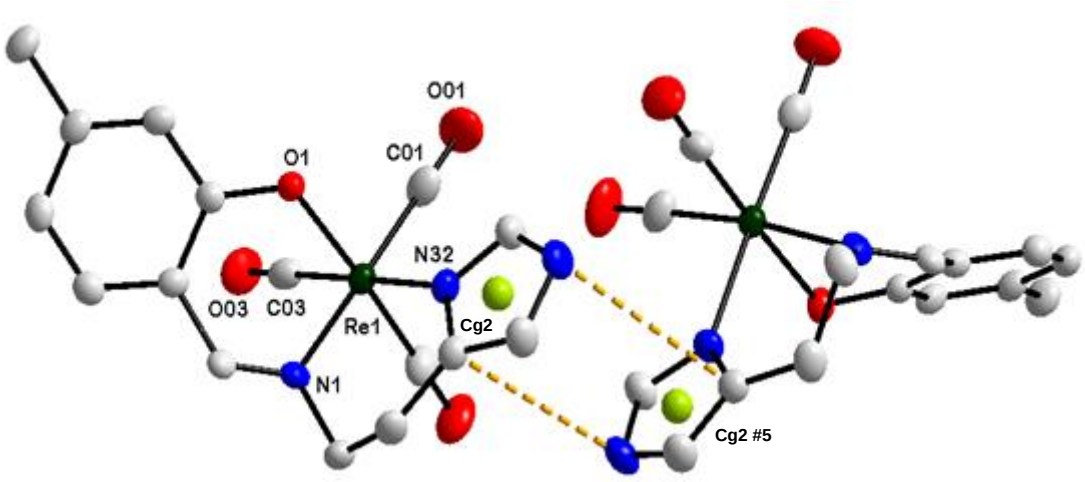

Figure 5.37: A schematic representation of a π-π interaction between the five-membered histamine rings of neighbouring molecules. H atoms are omitted for clarity.

Table 5.21: π-π interaction observed in the title complex [Å].

Centroid atom	Centroid atom	*d*(Cg…Cg)
Cg1	Cg1 #1	3.894(4)

Symmetry codes:
#5 -x, y, 1/2-z
Cg2 = centroid atom of C31, N32, C33, N34, C35

The molecules in the unit cell pack in a "head-to-head" manner when viewed along the *b*-axis as depicted in Figure 5.38. A weak π-π interaction occurs between the salicylidene aromatic rings of the neighbouring molecules.

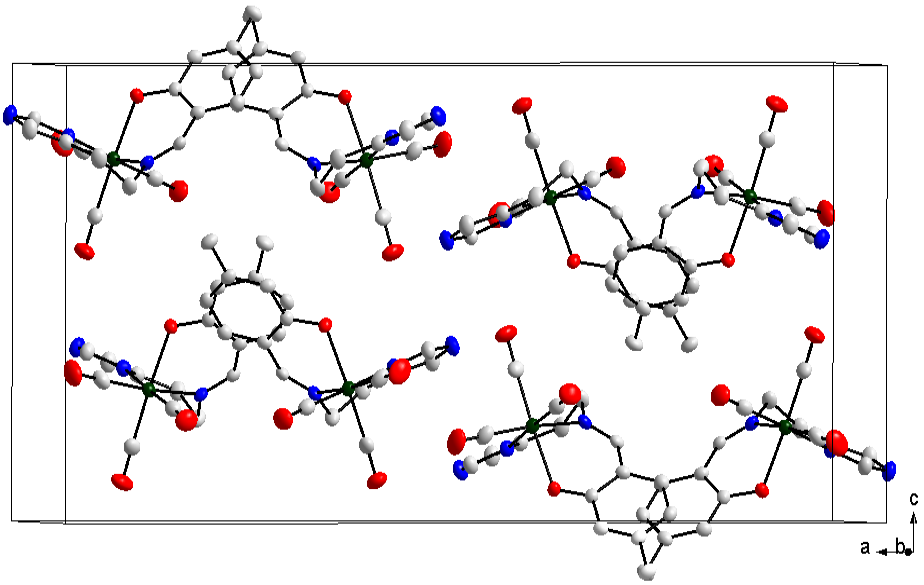

Figure 5.38: Packing of the molecules in the unit cell when viewed along the *b*-axis, showing weak π-π interaction between the salicylidene aromatic rings of the neighbouring molecules. H atoms are omitted for clarity.

5.4 Discussion

In this chapter, four new crystal structures of complexes of the type *fac*-[Re(L,L'-Bid)$(CO)_3$(L)] (L,L'-Bid = *N,O* Sal bidentate ligand; *L* = coordinated pyridine or imidazole) and a polymorphic form of a complex previously reported by Brink *et al.*(2013)[6] were presented. Crystallographic parameters of the five complexes as well as their selected bond lengths and angles are summarized for comparison in Table 5.22 and 5.23.

Table 5.22: Crystallographic parameters of *fac*-[Re(L,L'-Bid)$(CO)_3$(L)] complexes (L,L'-Bid = *N,O* Sal bidentate ligand; *L* = coordinated pyridine or imidazole).

Complex	**(4)**	**(5)**	**(6)**	**(7)**	**(8)**
Crystal system	Monoclinic	Monoclinic	Monoclinic	Monoclinic	Orthorhombic
Space group	$P2_1/c$	$P2_1/c$	$P2_1/c$	$P2_1/c$	*Pbcn*
Unit cell dimensions					
a (Å)	8.2805(3)	8.2371(4)	15.746(5)	11.2105(5)	28.3997(39)
b (Å)	13.7325(5)	15.0284(7)	7.983(5)	9.0638(5)	9.0380(11)
c (Å)	16.3560(6)	16.2958(7)	19.170(4)	22.9499(12)	14.3900(17)
α (^{o})	90	90	90	90	90
β (^{o})	92.431(2)	91.040(1)	126.407(17)	102.860(2)	90
γ (^{o})	90	90	90	90	90
Volume (Å^3)	1858.2(2)	2016.9(2)	1939.4(3)	2273.4(3)	3693.6(13)
Z	4	4	4	4	8

Table 5.23: Selected bond lengths and angles of *fac*-[Re(L,L'-Bid)$(CO)_3$(L)] complexes (L,L'-Bid = *N,O* Sal bidentate ligand; *L* = coordinated pyridine or imidazole).

Complex	**(4)**	**(5)**	**(6)**	**(7)**	**(8)**
Bond length (Å)					
Re1-O1	2.107(3)	2.093(4)	2.114(5)	2.132(3)	2.138(4)
Re1-N1	2.173(3)	2.170(5)	2.183(6)	-	2.167(5)
Re1-N3	2.231(4)	2.229(5)	2.189(6)	2.220(4)	-
Re1-N32	-	-	-	-	2.184(4)
Re1-Br	-	-	-	2.6279(7)	-
Re1-C01	1.898(5)	1.933(7)	1.896(8)	1.896(4)	1.917(7)
Re1-C02	1.905(5)	1.907(7)	1.871(9)	1.897(4)	1.894(6)
Re1-C03	1.907(5)	1.921(6)	1.905(8)	1.899(5)	1.925(6)
N1-C1	1.300(6)	1.291(8)	1.303(9)	1.304(6)	1.277(7)
Bond angle (^{o})					
N1-Re1-O1	85.73(12)	85.70(17)	85.1(2)	-	81.12(14)
N1-Re1-N32	-	-	-	-	81.23(18)
N1-Re1-N3	87.23(13)	86.22(18)	87.1(2)	-	-
Br1-Re1-N3	-	-	-	84.96(9)	
C03-Re1-N3	176.37(19)	176.2(3)	178.2(3)	175.93(15)	-
C03-Re1-N32	-	-	-	-	178.0(2)
C01-Re1-C02	86.95(19)	86.2(3)	84.9(4)	88.61(19)	88.7(3)
C1-N1-C2	-	-	-	-	117.4(5)
C1-N1-C21	117.9(4)	118.3(6)	115.9(6)	124.9(4)	-

Four of the complexes **(4-7)** presented in this chapter all crystallize in the monoclinic crystal system, $P2_1/c$ space group and contains four molecules ($Z = 4$) in the unit cell. Complex **(8)** is the odd one out crystallizing in an orthorhombic crystal system, *Pbcn* space group and consists of eight molecules ($Z = 8$) in the unit cell. Complexes **(4-6)** display similar packing modes of the molecules within the unit cell.

In complex **(4)** and **(5)**, the bidentate ligand coordinates to the rhenium center through the *N* and *O* donor atoms. Three carbonyl ligands are facially coordinated to the metal center and the sixth coordination site is occupied by a pyridine ligand. The bidentate ligand and carbonyl ligands in complex **(6)** coordinate to the rhenium center in a similar manner as in complex **(4)** and **(5)**. The only difference in complex **(6)** is the imidazole ligand that is coordinated to the sixth position instead of the pyridine ligand. Complex **(7)** and **(8)** adopts unique coordination modes of the Schiff-base ligands around the rhenium center. In complex **(7)**, the ligand coordinates to the rhenium center in a monodentate manner through the *O* donor atom and not in a standard bidentate manner through both *N* and *O* donor atoms. The mono-coordinated ligand in this complex crystallizes as the keto-amine tautomer (NH containing) resulting in the formation of a zwitterion. Three carbonyl ligands are facially coordinated to rhenium and the two remaining coordination sites are occupied by the pyridine ligand and a bromido ligand. The ligand in complex **(8)** coordinates to the metal center in a tridentate manner through two *N* donor atoms and one *O* donor atom.

Complexes **(5-7)** have the same salicylidene Schiff-base ligand coordinated to the rhenium center. The ligand coordinates in a standard bidentate manner, complex **(5)** and **(6)**, when the reaction is carried out at elevated temperature (70 ^{o}C). But, when the reaction is done at room temperature (25 ^{o}C), the same ligand coordinates in a monodentate manner through the phenolatido *O* donor atom as demonstrated by complex **(7)**.

The only difference between complex **(5)** and **(6)** is the pyridine and imidazole ligand that is coordinated to the sixth position on the metal center. Therefore, it comes as no surprise that both these complexes crystallize in the same crystal system, the same space group and contain the same amount of molecules in the unit cell. Furthermore, their cell dimensions do not differ significantly when compared to each other. Thus, it can be concluded that the two complexes are iso-structural.

From Table 5.23, it is evident that the Re1-O1 bond distances in complexes **(4)** and **(6)** are comparable to each another, but are significantly longer than the observed Re1-O1 bond

distance in complex **(5)**. This is rather peculiar considering the fact that the bidentate ligand in complex **(5)** and **(6)** is exactly the same. Furthermore, these complexes are iso-structural. Therefore, one would expect the Re1-O1 bond distances in complex **(5)** and **(6)** to be comparable since the ligand (pyridine and imidazole) occupying the sixth position on the metal center only introduces small variations in the complexes. The Re1-N1 bond distance in complexes **(4)-(6)** are comparable, which is in agreement with the iso-structural behaviour displayed by complex **(5)** and **(6)**. The Re1-N3 bond distances in complexes **(4)**, **(5)** and **(7)** are comparable to each other, but are significantly longer than the observed Re-N3 bond distance in complex **(6)**. Therefore, the imidazole ligand coordinates more strongly to the rhenium center than the pyridine ligand. This is further supported by the Re1-N32 bond distance of the histamine moiety in complex **(8)**, which is comparable to the Re1-N3 bond distance in complex **(6)**.

The bite angles of the bidentate ligands in complexes **(4)-(7)** are comparable to each other, but are significantly larger than the bite angles of the tridentate ligand in complex **(8)**. This is expected as the tridentate ligand would require more space on the metal center than the bidentate ligands. Thus, the tridentate ligand is significantly rotated and squeezed upon coordination to the rhenium center, which result in a decrease of the bite angles.

5.5 Conclusion

The initial aim of synthesizing complexes of the type *fac*-[Re(L,L'-Bid)$(CO)_3$(MeOH)] (L,L'-Bid = *N,O* Sal bidentate ligand) was achieved during this M.Sc. study. However, all attempts to obtain single crystals of the methanol substituted products that were suitable for X-ray diffraction were unsuccessful. The methanol solvento molecule was consequently substituted with more stable monodentate ligands to form single crystals of complexes of the type *fac*-[Re(L,L'-Bid)$(CO)_3$(L)] (L,L'-Bid = *N,O* Sal bidentate ligand; *L* = coordinated pyridine or imidazole), that were suitable for X-ray diffraction. As a result, four new crystal structures and a polymorphic form of a complex previously reported by Brink *et al*. (2013)[6] were presented in this chapter. The new complexes all crystallize in the same crystal system (monoclinic), same space group ($P2_1/c$) and contain the same amount of molecules ($Z = 4$) in the unit cell. Furthermore, two of the new complexes were found to be iso-structural. From the crystal structures that were discussed, it also became evident that the temperature, at which the reaction is carried out, has a major effect on how the bidentate Schiff-base ligands coordinate to the metal center in the final complex.

6 Preliminary Formation Kinetics of *fac*-[Re(L,L'-Bid)(CO)$_3$] complexes with L,L'-Bid = *N,O*- and *N,N'*-Bid Type Ligands

6.1 Introduction

Chemical kinetics is the study of the rate at which chemical reactions takes place.[1] Kinetic investigations make it possible to study the influence that temperature, concentration and pressure variation have on the rate of the reaction. Furthermore, chemical kinetics makes it possible to identify the mechanism that a certain reaction follows.[2] All this factors are indispensable in the design and development of radiopharmaceutical drugs as they give an insight into the formation, the stability of the drug *in vivo*, biodistribution tendencies and the rate of decomposition or clearance from the body.[3]

In chemical kinetics, the presence of time as a factor adds both interest and difficulty.[2] Chemical kinetics reflects a statistical average state of the molecules participating in the chemical reaction.[3,4] A combination of all these factors reveals only a general and not an absolute idea of the chemical reaction taking place, which makes interpretation difficult. Fortunately, this can be greatly simplified by selectively manipulating the experimental conditions of the reacting species.

6.2 Theoretical Aspects of Chemical Kinetics

The basic theory of using UV-Vis spectroscopy to study chemical kinetics is described by the Beer-Lambert Law.[5] This law gives a direct linear relationship between the concentration of the species, the intensity of the incident (I_0) and transmitted (I_t) monochromatic light as well as the electromagnetic radiation which the species absorbs.

$$A = -log\ (I_0/I_t) = \varepsilon cl \qquad (6.1)$$

[1] J. H. Espenson, *Chemical Kinetics and Reaction Mechanisms*, 2nd Ed., McGraw Hill, New York, 1995.
[2] K. A. Connors, *Chemical Kinetics*: *The Study of Reaction Rates Solution*, 1st Ed., VCH Publishers, New York, 1990.
[3] C. Capellos, B. H. J. Bielski, *Kinetic Systems*, Wiley-Interscience, New York, 1972.
[4] A. F. Frost, R. G. Pearson, *Kinetics and Mechanism*, John Wiley & Sons, New York, 1953.
[5] P. W. Atkins, *Physical Chemistry*, Oxford University Press, London, 1994.

where A is the absorbance, l is the path length through the sample, c is the concentration of the species and ε is the extinction coefficient.

For a pseudo-first order reaction, i.e. a reaction where the ligand concentration is usually in excess ([L] >> [M], aspects of the intimate mechanism as well as the observed rate constants can be determined from the relationship that exists between concentration and absorbance. After the components are mixed and the cuvette inserted into a UV-Vis spectrophotometer, a change in absorbance is observed and monitored as a function of time. This change in absorbance indicates that there is a reaction taking place between the mixed components. In the plot obtained, the change in absorbance can be seen as either increasing or decreasing. The observed first-order rate constant for the reaction can be obtained from a least squares fit of the A_{obs} *vs* time data to the following equation:

$$A_{obs} = A_f - (A_f - A_i)e^{-k_{obs}t} \tag{6.2}$$

where A_{obs} is the experimentally observed absorbance at time t, A_f = final absorbance (when the reaction is complete), A_i = initial absorbance (when the reaction has started) and k_{obs} = observed pseudo-first order rate constant.

6.2.1 Rate Laws and Equilibrium

In a closed system, the rate of a chemical reaction can be defined as the rate of disappearance of the reactants concentration or formation of the products with time. For a general chemical reaction shown in equation 6.4, where M = metal, L = ligand, C and D are products:

$$aM + bL \longrightarrow cC + dD \tag{6.3}$$

The rate of the reaction, is given by equation 6.5, where t = time and the brackets, [ ], indicate concentration of the species. The negative signs indicate the disappearance of the reactants, whereas the positive signs indicate the formation of products.

$$R = -\frac{d[M]}{dt} = -\frac{d[L]}{dt} = +\frac{d[C]}{dt} = +\frac{d[D]}{dt} \tag{6.4}$$

The general form of the rate law only incorporates the concentrations of the reactants and is given by the following equation:

$$R = k[M]^m[L]^n \tag{6.5}$$

where k = rate constant, m is the order of the reaction in concentration M and n is the order of the reaction in concentration L. The total order of the reaction is determined by adding the orders in concentration M and L.

Great difficulties are however encountered when determining the order of the reaction experimentally, so *pseudo* first-order conditions are employed to overcome this problem. When the concentration of one of the reactants, say L is much larger than that of M, the change in concentration of L will be less significant and hence assumed to be constant when compared to the change in concentration of M. Therefore, when $[L] >> [M]$, equation 6.5 simplifies to:

$$R = k_{obs}[M]^m \text{ where } k_{obs} = k[L]^n \tag{6.6}$$

Thus, for a simple equilibrium reaction:

$$[M] + [L] \underset{k_{-1}}{\overset{k_1, K_1}{\rightleftharpoons}} [C] \tag{6.7}$$

where $R = k_1[M][L] + k_{-1}[C]$, under *pseudo* first-order conditions ([L] >> [M]), the observed rate constant, k_{obs} is given by the following equation:

$$k_{obs} = k_1[L] + k_{-1} \tag{6.8}$$

where k_1 represent the forward reaction rate constant and k_{-1} is the reversed reaction rate constant. Thus, a plot of k_{obs} *vs* $[L]$ must be linear with a slope of k_1 and an intercept of k_{-1}. The equilibrium constant, K_1 can be determined from the following equation:

$$K_1 = \frac{k_1}{k_{-1}} \tag{6.9}$$

The above equilibrium equations however hold true for an associatively activated one-step mechanism, *A*. This mechanism involves a transition state that is formed during a slow rate determining step, whereby there's an increase in the coordination number of the metal, followed by the fast dissociation of the leaving groups.

The plot of k_{obs} *vs* $[L]$ can also give nonlinear, limiting plots which raises the possibility of the existence of a two-step interchange type mechanism, *I*, whereby there is an interchange with

L in the outersphere of the complex to form a rapid pre-equilibrium, followed by a slower rate determining second reaction as indicated in equation 6.10.[6,7,8]

$$[M] + [L] \underset{}{\overset{K_2}{\rightleftharpoons}} [M]\cdots(L)]^{\neq}$$

$$[M]\cdots(L)]^{\neq} \underset{k_{-3}}{\overset{k_3}{\rightleftharpoons}} [ML] \qquad (6.10)$$

The observed rate constant, k_{obs} for this equilibrium under *pseudo* first-order conditions is given by the following equation:

$$k_{obs} = \frac{k_3 K_2 [L]}{(1+K_2[L])} + k_{-3} \qquad (6.11)$$

where K_2 is the pre-equilibrium constant, k_3 is the observed second order limiting rate constant and k_{-3} is the reversed reaction rate constant.

6.2.2 Reaction Thermodynamics

Thermodynamics is primarily concerned with the initial and final state of a chemical system. It cannot reveal any information about the rate of the reaction or possible detail of the intermediate states which are important for chemical kinetics. The thermodynamic properties of a system under investigation can be obtained by repeating the same reaction experiment at different temperatures. At various temperatures, different rate constants are obtained and plotted in accordance with the Eyring equation to obtain the activation parameters, $\Delta H^{\neq}$ and $\Delta S^{\neq}$.

$$ln\frac{k}{T} = \frac{-\Delta H^{\neq}}{RT} + ln\frac{k_B}{h} + \frac{\Delta S^{\neq}}{R} \qquad (6.12)$$

where k = experimentally determined rate constants, T = absolute temperature, R = universal gas constant (8.314 J K^{-1} mol^{-1}), k_B = Boltzmann constant (1.381 J K^{-1}) and h = Planck's constant (6.626 x 10^{-34} J s). Thus, the enthalpy of activation ($\Delta H^{\neq}$) and entropy of activation ($\Delta S^{\neq}$) can be obtained from a linear plot of $ln\frac{k}{T}$ *vs* $\frac{1}{T}$, or from a non-linear least squares fit of

[6] A. Brink, H. G. Visser, A. Roodt, *Inorg. Chem*., 2013, 52, 8950.
[7] A. Brink, H. G. Visser, A. Roodt, *Inorg. Chem*., 2014, 53, 12480.
[8] R. G. Wilkins, *Kinetics and Mechanism of Reaction of Transition Metal Complexes*, 2nd Ed., VCH Publishers, Inc., New York, 2002.

the kinetic data as a function of temperature to the non-logarithmic form of the Eyring equation.

6.3 Reagents and Equipment

All reagents and chemicals used for the kinetic studies were of analytical grade. The methanol solvent was pre-dried over calcium hydride for 24 hours and distilled before use. Ethylenediamine and diethylenetriamine were purchased from Sigma Aldrich and used without further purification. The complex, *fac*-$[Et_4N]_2[Re(CO)_3Br_3]$ **(ReAA)** was synthesized according to a literature procedure[9] described under section 4.4.1.

Kinetic measurements were conducted using 1 cm tandem quartz cuvette cell on a Varian Carey 50 Conc. UV-Visible Spectrometer equipped with a Julabo F12-mV temperature cell regulator, accurate within 0.1°C. All kinetic reactions were performed under *pseudo* first-order conditions were the lowest concentration of the ligand was at least ten times more than that of **ReAA**. The obtained data was analysed using equations 6.2 and 6.8 in the program MicroMath Scientist for Windows, Version 2.01.[10]

The stability test of *fac*-$[Et_4N]_2[Re(CO)_3Br_3]$ in methanol was the first kinetic studies performed. The solution was scanned on the UV-Vis Spectrometer for 24 hours to ensure that the solvent does not react with the metal complex. No significant change was observed after 24 hours, which confirmed the stability of the complex in methanol. Fresh concentration solutions of the metal complex and ligands were however prepared for each day of doing kinetic experiments.

6.4 Motivation for Investigating Formation Kinetics of *fac*-$[Re(CO)_3]^+$ core with Ethylene Amine Type Ligands

The initial aim of this study was to investigate the formation kinetics of the reactions between *fac*-$[Et_4N]_2[Re(CO)_3Br_3]$ and the various Schiff-base ligands which resulted in the formation of complexes that were synthesized in chapter 4. However, after the synthesis part of this M.Sc. study was completed, it was found that the reaction between *fac*-$[Re(CO)_3]^+$ core and an excess of Schiff-base bidentate ligand ([*M*] : [*L*] = 1 : 2), result in the first ligand coordinating to rhenium in a standard bidentate manner and the second ligand replacing the

[9] R. Alberto, R. Schibli, P. A. Schubiger, *Polyhedron*, 1996, 15, 1079.
[10] MicroMath Scientist for Windows, Version 2.01, Copyright© 1986-1995, MicroMath, Inc.

Br^-/MeOH on the sixth position and coordinate as a monodentate to form zwitterionic type species illustrated in Figure 6.1. Further synthetic studies using rhenium to Schiff-base bidentate ligand ratios ([*M*] : [*L*] = 1 : 3, 1 : 4) were also evaluated. The coordination result, i.e. two ligands coordinating in a bi- and a monodentate fashion, was consistent. In addition, the coordination mode of the Schiff-base bidentate ligands to the *fac*-$[Re(CO)_3]^+$ core was found to be temperature dependent. At 70 ^oC, the reaction between the bidentate ligand 5Me-SalH-CyPent = 2-(cyclopentylimino)methyl-5-methylphenol and **ReAA** forms the commonly obtained *fac*-[Re(5Me-Sal-CyPent)$(CO)_3$(Pyridine)] **(5)** complex, whereas at 25 ^oC, the same bidentate ligand coordinates to rhenium as a monodentate yielding the zwitterionic complex, *fac*-[Re(*κO*-5Me-Sal-CyPent)$(CO)_3$(Pyridine)] **(7)**. Single crystal X-ray structures of **(9)** and **(10)** were obtained,[11] but are not included in this study and will be reported in subsequent work.

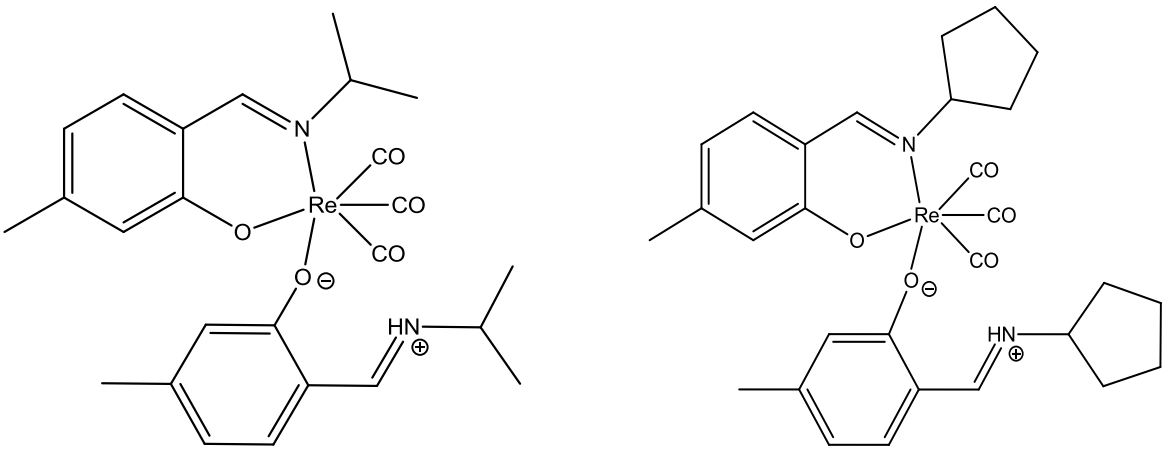

(9) **(10)**

Figure 6.1: Simultaneous bidentate and monodentate coordination of Schiff-base ligands to rhenium center.

Kinetic studies are investigated at various temperatures under *pseudo* first-order conditions, whereby the lowest concentration of the ligand is at least 10 times higher than the concentration of the metal complex. From the aforementioned observations made from the synthetic studies, it was concluded that the investigation of the formation kinetics between *fac*-$[Et_4N]_2[Re(CO)_3Br_3]$ and Schiff-base ligands would lead to the observation of complex, multiple reactions.

[11] T. D. Marake, A. Brink, A. Roodt, 2015, Unpublished results.

As a result, sodium picolinate (Pic^-Na^+) was used as a model for the *N,O* Schiff-base bidentate ligands to study the formation kinetics. However, it can be seen from a plot of the change in absorbance as a function of time (Figure 6.2) that there is more than one reaction taking place for the reaction between *fac*-$[Et_4N]_2[Re(CO)_3Br_3]$ and sodium picolinate. The first rapid reaction is followed by a slower second reaction. Therefore, it was assumed that an excess of sodium picolinate also result in the ligand coordinating to the rhenium in a similar manner as the *N,O* Schiff-base bidentate ligands illustrated in Figure 6.1. This explains the observation of more than one reaction. The change in absorbance for the reaction is also quite small to accurately calculate k_{obs} values.

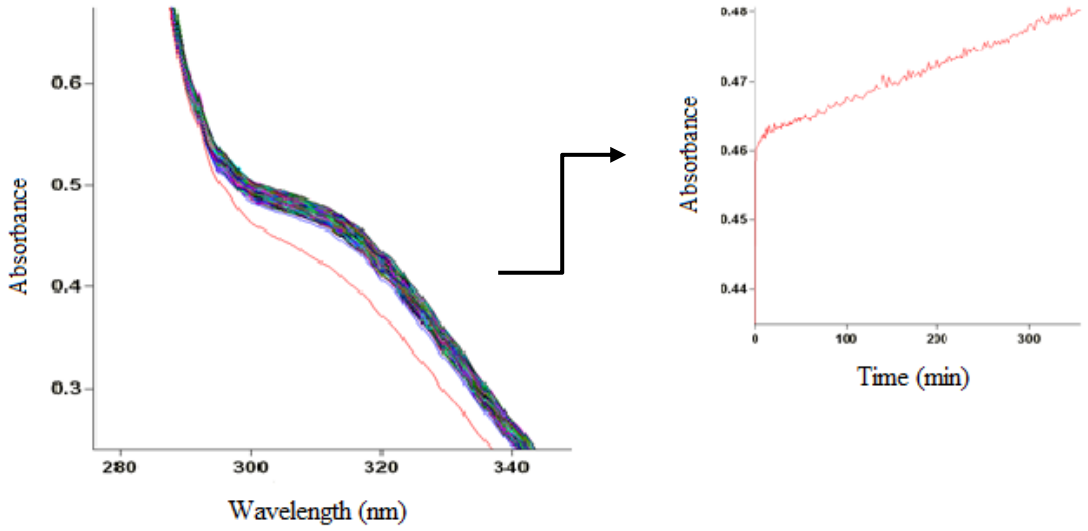

Figure 6.2: The change in absorbance for the reaction between *fac*-$[Et_4N]_2[Re(CO)_3Br_3]$ and sodium picolinate in methanol at 25 ^oC, [Re] = 1.99 x 10^{-4} M, [Pic^-Na^+] = 0.001 M, λ = 310 nm, Δt = 12 s.

Sodium picolinate was therefore replaced with more simple and symmetric ethylene amine type ligands, ethylenediamine (en) and diethylenetriamine (dien) depicted in Figure 6.3, to study the formation kinetics.

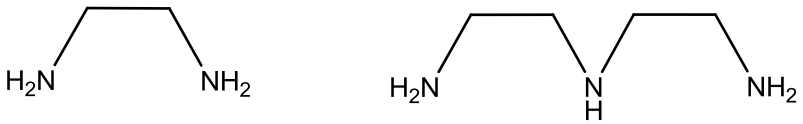

(11) **(12)**

Figure 6.3: Structures of ethylenediamine **(11)** and diethylenetriamine **(12)**.

The conscious choice of selecting a bidentate and a tridentate ligand for the formation kinetics was prompted by the observations made by Alberto,[12] whereby fast complex formation with the *fac*-$[M(CO)_3]^+$ core was obtained when a bidentate (histamine) or a tridentate (histidine) ligand was used. Furthermore, quantitative complex formation with histidine was achieved at a 1:1 ratio with respect to the metal concentration. These conditions are considered ideal when designing radiopharmaceutical drugs because the agent can be applied for diagnostic or therapeutic purposes immediately after preparation without any further purification. Another reason for the inclusion of **(12)** was to investigate if this tridentate ligand coordinate to the rhenium center *via* a one-step (i), two steps (ii) or three steps (iii) mechanism as shown in Figure 6.4.

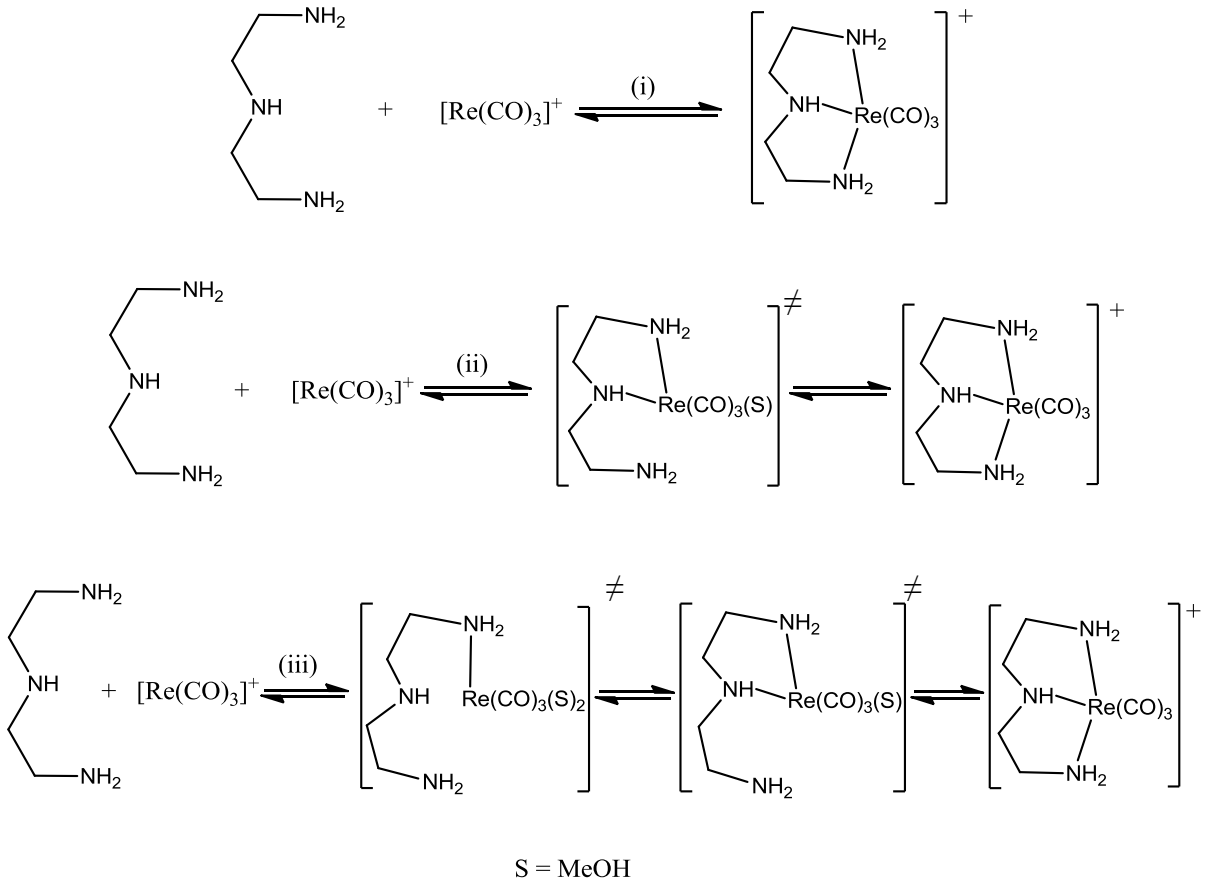

Figure 6.4: Three stepwise possibilities for the coordination of diethylenetriamine to the *fac*-$[Re(CO)_3]^+$ core.

[12] R. Alberto, R. Schibli, R. Waibel, U. Abram, P. A. Schubiger, *Coord. Chem. Rev*., 1999,190-192, 901.

6.5 Results of the Preliminary Formation Kinetics Between the *fac*-$[Re(CO)_3]^+$ core and Ethylene Amine Type Ligands

6.5.1 Reaction of *fac*-$[Re(CO)_3Br_3]^{2-}$ with Ethylenediamine

The reaction between *fac*-$[Et_4N]_2[Re(CO)_3Br_3]$ and ethylenediamine under *pseudo* first-order conditions was performed in methanol at 25 ^oC. The preliminary kinetic measurements were conducted using ligand concentrations ranging from 0.04-0.4 M and a metal concentration of 9.86×10^{-5} M. The change in absorbance as a function of wavelength as well as time (insert) obtained from a UV-Vis scan for the reaction between *fac*-$[Et_4N]_2[Re(CO)_3Br_3]$ and ethylenediamine is shown in Figure 6.5. From a plot of the change in absorbance as a function of wavelength, it is evident that there is a first rapid reaction taking place while manually mixing the metal complex with the ligand as indicated by the dramatic change in the absorbance from the first UV-Vis scan (before mixing) to the second one (after mixing). The second reaction was investigated during this study as the first one would require the use of a stopped-flow UV-Vis spectrophotometer for following fast kinetics, but this was believed to be beyond the scope of this study at present. Only one ethylenediamine ligand coordinate to rhenium in the final product as characterized by NMR in chapter 4, section 4.4.8. The observed rate constants, k_{obs} were calculated from equation 6.2 at 278 nm for each ligand concentration and are given in Table 6.1. Figure 6.7 shows a linear relationship between k_{obs} and ligand concentration at 25 ^oC, from which the forward reaction rate constant, k_2 for the second reaction can be obtained.

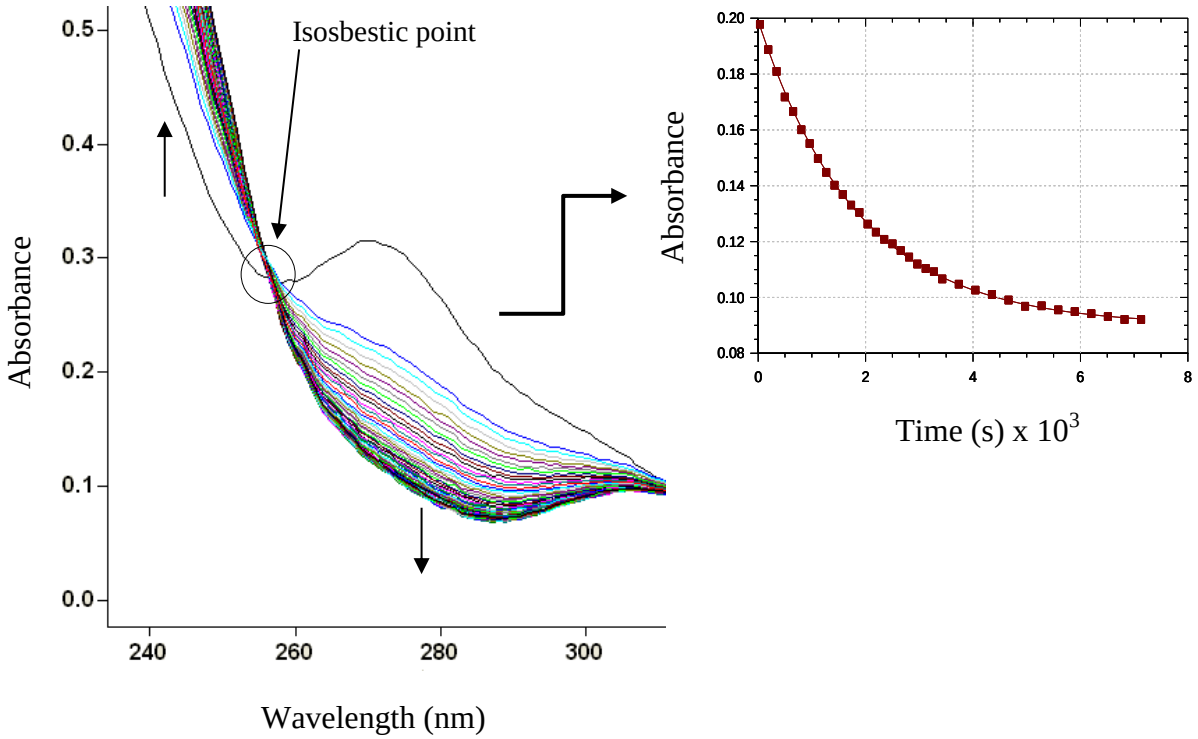

Figure 6.5: The change in absorbance for the reaction between *fac*-$[Et_4N]_2[Re(CO)_3Br_3]$ and ethylenediamine in methanol at 25 ^oC. [Re] = 9.86 x 10^{-5} M, [en] = 0.04 M, λ = 278 nm, Δt = 120 s.

Table 6.1: Calculated k_{obs} values for the reaction between *fac*-$[Et_4N]_2[Re(CO)_3Br_3]$ and ethylenediamine in methanol at 25 ^oC, [Re] = 9.86 x 10^{-5} M, [en] = 0.04-0.4 M, λ = 278 nm.

[en] (M)	k_{obs} (s^{-1})
0.040	0.000532(1)
0.080	0.000993(2)
0.101	0.001156(3)
0.200	0.002122(7)
0.401	0.003547(16)

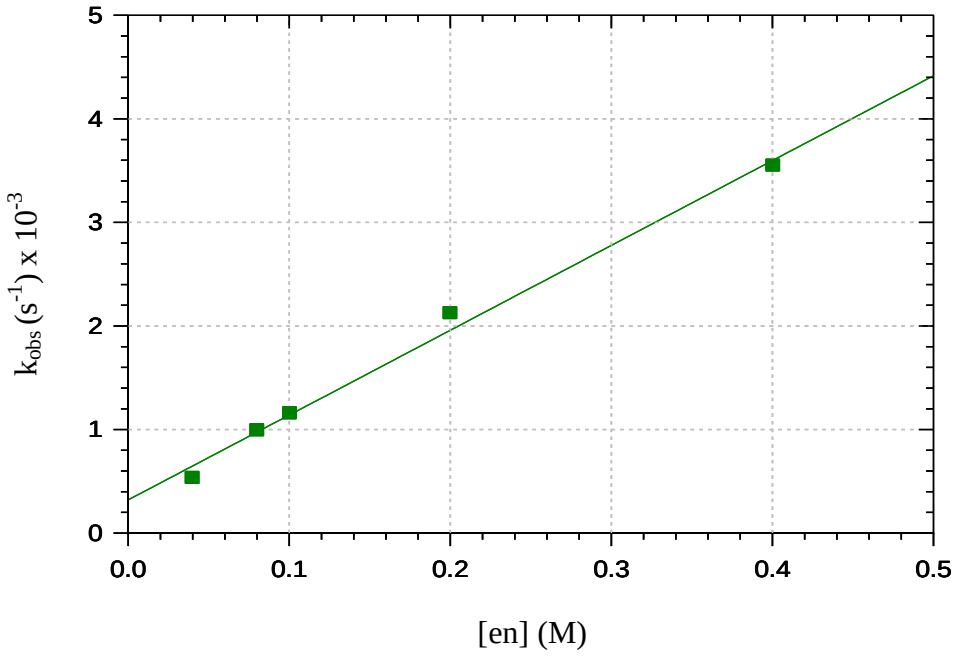

Figure 6.6: A graph of k_{obs} versus [en] for the reaction between *fac*-$[Et_4N]_2[Re(CO)_3Br_3]$ and ethylenediamine in methanol at 25 ^oC, [Re] = 9.86 x 10^{-5} M, [en] = 0.04-0.4 M, λ = 278 nm.

The forward reaction rate constant, k_2 and the reverse reaction rate constant, k_{-2} were obtained as 0.00826(4) $M^{-1}s^{-1}$ and 0.00031(9) s^{-1} respectively. The equilibrium constant for the second reaction, K_2 was calculated from equation 6.9 as 27(8) M^{-1}. The activation parameters, $\Delta H^{\neq}$ and $\Delta S^{\neq}$ could not be obtained at present as additional future kinetic temperature studies will be conducted at 15, 25, 35 and 45 ^oC.

6.5.2 Reaction of *fac*-$[Re(CO)_3Br_3]^{2-}$ with Diethylenetriamine

The reaction between *fac*-$[Et_4N]_2[Re(CO)_3Br_3]$ and diethylenetriamine under *pseudo* first-order conditions was performed in methanol at 25 ^oC using the ligand concentrations 0.04, 0.4 M and a metal concentration of 1.012 x 10^{-4} M. These results are included to indicate the type of reaction taking place between *fac*-$[Et_4N]_2[Re(CO)_3Br_3]$ and diethylenetriamine and that the absorbance change profiles are similar to the reaction with ethylenediamine. However, the graph of the change in absorbance as a function of wavelength shows a nice isosbestic point for the reaction between *fac*-$[Et_4N]_2[Re(CO)_3Br_3]$ and ethylenediamine (see Figure 6.5), whereas the reaction between *fac*-$[Et_4N]_2[Re(CO)_3Br_3]$ and diethylenetriamine does not show a clear isosbestic point (see Figure 6.7). This support beyond doubt that there are two reactions taking place between *fac*-$[Et_4N]_2[Re(CO)_3Br_3]$ and diethylenetriamine. The change in absorbance as a function of wavelength as well as time obtained for the reaction

between *fac*-$[Et_4N]_2[Re(CO)_3Br_3]$ and diethylenetriamine is shown in Figure 6.7. The observed rate constants were calculated at 280 nm for the two ligand concentrations and are given in Table 6.2. Figure 6.8 shows a linear relationship between k_{obs} and ligand concentration at 25 ^{o}C, from which the forward reaction rate constant, k_2 for the second reaction can be obtained. Rate constants for the reactions between *fac*-$[Et_4N]_2[Re(CO)_3Br_3]$ and ethylene amine type ligands are given in Table 6.3.

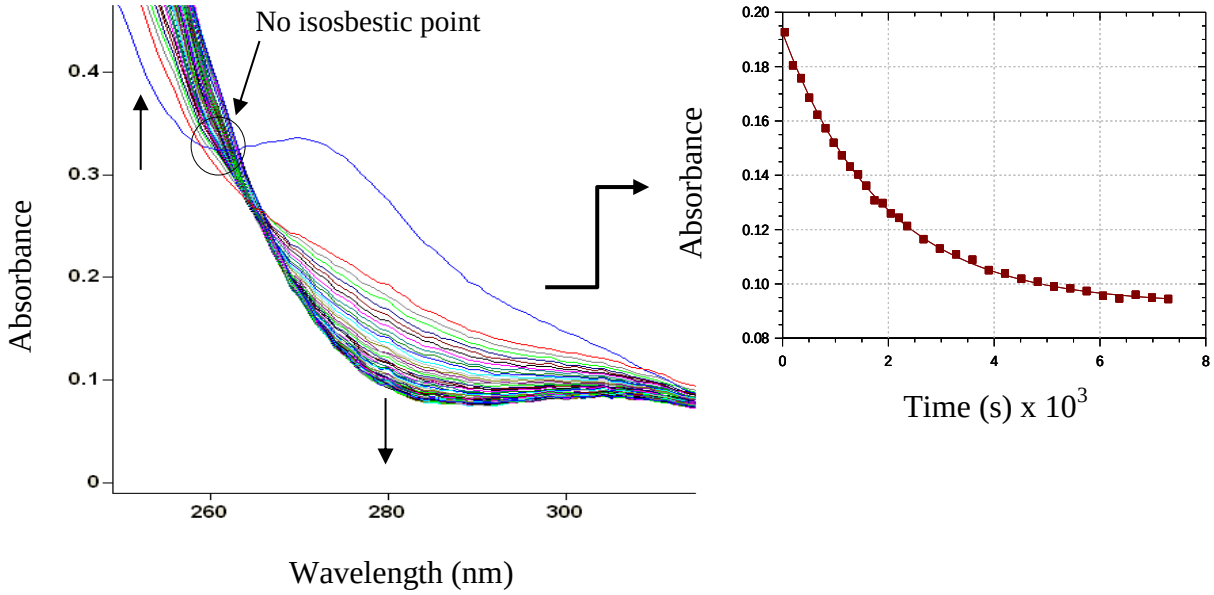

Figure 6.7: UV-Vis scans showing the change in absorbance for the reaction between *fac*-$[Et_4N]_2[Re(CO)_3Br_3]$ and diethylenetriamine in methanol at 25 ^{o}C. [Re] = 1.012 x 10^{-4} M, [dien] = 0.04 M, λ = 280 nm, Δt = 120 s.

Table 6.2: Calculated k_{obs} values for the reaction between *fac*-$[Et_4N]_2[Re(CO)_3Br_3]$ and diethylenetriamine in methanol at 25 ^{o}C, [Re] = 1.012 x 10^{-4} M, [en] = 0.04 and 0.4 M, λ = 280 nm.

[dien] (M)	k_{obs} (s^{-1})
0.040	0.000525(2)
0.400	0.00309(7)

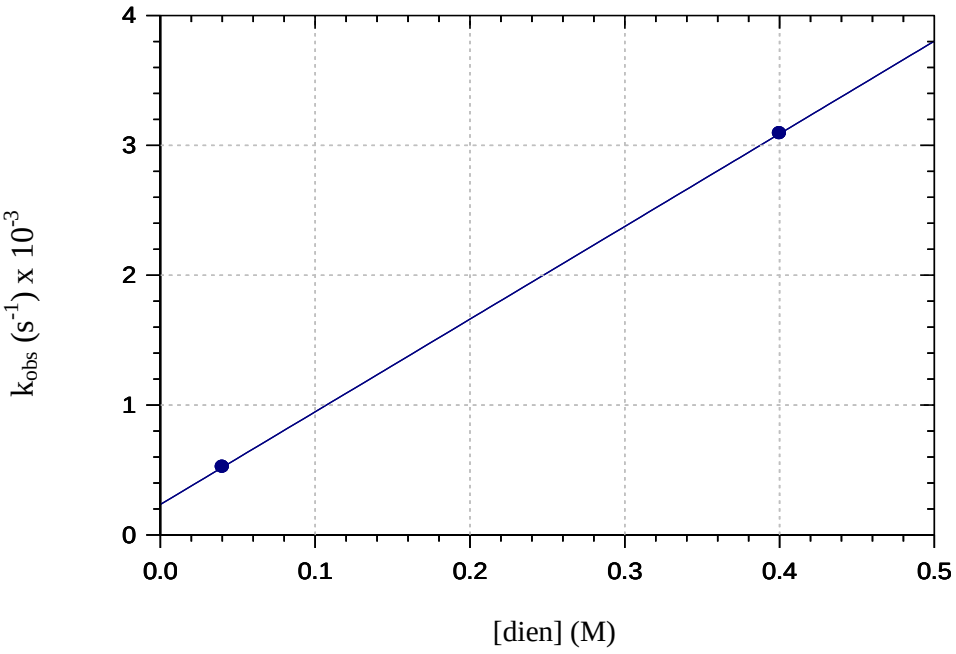

Figure 6.8: A graph of k_{obs} versus [dien] for the reaction between *fac*-$[Et_4N]_2[Re(CO)_3Br_3]$ and diethylenetriamine in methanol at 25 ^oC, [Re] = 1.012 x 10^{-4} M, [en] = 0.04 and 0.4 M, λ = 280 nm.

The second order rate constant, k_2 and the reverse reaction rate constant, k_{-2} were obtained as 0.00715(3) $M^{-1}s^{-1}$ and 0.00023(1) s^{-1} respectively. The pre-equilibrium constant, K_2 was calculated as 31(1) M^{-1} from equation 6.9.

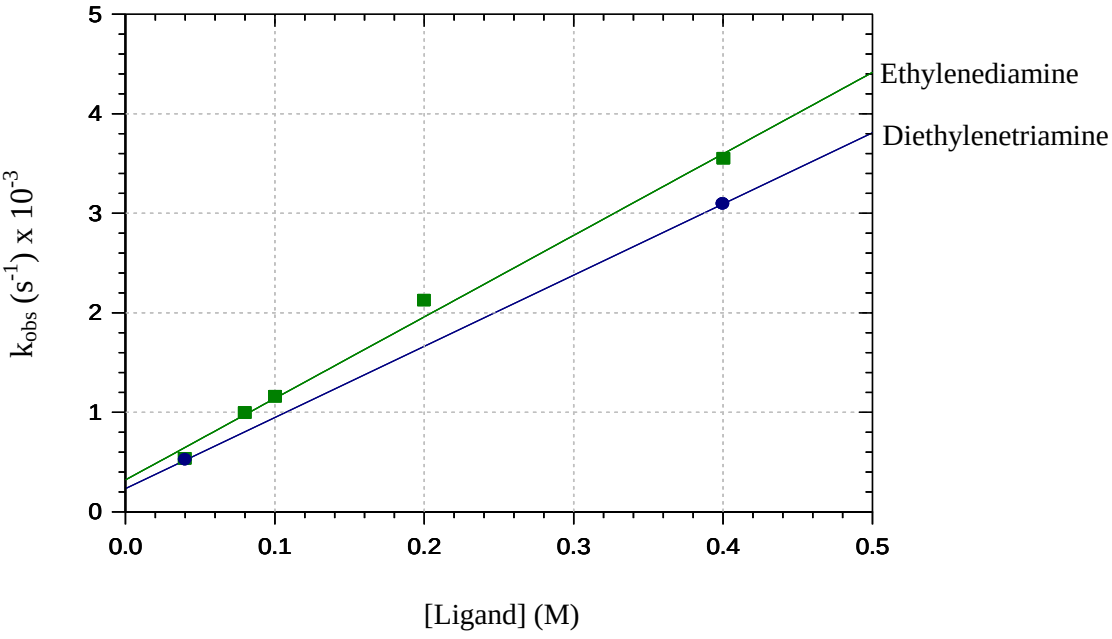

Figure 6.9: A plot of k_{obs} versus [Ligand] for the reactions between *fac*-$[Et_4N]_2[Re(CO)_3Br_3]$ and ethylene amine type ligands in methanol at 25 ^oC.

Table 6.3: Rate constants for the reactions between *fac*-$[Et_4N]_2[Re(CO)_3Br_3]$ and ethylene amine type ligands in methanol at 25 ^oC.

Ligand	k_2 ($M^{-1}s^{-1}$)	k_{-2} (s^{-1})	K_2 (M^{-1})
en	0.00826(4)	0.00031(9)	27(8)
dien	0.00715(3)	0.00023(1)	31(1)

From Figure 6.9 and the forward reaction rate constants, k_2 given in Table 6.3, it is evident that the reaction between *fac*-$[Et_4N]_2[Re(CO)_3Br_3]$ and ethylenediamine is slightly faster than that with diethylenetriamine. This can possibly be because of the simple, symmetrical nature of ethylenediamine ligand as opposed to the larger steric demand of diethylenetriamine ligand.

6.6 Conclusion

The initial objective of this study was to investigate the formation reactions between *fac*-$[Et_4N]_2[Re(CO)_3Br_3]$ and Schiff-base ligands. Sodium picolinate was used as a model for the *N*,*O* Schiff-base bidentate ligands for the preliminary formation kinetics, based on the synthetic work. However, it was found that sodium picolinate itself result in the observation of more than one reaction under *pseudo* first-order conditions, with small absorbance changes. Therefore, the ethylene amine type ligands, ethylenediamine and diethylenetriamine were chosen as alternatives to study the formation kinetic. The formation reactions between *fac*-$[Et_4N]_2[Re(CO)_3Br_3]$ and ethylene amine type ligands were studied under *pseudo* first-order conditions, i.e. $[L] >> [M]$, at 25 ^oC. However, also for these ligands, at least two reactions could be identified, a rapid first reaction, followed by a slower second reaction which was investigated during this study. The first reaction required stopped-flow UV-Vis spectrophotometer to be studied, which was considered to be beyond the scope of this study at present. A linear plot of k_{obs} versus [Ligand] was obtained for both ligands, from which k_2, k_{-2} and K_2 for the second reaction were deduced. The reaction between *fac*-$[Et_4N]_2[Re(CO)_3Br_3]$ and ethylenediamine was found to be faster than that with diethylenetriamine and is assumed to be related to the larger steric demand of diethylenetriamine ligand. The intimate mechanism for the reactions studied could not be assigned since the activation parameters, $\Delta H^{\neq}$ and $\Delta S^{\neq}$ can only be obtained if the kinetic measurements are performed at different temperatures.

Future endeavours will include a detailed formation kinetic study of the reactions between *fac*-$[Et_4N]_2[Re(CO)_3Br_3]$ and ethylene amine type ligands as well as other ligands at various temperatures. This is important as it will be possible to assign an intimate mechanism for the complex formation reaction. Stopped-flow UV-Vis spectrophotometer will also be used to follow the first rapid reaction which could not be studied on the slow UV-Vis spectrophotometer. Furthermore, the formation kinetics will be followed with multi nuclear NMR to identify any possible intermediates formed during the course of the reaction and to conclude with more certainty if the ethylenediamine ligand coordinates to the rhenium center *via* a one-step concerted mechanism or in two consecutive steps with the coordination of the first *N* donor atom followed by ring closure from the second *N* donor atom. A similar study will be conducted with the diethylenetriamine ligand and sodium picolinate to see if the latter behaves similar to ethylenediamine. The NMR kinetic studies will also be conducted to see if the diethylenetriamine ligand coordinates to the metal center *via* a one-step, two-step or three step mechanism.

7 Critical Evaluation of Study

7.1 Introduction

The initial objective of this study was to investigate the coordinative and kinetic behaviour of *fac*-[Re(L,L'-Bid)$(CO)_3$(MeOH)] (L,L'-Bid = monoanionic *N,O* bidentate Schiff-base ligands: 5Me-SalH-iProp = 2-(isopropylimino)methyl-5-methylphenol, 5Me-SalH-CyPent = 2-(cyclopentylimino)methyl-5-methylphenol and 5Me-SalH-Hist = 2-(2-imidazol-4-yl)ethyliminomethyl-5-methylphenol) complexes. The selection of salicylidene (Sal) type Schiff-base ligands was prompted by the fact that there are only a few crystal structures reported in literature whereby the salicylidene backbone is utilized and coordinated onto the *fac*-$[Re(CO)_3]^+$ core. Furthermore, the manipulative capabilities of Schiff-bases make it possible to design a range of mono-, bi- and tridentate ligands with varying steric and electronic character. The major advantage of utilizing bidentate ligands with the *fac*-$[Re(CO)_3(MeOH)_3]^+$ precursor is that the sixth coordination site on the metal center is left "open" and can be occupied by a different monodentate ligand leading to the [2+1] mixed ligand approach. This chapter include a description of the scientific relevance of this current study, a summary of the results obtained as well as some future endeavours.

7.2 Scientific Relevance and Results Obtained

In this study, three salicylidene type Schiff-base ligands with varying steric and electronic character afforded by the substituent on the nitrogen imine donor atom were synthesized and successfully coordinated to the *fac*-$[Re(CO)_3]^+$ core to give complexes of the type *fac*-[Re(L,L'-Bid)$(CO)_3$(MeOH)] (L,L'-Bid = *N,O* Sal bidentate ligand). However, single crystals of the methanol substituted products that were suitable for X-ray diffraction could not be obtained. Therefore, the methanol solvento molecule coordinated to the sixth position on the metal center, was substituted with stable monodentate ligands to form single crystals of complexes of the type *fac*-[Re(L,L'-Bid)$(CO)_3$(L)] (L,L'-Bid = *N,O* Sal bidentate ligand; *L* = coordinated pyridine or imidazole), that were suitable for X-ray diffraction.

From the synthesis of *fac*-[Re(L,L'-Bid)$(CO)_3$(L)] (L,L'-Bid = *N,O* Sal bidentate ligand; *L* = coordinated pyridine or imidazole) complexes, it was shown that the temperature at which the reaction is carried out, plays an integral part in determining the mode of coordination of the

bidentate ligand to the rhenium center. At high temperatures (70 ^{o}C), the bidentate ligand coordinate to rhenium in a standard bidentate manner, but when the reaction is carried out at room temperature, the same bidentate ligand coordinate as a monodentate ligand through the *O* donor atom.

Four new crystal structures and a polymorphic form of a complex previously reported were obtained during this study and characterized in detail with single crystal X-ray diffraction as well as other spectroscopic techniques. The new crystal structures reported all crystallize in the same crystal system (monoclinic), same space group ($P2_1/c$) and contain the same number of molecules in the unit cell (Z = 4). Two of the crystal structures, *fac*-[Re(5Me-Sal-CyPent)$(CO)_3$(Pyridine)] and *fac*-[Re(5Me-Sal-CyPent)$(CO)_3$(Imidazole)] met the criterion of being iso-structural. The different substituents on the nitrogen imine donor atom do not affect the bond distances significantly. However, the bond distance of the imidazole ligand coordinated to the sixth position is significantly shorter than that of the coordinated pyridine ligand. Thus, imidazole coordinates more strongly to the metal center than pyridine.

The preliminary formation kinetics of the *fac*-$[Re(CO)_3]^+$ core with Schiff-bases was altered based on the observation made from the synthesis chapter, whereby the reaction between *fac*-$[Re(CO)_3]^+$ core and an excess of the bidentate ligand result in the first ligand coordinating to rhenium in a standard bidentate manner and the second ligand replaces the Br^-/MeOH on the sixth position and coordinate as a monodentate through the *O* donor atom. Furthermore, it was found that the mode of coordination of the Schiff-base bidentate ligands to rhenium is temperature dependent. When the reaction is carried out at high temperatures (70 ^{o}C), the bidentate ligand coordinate to rhenium center in a standard bidentate manner, but at low temperatures (25 ^{o}C), the ligand coordinate as a monodentate through the *O* donor atom. Therefore, sodium picolinate was used as a model for *N*,*O* Schiff-base ligands as it was believed that complex, multiple reactions would be observed for the formation kinetics with Schiff-bases since kinetic studies are performed at various temperatures, under *pseudo* first-order conditions ([*L*] >> [*M*]). However, multiple reactions were observed for the formation reactions with sodium picolinate, indicating complex formation mechanism believed to be beyond the scope of this study. Furthermore, the change in absorbance for the reaction between *fac*-$[Re(CO)_3]^+$ core and sodium picolinate was too small to accurately calculate the rate constants.

Consequently, simpler ethylene amine type ligands, ethylenediamine and diethylenetriamine were used as the alternatives to study the formation kinetics. The formation reactions between the *fac*-$[Re(CO)_3]^+$ core and ethylene amine type ligands were studied under *pseudo* first-order conditions at 25 ^oC. Two reactions were also identified, a rapid first reaction, followed by a slower second reaction which was investigated during this study. The first reaction required stopped-flow UV-Vis spectrophotometer to be studied, which at present was considered to be beyond the scope of this study. The second reaction studied between the *fac*-$[Re(CO)_3]^+$ core and ethylenediamine was found to be faster than that with diethylenetriamine. This can possibly be because of the large steric demand of diethylenetriamine ligand. The intimate mechanism for the reactions studied could not at present be assigned and is the subject of current studies.

7.3 Future Research

Based on the results obtained during this M.Sc. study, it is clear that unknown parameters should be further investigated, specifically for the formation kinetic studies in order to expand on the current knowledge. Future research will consist of the following:

- Synthesize a range of *N*,*O* Schiff-base bidentate ligands with a biologically active substituent on the *N* imine donor atom.
- Coordinate the ligands onto the *fac*-$[M(CO)_3]^+$ (M = Re, $^{99/99m}Tc$) core.
- Perform cell testing with all the ligands and metal complexes.
- The use of stopped-flow UV-Vis spectrophotometer to study the first rapid reaction observed between *fac*-$[Re(CO)_3]^+$ core and ethylene amine type ligands.
- An extended formation kinetic study for the reaction between *fac*-$[Re(CO)_3]^+$ core and ethylene amine type ligands at four different temperature in order to propose a mechanism for complex formation.
- Follow the formation kinetics with ^1H NMR to identify if there are any intermediates formed during the course of the reaction and to conclude with certainty how these ligands coordinate to the rhenium center.
- Study the formation kinetics with the Schiff base ligands, sodium picolinate and other analogues to verify the mechanism.

APPENDIX

SUPPLEMENTARY DATA OF THE CRYSTAL STRUCTURES

1 Data of *fac*-[Re(5Me-Sal-iProp)(CO)$_3$(Py)]

Table 1.1: Atomic coordinates (x 10^4) and equivalent isotropic displacement parameters (Å^2 x 10^3) for *fac*-[Re(5Me-Sal-iProp)(CO)$_3$(Py)]. U(eq) is defined as one third of the trace of the orthogonalized U^{ij} tensor.

	x	y	z	U(eq)
Re(1)	1546(1)	1112(1)	7217(1)	37(1)
C(03)	3627(6)	1688(3)	7392(3)	50(1)
N(3)	-910(4)	445(2)	7097(2)	40(1)
O(02)	625(5)	2916(2)	6213(2)	71(2)
C(21)	105(6)	2643(3)	8442(3)	51(1)
O(1)	2140(4)	-197(2)	7832(2)	44(1)
C(32)	-3369(6)	154(4)	6347(4)	61(1)
O(01)	2625(5)	248(3)	5602(2)	71(1)
C(35)	-1497(5)	-69(4)	7726(3)	45(1)
C(16)	2462(6)	43(3)	10040(3)	52(1)
C(11)	2033(5)	296(3)	9226(3)	41(1)
C(13)	3343(6)	-1203(3)	8834(4)	45(1)
N(1)	876(4)	1648(2)	8405(2)	38(1)
C(14)	3770(6)	-1418(3)	9628(3)	50(1)
O(03)	4855(5)	2058(3)	7506(3)	81(1)
C(141)	4726(7)	-2317(3)	9853(4)	73(2)
C(1)	1214(6)	1203(3)	9092(3)	43(1)
C(34)	-3022(6)	-481(3)	7684(3)	51(1)
C(02)	939(5)	2244(3)	6605(3)	46(1)
C(31)	-1869(6)	555(3)	6422(3)	53(1)
C(22)	-1636(6)	2587(4)	8195(5)	70(2)
C(15)	3320(7)	-776(3)	10253(4)	58(1)
C(01)	2204(5)	570(3)	6217(3)	45(1)
C(12)	2483(5)	-346(3)	8590(3)	39(1)
C(33)	-3984(6)	-362(4)	6992(4)	59(1)
C(23)	321(9)	3150(4)	9261(4)	80(2)

Table 1.2: Bond lengths [Å] and angles [°] for *fac*-[Re(5Me-Sal-iProp)$(CO)_3$(Py)].

Atoms	Length	Atoms	Angle
Re(1)-C(01)	1.898(5)	C(01)-Re(1)-C(02)	86.95(19)
Re(1)-C(02)	1.905(5)	C(01)-Re(1)-C(03)	90.1(2)
Re(1)-C(03)	1.907(5)	C(02)-Re(1)-C(03)	87.5(2)
Re(1)-O(1)	2.107(3)	C(01)-Re(1)-O(1)	90.41(15)
Re(1)-N(1)	2.173(3)	C(02)-Re(1)-O(1)	176.21(16)
Re(1)-N(3)	2.231(4)	C(03)-Re(1)-O(1)	95.20(17)
C(03)-O(03)	1.145(6)	C(01)-Re(1)-N(1)	176.03(16)
N(3)-C(31)	1.340(6)	C(02)-Re(1)-N(1)	96.95(16)
N(3)-C(35)	1.355(5)	C(03)-Re(1)-N(1)	89.33(18)
O(02)-C(02)	1.147(5)	O(1)-Re(1)-N(1)	85.73(12)
C(21)-C(22)	1.483(7)	C(01)-Re(1)-N(3)	93.28(16)
C(21)-N(1)	1.510(5)	C(02)-Re(1)-N(3)	93.99(16)
C(21)-C(23)	1.513(8)	C(03)-Re(1)-N(3)	176.37(19)
C(21)-H(21)	0.98	O(1)-Re(1)-N(3)	83.44(12)
O(1)-C(12)	1.278(5)	N(1)-Re(1)-N(3)	87.23(13)
C(32)-C(31)	1.360(7)	O(03)-C(03)-Re(1)	177.9(5)
C(32)-C(33)	1.385(8)	C(31)-N(3)-C(35)	117.7(4)
C(32)-H(32)	0.93	C(31)-N(3)-Re(1)	122.2(3)
O(01)-C(01)	1.165(6)	C(35)-N(3)-Re(1)	120.1(3)
C(35)-C(34)	1.383(6)	C(22)-C(21)-N(1)	110.5(4)
C(35)-H(35)	0.93	C(22)-C(21)-C(23)	110.0(5)
C(16)-C(15)	1.367(6)	N(1)-C(21)-C(23)	114.6(4)
C(16)-C(11)	1.407(7)	C(22)-C(21)-H(21)	107.1
C(16)-H(16)	0.93	N(1)-C(21)-H(21)	107.1
C(11)-C(12)	1.426(6)	C(23)-C(21)-H(21)	107.1
C(11)-C(1)	1.430(5)	C(12)-O(1)-Re(1)	129.7(2)
C(13)-C(14)	1.363(8)	C(31)-C(32)-C(33)	120.2(5)
C(13)-C(12)	1.423(6)	C(31)-C(32)-H(32)	119.9
C(13)-H(13)	0.93	C(33)-C(32)-H(32)	119.9
N(1)-C(1)	1.300(6)	N(3)-C(35)-C(34)	122.1(4)
C(14)-C(15)	1.412(7)	N(3)-C(35)-H(35)	119
C(14)-C(141)	1.504(6)	C(34)-C(35)-H(35)	119
C(141)-H(14A)	0.96	C(15)-C(16)-C(11)	123.5(4)
C(141)-H(14B)	0.96	C(15)-C(16)-H(16)	118.3

C(141)-H(14C)	0.96	C(11)-C(16)-H(16)	118.3
C(1)-H(1)	0.93	C(16)-C(11)-C(12)	118.3(4)
C(34)-C(33)	1.366(9)	C(16)-C(11)-C(1)	117.3(4)
C(34)-H(34)	0.93	C(12)-C(11)-C(1)	124.3(4)
C(31)-H(31)	0.93	C(14)-C(13)-C(12)	123.5(4)
C(22)-H(23A)	0.96	C(14)-C(13)-H(13)	118.2
C(22)-H(23B)	0.96	C(12)-C(13)-H(13)	118.2
C(22)-H(23C)	0.96	C(1)-N(1)-C(21)	117.9(4)
C(15)-H(15)	0.93	C(1)-N(1)-Re(1)	124.1(3)
C(33)-H(33)	0.93	C(21)-N(1)-Re(1)	117.8(3)
C(23)-H(22A)	0.96	C(13)-C(14)-C(15)	119.2(4)
C(23)-H(22B)	0.96	C(13)-C(14)-C(141)	121.6(5)
C(23)-H(22C)	0.96	C(15)-C(14)-C(141)	119.2(5)
		C(14)-C(141)-H(14A)	109.5
		C(14)-C(141)-H(14B)	109.5
		H(14A)-C(141)-H(14B)	109.5
		C(14)-C(141)-H(14C)	109.5
		H(14A)-C(141)-H(14C)	109.5
		H(14B)-C(141)-H(14C)	109.5
		N(1)-C(1)-C(11)	128.7(4)
		N(1)-C(1)-H(1)	115.6
		C(11)-C(1)-H(1)	115.6
		C(33)-C(34)-C(35)	119.4(5)
		C(33)-C(34)-H(34)	120.3
		C(35)-C(34)-H(34)	120.3
		O(02)-C(02)-Re(1)	177.0(4)
		N(3)-C(31)-C(32)	122.4(5)
		N(3)-C(31)-H(31)	118.8
		C(32)-C(31)-H(31)	118.8
		C(21)-C(22)-H(23A)	109.5
		C(21)-C(22)-H(23B)	109.5
		H(23A)-C(22)-H(23B)	109.5
		C(21)-C(22)-H(23C)	109.5
		H(23A)-C(22)-H(23C)	109.5
		H(23B)-C(22)-H(23C)	109.5
		C(16)-C(15)-C(14)	118.7(5)
		C(16)-C(15)-H(15)	120.7

C(14)-C(15)-H(15)	120.7
O(01)-C(01)-Re(1)	179.0(4)
O(1)-C(12)-C(13)	119.5(4)
O(1)-C(12)-C(11)	123.7(4)
C(13)-C(12)-C(11)	116.8(4)
C(34)-C(33)-C(32)	118.1(5)
C(34)-C(33)-H(33)	120.9
C(32)-C(33)-H(33)	120.9
C(21)-C(23)-H(22A)	109.5
C(21)-C(23)-H(22B)	109.5
H(22A)-C(23)-H(22B)	109.5
C(21)-C(23)-H(22C)	109.5
H(22A)-C(23)-H(22C)	109.5
H(22B)-C(23)-H(22C)	109.5

Table 1.3: Anisotropic displacement parameters ($Å^2$ x 10^3) for *fac*-[Re(5Me-Sal-iProp)$(CO)_3$(Py)]. The anisotropic displacement factor exponent takes the form: $-2\pi^2[h^2a^{*2}U^{11} + ... + 2\ h\ k\ a^*\ b^*\ U^{12}]$.

	U^{11}	U^{22}	U^{33}	U^{23}	U^{13}	U^{12}
Re(1)	38(1)	37(1)	35(1)	1(1)	3(1)	-3(1)
C(03)	48(3)	52(2)	51(3)	2(2)	4(2)	-4(2)
N(3)	48(2)	38(2)	35(2)	2(1)	6(2)	-5(1)
O(02)	92(3)	60(2)	60(3)	15(2)	0(2)	5(2)
C(21)	61(3)	33(2)	59(3)	2(2)	7(3)	6(2)
O(1)	53(2)	37(1)	42(2)	-4(1)	6(2)	4(1)
C(32)	46(3)	82(3)	53(3)	7(3)	-11(2)	-6(2)
O(01)	77(3)	88(2)	48(2)	-6(2)	13(2)	6(2)
C(35)	47(3)	53(2)	36(3)	2(2)	3(2)	-6(2)
C(16)	75(3)	44(2)	38(3)	-1(2)	6(3)	7(2)
C(11)	49(2)	38(2)	34(2)	2(2)	3(2)	4(2)
C(13)	42(3)	37(2)	55(3)	-2(2)	4(2)	2(2)
N(1)	38(2)	35(2)	41(2)	-3(1)	2(2)	1(1)
C(14)	53(3)	41(2)	55(3)	8(2)	-1(2)	6(2)
O(03)	53(2)	87(3)	103(4)	-5(2)	-2(2)	-27(2)
C(141)	84(4)	55(3)	78(4)	12(3)	-9(3)	25(3)
C(1)	50(3)	39(2)	40(3)	-2(2)	9(2)	3(2)
C(34)	52(3)	54(2)	47(3)	3(2)	7(2)	-7(2)
C(02)	50(3)	45(2)	42(3)	1(2)	5(2)	-8(2)

C(31)	47(3)	65(3)	46(3)	0(2)	-2(2)	-6(2)
C(22)	60(3)	53(3)	94(5)	5(3)	-11(3)	13(2)
C(15)	75(4)	52(2)	48(3)	5(2)	0(3)	1(2)
C(01)	44(2)	50(2)	42(3)	-1(2)	1(2)	-1(2)
C(12)	39(2)	37(2)	41(3)	-3(2)	9(2)	-4(2)
C(33)	43(3)	65(3)	69(4)	-3(3)	3(3)	-9(2)
C(23)	116(5)	54(3)	69(4)	-19(3)	-17(4)	25(3)

2 Data of *fac*-[Re(5Me-Sal-CyPent)(CO)$_3$(Py)]

Table 2.1: Atomic coordinates (x 10^4) and equivalent isotropic displacement parameters (Å^2 x 10^3) for *fac*-[Re(5Me-Sal-CyPent)(CO)$_3$(Py)]. U(eq) is defined as one third of the trace of the orthogonalized U^{ij} tensor.

	x	y	z	U(eq)
Re(1)	3220(1)	1348(1)	2306(1)	45(1)
C(02)	3820(8)	2428(4)	1776(4)	57(2)
O(1)	2645(5)	106(2)	2805(2)	47(1)
C(13)	1572(7)	-932(4)	3719(4)	48(1)
N(3)	5656(5)	729(3)	2160(3)	44(1)
N(1)	4039(6)	1698(3)	3537(3)	55(1)
C(32)	8093(8)	578(5)	1413(4)	70(2)
C(31)	6589(7)	959(5)	1531(4)	57(2)
C(12)	2376(6)	-122(4)	3565(3)	44(1)
C(14)	1230(8)	-1214(4)	4500(4)	56(2)
C(01)	2425(7)	964(4)	1240(4)	51(1)
C(16)	2571(8)	81(5)	5040(4)	61(2)
C(11)	2896(7)	393(4)	4247(4)	50(1)
C(35)	6241(7)	132(4)	2687(4)	55(2)
O(01)	1913(6)	758(3)	613(3)	67(1)
C(34)	7757(8)	-253(5)	2616(4)	62(2)
C(33)	8703(8)	-36(5)	1967(5)	66(2)
C(1)	3726(7)	1237(4)	4184(4)	57(2)
C(15)	1750(9)	-693(5)	5170(4)	66(2)
C(141)	297(11)	-2067(5)	4638(5)	80(2)
O(02)	4144(7)	3065(3)	1428(3)	77(1)
O(03)	-11(7)	2252(4)	2635(4)	100(2)
C(03)	1158(8)	1896(5)	2507(5)	67(2)
C(21)	4807(10)	2588(5)	3646(5)	78(2)
C(22)	6521(8)	2632(5)	3338(5)	75(2)

C(25)	4792(17)	3044(7)	4386(8)	162(7)
C(23)	7162(10)	3507(5)	3679(5)	76(2)
C(24)	5876(14)	3852(6)	4240(6)	106(3)

Table 2.2: Bond lengths [Å] and angles [°] for *fac*-[Re(5Me-Sal-CyPent)$(CO)_3$(Py)].

Atoms	Length	Atoms	Angle
Re(1)-C(02)	1.907(7)	C(02)-Re(1)-C(03)	87.1(3)
Re(1)-C(03)	1.921(6)	C(02)-Re(1)-C(01)	86.2(3)
Re(1)-C(01)	1.933(7)	C(03)-Re(1)-C(01)	89.7(3)
Re(1)-O(1)	2.093(4)	C(02)-Re(1)-O(1)	175.3(2)
Re(1)-N(1)	2.170(5)	C(03)-Re(1)-O(1)	96.3(2)
Re(1)-N(3)	2.229(5)	C(01)-Re(1)-O(1)	90.5(2)
C(02)-O(02)	1.148(7)	C(02)-Re(1)-N(1)	97.7(3)
O(1)-C(12)	1.308(6)	C(03)-Re(1)-N(1)	90.0(3)
C(13)-C(14)	1.375(8)	C(01)-Re(1)-N(1)	176.1(2)
C(13)-C(12)	1.410(8)	O(1)-Re(1)-N(1)	85.70(17)
C(13)-H(13)	0.95	C(02)-Re(1)-N(3)	93.8(2)
N(3)-C(35)	1.327(7)	C(03)-Re(1)-N(3)	176.2(3)
N(3)-C(31)	1.337(7)	C(01)-Re(1)-N(3)	94.0(2)
N(1)-C(1)	1.291(8)	O(1)-Re(1)-N(3)	83.09(16)
N(1)-C(21)	1.489(8)	N(1)-Re(1)-N(3)	86.22(18)
C(32)-C(33)	1.381(9)	O(02)-C(02)-Re(1)	177.0(6)
C(32)-C(31)	1.381(9)	C(12)-O(1)-Re(1)	130.2(3)
C(32)-H(32)	0.95	C(14)-C(13)-C(12)	122.3(6)
C(31)-H(31)	0.95	C(14)-C(13)-H(13)	118.8
C(12)-C(11)	1.415(8)	C(12)-C(13)-H(13)	118.8
C(14)-C(15)	1.405(9)	C(35)-N(3)-C(31)	117.7(5)
C(14)-C(141)	1.515(9)	C(35)-N(3)-Re(1)	122.0(4)
C(01)-O(01)	1.141(7)	C(31)-N(3)-Re(1)	120.3(4)
C(16)-C(15)	1.364(9)	C(1)-N(1)-C(21)	118.3(6)
C(16)-C(11)	1.405(9)	C(1)-N(1)-Re(1)	124.2(4)
C(16)-H(16)	0.95	C(21)-N(1)-Re(1)	116.9(5)
C(11)-C(1)	1.445(9)	C(33)-C(32)-C(31)	120.1(6)
C(35)-C(34)	1.383(8)	C(33)-C(32)-H(32)	119.9
C(35)-H(35)	0.95	C(31)-C(32)-H(32)	119.9

N(3)-C(31)-C(32)	122.0(6)
N(3)-C(31)-H(31)	119
C(32)-C(31)-H(31)	119
O(1)-C(12)-C(13)	118.9(5)
O(1)-C(12)-C(11)	123.1(5)
C(13)-C(12)-C(11)	118.0(5)
C(13)-C(14)-C(15)	119.0(6)
C(13)-C(14)-C(141)	120.7(6)
C(15)-C(14)-C(141)	120.3(6)
O(01)-C(01)-Re(1)	177.6(5)
C(15)-C(16)-C(11)	122.1(6)
C(15)-C(16)-H(16)	119
C(11)-C(16)-H(16)	119
C(16)-C(11)-C(12)	118.7(6)
C(16)-C(11)-C(1)	117.2(5)
C(12)-C(11)-C(1)	124.1(6)
N(3)-C(35)-C(34)	123.1(6)
N(3)-C(35)-H(35)	118.5
C(34)-C(35)-H(35)	118.5
C(33)-C(34)-C(35)	119.7(6)
C(33)-C(34)-H(34)	120.2
C(35)-C(34)-H(34)	120.2
C(34)-C(33)-C(32)	117.4(6)
C(34)-C(33)-H(33)	121.3
C(32)-C(33)-H(33)	121.3
N(1)-C(1)-C(11)	129.1(6)
N(1)-C(1)-H(1)	115.5
C(11)-C(1)-H(1)	115.5
C(16)-C(15)-C(14)	120.0(6)
C(16)-C(15)-H(15)	120
C(14)-C(15)-H(15)	120
C(14)-C(141)-H(14A)	109.5
C(14)-C(141)-H(14B)	109.5
H(14A)-C(141)-H(14B)	109.5
C(14)-C(141)-H(14C)	109.5
H(14A)-C(141)-H(14C)	109.5

H(14B)-C(141)-H(14C)	109.5
O(03)-C(03)-Re(1)	176.8(7)
C(25)-C(21)-N(1)	122.5(7)
C(25)-C(21)-C(22)	106.9(8)
N(1)-C(21)-C(22)	113.5(6)
C(25)-C(21)-H(21)	104
N(1)-C(21)-H(21)	104
C(22)-C(21)-H(21)	104
C(21)-C(22)-C(23)	103.8(6)
C(21)-C(22)-H(22A)	111
C(23)-C(22)-H(22A)	111
C(21)-C(22)-H(22B)	111
C(23)-C(22)-H(22B)	111
H(22A)-C(22)-H(22B)	109
C(21)-C(25)-C(24)	104.1(8)
C(21)-C(25)-H(25A)	110.9
C(24)-C(25)-H(25A)	110.9
C(21)-C(25)-H(25B)	110.9
C(24)-C(25)-H(25B)	110.9
H(25A)-C(25)-H(25B)	109
C(24)-C(23)-C(22)	106.0(6)
C(24)-C(23)-H(23A)	110.5
C(22)-C(23)-H(23A)	110.5
C(24)-C(23)-H(23B)	110.5
C(22)-C(23)-H(23B)	110.5
H(23A)-C(23)-H(23B)	108.7
C(23)-C(24)-C(25)	103.9(7)
C(23)-C(24)-H(24A)	111
C(25)-C(24)-H(24A)	111
C(23)-C(24)-H(24B)	111
C(25)-C(24)-H(24B)	111
H(24A)-C(24)-H(24B)	109

Table 2.3: Anisotropic displacement parameters ($Å^2$ x 10^3) for *fac*-[Re(5Me-Sal-CyPent)$(CO)_3$(Py)]. The anisotropic displacement factor exponent takes the form: $-2\pi^2[h^2a^{*2}U^{11} + ... + 2\ h\ k\ a^*\ b^*\ U^{12}]$.

	U^{11}	U^{22}	U^{33}	U^{23}	U^{13}	U^{12}
Re(1)	39(1)	42(1)	54(1)	-1(1)	9(1)	5(1)
C(02)	54(4)	44(3)	74(4)	3(3)	6(3)	9(3)
O(1)	57(2)	44(2)	41(2)	-3(2)	5(2)	-8(2)
C(13)	46(3)	47(3)	50(3)	-2(3)	-3(2)	0(3)
N(3)	39(2)	44(3)	48(3)	-2(2)	2(2)	3(2)
N(1)	49(3)	51(3)	66(3)	-19(3)	21(2)	-9(2)
C(32)	51(4)	87(5)	71(4)	19(4)	21(3)	13(3)
C(31)	47(3)	67(4)	56(4)	12(3)	6(3)	5(3)
C(12)	33(3)	52(3)	46(3)	-3(2)	0(2)	4(2)
C(14)	54(4)	52(4)	60(4)	9(3)	2(3)	-1(3)
C(01)	40(3)	46(3)	67(4)	8(3)	10(3)	10(3)
C(16)	68(4)	72(4)	43(3)	-7(3)	-4(3)	-5(3)
C(11)	44(3)	60(4)	45(3)	-7(3)	-1(2)	-2(3)
C(35)	46(3)	65(4)	54(3)	6(3)	5(3)	6(3)
O(01)	66(3)	81(3)	53(3)	1(2)	-5(2)	4(2)
C(34)	49(4)	69(4)	66(4)	9(3)	-3(3)	15(3)
C(33)	43(3)	72(5)	85(5)	5(4)	7(3)	17(3)
C(1)	47(3)	67(4)	56(4)	-24(3)	6(3)	-9(3)
C(15)	76(5)	75(5)	47(4)	9(3)	0(3)	0(4)
C(141)	97(6)	67(5)	77(5)	17(4)	6(4)	-18(4)
O(02)	91(4)	48(3)	93(4)	13(3)	7(3)	3(3)
O(03)	66(3)	110(5)	127(5)	-10(4)	27(3)	32(3)
C(03)	44(3)	64(4)	92(5)	-7(4)	15(3)	13(3)
C(21)	75(5)	67(5)	92(5)	-29(4)	32(4)	-26(4)
C(22)	57(4)	61(4)	107(6)	-14(4)	27(4)	-15(3)
C(25)	212(13)	97(8)	181(11)	-79(8)	134(10)	-92(8)
C(23)	71(5)	64(5)	92(6)	16(4)	-10(4)	-21(4)
C(24)	159(10)	67(5)	93(6)	-19(5)	31(6)	-56(6)

3 Data of *fac*-[Re(5Me-Sal-CyPent)(CO)$_3$(Im)]

Table 3.1: Atomic coordinates (x 10^4) and equivalent isotropic displacement parameters (Å^2 x 10^3) for *fac*-[Re(5Me-Sal-CyPent)(CO)$_3$(Im)]. U(eq) is defined as one third of the trace of the orthogonalized U^{ij} tensor.

	x	y	z	U(eq)
Re(1)	2707(1)	8613(1)	1959(1)	43(1)
N(1)	1838(4)	10974(8)	1511(4)	44(1)
O(02)	2262(7)	7809(13)	3260(6)	101(3)
O(1)	3206(4)	9273(7)	1186(4)	56(1)
C(01)	3463(8)	6563(9)	2337(7)	59(2)
O(01)	3927(6)	5312(9)	2593(5)	88(2)
O(03)	776(7)	6563(9)	590(5)	89(2)
N(3)	4100(4)	10084(7)	2921(4)	49(1)
C(14)	3100(7)	11760(13)	-435(5)	61(2)
C(02)	2407(7)	8116(12)	2746(6)	60(2)
C(15)	2384(7)	12981(12)	-590(5)	62(2)
C(1)	1751(5)	11978(9)	935(4)	47(1)
C(13)	3348(6)	10539(11)	164(5)	60(2)
N(33)	5341(5)	11961(10)	3511(4)	61(2)
C(34)	4409(7)	11466(9)	2799(6)	52(2)
C(12)	2937(5)	10488(9)	630(4)	46(1)
C(11)	2229(5)	11822(11)	487(5)	51(2)
C(03)	1493(6)	7366(10)	1094(5)	57(2)
C(16)	1972(7)	12992(12)	-132(6)	62(2)
C(31)	4887(7)	9606(14)	3757(6)	83(3)
C(32)	5667(7)	10738(13)	4122(6)	82(3)
C(141)	3605(11)	11754(19)	-903(9)	94(4)
C(21)	1179(6)	11395(8)	1805(6)	51(2)
C(25)	847(8)	13192(13)	1782(7)	71(2)
C(22)	108(6)	10418(12)	1276(6)	66(2)
C(23)	-634(10)	11478(14)	1359(11)	94(4)
C(24)	4(8)	12962(15)	1922(7)	85(3)

Table 3.2: Bond lengths [Å] and angles [°] for *fac*-[Re(5Me-Sal-CyPent)$(CO)_3$(Im)].

Atoms	Length	Atoms	Angle
Re(1)-C(02)	1.871(9)	C(02)-Re(1)-C(01)	84.9(4)
Re(1)-C(01)	1.896(8)	C(02)-Re(1)-C(03)	89.3(4)
Re(1)-C(03)	1.905(8)	C(01)-Re(1)-C(03)	87.7(4)
Re(1)-O(1)	2.114(5)	C(02)-Re(1)-O(1)	173.8(3)
Re(1)-N(1)	2.183(6)	C(01)-Re(1)-O(1)	94.2(3)
Re(1)-N(3)	2.189(6)	C(03)-Re(1)-O(1)	96.8(3)
N(1)-C(1)	1.303(9)	C(02)-Re(1)-N(1)	95.8(3)
N(1)-C(21)	1.485(9)	C(01)-Re(1)-N(1)	179.3(3)
O(02)-C(02)	1.162(12)	C(03)-Re(1)-N(1)	92.2(3)
O(1)-C(12)	1.313(8)	O(1)-Re(1)-N(1)	85.1(2)
C(01)-O(01)	1.160(10)	C(02)-Re(1)-N(3)	92.3(3)
O(03)-C(03)	1.151(10)	C(01)-Re(1)-N(3)	93.0(3)
N(3)-C(34)	1.282(9)	C(03)-Re(1)-N(3)	178.2(3)
N(3)-C(31)	1.375(10)	O(1)-Re(1)-N(3)	81.5(2)
C(14)-C(13)	1.374(12)	N(1)-Re(1)-N(3)	87.1(2)
C(14)-C(15)	1.382(15)	C(1)-N(1)-C(21)	115.9(6)
C(14)-C(141)	1.510(14)	C(1)-N(1)-Re(1)	126.2(5)
C(15)-C(16)	1.366(12)	C(21)-N(1)-Re(1)	117.5(4)
C(15)-H(15)	0.95	C(12)-O(1)-Re(1)	132.8(4)
C(1)-C(11)	1.445(10)	O(01)-C(01)-Re(1)	177.7(8)
C(1)-H(1)	0.95	C(34)-N(3)-C(31)	105.9(7)
C(13)-C(12)	1.380(10)	C(34)-N(3)-Re(1)	127.4(5)
C(13)-H(13)	0.95	C(31)-N(3)-Re(1)	126.3(6)
N(33)-C(34)	1.340(10)	C(13)-C(14)-C(15)	118.1(8)
N(33)-C(32)	1.369(11)	C(13)-C(14)-C(141)	120.3(9)
N(33)-H(33)	0.88	C(15)-C(14)-C(141)	121.6(9)
C(34)-H(34)	0.95	O(02)-C(02)-Re(1)	177.4(9)
C(12)-C(11)	1.446(10)	C(16)-C(15)-C(14)	120.3(8)
C(11)-C(16)	1.369(11)	C(16)-C(15)-H(15)	119.8
C(16)-H(16)	0.95	C(14)-C(15)-H(15)	119.8
C(31)-C(32)	1.340(12)	N(1)-C(1)-C(11)	128.3(7)
C(31)-H(31)	0.95	N(1)-C(1)-H(1)	115.9
C(32)-H(32)	0.95	C(11)-C(1)-H(1)	115.9
C(141)-H(14A)	0.98	C(14)-C(13)-C(12)	123.5(8)
C(141)-H(14B)	0.98	C(14)-C(13)-H(13)	118.3
C(141)-H(14C)	0.98	C(12)-C(13)-H(13)	118.3
C(21)-C(25)	1.519(11)	C(34)-N(33)-C(32)	106.8(7)
C(21)-C(22)	1.565(11)	C(34)-N(33)-H(33)	126.6
C(21)-H(21)	1	C(32)-N(33)-H(33)	126.6
C(25)-C(24)	1.514(14)	N(3)-C(34)-N(33)	111.9(7)

C(25)-H(25A)	0.99	N(3)-C(34)-H(34)	124.1
C(25)-H(25B)	0.99	N(33)-C(34)-H(34)	124.1
C(22)-C(23)	1.526(13)	O(1)-C(12)-C(13)	120.0(6)
C(22)-H(22A)	0.99	O(1)-C(12)-C(11)	122.5(6)
C(22)-H(22B)	0.99	C(13)-C(12)-C(11)	117.5(6)
C(23)-C(24)	1.513(17)	C(16)-C(11)-C(1)	117.8(7)
C(23)-H(23A)	0.99	C(16)-C(11)-C(12)	117.7(7)
C(23)-H(23B)	0.99	C(1)-C(11)-C(12)	124.5(7)
C(24)-H(24A)	0.99	O(03)-C(03)-Re(1)	177.6(8)
C(24)-H(24B)	0.99	C(15)-C(16)-C(11)	122.9(8)
		C(15)-C(16)-H(16)	118.5
		C(11)-C(16)-H(16)	118.5
		C(32)-C(31)-N(3)	109.5(8)
		C(32)-C(31)-H(31)	125.2
		N(3)-C(31)-H(31)	125.2
		C(31)-C(32)-N(33)	105.8(7)
		C(31)-C(32)-H(32)	127.1
		N(33)-C(32)-H(32)	127.1
		C(14)-C(141)-H(14A)	109.5
		C(14)-C(141)-H(14B)	109.5
		H(14A)-C(141)-H(14B)	109.5
		C(14)-C(141)-H(14C)	109.5
		H(14A)-C(141)-H(14C)	109.5
		H(14B)-C(141)-H(14C)	109.5
		N(1)-C(21)-C(25)	120.6(7)
		N(1)-C(21)-C(22)	111.6(6)
		C(25)-C(21)-C(22)	103.4(7)
		N(1)-C(21)-H(21)	106.8
		C(25)-C(21)-H(21)	106.8
		C(22)-C(21)-H(21)	106.8
		C(24)-C(25)-C(21)	101.7(9)
		C(24)-C(25)-H(25A)	111.4
		C(21)-C(25)-H(25A)	111.4
		C(24)-C(25)-H(25B)	111.4
		C(21)-C(25)-H(25B)	111.4
		H(25A)-C(25)-H(25B)	109.3
		C(23)-C(22)-C(21)	104.7(8)
		C(23)-C(22)-H(22A)	110.8
		C(21)-C(22)-H(22A)	110.8
		C(23)-C(22)-H(22B)	110.8
		C(21)-C(22)-H(22B)	110.8
		H(22A)-C(22)-H(22B)	108.9
		C(24)-C(23)-C(22)	106.5(8)

C(24)-C(23)-H(23A)	110.4
C(22)-C(23)-H(23A)	110.4
C(24)-C(23)-H(23B)	110.4
C(22)-C(23)-H(23B)	110.4
H(23A)-C(23)-H(23B)	108.6
C(23)-C(24)-C(25)	104.4(9)
C(23)-C(24)-H(24A)	110.9
C(25)-C(24)-H(24A)	110.9
C(23)-C(24)-H(24B)	110.9
C(25)-C(24)-H(24B)	110.9
H(24A)-C(24)-H(24B)	108.9

Table 3.3: Anisotropic displacement parameters ($Å^2$ x 10^3) for *fac*-[Re(5Me-Sal-CyPent)$(CO)_3$(Im)]. The anisotropic displacement factor exponent takes the form: $-2\pi^2[h^2a^{*2}U^{11} + ... + 2\ h\ k\ a^*\ b^*\ U^{12}]$.

	U^{11}	U^{22}	U^{33}	U^{23}	U^{13}	U^{12}
Re(1)	38(1)	42(1)	55(1)	3(1)	31(1)	1(1)
N(1)	35(3)	51(3)	51(3)	-6(2)	28(2)	-2(2)
O(02)	107(6)	134(7)	113(5)	45(5)	94(5)	28(5)
O(1)	63(3)	56(3)	73(3)	13(3)	54(3)	13(2)
C(01)	77(6)	39(4)	80(5)	12(3)	56(5)	9(3)
O(01)	97(5)	73(4)	118(6)	33(4)	78(5)	36(4)
O(03)	78(5)	80(5)	72(4)	-3(3)	25(4)	-19(4)
N(3)	38(3)	49(3)	56(3)	9(2)	27(2)	3(2)
C(14)	59(5)	80(5)	52(4)	11(4)	38(4)	0(4)
C(02)	54(4)	59(4)	79(5)	3(4)	46(4)	1(4)
C(15)	66(5)	65(5)	63(4)	10(4)	41(4)	1(4)
C(1)	36(3)	50(4)	53(3)	6(3)	26(3)	5(3)
C(13)	46(4)	76(5)	62(4)	6(4)	34(3)	7(3)
N(33)	53(3)	66(4)	68(4)	-2(3)	38(3)	-13(3)
C(34)	50(4)	56(4)	57(4)	-1(3)	35(4)	-3(3)
C(12)	42(3)	50(4)	49(3)	6(3)	29(3)	1(3)
C(11)	37(3)	59(4)	60(4)	5(3)	31(3)	4(3)
C(03)	51(4)	56(4)	56(4)	5(3)	27(3)	-2(3)
C(16)	57(4)	60(5)	68(5)	17(4)	36(4)	11(4)
C(31)	63(5)	80(6)	69(5)	18(5)	18(4)	-5(5)
C(32)	51(4)	72(6)	70(5)	15(4)	7(4)	-9(4)
C(141)	86(8)	141(11)	82(7)	23(7)	65(7)	19(7)
C(21)	46(4)	56(4)	61(4)	6(3)	38(4)	7(3)
C(25)	63(5)	67(5)	98(7)	-11(5)	56(5)	8(4)

C(22)	51(4)	70(5)	90(6)	-5(4)	47(4)	-1(4)
C(23)	58(6)	105(10)	141(12)	17(7)	71(8)	10(5)
C(24)	67(5)	101(8)	103(7)	-18(6)	58(6)	11(6)

4 Data of *fac*-[Re(*κO*-5Me-Sal-CyPent)(CO)$_3$(Py)(Br)]

Table 4.1: Atomic coordinates (x 10^4) and equivalent isotropic displacement parameters (Å^2 x 10^3) for *fac*-[Re(*κO*-5Me-Sal-CyPent)(CO)$_3$(Py)(Br)]. U(eq) is defined as one third of the trace of the orthogonalized U^{ij} tensor.

	x	y	z	U(eq)
Re(1)	3166(1)	2637(1)	4047(1)	38(1)
O(1)	4542(3)	2010(4)	3587(1)	49(1)
C(14)	7688(4)	1784(7)	4455(2)	59(1)
C(12)	5716(4)	1765(5)	3744(2)	43(1)
C(13)	6443(4)	2117(6)	4303(2)	50(1)
C(11)	6292(4)	1103(5)	3318(2)	50(1)
C(141)	8446(6)	2167(10)	5066(3)	90(2)
C(16)	7554(4)	782(7)	3478(2)	64(1)
C(15)	8231(4)	1113(8)	4030(2)	69(2)
N(1)	4476(3)	968(5)	2522(2)	53(1)
C(1)	5631(4)	696(6)	2740(2)	54(1)
C(21)	3809(5)	568(6)	1921(2)	60(1)
C(22)	2548(5)	-57(8)	1925(3)	79(2)
O(02)	4243(3)	1321(4)	5274(1)	64(1)
C(02)	3857(4)	1802(5)	4806(2)	46(1)
N(3)	2393(3)	493(4)	3674(2)	44(1)
C(35)	1195(4)	355(6)	3403(2)	56(1)
C(33)	1409(6)	-2173(7)	3185(3)	71(2)
C(34)	702(5)	-945(7)	3163(2)	68(1)
C(31)	3101(4)	-689(5)	3694(2)	54(1)
C(32)	2664(6)	-2048(6)	3446(3)	65(1)
O(03)	4214(4)	5660(4)	4458(2)	79(1)
C(03)	3835(4)	4509(5)	4311(2)	49(1)
C(01)	1773(4)	3169(6)	4341(2)	53(1)
O(01)	930(3)	3476(6)	4521(2)	84(1)
Br(1)	2185(1)	3689(1)	2982(1)	54(1)
C(25)	3569(8)	1893(9)	1512(3)	90(2)
C(23)	1743(7)	576(13)	1371(4)	124(3)
C(24)	2453(9)	1516(13)	1073(4)	142(4)

Table 4.2: Bond lengths [Å] and angles [°] for *fac*-[Re(*κO*-5Me-Sal-CyPent)$(CO)_3$(Py)(Br)].

Atoms	Length	Atoms	Angle
Re(1)-C(01)	1.896(4)	C(01)-Re(1)-C(02)	88.61(19)
Re(1)-C(02)	1.897(4)	C(01)-Re(1)-C(03)	87.5(2)
Re(1)-C(03)	1.899(5)	C(02)-Re(1)-C(03)	90.73(19)
Re(1)-O(1)	2.132(3)	C(01)-Re(1)-O(1)	171.19(16)
Re(1)-N(3)	2.220(4)	C(02)-Re(1)-O(1)	98.96(15)
Re(1)-Br(1)	2.6279(7)	C(03)-Re(1)-O(1)	96.79(17)
O(1)-C(12)	1.303(5)	C(01)-Re(1)-N(3)	94.49(18)
C(14)-C(13)	1.394(7)	C(02)-Re(1)-N(3)	92.84(16)
C(14)-C(15)	1.398(7)	C(03)-Re(1)-N(3)	175.93(15)
C(14)-C(141)	1.510(8)	O(1)-Re(1)-N(3)	80.73(13)
C(12)-C(13)	1.394(6)	C(01)-Re(1)-Br(1)	91.79(14)
C(12)-C(11)	1.419(6)	C(02)-Re(1)-Br(1)	177.78(14)
C(13)-H(15)	0.95	C(03)-Re(1)-Br(1)	91.47(13)
C(11)-C(16)	1.411(7)	O(1)-Re(1)-Br(1)	80.47(9)
C(11)-C(1)	1.416(6)	N(3)-Re(1)-Br(1)	84.96(9)
C(141)-H(14A)	0.98	C(12)-O(1)-Re(1)	134.9(3)
C(141)-H(14B)	0.98	C(13)-C(14)-C(15)	119.1(4)
C(141)-H(14C)	0.98	C(13)-C(14)-C(141)	120.5(5)
C(16)-C(15)	1.358(7)	C(15)-C(14)-C(141)	120.3(4)
C(16)-H(12)	0.95	O(1)-C(12)-C(13)	124.3(4)
C(15)-H(13)	0.95	O(1)-C(12)-C(11)	117.9(4)
N(1)-C(1)	1.304(6)	C(13)-C(12)-C(11)	117.9(4)
N(1)-C(21)	1.459(6)	C(14)-C(13)-C(12)	121.9(4)
N(1)-H(1B)	0.88	C(14)-C(13)-H(15)	119
C(1)-H(1A)	0.95	C(12)-C(13)-H(15)	119
C(21)-C(25)	1.512(9)	C(16)-C(11)-C(1)	118.4(4)
C(21)-C(22)	1.524(8)	C(16)-C(11)-C(12)	119.5(4)
C(21)-H(21)	1	C(1)-C(11)-C(12)	122.1(4)
C(22)-C(23)	1.501(10)	C(14)-C(141)-H(14A)	109.5
C(22)-H(22A)	0.99	C(14)-C(141)-H(14B)	109.5
C(22)-H(22B)	0.99	H(14A)-C(141)-H(14B)	109.5
O(02)-C(02)	1.151(5)	C(14)-C(141)-H(14C)	109.5
N(3)-C(31)	1.328(6)	H(14A)-C(141)-H(14C)	109.5
N(3)-C(35)	1.354(5)	H(14B)-C(141)-H(14C)	109.5
C(35)-C(34)	1.365(7)	C(15)-C(16)-C(11)	121.2(4)
C(35)-H(35)	0.95	C(15)-C(16)-H(12)	119.4
C(33)-C(34)	1.360(9)	C(11)-C(16)-H(12)	119.4
C(33)-C(32)	1.406(9)	C(16)-C(15)-C(14)	120.4(4)
C(33)-H(33)	0.95	C(16)-C(15)-H(13)	119.8

C(34)-H(34)	0.95	C(14)-C(15)-H(13)	119.8
C(31)-C(32)	1.399(7)	C(1)-N(1)-C(21)	124.9(4)
C(31)-H(31)	0.95	C(1)-N(1)-H(1B)	117.5
C(32)-H(32)	0.95	C(21)-N(1)-H(1B)	117.5
O(03)-C(03)	1.149(6)	N(1)-C(1)-C(11)	125.4(4)
C(01)-O(01)	1.147(5)	N(1)-C(1)-H(1A)	117.3
C(25)-C(24)	1.461(10)	C(11)-C(1)-H(1A)	117.3
C(25)-H(25A)	0.99	N(1)-C(21)-C(25)	111.8(5)
C(25)-H(25B)	0.99	N(1)-C(21)-C(22)	111.6(4)
C(23)-C(24)	1.437(13)	C(25)-C(21)-C(22)	105.2(5)
C(23)-H(23A)	0.99	N(1)-C(21)-H(21)	109.4
C(23)-H(23B)	0.99	C(25)-C(21)-H(21)	109.4
C(24)-H(24A)	0.99	C(22)-C(21)-H(21)	109.4
C(24)-H(24B)	0.99	C(23)-C(22)-C(21)	103.7(5)
		C(23)-C(22)-H(22A)	111
		C(21)-C(22)-H(22A)	111
		C(23)-C(22)-H(22B)	111
		C(21)-C(22)-H(22B)	111
		H(22A)-C(22)-H(22B)	109
		O(02)-C(02)-Re(1)	177.5(4)
		C(31)-N(3)-C(35)	117.7(4)
		C(31)-N(3)-Re(1)	120.9(3)
		C(35)-N(3)-Re(1)	121.3(3)
		N(3)-C(35)-C(34)	122.4(5)
		N(3)-C(35)-H(35)	118.8
		C(34)-C(35)-H(35)	118.8
		C(34)-C(33)-C(32)	118.0(5)
		C(34)-C(33)-H(33)	121
		C(32)-C(33)-H(33)	121
		C(33)-C(34)-C(35)	120.7(5)
		C(33)-C(34)-H(34)	119.6
		C(35)-C(34)-H(34)	119.6
		N(3)-C(31)-C(32)	123.0(4)
		N(3)-C(31)-H(31)	118.5
		C(32)-C(31)-H(31)	118.5
		C(31)-C(32)-C(33)	118.1(5)
		C(31)-C(32)-H(32)	121
		C(33)-C(32)-H(32)	121
		O(03)-C(03)-Re(1)	178.0(4)
		O(01)-C(01)-Re(1)	179.3(5)
		C(24)-C(25)-C(21)	104.4(6)
		C(24)-C(25)-H(25A)	110.9
		C(21)-C(25)-H(25A)	110.9

C(24)-C(25)-H(25B)	110.9
C(21)-C(25)-H(25B)	110.9
H(25A)-C(25)-H(25B)	108.9
C(24)-C(23)-C(22)	109.7(6)
C(24)-C(23)-H(23A)	109.7
C(22)-C(23)-H(23A)	109.7
C(24)-C(23)-H(23B)	109.7
C(22)-C(23)-H(23B)	109.7
H(23A)-C(23)-H(23B)	108.2
C(23)-C(24)-C(25)	106.9(7)
C(23)-C(24)-H(24A)	110.3
C(25)-C(24)-H(24A)	110.3
C(23)-C(24)-H(24B)	110.3
C(25)-C(24)-H(24B)	110.3
H(24A)-C(24)-H(24B)	108.6

Table 4.3: Anisotropic displacement parameters ($Å^2$ x 10^3) for *fac*-[Re(*κO*-5Me-Sal-CyPent)$(CO)_3$(Py)(Br)]. The anisotropic displacement factor exponent takes the form: $-2\pi^2[h^2a^{*2}U^{11} + ... + 2\ h\ k\ a^*\ b^*\ U^{12}]$.

	U^{11}	U^{22}	U^{33}	U^{23}	U^{13}	U^{12}
Re(1)	35(1)	48(1)	31(1)	-2(1)	6(1)	0(1)
O(1)	41(2)	65(2)	41(2)	-11(2)	9(1)	3(1)
C(14)	44(2)	81(4)	49(3)	4(2)	8(2)	-8(2)
C(12)	41(2)	45(2)	44(2)	1(2)	13(2)	-2(2)
C(13)	42(2)	65(3)	47(3)	-5(2)	15(2)	-6(2)
C(11)	47(2)	57(3)	47(2)	-3(2)	14(2)	5(2)
C(141)	50(3)	161(7)	56(4)	-10(4)	5(3)	-5(4)
C(16)	51(3)	86(4)	59(3)	-10(3)	18(2)	10(2)
C(15)	36(2)	101(5)	71(4)	3(3)	10(2)	10(2)
N(1)	56(2)	64(2)	38(2)	-9(2)	12(2)	5(2)
C(1)	56(3)	63(3)	47(2)	-8(2)	19(2)	9(2)
C(21)	65(3)	71(3)	42(2)	-14(2)	7(2)	10(2)
C(22)	82(4)	90(4)	61(3)	-10(3)	6(3)	-21(3)
O(02)	73(2)	72(2)	43(2)	4(2)	2(2)	4(2)
C(02)	47(2)	51(2)	41(2)	-3(2)	10(2)	-1(2)
N(3)	41(2)	49(2)	39(2)	1(2)	5(1)	-3(1)
C(35)	40(2)	65(3)	59(3)	1(2)	2(2)	-2(2)
C(33)	81(4)	60(3)	67(4)	-13(3)	10(3)	-16(3)
C(34)	53(3)	80(4)	66(3)	-4(3)	-2(2)	-14(3)
C(31)	55(2)	55(3)	45(2)	8(2)	-2(2)	4(2)

C(32)	77(4)	53(3)	61(3)	-3(3)	8(3)	4(3)
O(03)	97(3)	58(2)	67(2)	-4(2)	-9(2)	-12(2)
C(03)	51(2)	50(2)	42(2)	0(2)	1(2)	-1(2)
C(01)	50(2)	62(3)	47(2)	3(2)	13(2)	5(2)
O(01)	53(2)	128(4)	78(3)	-14(3)	29(2)	13(2)
Br(1)	56(1)	64(1)	39(1)	10(1)	3(1)	-1(1)
C(25)	105(5)	106(5)	54(3)	14(4)	7(3)	-19(5)
C(23)	71(4)	177(10)	114(6)	0(7)	-5(4)	-8(5)
C(24)	137(8)	157(10)	100(6)	28(7)	-39(6)	-16(7)

5 Data of *fac*-[Re(5Me-Sal-Hist)(CO)$_3$].MeOH

Table 5.1: Atomic coordinates (x 10^4) and equivalent isotropic displacement parameters (Å^2 x 10^3) for *fac*-[Re(5Me-Sal-Hist)(CO)$_3$]. U(eq) is defined as one third of the trace of the orthogonalized U^{ij} tensor.

	x	y	z	U(eq)
Re(1)	3877(1)	3349(1)	7090(1)	24(1)
C(01)	4360(2)	1908(6)	6877(5)	36(1)
C(13)	2966(2)	2212(6)	4856(4)	24(1)
C(16)	2335(2)	3894(6)	5861(4)	28(1)
N(34)	4948(2)	6369(5)	6144(3)	36(1)
C(02)	4092(2)	3519(6)	8332(4)	33(1)
C(03)	3479(2)	1757(6)	7504(4)	31(1)
C(35)	4635(2)	7417(6)	6461(4)	35(1)
O(1)	3603(1)	3230(4)	5707(3)	25(1)
C(15)	2173(2)	2972(6)	5167(4)	28(1)
N(1)	3354(2)	5088(5)	7184(3)	25(1)
C(11)	2813(2)	3983(6)	6078(3)	24(1)
N(32)	4307(2)	5199(5)	6608(3)	26(1)
C(2)	3482(2)	6432(6)	7697(4)	32(1)
C(33)	4739(2)	5067(6)	6249(4)	31(1)
C(3)	3792(2)	7397(7)	7090(4)	33(1)
C(31)	4241(2)	6702(5)	6739(4)	28(1)
C(141)	2324(2)	1117(7)	3899(4)	34(1)
C(1)	2960(2)	5084(6)	6756(4)	24(1)
C(12)	3140(2)	3143(5)	5565(4)	22(1)
C(14)	2495(2)	2120(6)	4655(4)	26(1)
O(03)	3252(2)	793(5)	7770(3)	47(1)
O(02)	4214(2)	3583(5)	9102(3)	53(1)

O(01)	4654(2)	1061(5)	6733(4)	56(1)
O(04)	4227(2)	2314(5)	4456(3)	44(1)
C(04)	4234(3)	742(8)	4436(5)	50(2)

Table 5.2: Bond lengths [Å] and angles [°] for *fac*-[Re(5Me-Sal-Hist)$(CO)_3$].MeOH.

Atoms	Length	Atoms	Angle
Re(1)-C(02)	1.894(6)	C(02)-Re(1)-C(01)	88.7(3)
Re(1)-C(01)	1.917(7)	C(02)-Re(1)-C(03)	87.5(3)
Re(1)-C(03)	1.925(6)	C(01)-Re(1)-C(03)	87.8(3)
Re(1)-O(1)	2.138(4)	C(02)-Re(1)-O(1)	176.9(2)
Re(1)-N(1)	2.167(5)	C(01)-Re(1)-O(1)	94.4(2)
Re(1)-N(32)	2.184(4)	C(03)-Re(1)-O(1)	92.1(2)
C(01)-O(01)	1.150(8)	C(02)-Re(1)-N(1)	95.9(2)
C(13)-C(14)	1.368(7)	C(01)-Re(1)-N(1)	173.6(2)
C(13)-C(12)	1.412(7)	C(03)-Re(1)-N(1)	96.9(2)
C(13)-H(13)	0.95	O(1)-Re(1)-N(1)	81.12(14)
C(16)-C(15)	1.380(8)	C(02)-Re(1)-N(32)	93.4(2)
C(16)-C(11)	1.395(8)	C(01)-Re(1)-N(32)	94.0(2)
C(16)-H(16)	0.95	C(03)-Re(1)-N(32)	178.0(2)
N(34)-C(33)	1.326(7)	O(1)-Re(1)-N(32)	86.86(15)
N(34)-C(35)	1.376(8)	N(1)-Re(1)-N(32)	81.23(18)
N(34)-H(34)	0.88	O(01)-C(01)-Re(1)	178.5(7)
C(02)-O(02)	1.162(8)	C(14)-C(13)-C(12)	122.0(5)
C(03)-O(03)	1.150(7)	C(14)-C(13)-H(13)	119
C(35)-C(31)	1.354(8)	C(12)-C(13)-H(13)	119
C(35)-H(35)	0.95	C(15)-C(16)-C(11)	121.4(5)
O(1)-C(12)	1.333(6)	C(15)-C(16)-H(16)	119.3
C(15)-C(14)	1.405(8)	C(11)-C(16)-H(16)	119.3
C(15)-H(15)	0.95	C(33)-N(34)-C(35)	106.5(5)
N(1)-C(1)	1.277(7)	C(33)-N(34)-H(34)	126.7
N(1)-C(2)	1.467(7)	C(35)-N(34)-H(34)	126.7
C(11)-C(12)	1.409(7)	O(02)-C(02)-Re(1)	177.7(5)
C(11)-C(1)	1.454(7)	O(03)-C(03)-Re(1)	177.9(6)
N(32)-C(33)	1.339(7)	C(31)-C(35)-N(34)	107.7(5)
N(32)-C(31)	1.384(6)	C(31)-C(35)-H(35)	126.2
C(2)-C(3)	1.517(9)	N(34)-C(35)-H(35)	126.2
C(2)-H(2A)	0.99	C(12)-O(1)-Re(1)	120.3(3)
C(2)-H(2B)	0.99	C(16)-C(15)-C(14)	119.5(5)

C(33)-H(33)	0.95	C(16)-C(15)-H(15)	120.2
C(3)-C(31)	1.509(8)	C(14)-C(15)-H(15)	120.2
C(3)-H(3A)	0.99	C(1)-N(1)-C(2)	117.4(5)
C(3)-H(3B)	0.99	C(1)-N(1)-Re(1)	124.7(4)
C(141)-C(14)	1.497(7)	C(2)-N(1)-Re(1)	117.6(4)
C(141)-H(14A)	0.98	C(16)-C(11)-C(12)	119.5(5)
C(141)-H(14B)	0.98	C(16)-C(11)-C(1)	117.9(5)
C(141)-H(14C)	0.98	C(12)-C(11)-C(1)	122.1(5)
C(1)-H(1)	0.95	C(33)-N(32)-C(31)	105.3(5)
O(04)-C(04)	1.421(8)	C(33)-N(32)-Re(1)	124.6(4)
O(04)-H(141)	0.84	C(31)-N(32)-Re(1)	129.2(4)
C(04)-H(14D)	0.98	N(1)-C(2)-C(3)	109.2(5)
C(04)-H(14E)	0.98	N(1)-C(2)-H(2A)	109.8
C(04)-H(14F)	0.98	C(3)-C(2)-H(2A)	109.8
		N(1)-C(2)-H(2B)	109.8
		C(3)-C(2)-H(2B)	109.8
		H(2A)-C(2)-H(2B)	108.3
		N(34)-C(33)-N(32)	112.0(5)
		N(34)-C(33)-H(33)	124
		N(32)-C(33)-H(33)	124
		C(31)-C(3)-C(2)	116.4(5)
		C(31)-C(3)-H(3A)	108.2
		C(2)-C(3)-H(3A)	108.2
		C(31)-C(3)-H(3B)	108.2
		C(2)-C(3)-H(3B)	108.2
		H(3A)-C(3)-H(3B)	107.3
		C(35)-C(31)-N(32)	108.4(5)
		C(35)-C(31)-C(3)	126.9(5)
		N(32)-C(31)-C(3)	124.6(5)
		C(14)-C(141)-H(14A)	109.5
		C(14)-C(141)-H(14B)	109.5
		H(14A)-C(141)-H(14B)	109.5
		C(14)-C(141)-H(14C)	109.5
		H(14A)-C(141)-H(14C)	109.5
		H(14B)-C(141)-H(14C)	109.5
		N(1)-C(1)-C(11)	125.1(5)
		N(1)-C(1)-H(1)	117.4
		C(11)-C(1)-H(1)	117.4
		O(1)-C(12)-C(11)	122.5(5)
		O(1)-C(12)-C(13)	119.5(5)

C(11)-C(12)-C(13)	118.0(5)
C(13)-C(14)-C(15)	119.5(5)
C(13)-C(14)-C(141)	120.4(5)
C(15)-C(14)-C(141)	120.1(5)
C(04)-O(04)-H(141)	109.5
O(04)-C(04)-H(14D)	109.5
O(04)-C(04)-H(14E)	109.5
H(14D)-C(04)-H(14E)	109.5
O(04)-C(04)-H(14F)	109.5
H(14D)-C(04)-H(14F)	109.5
H(14E)-C(04)-H(14F)	109.5

Table 5.3: Anisotropic displacement parameters ($Å^2$ x 10^3) for *fac*-[Re(5Me-Sal-Hist)$(CO)_3$].MeOH. The anisotropic displacement factor exponent takes the form: $-2\pi^2[h^2a^{*2}U^{11} + ... + 2\ h\ k\ a^*\ b^*\ U^{12}]$.

	U^{11}	U^{22}	U^{33}	U^{23}	U^{13}	U^{12}
Re(1)	23(1)	22(1)	25(1)	-1(1)	-2(1)	-1(1)
C(01)	38(4)	29(3)	40(3)	-1(3)	-12(3)	2(3)
C(13)	31(3)	20(2)	22(3)	0(2)	0(2)	4(2)
C(16)	28(3)	28(3)	28(3)	2(2)	3(2)	1(2)
N(34)	28(3)	38(3)	43(3)	0(2)	8(2)	-7(2)
C(02)	32(3)	36(3)	31(3)	7(3)	1(3)	-7(3)
C(03)	35(3)	28(3)	30(3)	-5(2)	-3(3)	5(2)
C(35)	32(3)	25(3)	48(4)	1(3)	1(3)	-3(2)
O(1)	23(2)	28(2)	25(2)	-5(1)	-2(2)	2(2)
C(15)	25(3)	31(3)	28(3)	6(2)	-4(2)	-1(2)
N(1)	24(2)	28(2)	23(2)	-5(2)	7(2)	-1(2)
C(11)	29(3)	21(2)	21(3)	0(2)	2(2)	-1(2)
N(32)	25(2)	23(2)	30(2)	-1(2)	-1(2)	-5(2)
C(2)	29(3)	32(3)	34(3)	-13(2)	2(2)	-3(2)
C(33)	27(3)	31(3)	36(3)	-5(2)	4(2)	-4(2)
C(3)	32(3)	23(3)	44(4)	-8(2)	-1(2)	1(2)
C(31)	29(3)	26(3)	28(3)	0(2)	-2(2)	-2(2)
C(141)	38(3)	37(3)	28(3)	-3(3)	-10(3)	-3(3)
C(1)	23(3)	27(3)	21(2)	-1(2)	6(2)	-3(2)
C(12)	23(3)	20(2)	24(3)	3(2)	0(2)	1(2)
C(14)	31(3)	23(2)	25(3)	3(2)	-6(2)	-1(2)
O(03)	55(3)	34(3)	52(3)	4(2)	4(2)	-17(2)
O(02)	55(3)	72(3)	32(3)	2(2)	-14(2)	-13(3)

O(01)	53(3)	41(3)	74(3)	-12(3)	-13(3)	25(2)
O(04)	38(3)	39(2)	55(3)	-1(2)	15(2)	2(2)
C(04)	51(4)	44(4)	56(4)	-8(3)	5(3)	6(3)